

82814

STUDY ON MOMENT CURVATURE RELATIONSHIPS  
IN REINFORCED CONCRETE

A THESIS SUBMITTED TO  
THE GRADUATE SCHOOL OF NATURAL AND APPLIED SCIENCES  
OF  
THE MIDDLE EAST TECHNICAL UNIVERSITY

BY

AHMET YAĞCI

82814

IN PARTIAL FULFILLMENT OF THE REQUIREMENTS FOR THE DEGREE  
OF MASTER OF SCIENCE  
IN  
THE DEPARTMENT OF CIVIL ENGINEERING

TC. YÜKSEKÖĞRETİM KURULU  
DOKÜMANİTASYON BİRİMİ

FEBRUARY 1999

Approval of the Graduate School of Natural and Applied Sciences



Prof. Dr. Tayfur ÖZTÜRK

Director

I certify that this thesis satisfies all the requirements as a thesis for the degree of Master of Science.



Prof. Dr. Fuat ERBATUR

Head of Department

This is to certify that we have read this thesis and that in our opinion it is fully adequate, in scope and quality, as a thesis for the degree of Master of Science.



Prof. Dr. Uğur ERSOY

Supervisor

Examining Committee Members

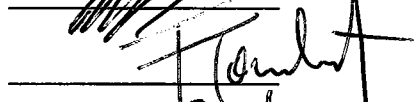
Prof. Dr. S. Tanvir WASTI



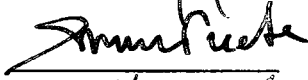
Prof. Dr. Uğur ERSOY



Prof. Dr. Tuğrul TANKUT



Prof. Dr. Güney ÖZCEBE



Dr. Halis GÜNEL



## ABSTRACT

### STUDY ON MOMENT CURVATURE RELATIONSHIPS IN REINFORCED CONCRETE

YAĞCI, Ahmet

M.S., Department of Civil Engineering

Supervisor: Prof. Dr. Uğur Ersoy

February, 1999, 234 pages

In this study the behaviour of reinforced concrete structural members having various characteristics were investigated. For this purpose a computer program which can draw moment-curvature diagrams was written. Main inputs to the program are; material characteristics used, geometry of the cross-section, and configuration of longitudinal and transverse reinforcement. For confined concrete in the core, mathematical models which have been tested by various researchers have been used. The moment-curvature diagrams obtained were grouped, in order to be able to make better comparisons and to reach to sound conclusions. Fifteen case studies were made in two main chapters: Studies on R/C beams and columns. The case studies considered were as follows:

- Influence of compression reinforcement (R/C beams)
- Influence of concrete strength (R/C beams & columns)
- Influence of confinement (R/C beams)
- Influence of steel model (R/C beams)

- Influence of tension reinforcement (R/C beams)
- Influence of confined concrete model (R/C beams and columns)
- Influence of flange width in T-beams
- Influence of lateral reinforcement configuration (R/C columns)
- Influence of lateral reinforcement ratio (R/C columns)
- Influence of lateral reinforcement spacing (R/C columns)
- Influence of ratio of longitudinal bars (R/C columns)
- Influence of axial load level (R/C columns)
- Influence of ratio of the gross area to the confined area (R/C columns)

The conclusions of each case study are presented at the end of the related sections. All moment-curvature diagrams are presented in Appendix A. The interaction diagrams of the columns studied are presented in Appendix B. As a general conclusion, it can be said that, for beams the ductility and behaviour was dominated by the quality of steel, while for columns the ductility and behaviour were dominated by the quality of concrete. It should be pointed out that concrete which dominates the behaviour of R/C columns is the confined concrete.

**Keywords:** Reinforced Concrete, Moment-Curvature, Stress-Strain Relationships, Confined Concrete, Steel Model, Axial Load, Interaction Diagrams, Ductility, Strength, Confinement

ÖZ

BETONARMEDE MOMENT EĞRİLİK İLİŞKİSİ  
ÜZERİNE BİR ÇALIŞMA

YAĞCI, Ahmet

Yüksek Lisans Tezi, İnşaat Mühendisliği Bölümü

Tez Yöneticisi: Prof. Dr. Uğur Ersoy

Şubat, 1999, 234 sayfa

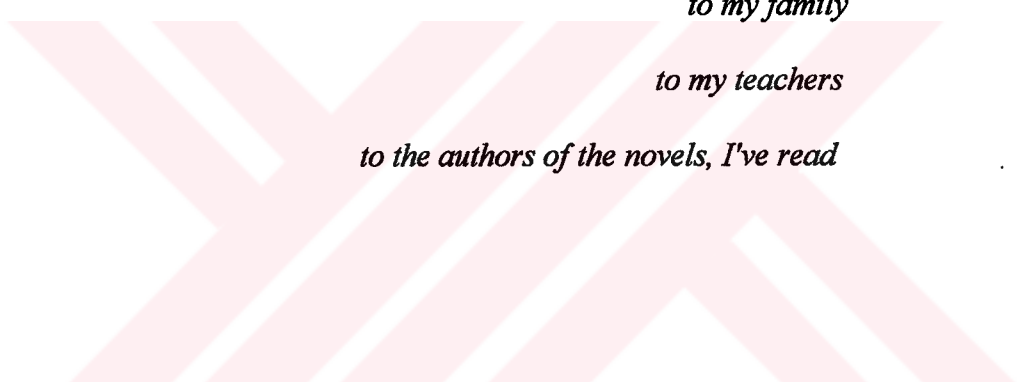
Bu tezde değişik özelliklere sahip betonarme elemanların davranışları incelenmiştir. Bu amaçla moment-eğrilik grafikleri çizebilen bir bilgisayar programı yazılmıştır. Bu program, problemden bağımsız olarak ve ancak incelenecek örneği oluşturan yapı malzemelerinin bütün özellikleri bilgisayara aktarıldıktan sonra çalışmaktadır. Sargılanmış betonun gerilme birim deformasyon ilişkisinin analitik çözümünde, sonuçlarının güvenilirliği daha önceki çalışmalarda kanıtlanmış bazı matematik modeller kullanılmıştır. Oluşturulan moment eğrilik grafikleri çeşitli karşılaştırmalar yapmak ve bazı sonuçlar elde etmek üzere gruplandırılmıştır. On beş durum çalışması iki genel konu altında incelenmiştir: Betonarme kirişler ve kolonlar. İncelenen durum çalışmaları şunlardır:

- Basınç donatısının betonarme kiriş davranışına etkisi
- Beton dayanımının betonarme kiriş ve kolon davranışlarına etkisi
- Sargılamanın betonarme kiriş davranışına etkisi
- Çelik modelinin betonarme kiriş davranışına etkisi
- Çekme donatısının betonarme kiriş davranışına etkisi

- Betonarme kiriş ve kolonlarda, sargılanmış beton modelinin, moment-eğrilik diyagramına etkisi
- T-kirişlerde, tabla genişliğinin etkisi
- Enine donatı konfigurasyonunun betonarme kolon davranışına etkisi
- Enine donatı oranının betonarme kolon davranışına etkisi
- Enine donatı aralığının betonarme kolon davranışına etkisi
- Boyuna donatı oranının betonarme kolon davranışına etkisi
- Eksenel yük düzeyinin betonarme kolon davranışına etkisi
- Toplam beton alanının sargılanmış alana oranının betonarme kolon davranışına etkisi

Her durum çalışması sonrasında elde edilen sonuçlar, ilgili bölümlerin sonunda sunulmuştur. Moment-eğrilik diyagramları Ek A'da sunulmuştur. İncelenen kolonların etkileşim diyagramları Ek B'de sunulmuştur. Genel bir sonuç olarak şu söylenebilir ki, kiriş davranışının sünekliliğini belirleyen baskın etken çelik kalitesi iken kolon davranışının sünekliliği beton kalitesine, yani dayanımına, sargılanmasına, vs. bağlıdır.

**Anahtar Kelimeler:** Betonarme, Moment-Eğrilik İlişkisi, Gerilme-Birim Deformasyon İlişkisi, Sargılanmış Beton, Çelik Modeli, Eksenel Yük, Etkileşim Diyagramı, Süneklilik, Dayanım, Sargılama



*to my family*

*to my teachers*

*to the authors of the novels, I've read*

## ACKNOWLEDGEMENTS

This study was conducted under the supervision of Prof. Dr. Uğur Ersoy. I wish to express my deepest appreciation for his professional guidance and nonstop encouragement.

I owe special thanks to Prof. Ş. Muvaffak Üzümeri, Prof. Dr. Tuğrul Tankut and Prof. Dr. Güney Özcebe for their valuable recommendations and continuous concerns.

I would like to extend my thanks to the structural mechanics laboratory staff, my friends, research assistants for their assistance during this study. I want to thank to Aytaç Korucu for his help in drawing the interaction diagrams.

Finally, I would like to give my heartfelt thanks to my mother, my father and my brother for their continuous encouragement, help and love.



## TABLE OF CONTENTS

ABSTRACT.....	iii
ÖZ.....	v
TABLE OF CONTENTS.....	ix
LIST OF TABLES.....	xiv
LIST OF FIGURES.....	xvi
LIST OF SYMBOLS.....	xxv
<b>CHAPTERS</b>	
1. INTRODUCTION.....	1
1.1 General.....	1
1.2 Object and Scope.....	3
2. LITERATURE SURVEY.....	6
3. METHOD OF ANALYSIS.....	18
3.1 General.....	18
3.2 Basic Assumptions and Models.....	22
3.2.1 General.....	22
3.2.2 Stress-Strain Relationships of Steel.....	24
3.2.3 Stress-Strain Relationships of Concrete Under Tension.....	25
3.2.4 Stress-Strain Relationships of Unconfined Concrete Under Compression.....	27
3.2.5 Stress-Strain Relationships of Confined Concrete Under Compression.....	29
3.2.5.1 Mechanics of Concrete Confinement by Reinforcement.....	29

3.2.5.2 Review of Mathematical Models Used in the	
Computer Program.....	33
3.2.5.2.1 Roy and Sozen Model.....	35
3.2.5.2.2 Sheikh and Uzumeri Model.....	36
3.2.5.2.3 Kent and Park Model.....	39
3.2.5.2.4 Modified Kent and Park Model.....	41
3.2.5.2.5 Saatcioglu Model.....	42
3.3 The Computer Program.....	44
4. NUMERICAL APPLICATIONS OF THE PROGRAM	
STUDIES ON R/C BEAMS.....	49
4.1 General.....	49
4.2 Case Study I: Influence of Compression Reinforcement	
in R/C Beams.....	51
4.2.1 Assumptions.....	51
4.2.2 Discussion of Results.....	54
4.2.3 Conclusions.....	56
4.3 Case Study II: Influence of Concrete Strength in R/C Beams.....	57
4.3.1 Assumptions.....	60
4.3.2 Discussion of Results.....	60
4.3.3 Conclusions.....	62
4.4 Case Study III: Influence of Confinement in R/C Beams.....	63
4.4.1 Assumptions.....	63
4.4.2 Discussion of Results.....	66
4.4.3 Conclusions.....	68
4.5 Case Study IV: Influence of the Steel Model in R/C Beams.....	69
4.5.1 Assumptions.....	69
4.5.2 Discussion of Results.....	72
4.5.3 Conclusions.....	74
4.6 Case Study V: Influence of Tension Reinforcement Ratio	
in R/C Beams.....	75

4.6.1 Assumptions.....	75
4.6.2 Discussion of Results.....	78
4.6.3 Conclusions.....	81
4.7 Case Study VI: Influence of Confined Concrete Models on Moment-Curvature Diagrams of R/C Beams.....	82
4.7.1 Assumptions.....	84
4.7.2 Discussion of Results.....	84
4.7.3 Conclusions.....	85
4.8 Case Study VII: Influence of Flange Width in T-Beams in R/C Beams.....	86
4.8.1 Assumptions.....	86
4.8.2 Discussion of Results.....	89
4.8.3 Conclusions.....	91
<b>5. NUMERICAL APPLICATIONS OF THE PROGRAM</b>	
<b>STUDIES ON R/C COLUMNS.....</b>	<b>92</b>
5.1 General.....	92
5.2 Case Study VIII: Influence of Lateral Reinforcement Configuration in R/C Columns.....	94
5.2.1 Assumptions.....	94
5.2.2 Discussion of Results.....	97
5.2.3 Conclusions.....	100
5.3 Case Study IX: Influence of Lateral Reinforcement Ratio " $\rho_s$ " in R/C Columns.....	101
5.3.1 Assumptions.....	101
5.3.2 Discussion of Results.....	104
5.3.3 Conclusions.....	106
5.4 Case Study X: Influence of Lateral Reinforcement Spacing in R/C Columns.....	107
5.4.1 Assumptions.....	107
5.4.2 Discussion of Results.....	110

5.4.3 Conclusions.....	111
5.5 Case Study XI: Influence of Concrete Strength in R/C Columns.....	111
5.5.1 Assumptions.....	111
5.5.2 Discussion of Results.....	114
5.5.3 Conclusions.....	117
5.6 Case Study XII: Influence of Ratio of Longitudinal Bars ( $\rho_t=A_{st}/A_c$ ) in R/C Columns.....	118
5.6.1 Assumptions.....	118
5.6.2 Discussion of Results.....	118
5.6.3 Conclusions.....	122
5.7 Case Study XIII: Influence of Confined Concrete Models on Moment-Curvature Diagrams of R/C Columns.....	123
5.7.1 Discussion of Results.....	124
5.7.2 Conclusions.....	129
5.8 Case Study XIV: Influence of Axial Load Level (' $N/f_{ck}A_c$ ' Ratio) in R/C Columns.....	129
5.8.1 Assumptions.....	130
5.8.2 Discussion of Results.....	130
5.8.3 Conclusions.....	135
5.9 Case Study XV: Influence of Ratio of the Gross Area to the Confined Area ( $A_g/A_{ck}$ ) in R/C Columns.....	136
5.9.1 Assumptions.....	136
5.9.2 Discussion of Results.....	139
5.9.3 Conclusions.....	140
6. CONCLUSIONS AND RECOMMENDATIONS.....	142
6.1 General.....	142
6.2 Conclusions.....	143
6.2.1 Beams.....	143
6.2.2 Columns.....	144
6.3 Recommendations .....	146

REFERENCES.....	147
APPENDIX A: Moment-Curvature Curves.....	150
APPENDIX B: Interaction Diagrams for Columns of Chapter 5.....	229



## LIST OF TABLES

### TABLE

4.1	List of sections and section properties; Influence of compression reinforcement in R/C beams.....	52
4.2	Results; Influence of compression reinforcement in R/C beams.....	53
4.3	List of sections and section properties; Influence of concrete strength in R/C beams.....	58
4.4	Results; Influence of concrete strength in R/C beams.....	59
4.5	List of sections and section properties; Influence of confinement in R/C beams.....	64
4.6	Results; Influence of confinement in R/C beams.....	65
4.7	List of sections and section properties; Influence of steel model in R/C beams.....	70
4.8	Results; Influence of steel model in R/C beams.....	71
4.9	List of sections and section properties; Influence of tension reinforcement ratio in R/C beams.....	76
4.10	Results; Influence of tension reinforcement ratio in R/C beams.....	77
4.11	List of sections and section properties; Influence of confined concrete models on moment-curvature diagrams of R/C beams.....	83
4.12	Results; Influence of confined concrete models on moment-curvature diagrams of R/C beams.....	83
4.13	List of sections and section properties; Influence of flange width in T-beams.....	87
4.14	Results; Influence of flange width in T-beams.....	88

5.1	List of sections and section properties; Influence of lateral reinforcement configuration in R/C columns.....	95
5.2	Results; Influence of lateral reinforcement configuration in R/C columns.....	96
5.3	List of sections and section properties; Influence of lateral reinforcement ratio " $\rho_s$ " in R/C columns.....	102
5.4	Results; Influence of lateral reinforcement ratio " $\rho_s$ " in R/C columns.....	103
5.5	List of sections and section properties; Influence of lateral reinforcement spacing in R/C columns.....	108
5.6	Results; Influence of lateral reinforcement spacing in R/C columns.....	109
5.7	List of sections and section properties; Influence of concrete strength in R/C columns.....	112
5.8	Results; Influence concrete strength in R/C columns.....	113
5.9	List of sections and section properties; Influence of ratio of longitudinal bars ( $\rho_t=A_{st}/A_c$ ) in R/C columns.....	119
5.10	Results; Influence of ratio of longitudinal bars ( $\rho_t=A_{st}/A_c$ ) in R/C columns.....	120
5.11	List of sections and section properties; Influence of confined concrete models on moment-curvature diagrams of R/C columns.....	125
5.12	Results; Influence of confined concrete models on moment-curvature diagrams of R/C columns.....	126
5.13	List of sections and section properties; Influence of axial load level ( $N/f_{ck}A_c$ ratio) in R/C columns.....	131
5.14	Results; Influence of axial load level ( $N/f_{ck}A_c$ ratio) in R/C columns.....	132
5.15	List of sections and section properties; Influence of ratio of the gross area to the confined area ( $A_g/A_{ck}$ ) in R/C columns.....	137
5.16	Results; Influence of ratio of the gross area to the confined area ( $A_g/A_{ck}$ ) in R/C columns.....	138

## LIST OF FIGURES

### FIGURES

3.1	Theoretical moment-curvature determination.....	20
3.2	Stress-strain diagram for steel in tension or compression.....	24
3.3	Assumed stress-strain diagram for concrete in tension.....	26
3.4	Hognestad's (1951) stress-strain diagram.....	28
3.5	Axial $\sigma$ - $\epsilon$ curves from triaxial compression tests (Richart et al).....	32
3.6	A uniaxially loaded member and free body diagrams of core concrete and spiral steel.....	32
3.7	Effectively confined concrete in square section and deformation of lateral steel between restraint points.....	34
3.8	Stress-strain diagrams for different amounts of lateral steel.....	34
3.9	Stress-strain curve proposed by Roy and Sozen.....	35
3.10	Stress strain curve for confined concrete. Sheikh and Üzümeri idealization (From Sheikh and Üzümeri, 1982).....	37
3.11	Stress strain curve for concrete. Kent and Park idealization (From Kent and Park, 1971).....	39
3.12	Stress strain curve for concrete. Modified Kent and Park idealization.....	41
3.13	Proposed stress strain relationship. Idealized by Saatcıođlu.....	44
3.14	Flowchart of the Program.....	46
3.15	Transverse steel configuration types.....	48
A.1	Influence of compression reinforcement in R/C beams; Group IA.....	150
A.2	Influence of compression reinforcement in R/C beams; Group IB.....	151
A.3	Influence of compression reinforcement in R/C beams; Group IC.....	151



A.4	Influence of compression reinforcement in R/C beams; Group ID.....	152
A.5	Influence of compression reinforcement in R/C beams; Group IE.....	152
A.6	Influence of compression reinforcement in R/C beams; Group IF.....	153
A.7	Influence of compression reinforcement in R/C beams; Group IG.....	153
A.8	Influence of compression reinforcement in R/C beams; Group IH.....	154
A.9	Influence of compression reinforcement in R/C beams; Group IJ.....	154
A.10	Influence of compression reinforcement in R/C beams; Group IK.....	155
A.11	Influence of compression reinforcement in R/C beams; Group IL.....	155
A.12	Influence of compression reinforcement in R/C beams; Group IM.....	156
A.13	Influence of concrete strength in R/C beams; Group IIA.....	156
A.14	Influence of concrete strength in R/C beams; Group IIB.....	157
A.15	Influence of concrete strength in R/C beams; Group IIC.....	157
A.16	Influence of concrete strength in R/C beams; Group IID.....	158
A.17	Influence of concrete strength in R/C beams; Group IIE.....	158
A.18	Influence of concrete strength in R/C beams; Group IIF.....	159
A.19	Influence of concrete strength in R/C beams; Group IIG.....	159
A.20	Influence of concrete strength in R/C beams; Group IIH.....	160
A.21	Influence of concrete strength in R/C beams; Group IIJ.....	160
A.22	Influence of concrete strength in R/C beams; Group IIK.....	161
A.23	Influence of concrete strength in R/C beams; Group IIL.....	161
A.24	Influence of confinement in R/C beams; Group IIIA.....	162
A.25	Influence of confinement in R/C beams; Group IIIB.....	162
A.26	Influence of confinement in R/C beams; Group IIIC.....	163
A.27	Influence of confinement in R/C beams; Group IIID.....	163
A.28	Influence of confinement in R/C beams; Group IIIE.....	164
A.29	Influence of confinement in R/C beams; Group IIIF.....	164
A.30	Influence of confinement in R/C beams; Group IIIG.....	165
A.31	Influence of confinement in R/C beams; Group IIIH.....	165
A.32	Influence of confinement in R/C beams; Group IIIJ.....	166
A.33	Influence of confinement in R/C beams; Group IIJK.....	166

A.34	Influence of confinement in R/C beams; Group IIII.....	167
A.35	Influence of the steel model in R/C beams; Group IVA.....	167
A.36	Influence of the steel model in R/C beams; Group IVB.....	168
A.37	Influence of the steel model in R/C beams; Group IVC.....	168
A.38	Influence of the steel model in R/C beams; Group IVD.....	169
A.39	Influence of the steel model in R/C beams; Group IVE.....	169
A.40	Influence of the steel model in R/C beams; Group IVF.....	170
A.41	Influence of the steel model in R/C beams; Group IVG.....	170
A.42	Influence of the steel model in R/C beams; Group IVH.....	171
A.43	Influence of the steel model in R/C beams; Group IVJ.....	171
A.44	Influence of the steel model in R/C beams; Group IVK.....	172
A.45	Influence of the steel model in R/C beams; Group IVL.....	172
A.46	Influence of the steel model in R/C beams; Group IVM.....	173
A.47	Influence of tension reinforcement ratio in R/C beams; Group VA.....	173
A.48	Influence of tension reinforcement ratio in R/C beams; Group VB.....	174
A.49	Influence of tension reinforcement ratio in R/C beams; Group VC.....	174
A.50	Influence of tension reinforcement ratio in R/C beams; Group VD.....	175
A.51	Influence of tension reinforcement ratio in R/C beams; Group VE.....	175
A.52	Influence of tension reinforcement ratio in R/C beams; Group VF.....	176
A.53	Influence of tension reinforcement ratio in R/C beams; Group VG.....	176
A.54	Influence of tension reinforcement ratio in R/C beams; Group VH.....	177
A.55	Influence of tension reinforcement ratio in R/C beams; Group VJ.....	177
A.56	Influence of tension reinforcement ratio in R/C beams; Group VK.....	178
A.57	Influence of confined concrete models on moment-curvature diagrams of R/C beams; Group VIA.....	178
A.58	Influence of confined concrete models on moment-curvature diagrams of R/C beams; Group VIB.....	179
A.59	Influence of confined concrete models on moment-curvature diagrams of R/C beams; Group VIC.....	179
A.60	Influence of confined concrete models on moment-curvature	

	diagrams of R/C beams; Group VID.....	180
A.61	Stress-strain diagrams of concrete for different confinement models; Ties $\Phi 10/90$ mm.....	180
A.62	Stress-strain diagrams of concrete for different confinement models; Ties $\Phi 8/120$ mm.....	181
A.63	Influence of flange width in T-beams; Group VIIA.....	181
A.64	Influence of flange width in T-beams; Group VIIB.....	182
A.65	Influence of flange width in T-beams; Group VIIC.....	182
A.66	Influence of flange width in T-beams; Group VIID.....	183
A.67	Influence of flange width in T-beams; Group VIIE.....	183
A.68	Influence of flange width in T-beams; Group VIIF.....	184
A.69	Influence of flange width in T-beams; Group VIIG.....	184
A.70	Influence of flange width in T-beams; Group VIIC.....	185
A.71	Influence of flange width in T-beams; Group VIID.....	185
A.72	Influence of flange width in T-beams; Group VIIE.....	186
A.73	Influence of lateral reinforcement configuration in R/C columns; Group VIIIA.....	186
A.74	Influence of lateral reinforcement configuration in R/C columns; Group VIIIB.....	187
A.75	Influence of lateral reinforcement configuration in R/C columns; Group VIIC.....	187
A.76	Influence of lateral reinforcement configuration in R/C columns; Group VIID.....	188
A.77	Influence of lateral reinforcement configuration in R/C columns; Group VIIE.....	188
A.78	Influence of lateral reinforcement configuration in R/C columns; Group VIIF.....	189
A.79	Influence of lateral reinforcement configuration in R/C columns; Group VIIG.....	189
A.80	Influence of lateral reinforcement configuration in	

	R/C columns; Group VIIIH.....	190
A.81	Influence of lateral reinforcement configuration in R/C columns; Group VIIIJ.....	190
A.82	Influence of lateral reinforcement ratio " $\rho_s$ " in R/C columns; Group IXA.....	191
A.83	Influence of lateral reinforcement ratio " $\rho_s$ " in R/C columns; Group IXB.....	191
A.84	Influence of lateral reinforcement ratio " $\rho_s$ " in R/C columns; Group IXC.....	192
A.85	Influence of lateral reinforcement ratio " $\rho_s$ " in R/C columns; Group IXD.....	192
A.86	Influence of lateral reinforcement ratio " $\rho_s$ " in R/C columns; Group IXE.....	193
A.87	Influence of lateral reinforcement ratio " $\rho_s$ " in R/C columns; Group IXF.....	193
A.88	Influence of lateral reinforcement ratio " $\rho_s$ " in R/C columns; Group IXG.....	194
A.89	Influence of lateral reinforcement ratio " $\rho_s$ " in R/C columns; Group IXH.....	194
A.90	Influence of lateral reinforcement ratio " $\rho_s$ " in R/C columns; Group IXJ.....	195
A.91	Influence of lateral reinforcement spacing in R/C columns; Group XA.....	195
A.92	Influence of lateral reinforcement spacing in R/C columns; Group XB.....	196
A.93	Influence of lateral reinforcement spacing in R/C columns; Group XC.....	196
A.94	Influence of lateral reinforcement spacing in R/C columns; Group XD.....	197
A.95	Influence of lateral reinforcement spacing in R/C columns;	

Group XE.....	197
A.96 Influence of lateral reinforcement spacing in R/C columns; Group XF.....	198
A.97 Influence of lateral reinforcement spacing in R/C columns; Group XG.....	198
A.98 Influence of lateral reinforcement spacing in R/C columns; Group XH.....	199
A.99 Influence of lateral reinforcement spacing in R/C columns; Group XJ.....	199
A.100 Influence of concrete strength in R/C columns; Group XIA.....	200
A.101 Influence of concrete strength in R/C columns; Group XIB.....	200
A.102 Influence of concrete strength in R/C columns; Group XIC.....	201
A.103 Influence of concrete strength in R/C columns; Group XID.....	201
A.104 Influence of concrete strength in R/C columns; Group XIE.....	202
A.105 Influence of concrete strength in R/C columns; Group XIF.....	202
A.106 Influence of concrete strength in R/C columns; Group XIG.....	203
A.107 Influence of concrete strength in R/C columns; Group XIH.....	203
A.108 Influence of concrete strength in R/C columns; Group XIJ.....	204
A.109 Influence of concrete strength in R/C columns; Group XIK.....	204
A.110 Influence of concrete strength in R/C columns; Group XIL.....	205
A.111 Influence of concrete strength in R/C columns; Group XIM.....	205
A.112 Influence of concrete strength in R/C columns; Group XIN.....	206
A.113 Influence of ratio of longitudinal bars ( $\rho_t=A_{st}/A_c$ ) in R/C columns; Group XIIA.....	206
A.114 Influence of ratio of longitudinal bars ( $\rho_t=A_{st}/A_c$ ) in R/C columns; Group XIIB.....	207
A.115 Influence of ratio of longitudinal bars ( $\rho_t=A_{st}/A_c$ ) in R/C columns; Group XIIC.....	207
A.116 Influence of ratio of longitudinal bars ( $\rho_t=A_{st}/A_c$ ) in R/C columns; Group XIID.....	208

A.117	Influence of ratio of longitudinal bars ( $\rho_t=A_{st}/A_c$ ) in R/C columns; Group XIIE.....	208
A.118	Influence of ratio of longitudinal bars ( $\rho_t=A_{st}/A_c$ ) in R/C columns; Group XIIF.....	209
A.119	Influence of ratio of longitudinal bars ( $\rho_t=A_{st}/A_c$ ) in R/C columns; Group XIIG.....	209
A.120	Influence of ratio of longitudinal bars ( $\rho_t=A_{st}/A_c$ ) in R/C columns; Group XIIH.....	210
A.121	Influence of ratio of longitudinal bars ( $\rho_t=A_{st}/A_c$ ) in R/C columns; Group XIJ.....	210
A.122	Influence of ratio of longitudinal bars ( $\rho_t=A_{st}/A_c$ ) in R/C columns; Group XIK.....	211
A.123	Influence of ratio of longitudinal bars ( $\rho_t=A_{st}/A_c$ ) in R/C columns; Group XII.....	211
A.124	Influence of confined concrete models on moment-curvature diagrams of R/C columns; Group XIII A.....	212
A.125	Influence of confined concrete models on moment-curvature diagrams of R/C columns; Group XIII B.....	212
A.126	Influence of confined concrete models on moment-curvature diagrams of R/C columns; Group XIII C.....	213
A.127	Influence of confined concrete models on moment-curvature diagrams of R/C columns; Group XIII D.....	213
A.128	Influence of confined concrete models on moment-curvature diagrams of R/C columns; Group XIII E.....	214
A.129	Influence of confined concrete models on moment-curvature diagrams of R/C columns; Group XIII F.....	214
A.130	Influence of confined concrete models on moment-curvature diagrams of R/C columns; Group XIII G.....	215
A.131	Influence of confined concrete models on moment-curvature diagrams of R/C columns; Group XIII H.....	215

A.132	Influence of confined concrete models on moment-curvature diagrams of R/C columns; Group XIIIJ.....	216
A.133	Influence of confined concrete models on moment-curvature diagrams of R/C columns; Group XIIIK.....	216
A.134	Influence of confined concrete models on moment-curvature diagrams of R/C columns; Group XIII L.....	217
A.135	Influence of axial load level ( $'N/f_{ck}A_c'$ ratio) in R/C columns; Group XIVA.....	217
A.136	Influence of axial load level ( $'N/f_{ck}A_c'$ ratio) in R/C columns; Group XIVB.....	218
A.137	Influence of axial load level ( $'N/f_{ck}A_c'$ ratio) in R/C columns; Group XIVC.....	218
A.138	Influence of axial load level ( $'N/f_{ck}A_c'$ ratio) in R/C columns; Group XIVD.....	219
A.139	Influence of axial load level ( $'N/f_{ck}A_c'$ ratio) in R/C columns; Group XIVE.....	219
A.140	Influence of axial load level ( $'N/f_{ck}A_c'$ ratio) in R/C columns; Group XIVF.....	220
A.141	Influence of axial load level ( $'N/f_{ck}A_c'$ ratio) in R/C columns; Group XIVG.....	220
A.142	Influence of axial load level ( $'N/f_{ck}A_c'$ ratio) in R/C columns; Group XIVH.....	221
A.143	Influence of axial load level ( $'N/f_{ck}A_c'$ ratio) in R/C columns; Group XIVJ.....	221
A.144	Influence of axial load level ( $'N/f_{ck}A_c'$ ratio) in R/C columns; Group XIVK.....	222
A.145	Influence of ratio of the gross area to the confined area ( $A_c/A_{ck}$ ) in R/C columns; Group XVA.....	222
A.146	Influence of ratio of the gross area to the confined area ( $A_c/A_{ck}$ ) in R/C columns; Group XVB.....	223



A.147	Influence of ratio of the gross area to the confined area ( $A_c/A_{ck}$ ) in R/C columns; Group XVC.....	223
A.148	Influence of ratio of the gross area to the confined area ( $A_c/A_{ck}$ ) in R/C columns; Group XVD.....	224
A.149	Influence of ratio of the gross area to the confined area ( $A_c/A_{ck}$ ) in R/C columns; Group XVE.....	224
A.150	Influence of ratio of the gross area to the confined area ( $A_c/A_{ck}$ ) in R/C columns; Group XVF.....	225
A.151	Influence of ratio of the gross area to the confined area ( $A_c/A_{ck}$ ) in R/C columns; Group XVG.....	225
A.152	Influence of ratio of the gross area to the confined area ( $A_c/A_{ck}$ ) in R/C columns; Group XVH.....	226
A.153	Influence of ratio of the gross area to the confined area ( $A_c/A_{ck}$ ) in R/C columns; Group XVJ.....	226
A.154	Influence of ratio of the gross area to the confined area ( $A_c/A_{ck}$ ) in R/C columns; Group XVK.....	227
A.155	Influence of ratio of the gross area to the confined area ( $A_c/A_{ck}$ ) in R/C columns; Group XVL.....	227
A.156	Influence of ratio of the gross area to the confined area ( $A_c/A_{ck}$ ) in R/C columns; Group XVM.....	228
B.1	Interaction diagrams; S220-C20 combination, 8 longitudinal bars.....	229
B.2	Interaction diagrams; S220-C20 combination, 12 longitudinal bars.....	230
B.3	Interaction diagrams; S420-C20 combination, 8 longitudinal bars.....	230
B.4	Interaction diagrams; S420-C20 combination, 12 longitudinal bars.....	231
B.5	Interaction diagrams; S420-C20 combination, 16 longitudinal bars.....	231
B.6	Interaction diagrams; S420-C30 combination, 8 longitudinal bars.....	232
B.7	Interaction diagrams; S420-C30 combination, 12 longitudinal bars.....	232
B.8	Interaction diagrams; S420-C40 combination, 8 longitudinal bars.....	233
B.9	Interaction diagrams; S420-C40 combination, 12 longitudinal bars.....	233
B.10	Interaction diagrams; S420-C40 combination, 16 longitudinal bars.....	234



## LIST OF SYMBOLS

$A_c$	Gross cross-sectional area
$A_{ck}$	Confined area
$A_s$	Area of tension reinforcement
$A_s'$	Area of compression reinforcement
$A_{st}$	Total area of longitudinal reinforcement (columns)
$b$	Width of the cross-section
$b_f$	Flange width in T-beams
$b_w$	Width of web in beams
$c$	Neutral axis depth
$d$	Effective depth in beams
$d'$	Distance from the extreme compression fiber to the centroid of compression reinforcement
$d''$	Distance between top and bottom steel layers
$dA_{cci}$	Area of a fiber in the confined region
$dA_{cti}$	Area of a fiber in the tension side
$dA_{cui}$	Area of a fiber in the unconfined region
$E$	Modulus of elasticity
$f_c$	Unconfined concrete strength in compression
$f_{cc}$	Compressive strength of confined concrete
$f_{ck}$	Characteristic concrete strength in compression
$f_{ct}$	Ultimate strength of concrete in tension
$f_{su}$	Ultimate strength of longitudinal steel
$f_y$	Yield strength of longitudinal steel

$f_{yk}$	Characteristic yield strength of longitudinal steel
$f_{yw}$	Yield strength of transverse steel
$f_{ywk}$	Characteristic yield strength of transverse steel
$h$	Height of the cross-section
$h_f$	Flange height in T-beams
$k_3$	Factor by which the concrete cylinder strength has to be multiplied
$M$	Moment
$N$	Axial load
$N_0$	Axial load capacity of the section
$q$	Lateral pressure
$s$	Tie spacing
$\epsilon_c$	Concrete strain at $\sigma_c$
$\epsilon_{cci}$	Compressive strain at the middle of any fiber
$\epsilon_{cj}$	Compressive strain at the extreme concrete fiber
$\epsilon_{cti}$	Tensile strain at the middle of any fiber
$\epsilon_{ctu}$	Ultimate tensile strain in concrete
$\epsilon_{c0}$	Concrete strain at $f_c$ (unconfined)
$\epsilon_{cc0}$	Concrete strain at $f_{cc}$ (confined)
$\epsilon_s$	Strain in steel
$\epsilon_{si}$	Longitudinal steel strain
$\epsilon_{sp}$	Strain which corresponds to strain hardening
$\epsilon_{su}$	Ultimate strain of steel
$\epsilon_{sy}$	Yield strain of steel
$\rho$	Ratio of tension reinforcement in beams
$\rho'$	Ratio of compression reinforcement in beams
$\rho_s$	Volumetric lateral steel ratio in columns
$\rho_t$	Ratio of longitudinal bars (columns)
$\rho_w$	Web reinforcement ratio in beams
$\sigma_c$	Compressive stress in concrete

- $\sigma_{cci}$  Compressive stress at the middle of any fiber in the confined region
- $\sigma_{cui}$  Compressive stress at the middle of any fiber in the unconfined region
- $\sigma_s$  Stress in longitudinal reinforcement
- $\sigma_{si}$  Stress in steel corresponding to the strain  $\epsilon_{si}$
- $\sigma_2$  Lateral confining pressure



UNIVERSITY OF  
BORNEO TRUST  
BORNEO TRUST

## **CHAPTER I**

### **INTRODUCTION**

#### **1.1 General**

Concrete is the most widely used material in constructions. After being popular in the 19<sup>th</sup> century, it has been significantly improved. Since the middle of the 19<sup>th</sup> century, innumerable studies have been made on concrete, reinforced concrete and reinforced concrete structures. In the light of these studies, today we know quite a lot about reinforced concrete theory. Some people believe and claim that they know everything about these technologies. But bearing in mind the catastrophic failures which arise after the earthquakes, in Turkey and other countries, it becomes obvious that more studies are needed to learn about the behaviour of reinforced concrete members and structures.

While improving engineering theories, experimental studies are very important. To perform these experiments, first a laboratory is needed, then mechanical equipment, technicians, etc. After the exhausting work continuing several weeks, the researchers obtain a limited number of results and get some conclusions with the help of these results. In the last few years, following the incredible advances in the computer technology, the researchers found an alternative method. Instead of realizing these expensive experiments, they prefer to simulate them in computerizing environments. However it should not forgotten that the computer simulation for

reinforced concrete is only possible if some experimental data is available which enables the formulation of nonlinear behaviour. Also related softwares have to be checked by tests.

Simulating computer experiments are used in different engineering areas such as automotive, construction, electronics, aeronautical, etc. This technique recovers the researchers from struggling with the performance of equipment, the required standards of materials, the technical elements, etc. More important than these, time saving is maintained when this method is carried out. For example, a researcher who intends to prepare a simple reinforced concrete beam and subject it to a simple flexure test, in order to get its moment-curvature diagram and examine the behaviour, he needs at least 4-5 weeks. He has to wait at least 28 days only for concrete to gain its characteristic strength. Instead, the researcher, after preparing a computer program, can simulate the same experiment in a few minutes.

In practice, the first thing that is considered is the ultimate strength capacity. In the analysis of sections or members or the structure, the design regulations are very important. Indeed these are the basic knowledge that should be learned. However another important subject is the behaviour. To understand, to investigate, to know how the reinforced concrete sections, members or structures behave, is as important as, maybe more important than the capacity design. Every good engineer should know that there is more to design than proportioning a structural section. To choose the appropriate sectional dimensions, to reinforce a concrete structure correctly, to know about detailing, to feel the structural psychology, the engineer needs a good background in behaviour. A good engineer (both the design and constructing engineers) is the one who, like a psychologist who tries to understand his patient, realizes in his mind the correct behaviour of the structure.

The moment-curvature relationship of reinforced concrete cross-sections is very crucial to understand behaviour of reinforced concrete structural elements. For

this purpose innumerable experiments were and are made all over the world. Before the computer technology and knowledge on the behaviour of reinforced concrete was limited, experiments were the only means to obtain moment-curvature relationship. Today, researchers using the previous knowledge obtained and inputting them into computers, may simulate so many experiments during a very limited time and improve reinforced concrete theory much faster.

## **1.2 Object and Scope**

This thesis is an attempt to study the influence of different variables on the behaviour of R/C sections analytically. For this purpose reinforced concrete sections with various characteristics were tested by simulation method. These sections can be grouped mainly into two categories: Reinforced concrete beams and columns. Indeed the main difference between these two groups is that while beams are subjected to only flexure, columns are subjected to combined flexure and axial load. In order to test the sections by a simulation method, a computer program was written.

The first problem that needs to be considered in writing a computer program which serves to simulate the behaviour of a section realistically, is the choice of appropriate mathematical models for steel and concrete. Without these models, no matter how good the computer software is, it is not possible to get reasonable results.

It is stated in the previous paragraphs that in order to investigate the flexural behaviour of reinforced concrete sections, one should have moment-curvature diagram for this section. To draw the moment-curvature diagrams, the most important thing is the stress-strain diagram of concrete. The choice of the model plays a crucial role on the reliability of the study. For this purpose, while forming the computer program, most popular mathematical models for the stress-strain diagrams of confined concrete were used. These models were proposed by Park, Priestley & Gill (Modified

Kent & Park Model); Sheikh & Uzumeri; and Saatcioglu [1] [2] [3] [4] [5] [6]. The common characteristic of these models is that, they all keep in view the effect of confinement. Although consideration of this effect differs from model to model, the analytical moment-curvature curves obtained using any of these models yield reasonably satisfactory results when compared with experimental ones.

In this study the influence of the following variables on the flexural behaviour (moment-curvature) of reinforced concrete members were investigated.

- Influence of compression reinforcement in reinforced concrete beams
- Influence of concrete strength in reinforced concrete beams
- Influence of confinement in reinforced concrete beams
- Influence of the steel model in reinforced concrete beams
- Influence of tension reinforcement ratio in reinforced concrete beams
- Influence of confined concrete models on moment-curvature diagrams of reinforced concrete beams
- Influence of flange width in T-beams
- Influence of lateral reinforcement configuration in reinforced concrete columns
- Influence of lateral reinforcement ratio " $\rho_s$ " in reinforced concrete columns
- Influence of lateral reinforcement spacing in reinforced concrete columns
- Influence of concrete strength in reinforced concrete columns
- Influence of ratio of longitudinal bars ( $\rho_r = A_{sr}/A_c$ ) in reinforced concrete columns
- Influence of confined concrete models on moment-curvature diagrams of reinforced concrete columns
- Influence of axial load level (' $N/f_{ck}A_c$ ' ratio) in reinforced concrete columns

- Influence of ratio of the gross area to the confined area ( $A_g/A_{ck}$ ) in reinforced concrete columns

The range of variables were selected to remain within the practical ranges. Only rectangular and flanged sections were considered. Triangular shapes were left out of the scope of this study.





## CHAPTER II

### LITERATURE SURVEY

There have been many studies to investigate the behaviour of reinforced concrete beams and columns by using moment-curvature relationships. Especially after the stress-strain models which realize the influence of confinement, many researchers studied analytically the moment-curvature diagrams and compared them with the experimental results. First study in this area was presented by Corley and Sozen in the 1960's.

One of the earliest studies in this area was done by Park and Sampson [8] in 1972. They discussed the ductility required for eccentrically loaded reinforced concrete column sections in seismic design by using theoretical moment-curvature relationships. For concrete stress-strain relationships, both confined and unconfined, they used Kent and Park model. Their aim was to develop a method for the determination of the amount of special transverse steel required for ductility. They concluded that the required content of transverse steel for ductility depended on the level of axial load, the longitudinal steel content and the material strengths. They pointed out that the code recommendations of those days for transverse steel could be less than the required values when the member was subjected to high axial loads and had low ratios of longitudinal reinforcement. However in some other cases the requirements could have been relaxed. Park and Sampson also concluded that the effect of strain hardening of the longitudinal reinforcement of columns gave a reserve

moment capacity at large curvatures. They also pointed out that the buckling of the compression steel was possible and this pointed to the need for closely spaced transverse steel.

Sheikh [9] in 1982 published a comparative study on confinement models. In this study various analytical models available in the literature for the confined concrete by rectilinear ties was investigated by comparing theoretical and experimental moment-curvature relationships of various reinforced concrete sections. The models were applied to the specimens tested by the author as well as by other investigators to check the validity of models. Loadings on these specimens included were uniaxial and combined axial and bending, monotonic as well as cyclic. In the case of cyclic loading, only the envelope curves were determined using the analytical models. Experimental results were compared with results predicted by various models. It was concluded that in addition to the commonly acknowledged variables such as the amount of lateral reinforcement and steel strength, two other variables played important roles in determining the behaviour of the confined concrete. These were the distribution of the longitudinal steel around the core perimeter and the resulting tie configuration, and the spacing of ties. From the limited work reported in this study, the author concluded that the envelope moment-curvature curves for reinforced concrete section under cyclic bending could be determined with reasonable accuracy by using Sheikh and Uzumeri's stress-strain relationship for confined concrete.

In 1983, Park, Fafitis and Shah wrote discussions on Sheikh's paper [10]. They discussed Sheikh's comparative study on confinement models. All discussors defended their own models and supplemented the comparative studies.

Fafitis and Shah [11] (1985) proposed a stress-strain relationship for unconfined and confined concrete. Their aim was to get an expression to predict the stress-strain curve of concrete. Using this expression, the predicted behaviour of confined columns was compared with the available experimental data. The proposed

model satisfactorily predicted ultimate loads, moments, curvatures and rotations of round and square columns subjected to cyclic loading. In conclusion they found that; (a) under constant axial load, the moment resistance of the column might exhibit a peak followed by a drop; (b) the extent in drop in moment depended on compressive strength of concrete, axial load level, shape of the section and confinement; (c) the square sections examined exhibited higher moment capacity than those of the circular section, especially at large deformations; (d) the contribution of the cover concrete became negligible beyond axial strains of 0.01; and (e) the contribution of confined concrete to moment was substantial.

Moehle and Cavanagh [12] (1985) realized an experimental study which investigated the confinement effectiveness of cross-ties in reinforced concrete columns subjected to monotonically increasing axial compression. Ten columns were constructed, of which eight were reinforced. The main variable was the type of the transverse reinforcement. Comparison was made between strength and ductility obtained by the different types of transverse steel, and analytical moment-curvature studies were used to estimate the influence of different confined concrete models on flexural behaviour of columns and structural walls. It was observed that cross-ties having 180° hooks were as effective in confining concrete as intermediate hoops. Cross-ties having 135° and 90° hooks were nearly as effective. It was concluded that both types of crossties were acceptable details for confinement of concrete where large inelastic strains would be applied monotonically.

Sheikh and Yeh [13] in 1986 published a paper, and with this paper they modified Sheikh and Uzumeri Model which was proposed in 1982 by including the effects of strain gradient caused by flexure. The proposed model along with some other models available in the literature was used to predict the behaviour of several specimens tested by various researchers including those recently tested at the University of Houston. The behaviour of reinforced concrete sections confined by rectilinear ties and subjected to axial and flexural loads had been studied by comparing

experimental and theoretical moment-curvature relationships. The following conclusions were drawn from this study.

- There was no conclusive evidence in the available test data that the strain gradient in a section enhanced the strength of concrete over that measured under concentric compression. The ductility, however, was improved and the increase in strain at peak stress appeared to be a function of the ratio of the section depth to the depth of neutral axis.
- The proposed stress-strain curve predicted the behaviour of confined concrete sections under axial and flexural loads in a satisfactory manner.
- The ACI confinement requirements have produced columns that showed inconsistent results under axial and flexural loads. Depending on the criterion against which the columns were tested, the ACI requirements might be either too conservative for columns with well distributed steel or unsafe for columns with only four corner bars fully supported by a tie. Based on the results from this and previous studies, it was suggested that in columns with high axial loads a minimum of eight fully supported longitudinal bars should be used when confinement of concrete was required. The maximum tie spacing should have been related to the size of the confined core.

Sakai and Sheikh [14] [15] (1989), based on an extensive review of the literature, presented a state of the art report on concrete confinement again by studying experimental and theoretical moment-curvature relationships. It was aimed to define the status of the problem and the future direction of work including revision of the design codes' provisions. The objectives of the research can be divided fundamentally into four categories: 1) Characteristics of materials; 2) characteristics of cross section; 3) behaviour of reinforced concrete columns; and 4) other mechanical characteristics and design constraints, such as structural detailing.

An important point declared in this paper was that the displacement ductility in columns was closely related to the curvature ductility of the column sections. They showed by a figure the relationships between curvature ductility factors and displacement ductility factors in which the effect due to additional deformations such as slippage of longitudinal bars and shear cracking was neglected.

Sakai and Sheikh arranged the factors considered in the previous studies related to the stress-strain relationships and therefore the moment-curvature relationships of reinforced concrete elements. These were: 1) Type and strength of concrete; 2) amount and distributions of longitudinal reinforcement; 3) amount, spacing and configurations of transverse reinforcement; 4) size and shape of confined concrete; 5) ratio of confined area to gross area; 6) strain rate; 7) strain gradient; 8) supplementary cross-ties; 9) cyclic loading; 10) characteristics of lateral steel; and 11) level of axial load.

Several models for the stress-strain relationship of confined concrete were studied in this paper. A comparative study showed that most of these analytical models were effective only to interpret their own test results or data used. According to the writers, the two models, Sheikh and Uzumeri [2] and modified Kent and Park [4], which were based on the test results using large-size specimens with practical detailing of transverse and longitudinal reinforcements, had appeared most promising. The results of this study were summarized as follows:

- The necessity of a reexamination of the ACI code provisions for confinement was obvious. Because the performance in terms of strength and ductility, expected of a column during a severe earthquake, was not well defined in the literature and lacking this information, it was difficult to propose a specific design for concrete confinement. Especially the following five areas should have been investigated: 1) distribution of longitudinal and lateral steel; 2) amount and spacing of transverse

reinforcement; 3) level of axial load; 4) cross-ties with 90° hooks; and 5) zone of inelastic deformations.

- Experimental evidence suggested that columns with single hoops and 90° hoops might not provide sufficient ductility, particularly when they were subjected to high axial loads and cyclic flexure.
- Further research was needed to study several variables such as steel configuration, amount of tie steel, spacing of ties, and level of axial loads also for high strength and lightweight concretes.

Sheikh and Yeh [16] (1990) made an experimental research and tested fifteen 305 mm square and 2.74 m long reinforced concrete columns under axial load and flexure. The main purpose of this research was to investigate the behaviour of column sections confined by rectilinear ties. The effects of different variables were studied by comparing moment-curvature relationships of the sections of those columns in which only one major variable had differed significantly. These variables included distribution of longitudinal and lateral steel, including unsupported longitudinal bars and supplementary cross-ties, amount of lateral steel, spacing of ties, and level of axial load.

Effect of different variables were studied on the flexural strength of sections, extreme fiber concrete compressive strains, and curvature ductilities. The conclusions drawn were as follows:

- As in the case of concentric compression, distribution of longitudinal and lateral steel played an important role on the behaviour of columns under axial load and flexure. A larger number of laterally supported longitudinal bars resulted in higher flexural strength and ductility. Reduced spacing of ties for the same amount of

lateral steel would have also resulted in higher strength and ductility if the anchorage of lateral steel could have been assured.

- Unsupported longitudinal bars, although effective in confining the concrete at small deformations, tended to buckle and pushed the ties outward at large deformations, resulting in a brittle behaviour caused by a loss of confinement. A similar phenomenon had been also observed for bars that were supported by 90° hooks, which had opened at large deformations.
- Higher axial loads reduced strength and ductility of confined concrete sections very significantly. Several columns in which the amount of lateral reinforcement was about 50% of that required for seismic design did not even reach the theoretical moment capacity for unconfined sections, although the tie steel provided was more than that required for nonseismic design. It appeared that the compressive strength of concrete in flexure reduced with an increase in the axial load.
- An increase in the amount of lateral steel resulted in a significant improvement in flexural behaviour of a section. Design of confining steel according to the ACI code have provided reasonably ductile behaviour of columns when axial load was less than  $0.6 f_c A_g$  and the steel was appropriately detailed. The results from this study pointed the need to link the required amount of steel and the use of unsupported bars and 90° hooks to the level of axial load and the expected performance of a column.

Samra [17] (1990) published a paper, and with this paper he described in detail the weakness of the procedure in the ACI Building Code used for detailing columns for ductility. The paper presented an approach for calculating the amount of transverse steel required in confined columns at various load levels by using idealized stress-strain diagrams for confined concrete and steel and moment-curvature curves.



The amount of transverse steel required in columns could have been determined from moment-curvature curves, for a curvature ductility factor of 12 at a moment capacity of not less than 75% of the maximum moment capacity. In the steel diagram, strain hardening was assumed to commence at four times the yield strain. This assumption was partly judgemental, since the point at which strain hardening has begun was not stipulated in specifications for steel and therefore including it, was difficult. Normally, it was unwise to rely on any increase in strength due to strain hardening, because this could have been associated with very large deformations of the member. Nevertheless, including its effect was realistic.

Sheikh and Yeh [18] (1992) reported a research on experimental work where sixteen 305 mm square and 2.74 m long columns were tested under flexure to large inelastic deformations while simultaneously subjected to axial load that remained constant throughout the test. The main variables included the distribution of longitudinal and lateral steel, amount of lateral steel, tie spacing, and axial load level. In this paper, the predictions for the behaviour of these specimens from the available stress-strain models for confined concrete were compared with the test results. After a critical examination of the analytical models and the variables that affected the behaviour of the specimens, a model originally proposed for concentric compression was modified to include the effects of strain gradient and the level of axial load.

A computer program was developed to carry out calculations for theoretical moment-curvature relationships of the test specimens using the concrete stress-strain curves from the four analytical models. These were modified Kent and Park, Sheikh and Uzumeri, Fafitis and Shah, and Mander et al. models. The required input data included cross-sectional dimensions of specimens, position, and amount of longitudinal steel including the location of laterally supported longitudinally bars, properties of longitudinal steel, stress in tie steel at maximum moment, unconfined concrete strength, and applied axial load. The section was divided into 40 small slices, each one containing two kinds of elements, core and cover.



After several available stress-strain models for confined concrete were briefly reviewed and used to predict the moment-curvature behaviour of the specimens, the authors claimed that most of the models had resulted in inaccurate predictions, because they did not consider all the variables investigated in the study.

The model proposed by Sheikh and Uzumeri (1982), originally developed for concentric compression, had been modified to reflect the effects of strain gradient and the level of axial load. After the analytical results for both the original model and from the modified version were presented in the paper, there was no convincing experimental evidence that strain gradient enhanced strength of concrete. The effect of strain gradient on the fraction of the core area which was effectively confined was also not significant. The major changes in the model reflected enhanced ductility due to strain gradient and the dependence of the concrete strength on the level of axial load. Above the balanced load level, strength of concrete reduced with an increase in axial load. Although the original model had predicted the moment-curvature behaviour of the confined concrete sections under axial load and flexure quite well, the modified model resulted in more accurate representations of the experimental results.

Watson, Zahn and Park [19] (1994), using previously derived stress-strain relationships for compressed concrete confined by various quantities and arrangements of transverse reinforcement in cyclic moment-curvature analyses of a range of reinforced concrete columns, derived some design charts. The column section was considered to have reached its available ultimate curvature when either the moment resisted had reduced to 80% of the ideal flexural strength, or the strain energy absorbed by the transverse reinforcement had reached its strain energy absorption capacity, or when the longitudinal steel had reached its limiting tensile or compressive strain, whichever occurred first. Refined design equations to determine the quantities of transverse reinforcement required for specified ductility levels were derived on the basis of design charts. The authors concluded that:

- Design charts for the available curvature ductility factor could be derived using theoretical cyclic moment-curvature analysis incorporating cyclic stress-strain relationships for confined and unconfined concrete and for longitudinal reinforcing steel. The cyclic stress-strain curves for confined concrete have taken into account the quantity and arrangement of the transverse reinforcement and the accumulation of strain energy in the transverse reinforcement.
- The quantity of transverse reinforcement required for confinement to achieve a curvature ductility factor in the order of 15-20 was less than that calculated using the code equations for axial compression load levels  $N/f_{ck}A_c < 0.4$ , but may be greater for  $N/f_{ck}A_c > 0.4$ .
- The quantity of transverse reinforcement required for confinement to meet any particular curvature ductility factor demand increased with increasing axial load level, increasing concrete strength, decreasing longitudinal reinforcement ratio, and increasing relative cover concrete thickness. Also more transverse reinforcement was required for the confinement of square and rectangular columns than for circular columns.
- The refined design equations gave only the transverse reinforcement required for concrete confinement. The transverse reinforcement provided must also be checked to ensure that it is sufficient to prevent premature buckling of the longitudinal compression bars and to prevent shear failure. For low axial load levels, the transverse reinforcement required for lateral restraint of longitudinal bars and for shear governed the design.
- There was a significant increase in the flexural strength of columns due to confinement of the concrete by transverse reinforcement for axial compression load levels  $N/f_{ck}A_c$  greater than about 0.3. This enhancement in flexural strength could have been taken as an advantage in the design of the longitudinal

reinforcement and should have been included in the calculation of the design shear forces corresponding to the development of plastic hinges in columns.

Saatcioglu, Salamat and Razvi [20] (1995) studied the behaviour of confined concrete columns under strain gradient. Twelve columns were tested under two different levels of end eccentricity. The test parameters included the arrangement, spacing, and volumetric ratio of confinement reinforcement. A confined concrete model developed on the basis of the column tests under concentric loading, was used to compute analytical moment-curvature relationships of the critical column section. The analytical relationships were compared with those recorded experimentally, for columns with different eccentricity of loading and parameters of confinement. The following conclusions were drawn from the combined experimental and analytical research reported in this paper [20]:

- Square columns with well distributed longitudinal reinforcements, laterally supported by closely spaced transverse reinforcement, resulted in improved strength and deformability under eccentric loading. Square columns with 12 bars uniformly distributed along the perimeter of the section, resulting in an approximate spacing of  $h/4$  between the longitudinal bars, laterally supported by corners of rectilinear hoops with a volumetric ratio of 2.7% and a spacing of approximately  $h/4$  showed extremely ductile responses. Columns with 8 longitudinal reinforcements, spaced at approximately  $h/3$ , and similar volumetric ratio and spacing of hoop reinforcements developed progressively increasing strength degradation immediately starting beyond the peak load. When the spacing of laterally supported longitudinal reinforcements approached  $h$  (as in the case of columns with perimeter ties only), the 20% strength decay was observed at approximately a 2% drift ratio.
- Columns with reduced volumetric ratio of transverse reinforcement, and a tie spacing of approximately  $h/2$ , showed 2-2.5% drift ratios at a 20% strength decay.

These columns showed little improvement in column deformability, with improvement in the reinforcement arrangement. There appeared to be a threshold value for the volumetric ratio and spacing of transverse confinement reinforcement below which the improvement in the longitudinal reinforcement arrangement was not effective.

- The flexural analysis of confined columns can be conducted fairly accurately by the confined concrete model proposed by Saatcioglu and Razvi (1992), and by considering the strain hardening of steel in reinforcement. Moment-curvature relationships obtained with the use of this confinement model showed good correlations with test data under different levels of strain gradient. The analytical relationships also showed good agreement with the envelopes of moment-curvature hysteretic relationships obtained experimentally under different levels of constant axial compression. The model had been extensively verified for columns subjected to concentric compression. This indicated that a concrete model based on concentric column tests could be used for columns under strain gradient, provided the model incorporated the relevant parameters of confinement.

## CHAPTER III

### METHOD OF ANALYSIS

#### 3.1 General

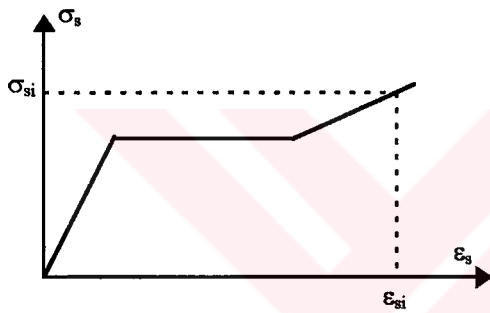
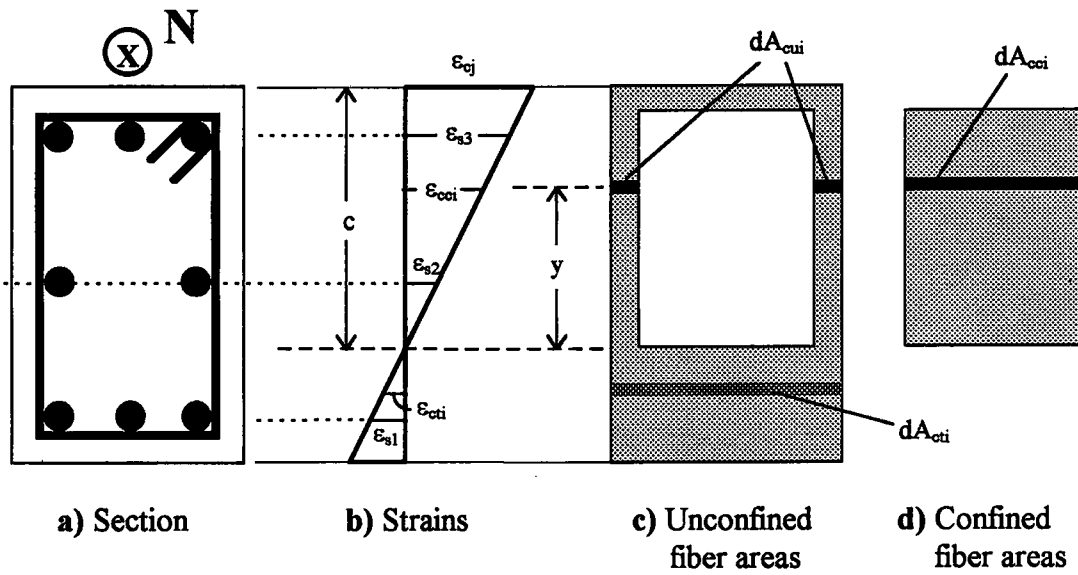
To investigate the behaviour of various reinforced concrete sections, a Fortran program which can generate moment-curvature diagrams was written. In this program the cross-section was divided into fibers. The program constructs the data file by increasing the extreme fiber strain of section gradually.

To determine the bending moments and curvatures of a section, it has been found convenient to divide the section into a number of discrete fibers each parallel to the neutral axis. Each fiber is then divided into confined and unconfined areas. The stresses in the concrete and steel in each fiber are found from the average strain in the fiber and the assumed stress-strain relations. The theoretical moment-curvature relation for a given axial load level can be determined by increasing the concrete strain in the extreme compression fiber. Iteration was started with a low extreme concrete fiber strain. This is a rather small strain value for concrete in compression. Referring to Figure 3.1, the analysis procedure involves following steps:

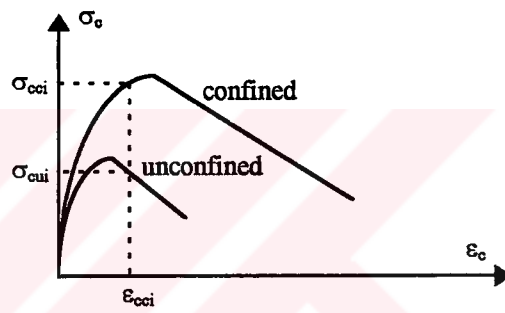
- 1) Assign an initial value for the compressive strain at the extreme concrete fiber. ( $\epsilon_{cj}$  in Figure 3.1.b)
- 2) Assume a neutral axis depth. ( $c$  in Figure 3.1.b)
- 3) Calculate strains at the middle of each fiber. ( $\epsilon_{cci}$ ,  $\epsilon_{cti}$ , etc.)

- 4) Use the chosen stress-strain models for confined and unconfined concrete to determine stress values at each fiber. (Figure 3.1.f)
- 5) Determine the longitudinal steel strains from similar triangles of the strain diagram. ( $\epsilon_{si}$ )
- 6) With the steel strain at each level, steel stresses are determined from stress-strain diagram of steel, Figure 3.1.e. Forces in steel at each level are obtained by multiplying these stresses by the respective steel areas.
- 7) On the compressive side, with the concrete strains at each fiber, concrete stresses ( $\sigma_{cci}$  &  $\sigma_{cui}$  in confined and unconfined fibers) are determined by entering the stress-strain curves of confined and unconfined concrete, Figure 3.1.f. Finite forces in confined and unconfined fibers are obtained by multiplying these stresses by the respective areas  $dA_{cci}$  and  $dA_{cui}$ :  $F_{cci} = \sigma_{cci} * dA_{cci}$  and  $F_{cui} = \sigma_{cui} * dA_{cui}$ .
- 8) On the tension side, tensile stress at each fiber is obtained by entering the stress-strain curve of concrete in tension, Figure 3.1.g. Finite forces in concrete on the tension side is obtained by multiplying these stresses by the filament area  $dA_{cti}$ . Areas corresponding to tensile strains exceeding  $\epsilon_{ctu}$  (Figure 3.1.g) are disregarded.
- 9) Compute the sum of the internal forces and compare this with the external axial force. (If the difference is less than or equal to 0.1%, results are acceptable and moment and curvature values are computed. Otherwise, neutral axis depth is changed returning to step 3. The neutral axis is changed until the equilibrium is satisfied. If convergence does not occur in 30 iterations, the program moves to the next point.)
- 10) Set new concrete strain and go back to step 2.

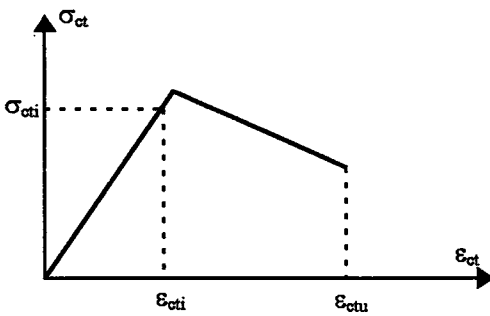
To adjust the neutral axis depth, a different technique was used in the program. The first assumed neutral axis depth is say 4 or 8 times (maximum) the section height; the second one is just a little greater than zero (minimum). Third one is the average of the minimum and maximum assumed values. The fourth value to be assumed is determined by comparing the summation of internal and external forces obtained from the previous step. If the sum of internal forces is greater than that of



e) Steel stress-strain diagram



f) Concrete stress-strain diagrams in compression



g) Concrete stress-strain diagram in tension

Figure 3.1: Theoretical moment-curvature determination

the external forces, a smaller value has to be assigned for the neutral axis depth. The fourth value is taken as the average of the smaller two of the previous values. If the sum of the external forces are greater than that of the internal forces, then the average of the larger two of the previous values. These steps are repeated until the sum of internal and external forces are approximately the same.

After the neutral axis depth corresponding to an extreme fiber strain is found, total moment is calculated by summing up the fiber moments and the moments of longitudinal reinforcements about the centroid of the section. Fiber moment are calculated by multiplying the fiber force by the distance from the middle of fiber to the geometric center of the section. Curvature is obtained by dividing top fiber strain by the neutral axis depth.

An important point with the program is about the termination. The termination of the program should be realized when the ultimate curvature is reached. The section can be considered to have reached its curvature capacity when either the resisting moment has reduced to some percentage of the maximum value due to crushing of concrete core, or when one of the longitudinal reinforcements has reached its rupturing tensile or compressive strain, whichever occurs first. Since it is difficult to decide about the percentage of drop in the moment at which the program will be terminated, it was decided to terminate the program only when the steel is ruptured. The decision on the ultimate curvature is left to the user.

For confined concrete, various mathematical models were used. The most commonly used ones are, Saatcioglu, Sheikh & Uzumeri, and Modified Kent & Park models. Detailed information about these models will be presented in the next sections. In addition to these three models, there is a fourth alternative in the program. This is similar to Modified Kent & Park, but with linear ascending part. It was originally proposed by Roy & Sozen [6] in 1963, and this study was one of the



first models proposed in this area. It can also be said that Kent & Park model was based on this model.

The program generates monotonic moment-curvature diagrams of sections which also can be considered as envelope curves in case of cyclic loading.

## **3.2 Basic Assumptions and Models**

### **3.2.1 General**

Analytical moment-curvature curves for reinforced concrete sections subjected to flexure or flexure and axial load can be derived on the bases of some assumptions. It is assumed that plane sections before bending remain plane after bending and that the stress-strain curves for concrete and steel are known. Also perfect bond between steel and concrete is assumed and effect of shear was neglected. It is also assumed that longitudinal bars do not buckle. The curvatures associated with a range of bending moments and axial loads can be determined using these assumptions and from the requirements of strain compatibility and equilibrium of forces.

To understand the behaviour of reinforced concrete sections, a knowledge of the fundamental properties of concrete and steel is required. The concrete in sections with transverse reinforcement consists of cover (unconfined) concrete and core (confined) concrete. The behaviour of cover concrete is generally different from that of plain concrete cylinders or prisms, because the behaviour will be affected by the thickness of cover and the spacing of transverse reinforcement.

Transverse reinforcement improves, strength and ductility of core concrete depending on the degree of confinement. The stress-strain relationship of confined

concrete is a function of many variables. Therefore, the main objective of this research was to study the effects of an array of variables using the analytical models for the stress-strain curve of confined concrete.

In the previous paragraph, the importance of assumptions relating to characteristics of materials was highlighted. Cross-sectional characteristics are also important. Dimensions and geometry of the cross-section, reinforcement ratios, thicknesses of clear covers, spacings of transverse reinforcements, axial load levels for columns, etc. are such important parameters. All these, influence the behaviour of reinforced concrete sections. Therefore, to make reasonable assumptions is very important and this requires extensive care.

One of the common assumptions is the factor by which the concrete cylinder strength has to be multiplied. This factor is  $k_3$ . In this study,  $k_3$  was taken as 1.0 for the cover concrete.

Curvature ductility ratios are calculated by dividing ultimate curvatures by yield curvatures. There is no universal agreement on the definition of ultimate curvature. Here the ultimate curvature will be taken as the curvature that corresponds to 85% of maximum moment value in the descending portion of the diagram. Yield curvature is the curvature where tensile reinforcement (bottom steel) starts to yield. For sections where there are many steel layers and therefore the above definition is controversial, an appropriate assumption will be presented in the "Assumptions" part of relevant chapter.

The moment values calculated, were divided by " $f_c b_w d^2$ " for all beam sections, and by " $f_c b h^2$ " for all column sections to get dimensionless values. (There is warning if there is an exception.) The symbols  $f_c$ ,  $b_w$ ,  $d$ ,  $b$  and  $h$  are the characteristic strength, width of web, effective depth, width and height of the cross sections respectively.

### 3.2.2 Stress-Strain Relationships of Steel

In general the stress-strain relation for the reinforcing steel is assumed to be elasto-plastic with strain hardening, and identical under compression and tension. The most important properties of the stress-strain diagram of the reinforcing steel are (a) the yield strength, (b) the ultimate strength, (c) strain hardening starting point, and (d) the strain capacity. The diagram in Figure 3.2 represents the stress-strain relationships of hot rolled steel. Hot rolled steel has a definite yield point and a significant yield plateau. Strain hardening starts at the end of this plateau, and it goes on a concavely downward parabolic line. The linear assumption for the part does not introduce significant error.

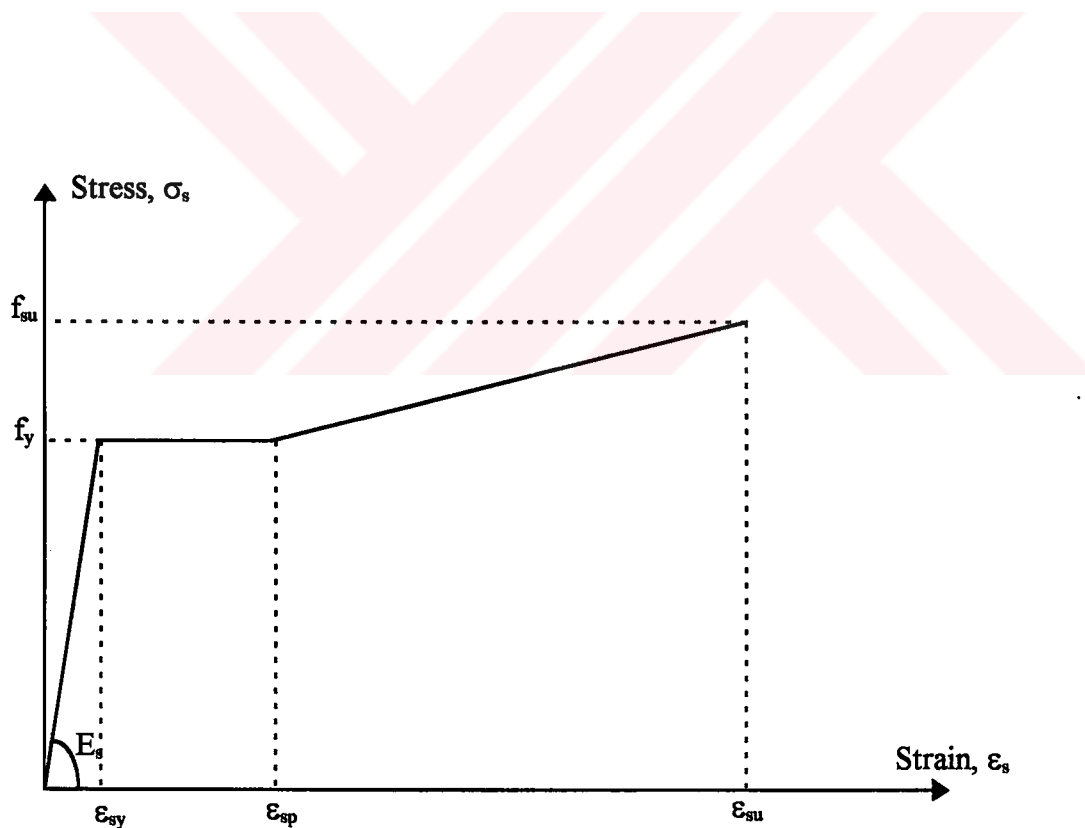


Figure 3.2: Stress-strain diagram for steel in tension or compression

In the program there is also an alternative for stress-strain diagram of reinforcing steel, where there is no strain hardening (elasto-plastic with no strain hardening).

In most of the examples in this study, either S220 or S420 steels were used. (There is a warning if there is an exception.) The numbers 220 and 420 corresponds to the characteristic yield strengths. Although the ultimate strengths for the S220 and S420 steels are taken as 340 MPa and 525 MPa respectively [7] (Ersoy, 1991), it is possible to change these values, in inputting the variables before the execution of the program. Also the strain hardening starting points and ultimate strains of any steel should be specified in the input.

Unlike concrete, the modulus of elasticity of steel does not vary with strength. TS-500 [23] recommends the use of  $E_s = 200$  GPa for the modulus of elasticity for nonprestressed reinforcement.

### **3.2.3 Stress-Strain Relationships of Concrete Under Tension**

Since the tensile strength of concrete is very low and since concrete cracks, tensile strength is generally neglected in strength calculations. However in serviceability conditions, such as deflections, tensile strength of concrete should be considered. The program allows the user to decide whether the tensile strength of concrete will be neglected or not.

The shape of the concrete stress-strain diagram in tension depends heavily on the testing procedure used. Only the direct tension test performed under constant strain can provide the complete stress-strain diagram in tension, namely with ascending and descending branches. The most realistic stress-strain curves for concrete in tension were obtained by Rusch [24] who tested concentrically loaded

specimens which were tested under strain controlled loading. Rusch found out that the shape of the curve changed significantly with the rate of loading and the strength of concrete.

In the light of Rusch's test results, it is decided to use the stress-strain curve shown in Figure 3.3. The diagram is approximated by two straight lines. Values for the strain corresponding to maximum stress, and the ultimate strain were assumed as 0.0001 and 0.0002 respectively (Ersoy, 1991) [7]. The direct tensile strength of plain concrete is expressed as a function of the square root of  $f_c$ . In the Turkish Code (TS500, 1985), this relationship is given as:  $f_{ct} = 0.35 \sqrt{f_c}$  (in MPa).

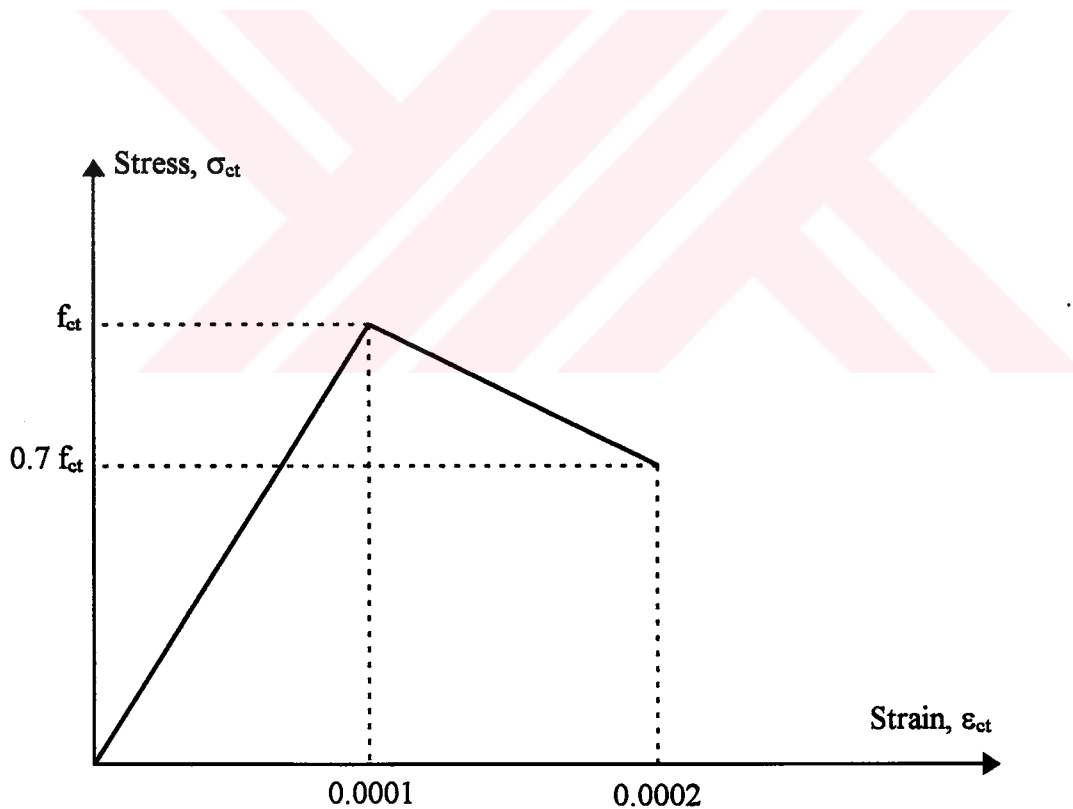


**Figure 3.3:** Assumed stress-strain diagram for concrete in tension

### **3.2.4 Stress-Strain Relationships of Unconfined Concrete Under Compression**

The stress-strain relationships of unconfined concrete under compression applies only to the clear cover of the section. Clear cover is simply the outside part of the core, which is not transversely reinforced. There is no universally accepted definition for the clear cover. Some researchers assume it as the area between the face of the section and the center of perimeter hoop, some others define it as the distance between the face of the section and outside of the perimeter of the hoop. Nevertheless since the difference between these two assumptions is small, in the program it is defined according to the model which the user chooses.

In general the behaviour of concrete in the compression zone of a member subjected to pure or combined flexure is assumed to be similar to that obtained from uniaxial compression tests. Stress-strain models proposed by different researchers simplify the actual stress-strain relations obtained experimentally. These models do not differ much in the ascending portion. In making a mathematical model for concrete, the initial portion of the stress-strain curve is often approximated by a second degree curve. However different assumptions are made for the descending portion.

A very commonly used approximation for the stress-strain diagram is the one known as the Hognestad curve. Hognestad [25] (1951) has developed a stress-strain diagram for concrete in flexural compression, from the tests of vertically cast short columns subjected to combined bending and axial load. The proposed stress-strain curve and limiting strain value have been widely accepted by other researchers. The model proposed by Hognestad (1951) is shown in Figure 3.4.

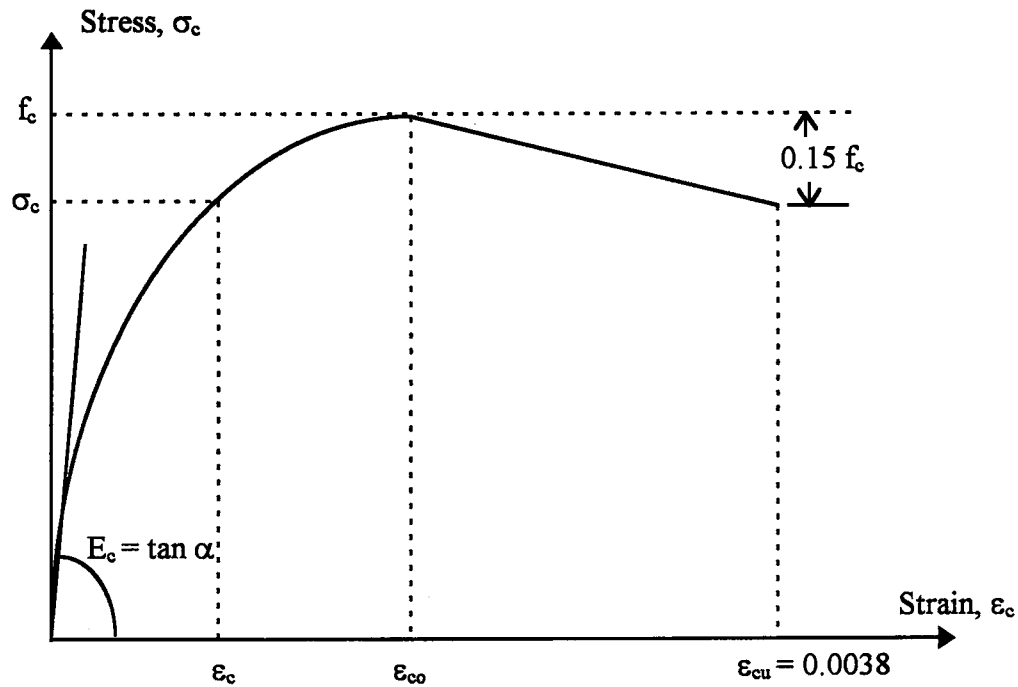


**Figure 3.4:** Hognestad's (1951) stress-strain diagram

The initial part of the curve is a second degree parabola, expressed by Equation 3.1,

$$\sigma_c = f_c [2\varepsilon_c/\varepsilon_{co} - (\varepsilon_c/\varepsilon_{co})^2] \quad (3.1)$$

$$f_c = 0.85 f_{ck}$$

where

$\varepsilon_c, \varepsilon_{co}$  : Concrete strains at  $\sigma_c$  and  $f_c$  respectively

$$\varepsilon_{co} = 2f_c/E_c$$

$$E_c = 12680 + 460 f_c \text{ (MPa)}$$

Between the strains corresponding the maximum stress,  $\varepsilon_{co}$  and the ultimate strain  $\varepsilon_{cu}$ , the stress-strain relationship is assumed to be a descending straight line.

$$\sigma_c = f_c [1.0 - 0.15 ((\epsilon_c - \epsilon_{co}) / (\epsilon_{cu} - \epsilon_{co}))] \quad (3.2)$$

where

$$\epsilon_{cu} = 0.0038$$

The above stress-strain diagram is general for the unconfined concrete. Preparing the input data of the program, if Kent & Park model is chosen for core concrete, the stress-strain diagram of the unconfined concrete is accepted as proposed by these researchers. This model is presented in following sections (Section 3.2.5.2.3). Anyway there is no such a big difference between these two models for unconfined concrete. The difference is only in the descending portion (slope and maximum strain).

### **3.2.5 Stress-Strain Relationships of Confined Concrete Under Compression**

#### **3.2.5.1 Mechanics of Concrete Confinement by Lateral Reinforcement [22]**

Strength and deformability of concrete in compression can improve significantly when confined by lateral reinforcement. Concrete in compression develops transverse strains which may lead to internal cracking. The presence of lateral reinforcement in concrete limits the internal cracking and improves ability of concrete to sustain higher stresses and strains.

Confined concrete shows stress-strain characteristics that are distinctly different from those of unconfined concrete. Early research conducted by Richart et al. in 1928 [26] on concrete cylinders with lateral stresses by uniform fluid pressure provided useful data for confinement. In this research, concrete cylinders were subjected to equal compression in two opposite directions ( $\sigma_2 = \sigma_3$ ) and then the load



in the other direction ( $\sigma_1$ ) was increased until failure was reached. As a result of these tests, Richart et al observed that both the strength and strain capacity of concrete increased significantly and this increase was a function of the lateral pressure ( $\sigma_2 = \sigma_3$ ) applied. Some typical results obtained by Richart et al are shown in Figure 3.5.

Confinement by lateral reinforcement was a topic of interest for many researchers. It can be said that almost every Ph.D. student studying on mechanics of confined concrete tried to create his own analytical model of confinement. Chan [27] (1955), Roy and Sozen [6] (1963), Soliman and Yu [28] (1967), Sargin et al [29] (1971), Kent and Park [3] (1971), Vallenar Bertero and Popov [30] (1977), Sheikh and Uzumeri [2] (1982), and Saatcioglu [1] (1991) investigated the behaviour of confined concrete and proposed analytical models. The main variables considered in these models were the diameter, strength, amount and spacing of lateral reinforcement. Other variables considered include concrete strength and type, cross-sectional size and shape, type and rate of loading and amount and arrangement of longitudinal reinforcement.

A revised version of Mohr's Failure Theory for concrete under triaxial stresses has been developed by Zia and Cowan [31]. If  $\sigma_2 = \sigma_3$  and if all stresses are compressive, then the behaviour of concrete can be predicted by Equation 3.3.

$$f_{cc} = f_c + 4\sigma_2 \quad (3.3)$$

where:

$f_{cc}$ : Axial compressive strength of confined specimen,

$f_c$ : Uniaxial compressive strength of unconfined specimen,

$\sigma_2$ : Lateral confining pressure.

In many of our structural members concrete is confined by lateral reinforcement either in the form of continuous spirals or rectangular hoops. A

concrete cross-section fully or partly subjected to compression will reach its limiting strain value at very high compressive stresses and the concrete outside the lateral reinforcement, which is not confined will crush and start to spall. Due to Poisson's effect, concrete inside the lateral reinforcement tries to expand laterally. Such a deformation is prevented by the lateral reinforcement which applies lateral passive pressure on concrete. Then it becomes obvious that the concrete inside the lateral reinforcement is no longer uniaxially loaded but is under triaxial state of stresses.

A uniaxially loaded member shown in Figure 3.6 has lateral reinforcement in the form of continuous spirals. When the longitudinal strain in the concrete reaches the limiting strain value, the concrete cover outside the spiral steel crushes, then the concrete in the core is subjected to triaxial compression with  $\sigma_2 = \sigma_3 = q$ .

Ideally, the increase of strength in the core area due to confinement should at least be equal to the strength loss due to crushing of the shell concrete outside the spiral steel.

The confinement provided by the rectangular hoop is not as effective as the circular spiral, due to the different behaviour caused by geometry. The circular spiral is subjected to uniaxial tension and thus axial elongation, whereas the rectangular hoop deformation is mainly due to flexure and therefore depends on the flexural stiffness of the bar. Since flexural stiffness is much smaller than the axial stiffness and since maximum flexural deformation takes place at the midspan, the passive pressure provided by the lateral reinforcement disappears rapidly moving from the corner to the midspan of the hoop. As shown in Figure 3.7 the confining pressure becomes significant only at the restraining end zones where the flexural deformation is negligible. The effectiveness of the confinement decreases significantly between the two adjacent hoops as shown in Figure 3.7. In practice it is assumed that rectangular hoops are only 50% as effective as the circular spirals.

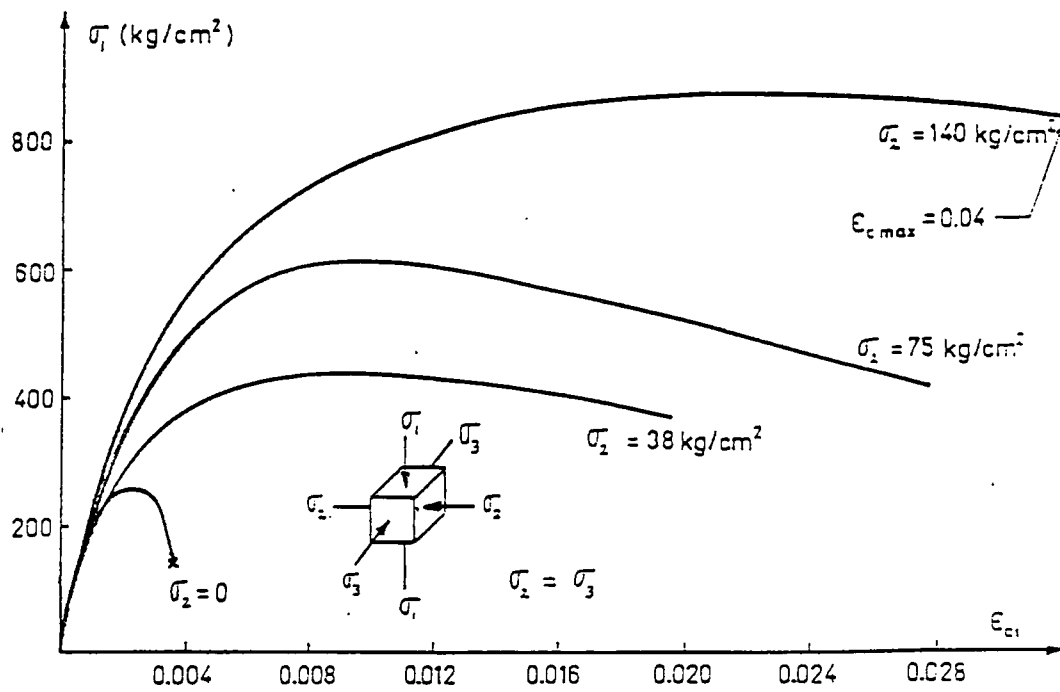


**Figure 3.5:** Axial  $\sigma$ - $\epsilon$  curves from triaxial compression tests (Richart et al)

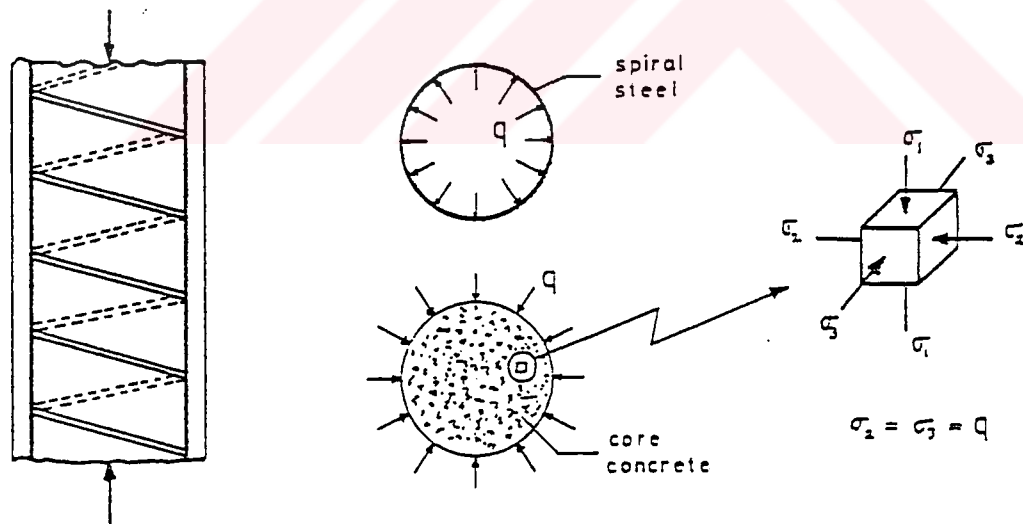


**Figure 3.6:** A uniaxially loaded spiral column and free body diagrams of the core concrete and the spiral steel

Confinement of concrete with properly designed spiral reinforcement not only changes the shape of the stress-strain curve, but also increases both the strength and strain capacity. Rectangular hoops improve the strain capacity significantly but do not increase the strength unless large amounts are used. Some typical stress-strain diagrams obtained by testing uniaxially loaded specimens in which lateral reinforcement was the main variable are shown in Figure 3.8.

### **3.2.5.2 Review of Mathematical Models Used in the Computer Program**

Most of the mathematical models developed were based on tests of specimens which were uniaxially loaded and which had simple tie configurations (four corner bars and a single tie). It should also be mentioned that most of the mathematical models developed were empirical, only a few being semi-empirical. There is yet no rational model to predict the force-deformation characteristics of confined concrete. Some of the models proposed by researchers will be reviewed briefly. The below reviewed models are arranged as subroutine programs which idealizes the stress-strain relationships of the core concrete in order to form moment-curvature diagrams in the main program.

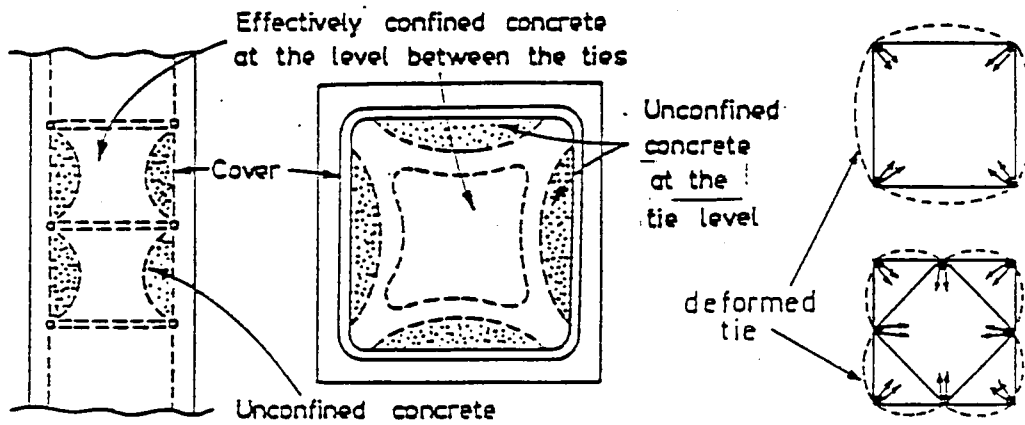


**Figure 3.7:** Effectively confined concrete in a square section and deformation of lateral steel between restraint points

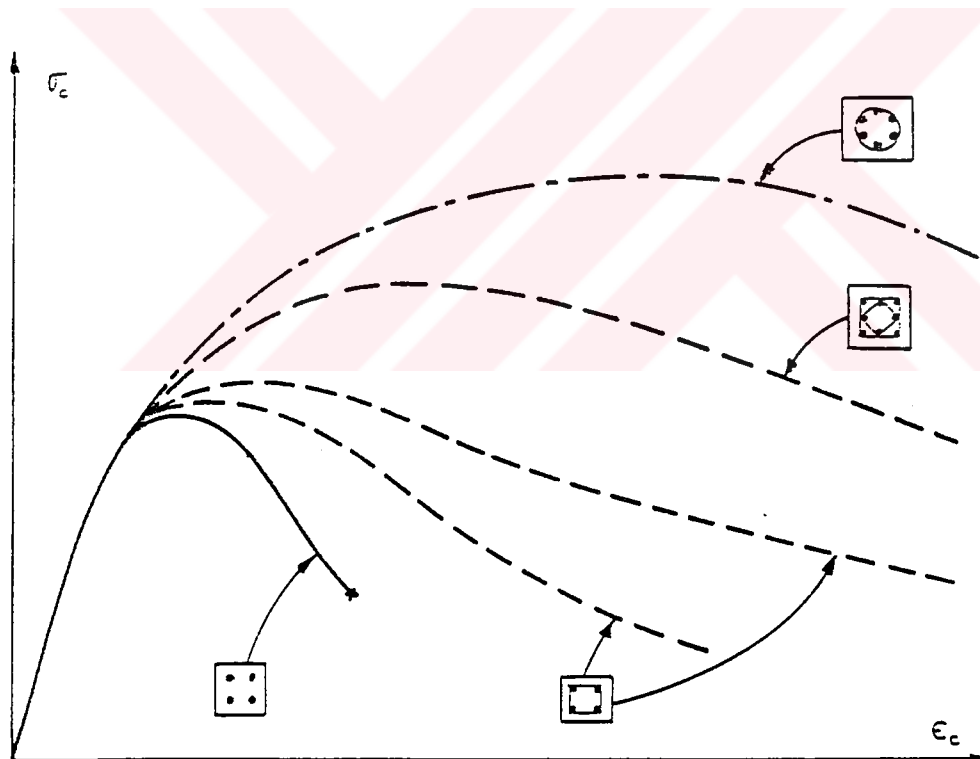


**Figure 3.8:** Stress-strain diagrams for different amounts of lateral steel [22]

### 3.2.5.2.1 Roy and Sozen Model

An idealized bilinear stress-strain relationship was proposed [6] for laterally reinforced concrete as shown in Figure 3.9. The strain  $\epsilon_{50}$  is defined as the point on the curve where the concrete stress drops to 50% of the maximum stress on the descending branch of the curve.  $\epsilon_{50}$  was given by the following equation:

$$\epsilon_{50} = (3 / 4) (\rho_s h / s) \quad (3.4)$$

where:

$h$ : The short dimension of the cross section

$\rho_s$ : Volumetric lateral steel ratio

$s$ : Tie spacing

$f_c$ : Strength of unconfined concrete

$f_{cc}$ : Strength of confined concrete

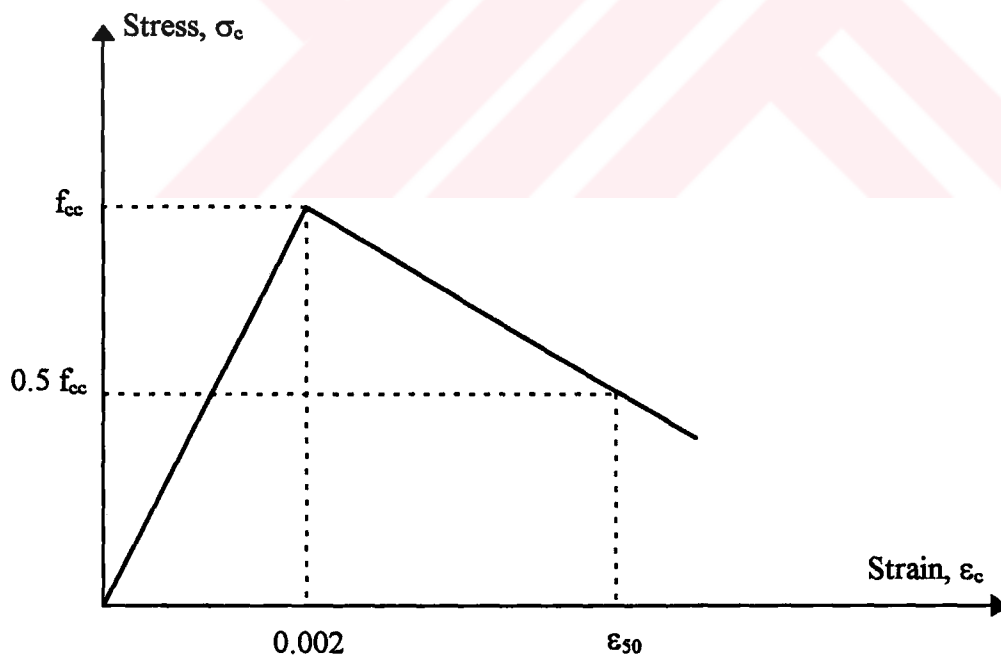


Figure 3.9: Stress-strain curve proposed by Roy and Sozen

The model known as Kent & Park model was inspired from the model proposed by Roy & Sozen

### **3.2.5.2.2 Sheikh and Uzumeri Model**

The main purpose of the model proposed by Sheikh and Uzumeri was to simulate the behaviour of confined concrete. [2]

In this model, the increase in the strength of confined concrete is calculated on the basis of effectively confined concrete area, which is less than the core concrete area enclosed by the center line of the perimeter ties.

In the development of this model the following variables were considered; (a) volumetric ratio of lateral reinforcement to concrete core, (b) distribution of longitudinal steel around the core perimeter, and (c) the resulting tie configuration, tie spacing, characteristics of lateral steel and strength of plain concrete.

A stress-strain relationship proposed by Sheikh & Uzumeri for confined concrete as shown in Figure 3.10 consists of four parts. The first part of the curve, upto a strain of  $\epsilon_{s1}$ , is a second degree parabola (Equation 3.5). Between  $\epsilon_{s1}$  and  $\epsilon_{s2}$ , the curve has a horizontal straight line portion. Beyond  $\epsilon_{s2}$  the descending part of the curve is a straight line (Equation 3.6) which is suggested to continue decreasing to 30% of the maximum stress, after which a horizontal line represents the concrete behaviour. Four equations were given to define the curve completely.

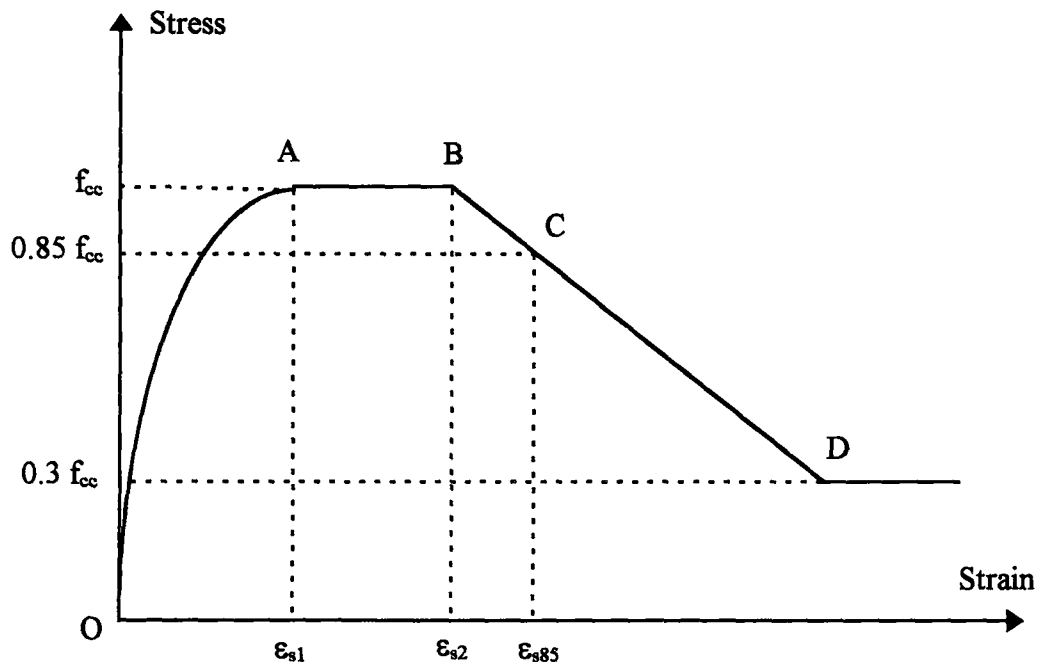


**Figure 3.10:** Stress-strain curve for confined concrete. Sheikh and Uzumeri idealization (From Sheikh and Uzumeri, 1982)

Part OA:

$$\sigma_c = f_{cc} [2\varepsilon_c / \varepsilon_{s1} - (\varepsilon_c / \varepsilon_{s1})^2] \quad (3.5)$$

Part BD:

$$\sigma_c = f_{cc} \left[ 1 - \frac{0.15 (\varepsilon_c - \varepsilon_{s2})}{\varepsilon_{s85} - \varepsilon_{s2}} \right] \quad (3.6)$$

where:

$$\begin{aligned} f_{cc} &= K_s \cdot f_{cp} \\ &= K_s \cdot 0.85 f_c \end{aligned}$$



where:

$$K_s = 1.0 + \frac{B^2}{0.119 f_c' (A_{ck} - A_{st})} \left[ \left(1 - \frac{n C^2}{5.5 B^2}\right) \left(1 - \frac{s}{2B}\right)^2 \right] \sqrt{\rho_s f_y}$$

$$\epsilon_{s1} = 80 \times 10^{-6} K_s f_c'$$

$$\epsilon_{s2} = 0.0022 \left[ 1 + \frac{248}{C} \left\{ 1 - 5.0 \left(\frac{s}{B}\right)^2 \right\} \frac{\rho_s f_y}{\sqrt{f_c'}} \right]$$

$$\epsilon_{s85} = \epsilon_{s2} + 0.225 \rho_s \sqrt{B/s}$$

where:

$f_{cc}$  : Compressive strength of confined concrete in MPa.

$f_{cp}$  : Compressive strength of concrete in plain specimen in MPa.

$f_c$  : Concrete cylinder strength in MPa.

$f_y$  : Yield strength of longitudinal steel in MPa.

$K_s$  : The strength gain factor

$\epsilon_{s1}$  &  $\epsilon_{s2}$  : Minimum and maximum strains corresponding to the maximum stress in concrete

$\epsilon_{s85}$  : The strain corresponding to 85 percent of the maximum stress on the descending part of the curve

$n$  : Number of arcs between longitudinal bars

$B$  : Center to center distance of perimeter tie in mm.

$C$  : Center to center distance between longitudinal bars in mm.

$s$  : Spacing of ties in mm.

$\rho_s$  : Volumetric ratio of total lateral reinforcement to the volume of core

$A_{ck}$  : Area of core concrete in mm<sup>2</sup>.

$A_{st}$  : Area of the longitudinal steel in mm<sup>2</sup>.

It is claimed that the model is also able to determine the stress-strain curve of the confined concrete in the core even when a strain gradient is present.

### 3.2.5.2.3 Kent and Park Model

The stress-strain curve proposed by Kent and Park is for concrete confined by rectangular ties. In the derivation of the model for confined concrete the effects of volumetric ratio of lateral steel to concrete core, tie spacing and strength of concrete are included but the effect of strain gradient is ignored. [3]

The stress-strain model consists of three parts. (See Figure 3.11) The ascending part of the curve is represented by a second degree parabola in which the strain  $\epsilon_{c0}$  at maximum stress is equal to 0.002 (Equation 3.7). Due to rectangular confinement no increase in the strength of confined concrete is considered. The falling

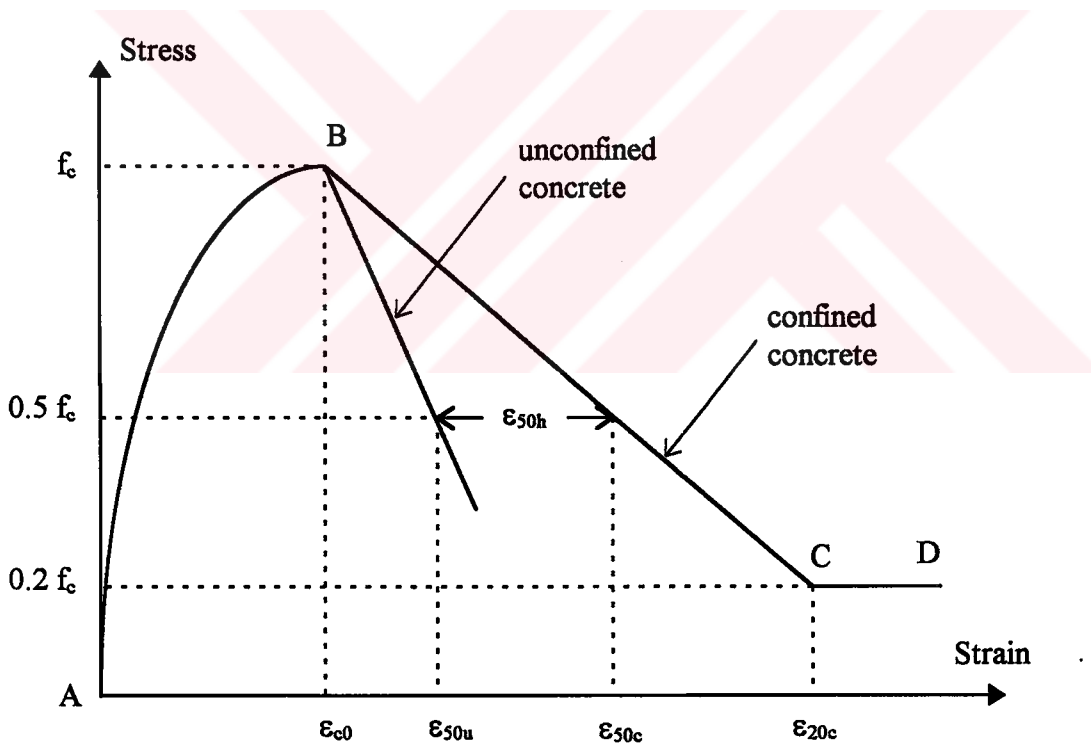


**Figure 3.11:** Stress-strain curve for concrete. Kent and Park idealization  
(From Kent and Park, 1971)

branch of the curve is assumed to be linear and its slope is specified by determining the strain when the stress on concrete falls to half of maximum strength (Equation 3.8). A horizontal portion with a constant stress at 0.2 of the maximum stress defines the rest of the curve.

Part AB:

$$\sigma_c = f_c [2\varepsilon_c / \varepsilon_{c0} - (\varepsilon_c / \varepsilon_{c0})^2] \quad (3.7)$$

Part BC:

$$\sigma_c = f_c [1 - Z (\varepsilon_c - \varepsilon_{c0})] \quad (3.8)$$

where:

$$Z = \frac{0.5}{\varepsilon_{50u} + \varepsilon_{50h} - \varepsilon_0}$$

$$\varepsilon_{50u} = \frac{0.021 + 0.002 f_c}{f_c - 7.0}$$

$$\varepsilon_{50h} = (3/4) \rho_s \sqrt{a / s}$$

where:

$f_c$  : Unconfined concrete strength in MPa.

$\rho_s$  : Ratio of volume of lateral reinforcement to volume of concrete core

$a$  : Width of confined core

$s$  : Tie spacing

In the derivation of the above stress-strain relationship it is assumed that the stress-strain curve for the cover concrete in compression is identical to that of the

confined concrete core at strains equal to or less than 0.002. The cover concrete at strains greater than 0.004 is considered to have spalled and to have zero strength.

#### 3.2.5.2.4 Modified Kent and Park Model (From Park et al, 1982)

The original model of Kent and Park has been improved by the same researchers. In this modified model, the increase in the concrete strength due to confinement is considered.

Figure 3.12 shows the modified Kent and Park stress-strain model. The maximum stress reached is assumed to be  $Kf_c$  at a strain  $\epsilon_{cc0} = 0.002 K$ , in which:

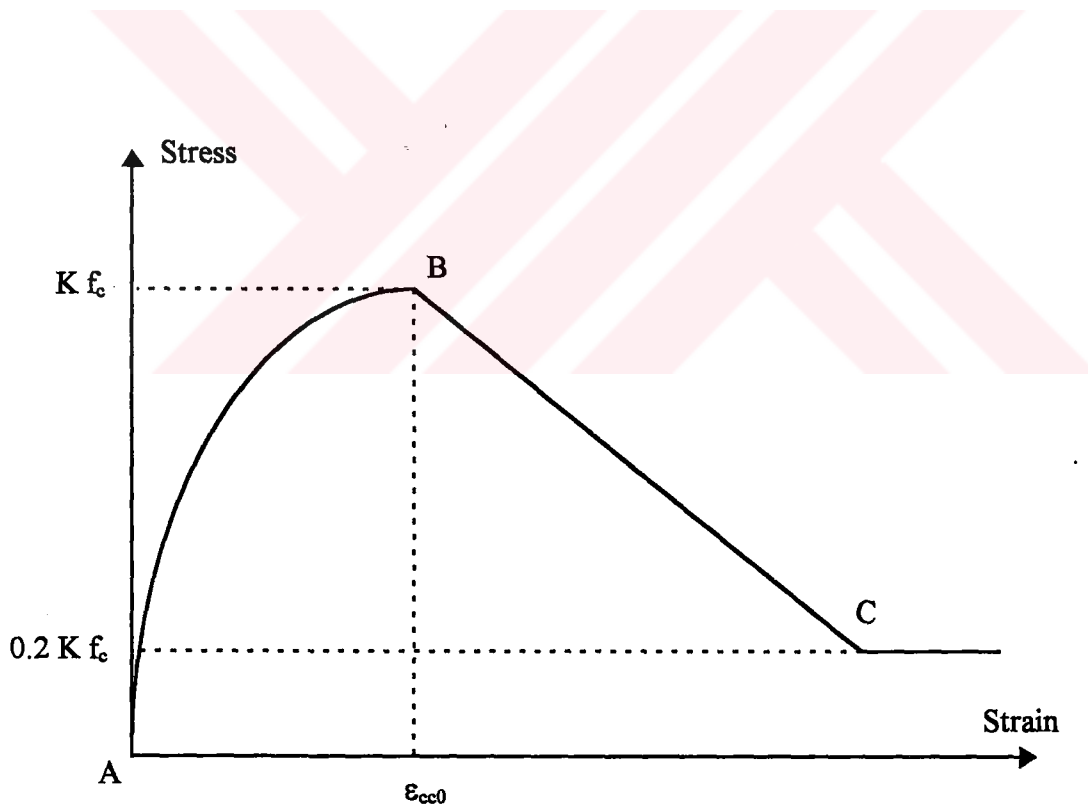


**Figure 3.12:** Stress-strain curve for concrete. Modified Kent and Park idealization

$$K = 1 + [ (\rho_s f_{yw}) / f_c ]$$

where:

$\rho_s$  : Ratio of volume of rectangular steel hoops to volume of concrete core

$f_{yw}$  : Yield strength of steel hoops

Part AB:

$$\sigma_c = K f_c [ 2\varepsilon_c / \varepsilon_{cc0} - (\varepsilon_c / \varepsilon_{cc0})^2 ] \quad (3.9)$$

Part BC:

$$\sigma_c = K f_c [ 1 - Z_m (\varepsilon_c - \varepsilon_{cc0}) ] \quad (3.10)$$

where:

$$Z_m = \frac{0.5}{\left[ \frac{0.021 + 0.002 f_c}{f_c - 7.0} \right] + \left[ (3/4) \rho_s \sqrt{a/s} \right] - \varepsilon_{cc0}}$$

### 3.2.5.2.5 Saatcioglu Model

An analytical model is developed for stress-strain relationship of confined concrete by Razvi and Saatcioglu. [1] [5] The model consists of a parabolic ascending branch, followed by a linear descending segment and a residual strength. The peak stress and the corresponding strain are established on the basis of lateral confinement pressure,  $\sigma_s$ . The confinement pressure is computed from equilibrium of internal forces and sectional characteristics.

The descending branch is constructed by defining the strain corresponding to 85% of confined strength. This strain level is expressed in terms of lateral reinforcement ratio and the strain corresponding to peak stress. The corresponding stress-strain curve of the model is shown in Figure 3.13.

The proposed model requires little computational effort to construct. It is general enough to cover the majority of applications in practice. The capabilities of the model include circular, square and rectangular concrete sections confined with circular and/or rectilinear reinforcement. Both concentric and eccentric loading, under low and high strain rates are covered. Here are the equations:

$$f_{cc} = f_c + k_1 \sigma_{1e} \quad (3.11)$$

$$\sigma_{1e} = k_2 \sigma_1 \quad (3.12)$$

$$\sigma_1 = (\sum A_0 f_{yw} \sin \alpha) / (s b_k) \quad (3.13)$$

$$k_1 = 6.7 (\sigma_{1e})^{-0.17} \quad (3.14)$$

$$k_2 = 0.26 \sqrt{(b_k / s) (b_k / s_1) (1 / \sigma_1)} \quad (3.15)$$

$$\sigma_{1e} = (\sigma_{1ex} b_{kx} + \sigma_{1ey} b_{ky}) / (b_{kx} + b_{ky}) \quad (3.16)$$

$$\epsilon_{cc0} = \epsilon_{c0} (1 + 5K) \quad (3.17)$$

$$K = (k_1 \sigma_{1e}) / f_c \quad (3.18)$$

$$\epsilon_{85c} = 260 \rho \epsilon_{cc0} + \epsilon_{85u} \quad (3.19)$$

$$\rho = (\sum A_0) / [s (b_{kx} + b_{ky})] \quad (3.20)$$

$$\sigma_c = f_{cc} [2\epsilon_c / \epsilon_{cc0} - (\epsilon_c / \epsilon_{cc0})^2]^{1/(1+2K)} \quad (3.21)$$

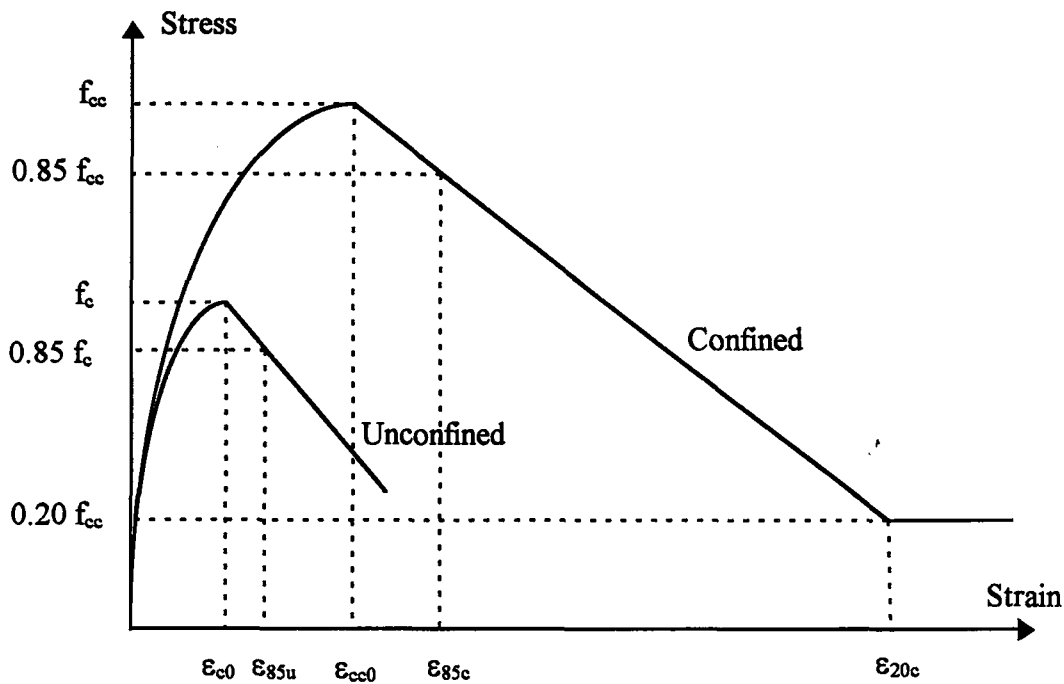


**Figure 3.13:** Proposed stress-strain relationship. Idealized by Saatcioglu

where:

$b_k$  : Core dimension, measured center to center of perimeter hoop, or circular spiral, or tie, in mm.

$s_l$  : Spacing of longitudinal reinforcement laterally, supported by the corner of a hoop or the hook of a cross tie, center to center, in mm.

$\alpha$  : Angle between transverse reinforcement and the side of the cross-section crossed by the reinforcement.

### 3.3 The Computer Program

The basic steps of the computer program written were given in Section 3.1. The assumptions and the material models which could be used with the program were discussed in Section 3.2.

The flowchart of the program is given in Figure 3.14. With this program the moment-curvature relationships of reinforced concrete sections having either rectangular or square sections can be obtained. Any number of layers of longitudinal reinforcement and different tie configurations can be considered. Any material model can be used. To run the program, the following input data is needed:

- Name or designation
- Yield strength of transverse steel (180, 220, 350, 500, etc... in MPa)
- Diameter of transverse steel (6, 8, 12, 12.28, etc... in mm)
- Spacing of transverse steel
- Unconfined concrete strength (10, 11, 15, 15.82, etc... in Mpa)
- Model for confined concrete (Saatcioglu, Sheikh & Uzumeri, Modified Kent & Park, Roy & Sozen)
- Clear cover
- Transverse and longitudinal steel configuration type of the cross section (See Figure 3.15)
- Height and width of cross section
- Longitudinal steel diameter (14, 15, 18.8, 32, etc... in mm)
- Number of longitudinal bars for each steel layer (1, 3, 6, 10, etc...)
- Whether the concrete carries tension or not
- Yield strength of longitudinal steel (180, 220, 350, 500, etc... in MPa)
- Whether there is strain hardening for the longitudinal strain or not
- If there is strain hardening, the strain where strain hardening starts (it should be greater than yield strain)
- Ultimate strain for longitudinal strain
- Ultimate strength of longitudinal steel (it should be greater than yield strength)
- If it is a beam, whether it is a T-beam or rectangular beam
- If it is a T-beam, thickness and width of flange



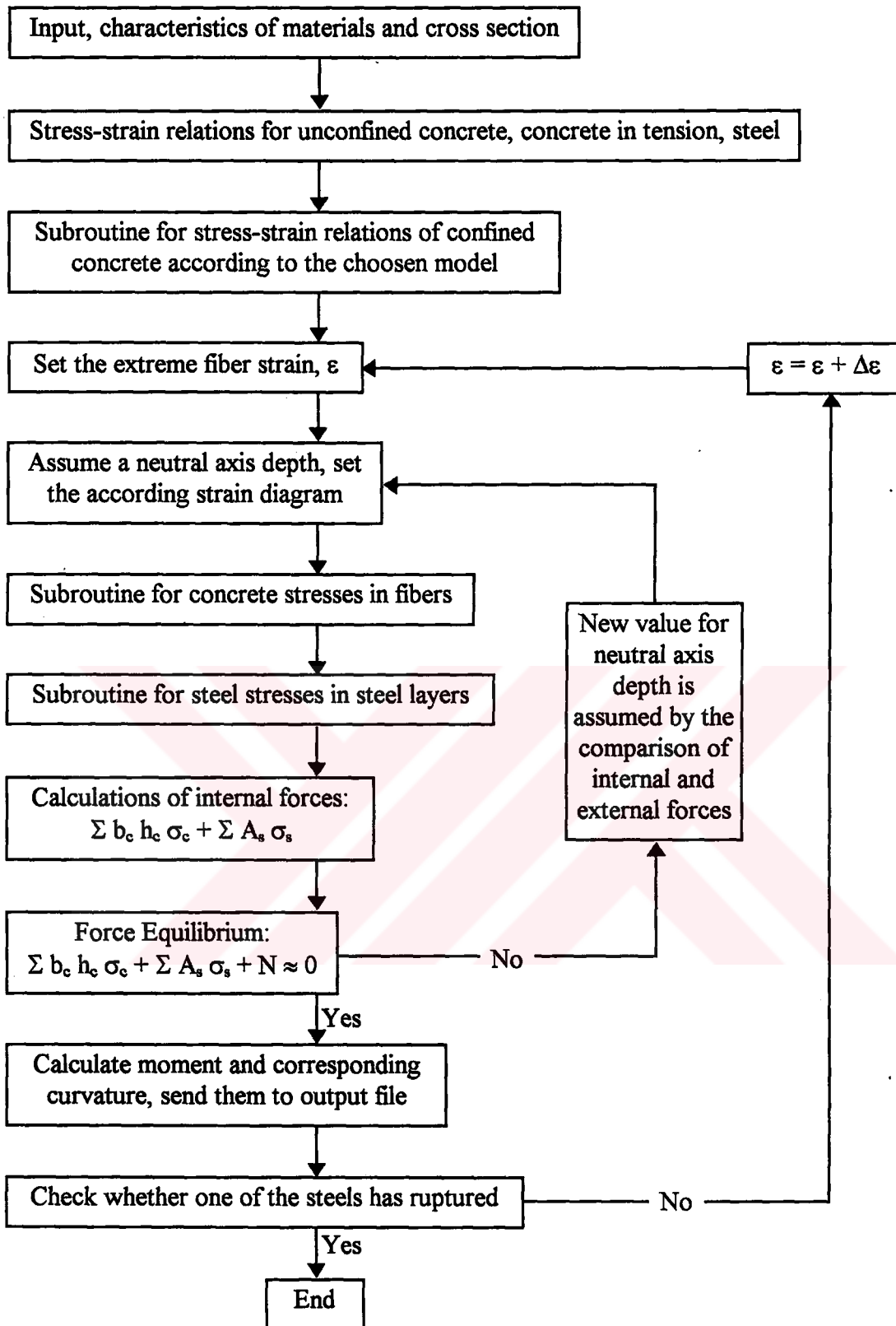
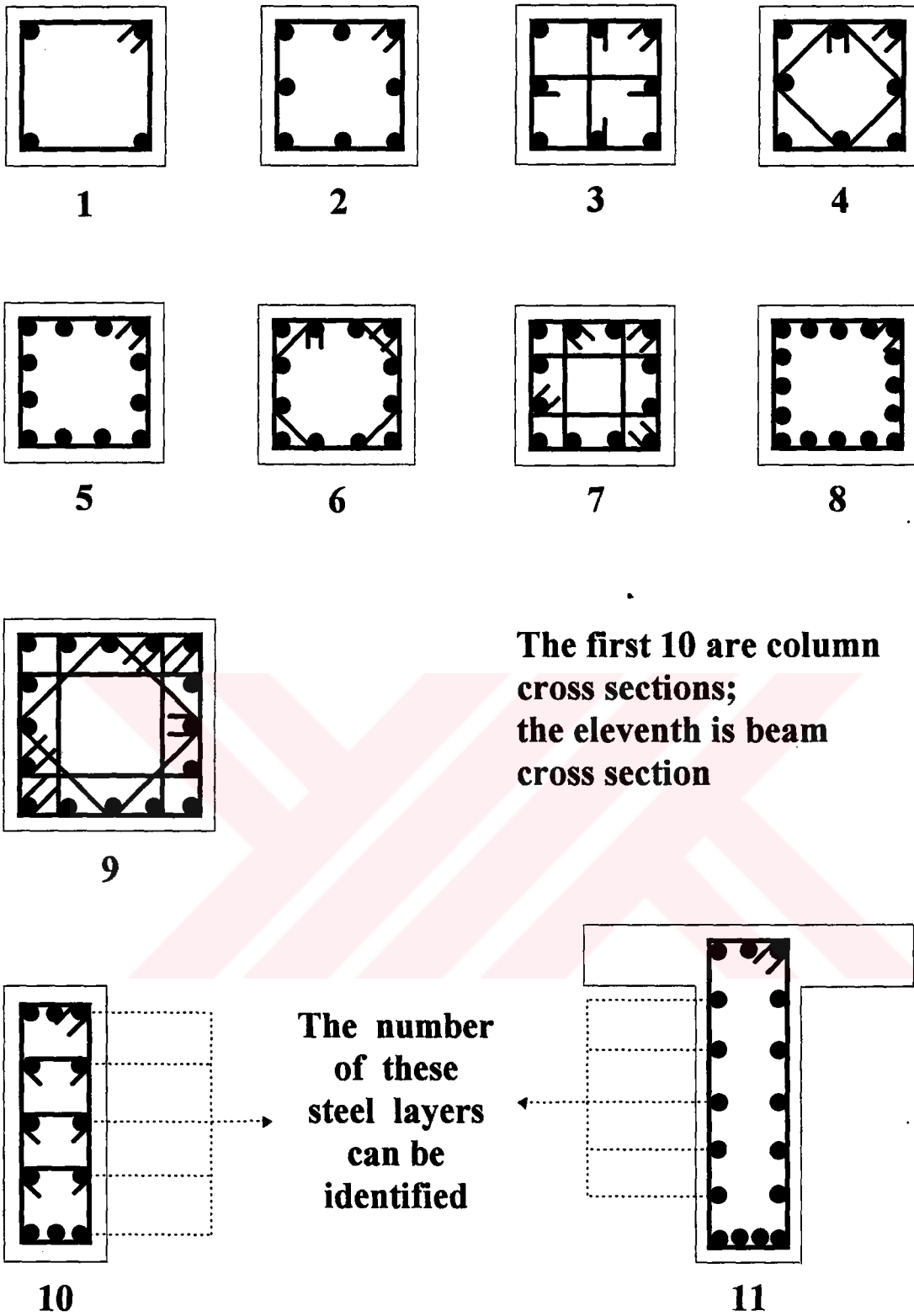


Figure 3.14: Flowchart of the Program

For each problem (sample) there will be three files in the program. One is the input file which shows different properties of the sample, the other is the output file which gives the curvature, moment, top fiber strain and neutral axis position. In this file there exists also the observations (such as, starting point of clear cover or core concrete crushing, yielding or strain hardening starting points of tension and compression reinforcements, etc.). The last one is the "XLS" file which serves to draw the moment-curvature diagram of the sample. The cross-sections and reinforcement configurations considered in this thesis are shown in Figure 3.15. The first 10 sections of the figure are column cross-sections and they are symmetrical in both horizontal and vertical directions. The eleventh section is a T-beam. The upper part of the section, that is the flange of the beam has to be in compression.





**Figure 3.15:** Different longitudinal and transverse steel configurations considered

**CHAPTER IV**

**NUMERICAL APPLICATIONS OF THE PROGRAM**

**STUDIES ON R/C BEAMS**

**4.1 General**

In this chapter the observed behaviour of the simulated samples will be presented and discussed. There are seven main case studies (listed in the first chapter). Every case study consists of some examples where related moment-curvature diagrams are drawn and presented in Appendix A. The examples and related diagrams are grouped for an easier comparison.

The grouping system is as follows. The title of a group consists of two parts. First part gives the case study number and is written by Roman numerals, second part shows the group in that case study and is written by a letter. For example, "IVF" means group "F" (or sixth group) in the "Case study IV". Fourth case study is the "Influence of the Steel Model in R/C Beams", and will be discussed in Section 4.5.

Each group has either 2, 3 or 4 examples. The examples are designated by a number which follows the group designation. For example, IVF2 means second example of Group IVF.

Case studies made are presented in the following paragraphs. Each case study has three subsections named as, "Assumptions", "Discussion of Results", and "Conclusions".

In the "Discussion of Results", all paragraphs begin with the related group names, such as Group IVD, Group VIIF, etc. This identification is required, in order to organise and to prevent the confusion of variables that affect the behaviour, while making the discussions.

In order to prevent the repetition of assumptions which are valid for all beams, such assumptions are presented before the case studies. Here are the common assumptions:

- Except for those in the case study named "Influence of Confined Concrete Model on Moment-Curvature Diagrams of R/C Beams" (Section 4.7), all moment-curvature diagrams drawn are based on the Modified Kent & Park model for confined concrete. This model was assumed to be valid only for the core concrete.

- The other common assumption was the model for concrete in tension which was presented previously in Chapter 3. (Figure 3.3)

- Strain hardening in reinforcing steel starts generally at a strain of five times the yield strain. The exception to this is for case studies for the purpose of investigating "Influence of Concrete Strength in R/C Beams" (Section 4.3) and "Influence of the Steel Model in R/C Beams" (Section 4.5). In these two studies different values were used for strain corresponding to strain hardening.

- For all sections, height is 600 mm and the width is 300 mm. Effective depth is generally 560 mm. Therefore the ratio of  $d'/d$  is generally 0.0714 ( $d'$  is height minus effective depth;  $d$  is effective depth). However for the investigation

designated as "Influence of Tension Reinforcement Ratio in R/C Beams", different "d'/d" ratios are used. Although dimensions were assigned to the beam, in general the results are presented in a dimensionless form.

- If the cross section of beam is rectangular, upper limit of the tensile reinforcement ratio is either  $\rho_m$  (TS500) or 0.02 (Turkish Seismic Code), whichever is smaller. T-beams, upper limit was exceeded in some cases. The lower limit for the tensile reinforcement ratio is again taken from TS500 (minimum flexural reinforcement).

- Compression steel ratio means compression reinforcement area divided by tensile reinforcement area.

## **4.2 Case Study I: Influence of Compression Reinforcement in R/C Beams**

This study aims to investigate the influence of compression steel on beam behaviour. For this purpose 40 moment-curvature diagrams for rectangular sections and 8 for flanged sections were drawn. The main variables investigated were concrete and steel strengths, ultimate strain of steel, and the ratio of tension reinforcement. In each group, beams having different amounts of compression steels were investigated. The list of all 48 sections with their properties are given in Table 4.1. The results are presented in Table 4.2. Curvature ductility ratio in Table 4.2 was the ratio of ultimate to yield curvature.

### **4.2.1 Assumptions**

- Transverse reinforcement (web) ratio ( $\rho_w$ ) for all beams is 0.0044 ( $\phi 10/120$  mm). This ratio was kept the same in all groups of this study.

**Table 4.1: List of sections and section properties; Influence of compression reinforcement in R/C beams**

		Steel & concrete properties	Ultimate strain of longitudinal steel	Tension steel ratio ( $A_s/bw/d$ )	Comp. steel ratio ( $A_s'/A_s$ )	
IA	IA1	S220 - C16  Rect. Sec. 300*600 mm	0.1	0.0048	0.00	IA1
	IA2				0.50	IA2
	IA3				1.00	IA3
	IA4				2.00	IA4
IB	IB1			0.0126	0.00	IB1
	IB2				0.50	IB2
	IB3				1.00	IB3
	IB4				2.00	IB4
IC	IC1			0.0191	0.00	IC1
	IC2				0.50	IC2
	IC3				1.00	IC3
	IC4				2.00	IC4
ID	ID1	S220 - C16  Rect. Sec. 300*600 mm	0.18	0.0048	0.00	ID1
	ID2				0.50	ID2
	ID3				1.00	ID3
	ID4				2.00	ID4
IE	IE1			0.0126	0.00	IE1
	IE2				0.50	IE2
	IE3				1.00	IE3
	IE4				2.00	IE4
IF	IF1			0.0191	0.00	IF1
	IF2				0.50	IF2
	IF3				1.00	IF3
	IF4				2.00	IF4
IG	IG1	S420 - C16  Rect. Sec. 300*600 mm	0.18	0.0027	0.00	IG1
	IG2				0.50	IG2
	IG3				1.00	IG3
	IG4				2.00	IG4
IH	IH1			0.0075	0.00	IH1
	IH2				0.50	IH2
	IH3				1.00	IH3
	IH4				2.00	IH4
IJ	IJ1			0.0117	0.00	IJ1
	IJ2				0.50	IJ2
	IJ3				1.00	IJ3
	IJ4				2.00	IJ4
IK	IK1	S420 - C40 Rect. Sec. 300*600 mm	0.18	0.0168	0.00	IK1
	IK2				0.50	IK2
	IK3				1.00	IK3
	IK4				2.00	IK4
IL	IL1	S420 - C16 T-beam $b_f = 1500$ mm $h_f = 150$ mm	0.18	0.0075	0.00	IL1
	IL2				0.50	IL2
	IL3				1.00	IL3
	IL4				2.00	IL4
IM	IM1			0.0117	0.00	IM1
	IM2				0.50	IM2
	IM3				1.00	IM3
	IM4				2.00	IM4

**Table 4.2: Results; Influence of compression reinforcement in R/C beams**

		Curvature (rad/m)						Curvature ductility ratio	Maximum M**	
		Yield A <sub>s</sub>	Str. Hard. A <sub>s</sub>	Cover Crush	Core Crush	Yield A <sub>s</sub> '	Str. Hard. A <sub>s</sub> '			
IA	IA1	0.0041	0.0153	0.0385	0.0726	*	*	51	0.087	IA1
	IA2	0.0033	0.0136	0.0448	0.0912	0.1085	*	55	0.090	IA2
	IA3	0.0040	0.0132	0.0478	0.1023	0.1830	*	49	0.095	IA3
	IA4	0.0032	0.0132	0.0505	0.1165	*	*	58	0.093	IA4
IB	IB1	0.0042	0.0139	0.0160	0.0200	*	*	30	0.168	IB1
	IB2	0.0038	0.0125	0.0276	0.0393	0.0308	0.0920	87	0.203	IB2
	IB3	0.0039	0.0133	0.0363	0.0637	0.1027	0.1646	51	0.241	IB3
	IB4	0.0030	0.0119	0.0440	0.0778	*	*	65	0.250	IB4
IC	IC1	0.0051	0.0149	0.0107	0.0121	*	*	16	0.231	IC1
	IC2	0.0043	0.0145	0.0192	0.0237	0.0121	0.0659	67	0.278	IC2
	IC3	0.0040	0.0152	0.0331	0.0513	0.0823	0.1413	57	0.359	IC3
	IC4	0.0040	0.0132	0.0425	0.0666	*	*	48	0.378	IC4
ID	ID1	0.0041	0.0153	0.0398	0.0776	*	*	96	0.077	ID1
	ID2	0.0033	0.0136	0.0459	0.0992	0.1279	0.2635	114	0.089	ID2
	ID3	0.0040	0.0132	0.0487	0.1085	0.3141	*	79	0.091	ID3
	ID4	0.0032	0.0132	0.0512	0.1184	*	*	94	0.090	ID4
IE	IE1	0.0042	0.0139	0.0160	0.0201	*	*	32	0.162	IE1
	IE2	0.0038	0.0125	0.0282	0.0415	0.0321	0.1052	95	0.188	IE2
	IE3	0.0039	0.0134	0.0370	0.0654	0.1451	0.2265	96	0.236	IE3
	IE4	0.0030	0.0119	0.0446	0.0839	*	*	99	0.236	IE4
IF	IF1	0.0051	0.0149	0.0107	0.0121	*	*	16	0.230	IF1
	IF2	0.0043	0.0146	0.0195	0.0242	0.0121	0.0708	64	0.263	IF2
	IF3	0.0040	0.0152	0.0337	0.0526	0.1076	0.1944	110	0.353	IF3
	IF4	0.0040	0.0132	0.0430	0.0676	*	*	74	0.357	IF4
IG	IG1	0.0052	0.0237	0.0384	0.0776	*	*	82	0.074	IG1
	IG2	0.0058	0.0214	0.0427	0.1005	0.1820	*	57	0.080	IG2
	IG3	0.0065	0.0235	0.0455	0.1176	*	*	42	0.079	IG3
	IG4	0.0057	0.0210	0.0486	0.1364	*	*	51	0.080	IG4
IH	IH1	0.0069	0.0242	0.0145	0.0223	*	*	18	0.178	IH1
	IH2	0.0066	0.0240	0.0208	0.0376	0.0567	0.1651	54	0.194	IH2
	IH3	0.0057	0.0235	0.0277	0.0626	0.2924	*	56	0.223	IH3
	IH4	0.0069	0.0225	0.0372	0.0852	*	*	41	0.220	IH4
IJ	IJ1	0.0081	0.0293	0.0094	0.0120	*	*	9	0.262	IJ1
	IJ2	0.0079	0.0257	0.0147	0.0228	0.0315	0.1089	31	0.287	IJ2
	IJ3	0.0059	0.0223	0.0223	0.0431	0.1963	0.3079	63	0.350	IJ3
	IJ4	0.0068	0.0245	0.0341	0.0728	*	*	42	0.343	IJ4
IK	IK1	0.0076	0.0244	0.0157	0.0194	*	*	14	0.160	IK1
	IK2	0.0071	0.0246	0.0216	0.0277	0.0513	0.1569	40	0.173	IK2
	IK3	0.0060	0.0237	0.0277	0.0397	0.2506	*	57	0.202	IK3
	IK4	0.0068	0.0221	0.0366	0.0598	*	*	42	0.198	IK4
IL	IL1	0.0047	0.0256	0.0669	0.1277	*	*	46	0.208	IL1
	IL2	0.0050	0.0264	0.0626	0.1358	0.2452	0.3007	77	0.216	IL2
	IL3	0.0054	0.0201	0.0607	0.1363	*	*	52	0.219	IL3
	IL4	0.0061	0.0212	0.0589	0.1368	*	*	48	0.222	IL4
IM	IM1	0.0060	0.0216	0.0437	0.0861	*	*	23	0.310	IM1
	IM2	0.0049	0.0238	0.0468	0.0941	0.1642	0.2203	53	0.316	IM2
	IM3	0.0053	0.0257	0.0486	0.0973	*	*	51	0.340	IM3
	IM4	0.0063	0.0224	0.0507	0.1041	*	*	46	0.345	IM4

\* Tension reinforcement ruptured, before the event occurred.  
 \*\* M: M/b<sub>v</sub>d<sup>2</sup>f<sub>c</sub>.



- For T-beams flange width is 1500 mm, and height of flange is 150 mm. ( $b/b_w=5.0$  and  $h_f/h=0.25$ )
- Grouping was made with respect to the tension reinforcement ratio. While one group had  $\rho=\rho_{min}$ , second group had  $\rho=\rho_b$ , third group had  $\rho=\rho_m$  (or 0.02). However due to the limitation in bar sizes it was not possible to obtain these ratios exactly. Therefore  $\rho$  values used are not exact, but close to  $\rho_{min}$ ,  $\rho_b$  and  $\rho_m$  (or 0.02).

#### 4.2.2 Discussion of Results

Group IA - Beams with C16 concrete and S220 steel was investigated. Tension reinforcement ratio was minimum ( $\rho=\rho_{min}$  of TS500). The strain capacity of steel was taken as  $\epsilon_{su}=0.1$ . The moment-curvature curves obtained for different  $\rho'/\rho$  ratios (0.0, 0.5, 1.0, and 2.0) are presented in Figure A.1 in Appendix A. As can be seen from this figure, the behaviour is not influenced by the compression reinforcement. Strength and ductility in all beams were almost the same. Only the one in which there was no compression steel exhibited higher ultimate curvature, because since it has no steel at top of the section, neutral axis height decrease and thus tension reinforcement rupture was delayed.

Group IB - Beams of this group were identical with those of IA, the only difference being that the ratio of tension reinforcement which was increased to ( $\rho\cong\rho_b$ ). The moment-curvature curves for Group IB are shown in Figure A.2 in Appendix A. From these curves it can be seen that although increasing compression steel increases the moment capacity, it does not improve the ductility after the ratio of  $\rho'/\rho>0.5$ . On the contrary when  $\rho'/\rho$  increases beyond 0.5, curvature ductility decreases. The curvature ductility ratio of beam IB2 ( $\rho'/\rho = 0.5$ ) is approximately 2.9 times that of the beam IB1 ( $\rho'/\rho = 0.0$ ), but is also 1.7 times that of IB3 ( $\rho'/\rho = 1.0$ ) and 1.3 times that of IB4 ( $\rho'/\rho = 2.0$ ). When we increase the compression steel ratio beyond 0.5, the neutral axis height of sections reduces rapidly and tension steel strain reaches its

ultimate value faster. However it should be noted that even for beam IB3 ( $\rho'/\rho = 1.0$ ), the curvature ductility ratio was about 51.

Group IC - Increasing tensile reinforcement up to the maximum percentage ( $\rho = 0.0191$ ), keeping all other variables identical with those of Group IB, did not change the behaviour. Same trend as observed for Group IB beams were observed. Again the curvature ductility ratio of beam IC2 ( $\rho'/\rho = 0.5$ ) is about 4.2 times that of the beam IC1 ( $\rho'/\rho = 0.0$ ), but is also 1.2 times that of IC3 ( $\rho'/\rho = 1.0$ ) and 1.4 times that of IC4 ( $\rho'/\rho = 2.0$ ). When the limit of 0.5 for the compression steel ratio is exceeded, the ductility does not improve; because tension steel ruptures earlier. Only moment capacities increase with increasing compression steel ratio (See Figure A.3, Appendix A).

Group ID - For beams in this group, C16 concrete and S220 steel were used. Tension reinforcement ratios was minimum ( $\rho = \rho_{\min}$  of TS500). The basic difference with the previous groups was the ultimate steel strain which was increased from  $\epsilon_{su} = 0.1$  to  $\epsilon_{su} = 0.18$ . The moment-curvature curves obtained for different  $\rho'/\rho$  ratios (0.0, 0.5, 1.0, and 2.0) are presented in Figure A.4 in Appendix A. For low tensile reinforcement ( $\rho = \rho_{\min}$ ), strain capacity of steel being 0.18, discussions presented for beams of Group IA were valid. Only the ultimate curvature values and thus the curvature ductility ratios were about twice as much as those of the beams in Group IA with the strain capacity of steel 0.1.

Groups IE & IF - Beams in Groups IE & IF were identical with those of Groups IB & IC respectively. However the strain capacity of reinforcing steel was 0.18. For Groups IB & IC, it was said that ductility of beams did not improve when the compression steel ratio of 0.5 was exceeded. For beams of Groups IE & IF, with strain capacity of steel 0.18, this limit for the compression steel ratio went up to 1.0. That is, till this value, ductility and moment capacity increased with increasing compression steels; but after this value, ductility reduced due to the early rupturing of

the tension reinforcement. This trend was more clear in beams reinforced with the maximum tensile steel ratios (See Figure A.5 & Figure A.6 of Appendix A).

Beams of Groups IG, IH & IJ were same as those of ID, IE & IF respectively. However the yield strength of steel was increased from 220 MPa to 420 MPa, and therefore the values of  $\rho_{min}$ ,  $\rho_c$  and  $\rho_m$  were reduced. Discussions made for Groups ID, IE and IF were also valid for Groups IG, IH & IJ. However all the curvature ductility ratios reduced approximately to one half (See Figures from A.7 to A.9, Appendix A).

Group IK - For beams in this group, concrete strength was increased from 20 to 40 MPa (C40 concrete and S420 steel was used). Tension reinforcement ratios was the limiting value ( $\rho \cong \rho_c$  of TS500). The strain capacity of steel was taken as  $\epsilon_{su} = 0.18$ . When compared with beams of Group IH, it can be seen that increasing the concrete strength from C16 to C40, only for the compression steel ratio of 0.5, there was a little decrease in ductility. For other ratios, the behaviour of beams in this group were same as those of Group IH (See Figure A.10, Appendix A).

Groups IL & IM - Adding flanges whose widths and heights were 1500 and 150 mm respectively to the beams of Groups IH & IJ, T-beams were obtained. All beams in these groups behaved similarly till the clear cover crushing; after that, for the compression steel ratio less than 0.5, as the compression steel increased, ductility increased. But after the ratio of 0.5, as the compression steel increased, ductility decreased (See Figure A.11 & Figure A.12, Appendix A).

#### **4.2.3 Conclusions**

Compression steel increases both the ductility and the moment capacity of beams.

The increase in ductility is evident in the compression steel ratio ( $\rho'/\rho$ ) range between 0 and 0.5. However when ( $\rho'/\rho$ )>0.5, the ductility decreases.

If tension steel ratio ( $\rho$ ) is low, that is near  $\rho_{\min}$ , and the ultimate strain capacity of steel is about 0.1, the designer should be aware of rapid rupturing of tension reinforcement when compression steel ratio ( $\rho'/\rho$ ) is over 0.5.

If it is certain that ultimate strain capacity of steel is near 0.18, and tension steel ratio is between  $\rho_t$  and  $\rho_m$ , ductility increases significantly by increasing compression steel ratio up to 1.0.

For very low ratios of tensile reinforcement and for small strain capacity of steel, compression steel is not very effective.

#### **4.3 Case Study II: Influence of Concrete Strength in R/C Beams**

This study aims to investigate the influence of concrete strength on beam behaviour. For this purpose 33 moment-curvature diagrams for different sections were drawn. The main variables investigated were cross section of beams (T-beam or rectangular), strain hardening starting points and ultimate strains of steel, and tension steel ratios. In each group, beams having different characteristic concrete strengths ( $f_{ck}$ =20, 30, 40 MPa.) were investigated and discussed. The list of all 33 sections with their properties are given in Table 4.3. The results are presented in Table 4.4.

It is well known that in underreinforced beams concrete strength has a negligible effect on the ultimate strength. In this study the overall behaviour at post-yield stages and the ductility were of main interest.

**Table 4.3: List of sections and section properties; Influence of concrete strength in R/C beams**

		Beam Cross Section	Strain Harden. Starts at	Ultimate Strain of Steel	Tension Steel Ratio ( $A_s/b_wd$ )	Concrete Strength							
IIA	IIA1	Rectangular 30x60 cm	$\epsilon_{sp} = 2\epsilon_{sy}$	0.1	$\rho = 0.004$	C20	IIA1						
	IIA2					C30	IIA2						
	IIA3					C40	IIA3						
IIB	IIB1				Rectangular 30x60 cm	$\epsilon_{sp} = 2\epsilon_{sy}$	0.1	$\rho = 0.0091$	C20	IIB1			
	IIB2								C30	IIB2			
	IIB3								C40	IIB3			
IIC	IIC1							Rectangular 30x60 cm	$\epsilon_{sp} = 2\epsilon_{sy}$	0.1	$\rho = 0.0136$	C20	IIC1
	IIC2											C30	IIC2
	IIC3											C40	IIC3
IID	IID1	Rectangular 30x60 cm	$\epsilon_{sp} = 2\epsilon_{sy}$	0.18							$\rho = 0.004$	C20	IID1
	IID2											C30	IID2
	IID3											C40	IID3
IIE	IIE1			Rectangular 30x60 cm	$\epsilon_{sp} = 2\epsilon_{sy}$	0.18	$\rho = 0.0091$				C20	IIE1	
	IIE2										C30	IIE2	
	IIE3										C40	IIE3	
IIF	IIF1						Rectangular 30x60 cm	$\epsilon_{sp} = 2\epsilon_{sy}$	0.18	$\rho = 0.0136$	C20	IIF1	
	IIF2										C30	IIF2	
	IIF3										C40	IIF3	
IIG	IIG1	T-beam $b_f=1500$ mm $h_f=150$ mm	$\epsilon_{sp} = 10\epsilon_{sy}$							0.18	$\rho = 0.004$	C20	IIG1
	IIG2											C30	IIG2
	IIG3											C40	IIG3
IIH	IIH1			T-beam $b_f=1500$ mm $h_f=150$ mm	$\epsilon_{sp} = 10\epsilon_{sy}$	0.18					$\rho = 0.0091$	C20	IIH1
	IIH2											C30	IIH2
	IIH3											C40	IIH3
IIJ	IIJ1						T-beam $b_f=1500$ mm $h_f=150$ mm	$\epsilon_{sp} = 10\epsilon_{sy}$	0.18		$\rho = 0.0136$	C20	IIJ1
	IIJ2											C30	IIJ2
	IIJ3											C40	IIJ3
IIK	IIK1	T-beam $b_f=1500$ mm $h_f=150$ mm	$\epsilon_{sp} = 5\epsilon_{sy}$							0.18	$\rho = 0.0091$	C20	IIK1
	IIK2											C30	IIK2
	IIK3											C40	IIK3
IIIL	IIIL1			T-beam $b_f=1500$ mm $h_f=150$ mm	$\epsilon_{sp} = 5\epsilon_{sy}$	0.18					$\rho = 0.0136$	C20	IIIL1
	IIIL2											C30	IIIL2
	IIIL3											C40	IIIL3

**Table 4.4: Results; Influence of concrete strength in R/C beams**

		Curvature (rad/m)						Curvature ductility ratio	Maximum M**	
		Yield A <sub>s</sub>	Str. Hard. A <sub>s</sub>	Cover Crush	Core Crush	Yield A <sub>s</sub> '	Str. Hard. A <sub>s</sub> '			
IIA	IIA1	0.0064	0.0099	0.0369	0.0790	0.1093	0.1875	29	181.3	IIA1
	IIA2	0.0053	0.0093	0.0482	0.0938	0.1709	*	35	183.6	IIA2
	IIA3	0.0048	0.0094	0.0582	0.1035	*	*	36	181.6	IIA3
IIB	IIB1	0.0068	0.0118	0.0207	0.0367	0.0529	0.0789	46	371.1	IIB1
	IIB2	0.0055	0.0097	0.0275	0.0480	0.0713	0.1142	38	392.5	IIB2
	IIB3	0.0057	0.0124	0.0334	0.0542	0.0936	0.1437	33	404.4	IIB3
IIC	IIC1	0.0064	0.0128	0.0152	0.0231	0.0313	0.0531	36	519.7	IIC1
	IIC2	0.0067	0.0117	0.0204	0.0293	0.0484	0.0769	42	546.5	IIC2
	IIC3	0.0061	0.0116	0.0249	0.0374	0.0595	0.1007	39	569.7	IIC3
IID	IID1	0.0064	0.0099	0.0374	0.0808	0.1311	0.2037	56	177.9	IID1
	IID2	0.0053	0.0093	0.0491	0.0983	0.2427	0.3139	64	182.9	IID2
	IID3	0.0048	0.0094	0.0595	0.1094	0.3149	*	65	182.2	IID3
IIE	IIE1	0.0068	0.0118	0.0208	0.0372	0.0548	0.0876	48	353.8	IIE1
	IIE2	0.0055	0.0097	0.0277	0.0489	0.0789	0.1274	72	368.8	IIE2
	IIE3	0.0057	0.0124	0.0338	0.0552	0.1058	0.1846	73	383.6	IIE3
IIF	IIF1	0.0064	0.0128	0.0153	0.0233	0.0320	0.0548	37	503.7	IIF1
	IIF2	0.0067	0.0117	0.0205	0.0296	0.0499	0.0806	43	523.0	IIF2
	IIF3	0.0061	0.0116	0.0252	0.0380	0.0617	0.1066	57	539.2	IIF3
IIG	IIG1	0.0064	0.0428	0.0380	0.0817	0.1333	*	57	177.3	IIG1
	IIG2	0.0053	0.0440	0.0499	0.0992	0.2441	*	64	182.7	IIG2
	IIG3	0.0048	0.0467	0.0601	0.1104	0.3154	*	65	181.9	IIG3
IIH	IIH1	0.0068	0.0450	0.0210	0.0379	0.0566	0.2032	49	349.4	IIH1
	IIH2	0.0055	0.0429	0.0281	0.0498	0.0808	0.2600	72	365.5	IIH2
	IIH3	0.0057	0.0426	0.0343	0.0593	0.1077	0.3141	73	381.0	IIH3
IIJ	IIJ1	0.0064	0.0484	0.0153	0.0235	0.0350	0.1464	37	495.9	IIJ1
	IIJ2	0.0067	0.0462	0.0207	0.0333	0.0517	0.1906	44	516.1	IIJ2
	IIJ3	0.0061	0.0450	0.0254	0.0387	0.0655	0.2343	57	533.5	IIJ3
IIK	IIK1	0.0052	0.0199	0.0638	0.1345	0.2455	0.3040	74	392.9	IIK1
	IIK2	0.0049	0.0233	0.0818	0.1582	0.3087	*	64	406.3	IIK2
	IIK3	0.0065	0.0193	0.0973	0.1707	*	*	51	414.2	IIK3
IIL	IIL1	0.0052	0.0253	0.0491	0.0972	0.1654	0.2183	50	552.2	IIL1
	IIL2	0.0053	0.0200	0.0638	0.1168	0.2337	0.2800	67	576.6	IIL2
	IIL3	0.0070	0.0213	0.0763	0.1288	0.2814	0.3311	54	595.8	IIL3

\* Tension reinforcement ruptured, before the event occurred.  
 \*\* M (in kN.m)

### 4.3.1 Assumptions

- For all beams S420 steel is used as reinforcements.
- In T-beams width of flange was 1500 mm and the height of flange was 150 mm. ( $b/b_w=5.0$  and  $h_f/h=0.25$ )
- Throughout this case study, three different ratios of tension reinforcement were considered: 0.004, 0.0091 and 0.0136. The first ratio,  $\rho=0.004$  corresponds to minimum ratio given in TS500 for S420 and C40; the second ratio  $\rho=0.0091$  corresponds to the limiting ratio  $\rho_l$  for S420 & C20. The third ratio,  $\rho=0.0136$  corresponds to  $\rho_m$  given in TS500 for the material combination S420 & C20.
- Web reinforcement ratio ( $\rho_w$ ) for all beams was taken as 0.0044 ( $\Phi$  10/120 mm).
- Compression steel ratio was equal to 0.5 for all sections.

### 4.3.2 Discussion of Results

Group IIA - Cross section was rectangular. Tensile reinforcement ratio was 0.004. Strain capacity and strain hardening starting point of steel was 0.1 and 0.0042 ( $\epsilon_{sp}=2\epsilon_{sy}$ ) respectively. The moment-curvature curves obtained for different concrete strengths ( $f_{ck} = 20; 30; 40$  MPa) are presented in Figure A.13 of Appendix A. Behaviour of all beams resemble to each other. The ductility ratios were almost the same. When the concrete strength was increased, yielding, strain hardening and rupturing of tension steel occurred earlier (since neutral axis heights get smaller); crushing of core concrete and yielding of compression steel was delayed.

Group IIB - Beams of this group were identical with those of IIA, the only difference was that the ratio of tension reinforcement which was increased to 0.0091. It is observed that as the concrete strength increased, ultimate moment capacity of beam increased, but curvature ductility ratio decreased. Ultimate curvature of the beams IIB2 ( $f_{ck} = 30$  MPa) and IIB3 ( $f_{ck} = 40$  MPa) were almost the same. Ultimate



curvature of IIB1 ( $f_{ck} = 20$  MPa) was about 50% greater than that of the others. Ductility was not improved when the concrete strength was increased for the beams having the steel characteristics and reinforcement percentage stated above, since neutral axis height decreased more rapidly and tension steel ruptured earlier (See Figure A.14, Appendix A).

Group IIC - These beams were same as those of Groups IIA & IIB, but tensile reinforcement ratio was increased to 0.0136. Both the moment capacity and the ductility increased, when the concrete strength was increased from 20 MPa to 30 MPa. However again a slight decrease in ductility was observed when the concrete strength increased from 30 MPa to 40 MPa (See Figure A.15, Appendix A).

Group IID - Cross section was rectangular. Strain hardening starting point of steel was same as before, 0.0042 ( $\epsilon_{sp}=2\epsilon_{sy}$ ). However ultimate strain capacity of steel was increased to 0.18. The tensile reinforcement ratio was 0.004. The moment-curvature diagrams obtained for different concrete strengths ( $f_{ck} = 20; 30; 40$  MPa) are presented in Figure A.16 in Appendix A. When these curves are compared with those in Figure A.13 (Group IIA), it will be seen that when the tension reinforcement ratio is very low, increasing the ultimate strain of steel from 0.1 to 0.18 did not change the general trend, i.e concrete strength did not change the behaviour. However comparing Figures A.13 & A.16, it will be seen that ultimate curvature increased significantly when the ultimate steel strain was increased.

Group IIE - The beams were identical with those of Group IIB ( $\rho=0.0091$ ), the only difference was that the strain capacity of steel was increased from 0.1 to 0.18. It was observed that, different from beams of Group IIB, as the concrete strength increased, the curvature ductility ratio of beams increased. The curvature ductility ratio of the beam with concrete strength of 30 MPa was 50% greater than that of the one with concrete strength of 20 MPa (See Figure A.17, Appendix A).



Group IIF - Tensile reinforcement ratio was 0.0136. Strain capacity of steel was 0.18. Other variables were same as in the previous paragraphs. When concrete strength was increased from 20 MPa, to first 30 MPa, then 40 MPa, there was considerable improvement in both the moment capacity and the ductility. The curvature ductility ratio of IIF2 ( $f_{ck} = 30$  MPa) was 16% greater than that of IIF1 ( $f_{ck} = 20$  MPa), the curvature ductility ratio of IIF3 ( $f_{ck} = 40$  MPa) was 33% greater than that of IIF2 (See Figure A.18, Appendix A).

Groups from IIG to IIJ - Beams of these groups were same as those of Groups IID, IIE & IIF, the only difference being the strain hardening of steel. In Groups IIG, IIH & IIJ strain hardening started at a strain 10 times the yield strain. No significant changes were observed in the behaviour due to the change of strain hardening strain. Ultimate moments and curvatures of the beams in these groups were almost the same as those in the previous groups (See Figures from A.19 to A.21, Appendix A).

Groups IIK & IIL - These were T-beams. Flange height and width were 150 and 1500 mm respectively. Strain capacity and strain hardening starting point of steel was 0.18 and 0.01 ( $\epsilon_{sp}=5\epsilon_{sy}$ ) respectively. Tensile reinforcement ratio was 0.0091 for Group IIK, and 0.0136 for Group IIL. Beams of Group IIK behaved almost the same regardless of the concrete strength. However in Group IIL, increasing concrete strength resulted in increased ductility (See Figure A.22 & Figure A.23, Appendix A).

### 4.3.3 Conclusions

An increase in the concrete strength increases the ductility only if tension steel ratio and ultimate strain capacity of steel are high. High means above limiting ratio ( $\rho_l$ ), and 0.18 for the capacity of ultimate strain. Otherwise ductility can decrease with increasing concrete strength.

An increase in the concrete strength increases the ultimate moment capacity a little when the tension steel ratio is above the limiting value,  $\rho_l$ .

Beams made of higher strength concrete ( $f_{ck} = 40$  MPa), with low tension steel ratio ( $\rho_{min} < \rho < \rho_l$ ) exhibited less ductility.

For low tension steel ratios, increasing concrete strength did not change the behaviour. Because since tension steel was insufficient, it dominated both the behaviour and the failure. For this kind of beams, the designer should be careful of sudden rupturing of tension steel.

#### 4.4 Case Study III: Influence of Confinement in R/C Beams

This study aims to investigate the influence of confinement (transverse steel reinforcement) on the beam behaviour. For this purpose 44 moment-curvature diagrams for different sections were drawn. The main variables investigated were concrete and steel strengths, ultimate strain of steel, and tensile reinforcement ratios. In each group, beams having different confinement (Ties:  $\varnothing 8/110$ ;  $\varnothing 8/80$ ;  $\varnothing 10/100$ ;  $\varnothing 12/120$  mm) were investigated. The list of all 44 sections with their properties are given in Table 4.5. The results are presented in Table 4.6.

##### 4.4.1 Assumptions

- Unconfined concrete strength ( $f_c$ ) for all sections is equal to 20 MPa.
- Compression steel ratios of all sections are 0.5. ( $\rho'/\rho=0.5$ )
- Ties:  $\varnothing 8/110$ ;  $\varnothing 8/80$ ;  $\varnothing 10/100$ ;  $\varnothing 12/120$  correspond to  $\rho_w = 0.0030$ ; 0.0042; 0.0052; 0.0063 respectively.

**Table 4.5: List of sections and section properties; Influence of confinement in R/C beams**

		Steel & concrete properties	Ultimate strain of longitudinal steel	Tension steel ratio ( $A_s/b_w/d$ )	Ties			
IIIA	IIIA1	S220 - C20	0.1	0.0061 (low)	φ 8/110 mm	IIIA1		
	IIIA2				φ 8/80 mm	IIIA2		
	IIIA3				φ 10/100 mm	IIIA3		
	IIIA4				φ 12/120 mm	IIIA4		
IIIB	IIIB1			S220 - C20	0.1	0.0190 (high)	φ 8/110 mm	IIIB1
	IIIB2						φ 8/80 mm	IIIB2
	IIIB3						φ 10/100 mm	IIIB3
	IIIB4						φ 12/120 mm	IIIB4
IIIC	IIIC1	S220 - C20	0.18			0.0061 (low)	φ 8/110 mm	IIIC1
	IIIC2						φ 8/80 mm	IIIC2
	IIIC3						φ 10/100 mm	IIIC3
	IIIC4						φ 12/120 mm	IIIC4
IIID	IIID1		S220 - C20	0.18	0.0190 (high)	φ 8/110 mm	IIID1	
	IIID2					φ 8/80 mm	IIID2	
	IIID3					φ 10/100 mm	IIID3	
	IIID4					φ 12/120 mm	IIID4	
IIIE	IIIE1	S420 - C20		0.1	0.0037 (low)	Φ 8/110 mm	IIIE1	
	IIIE2					Φ 8/80 mm	IIIE2	
	IIIE3					Φ 10/100 mm	IIIE3	
	IIIE4					Φ 12/120 mm	IIIE4	
IIIF	IIIF1		S420 - C20		0.1	0.0136 (high)	Φ 8/110 mm	IIIF1
	IIIF2						Φ 8/80 mm	IIIF2
	IIIF3						Φ 10/100 mm	IIIF3
	IIIF4						Φ 12/120 mm	IIIF4
IIIG	IIIG1	S420 - C20		0.18	0.0037 (low)	Φ 8/110 mm	IIIG1	
	IIIG2					Φ 8/80 mm	IIIG2	
	IIIG3					Φ 10/100 mm	IIIG3	
	IIIG4					Φ 12/120 mm	IIIG4	
IIIH	IIIH1		S420 - C20	0.18	0.0136 (high)	Φ 8/110 mm	IIIH1	
	IIIH2					Φ 8/80 mm	IIIH2	
	IIIH3					Φ 10/100 mm	IIIH3	
	IIIH4					Φ 12/120 mm	IIIH4	
IIIJ	IIIJ1	S420 - C20 T-beam $b_f = 1500$ mm $h_f = 150$ mm		0.12	0.0037 (low)	Φ 8/110 mm	IIIJ1	
	IIIJ2					Φ 8/80 mm	IIIJ2	
	IIIJ3					Φ 10/100 mm	IIIJ3	
	IIIJ4					Φ 12/120 mm	IIIJ4	
IIIK	IIIK1		S420 - C20 T-beam $b_f = 1500$ mm $h_f = 150$ mm		0.12	0.0287 (high)	Φ 8/110 mm	IIIK1
	IIIK2						Φ 8/80 mm	IIIK2
	IIIK3						Φ 10/100 mm	IIIK3
	IIIK4						Φ 12/120 mm	IIIK4
IIIL	IIIL1	S420 - C20		0.12	Multi Layered Sections	Φ 8/110 mm	IIIL1	
	IIIL2					Φ 8/80 mm	IIIL2	
	IIIL3					Φ 10/100 mm	IIIL3	
	IIIL4					Φ 12/120 mm	IIIL4	

**Table 4.6: Results; Influence of confinement in R/C beams**

		Curvature (rad/m)						Curvature ductility ratio	Maximum M**	
		Yield A <sub>s</sub>	Str. Hard. A <sub>s</sub>	Cover Crush	Core Crush	Yield A <sub>s</sub> '	Str. Hard. A <sub>s</sub> '			
IIIA	IIIA1	0.0033	0.0134	0.0443	0.0891	0.1032	0.1719	58	0.091	IIIA1
	IIIA2	0.0033	0.0134	0.0444	0.0893	0.1038	*	54	0.090	IIIA2
	IIIA3	0.0033	0.0134	0.0444	0.0872	0.1069	*	56	0.092	IIIA3
	IIIA4	0.0033	0.0134	0.0445	0.0848	0.1072	*	57	0.093	IIIA4
IIIB	IIIB1	0.0041	0.0141	0.0231	0.0303	0.0204	0.0703	63	0.220	IIIB1
	IIIB2	0.0042	0.0141	0.0232	0.0305	0.0205	0.0726	74	0.230	IIIB2
	IIIB3	0.0042	0.0142	0.0233	0.0307	0.0206	0.0748	77	0.234	IIIB3
	IIIB4	0.0042	0.0142	0.0234	0.0310	0.0207	0.0805	79	0.239	IIIB4
IIIC	IIIC1	0.0033	0.0135	0.0455	0.0971	0.1179	0.2212	121	0.087	IIIC1
	IIIC2	0.0033	0.0135	0.0455	0.0972	0.1187	0.2300	114	0.090	IIIC2
	IIIC3	0.0033	0.0135	0.0456	0.0935	0.1233	0.2663	110	0.091	IIIC3
	IIIC4	0.0033	0.0135	0.0457	0.0912	0.1290	0.2756	107	0.092	IIIC4
IIID	IIID1	0.0041	0.0141	0.0236	0.0315	0.0208	0.0791	57	0.208	IIID1
	IIID2	0.0042	0.0142	0.0237	0.0316	0.0209	0.0820	76	0.215	IIID2
	IIID3	0.0042	0.0142	0.0239	0.0319	0.0210	0.0848	83	0.218	IIID3
	IIID4	0.0042	0.0142	0.0240	0.0322	0.0211	0.0917	90	0.221	IIID4
IIIE	IIIE1	0.0054	0.0248	0.0397	0.0820	0.1196	*	35	0.088	IIIE1
	IIIE2	0.0054	0.0249	0.0398	0.0863	0.1212	*	30	0.086	IIIE2
	IIIE3	0.0054	0.0249	0.0399	0.0875	0.1344	*	32	0.087	IIIE3
	IIIE4	0.0054	0.0250	0.0400	0.0846	0.1567	*	33	0.088	IIIE4
IIIF	IIIF1	0.0063	0.0232	0.0152	0.0232	0.0314	0.0935	29	0.268	IIIF1
	IIIF2	0.0064	0.0234	0.0153	0.0262	0.0319	0.1030	40	0.275	IIIF2
	IIIF3	0.0064	0.0237	0.0154	0.0265	0.0324	0.1080	44	0.279	IIIF3
	IIIF4	0.0064	0.0239	0.0155	0.0268	0.0350	0.1129	49	0.283	IIIF4
IIIG	IIIG1	0.0054	0.0249	0.0401	0.0882	0.1347	0.2994	71	0.085	IIIG1
	IIIG2	0.0054	0.0249	0.0402	0.0903	0.1447	0.3516	65	0.087	IIIG2
	IIIG3	0.0054	0.0250	0.0403	0.0895	0.1599	*	64	0.088	IIIG3
	IIIG4	0.0054	0.0251	0.0404	0.0866	0.1942	*	62	0.088	IIIG4
IIIH	IIIH1	0.0063	0.0232	0.0152	0.0232	0.0317	0.0982	29	0.265	IIIH1
	IIIH2	0.0064	0.0234	0.0153	0.0263	0.0322	0.1091	41	0.266	IIIH2
	IIIH3	0.0064	0.0237	0.0154	0.0266	0.0348	0.1147	45	0.269	IIIH3
	IIIH4	0.0064	0.0239	0.0155	0.0269	0.0355	0.1203	48	0.272	IIIH4
IIIJ	IIIJ1	0.0077	0.0226	0.1094	*	*	*	27	0.095	IIIJ1
	IIIJ2	0.0077	0.0226	0.1094	*	*	*	27	0.095	IIIJ2
	IIIJ3	0.0076	0.0226	0.1091	*	*	*	27	0.095	IIIJ3
	IIIJ4	0.0076	0.0227	0.1099	*	*	*	27	0.095	IIIJ4
IIIK	IIIK1	0.0059	0.0211	0.0290	0.0442	0.0772	0.1043	18	0.595	IIIK1
	IIIK2	0.0059	0.0212	0.0290	0.0479	0.0775	0.1088	19	0.595	IIIK2
	IIIK3	0.0059	0.0212	0.0290	0.0480	0.0789	0.1124	20	0.596	IIIK3
	IIIK4	0.0059	0.0212	0.0291	0.0444	0.0795	0.1148	21	0.597	IIIK4
IIIL	IIIL1	0.0060	0.0251	0.0137	0.0187	0.0201	0.0757	14	0.202	IIIL1
	IIIL2	0.0061	0.0254	0.0138	0.0188	0.0203	0.0784	36	0.203	IIIL2
	IIIL3	0.0061	0.0244	0.0138	0.0190	0.0205	0.0798	36	0.205	IIIL3
	IIIL4	0.0061	0.0247	0.0139	0.0191	0.0207	0.0830	36	0.206	IIIL4

\* Tension reinforcement ruptured, before the event occurred.  
\*\* M:  $M/b_w d^2 f_c$

#### 4.4.2 Discussion of Results

Group IIIA - In this group beams, concrete was C20 concrete and steel was S220. Tensile reinforcement ratio was 0.0061 (low). Strain capacity of steel was 0.1. The moment-curvature diagrams obtained for different tie ratios (Ties:  $\varnothing 8/110$ ,  $\varnothing 8/80$ ,  $\varnothing 10/100$ ,  $\varnothing 12/120$  mm) are presented in Figure A.24 in Appendix A. The behaviour of all beams were almost identical. Their ductility ratios, yield and ultimate moments were almost the same. Diagrams of beams were absolutely same till the initiation of core crushing. Tensile reinforcements in all beams ruptured before the confinement became fully effective. Ductility ratio of IIIA1 (Ties:  $\varnothing 8/110$ ) was somewhat higher than the others in the same group. In less confined sections the neutral axis was lower as compared to the ones with higher confinement ratios, which resulted in lower strains in tension reinforcement. Therefore in less confined sections, rupture of tension reinforcement was delayed.

Group IIIB - Beams of this group were identical with those of IIIA, the only difference being that the ratio of tension reinforcement, which was increased to 0.019 (high). Beams exhibited identical behaviour regardless of the confinement ratio, until the clear cover crushed. After this point, as the confinement increased, ductility increased (See Figure A.25, Appendix A). Increase in ductility ratio is more clear comparing IIIB1 (Ties:  $\varnothing 8/110$ ) with IIIB2 (Ties:  $\varnothing 8/80$ ) (17% greater due to increased confinement), but not so clear comparing IIIB2 with IIIB3 (Ties:  $\varnothing 10/100$ ) and IIIB3 with IIIB4 (Ties:  $\varnothing 12/120$ ). In beams having low confinement ratios, there is also strength decay beyond the cover crushing.

Groups IIIC & IIID - Beams in Groups IIIC & IIID were identical with those of Groups IIIA & IIIB respectively. However the strain capacity of reinforcing steel was 0.18 in the examples of these groups. The discussions presented for Group IIIB are valid also for beams reinforced with steel having 0.18 of strain capacity (See Figure A.26 & Figure A.27, Appendix A). However for low tensile reinforcement

ratios, the curvature ductility ratios of beams with steel of higher strain capacity ( $\epsilon_{su}=0.18$ ) were about 100% higher than beams reinforced with steel of lower strain capacity ( $\epsilon_{su}=0.1$ ). On the other hand for high tensile reinforcement ratios, the curvature ductilities of beams with different confinement were almost same. Comparing Group IIIB with Group IIID (everything is same only ultimate strains are different), it was observed that ultimate moments of sections where strain capacity of steel is 0.1, are greater than those beams with steel of higher strain capacity ( $\epsilon_{su}=0.18$ ). Ultimate strength for both steels ( $\epsilon_{su}=0.1$  & 0.18) was 525 MPa. This means that for steel with  $\epsilon_{su}=0.1$ , the slope of the strain hardening portion is greater. This increased slope resulted in higher moment capacity.

Beams of Groups from IIIE to IIIH - Groups IIIE, IIIF, IIIG, IIIH were same as those of IIIA, IIIB, IIIC, IIID respectively. However the yield strength of steel was increased from 220 MPa to 420 MPa. As a result of this, low tensile reinforcement ratios and high tensile reinforcement ratios were reduced to 0.0037 and 0.0136 respectively. The general discussions made in the previous three paragraphs are valid for these groups also. Curvature ductility ratios of the beams having steel strength of 420 MPa were almost 40% less than those of the sections with a steel strength of 220 MPa (See Figures from A.28 to A.31, Appendix A).

Groups IIIJ & IIIK - These were T-beams. Flange height and widths were 150 and 1500 mm respectively. Strain capacity of steel was 0.12. Tensile reinforcement ratios were 0.0037 (low) for Group IIIK and 0.0287 (high) for Group IIIJ. Moment-curvature diagrams of sections with various confinement ratios, showed identical behaviour when the tensile reinforcement ratio was low. For beams with high reinforcement ratio, confinement seems to have little effect. This is not surprising, since the compression zone in general remains in the unconfined flange. Therefore confinement of web only, does not improve the behaviour (See Figure A.32 & Figure A.33, Appendix A).

Group III L - In beams of this group, reinforcement was placed at different levels (multi-layer). Concrete was C20 and the steel was S420 type. Strain capacity of steel was 0.12. All bars were 20 mm in diameter. There were 4 bars at the bottom layer, and 2 at the top. Also there were 2 intermediate steel layers, each with 2 bars. Beams with different confinement ratios showed almost the same behaviour, except the one which had very low ratio of confinement (III L1). Curvature ductility ratio of III L1 (Ties:  $\varnothing 8/110$ ) was 60% less than those of the others (See Figure A.34, Appendix A).

#### 4.4.3 Conclusions

Confinement in general increases the ductility of R/C beams.

If tension reinforcement ratios are low, steel ruptures before the confinement starts to be fully effective. Therefore in beams with low ratios of tensile reinforcement confinement does not improve the ductility.

Up until cover crushing (the point where there is a sudden decrease in diagram), all beams behaved almost the same. The confinement became effective only after cover crushing. Therefore it would not be wrong to say that confinement does not improve ultimate moment capacity of beams.

It is clear that confinement does not improve neither the moment capacity nor the ductility in T-beams. Since the compression zone falls into the unconfined flange, such a behaviour is not surprising.

Although confining the beams with transverse reinforcement improves the behaviour, excessive amount of confinement does not improve the behaviour further.



## 4.5 Case Study IV: Influence of Steel Model in R/C Beams

This study aims to investigate the influence of steel model on beam behaviour. For this purpose 36 moment-curvature diagrams for different sections were drawn. The investigation consists of two parts. In the first part (Groups from IVA to IVF), 12 examples were solved by keeping ultimate strain as 0.1 and changing strain hardening starting point; In second part (Groups from IVG to IVM), 24 examples were solved by keeping strain hardening starting point as 5 times of yield strain and changing ultimate strain values. Variables investigated at both parts of the study were tension steel ratio, steel and concrete strengths. In first part, in each group, 2 beams having different strain hardening strains ( $\epsilon_{sp}=2\epsilon_{sy}$ ;  $10\epsilon_{sy}$ ) were investigated. In second part, in each group, 4 beams having different strain capacities of steels ( $\epsilon_{su}=0.05$ ; 0.10; 0.15; 0.20) were investigated and discussed. The list of all 36 sections with their properties are given in Table 4.7. The results are presented in Table 4.8.

### 4.5.1 Assumptions

- Web reinforcement ratio ( $\rho_w$ ) for all beams was taken equal to 0.0044 ( $\Phi$  10/120 mm).
- Compression steel ratio was kept constant for all beams of this case study ( $\rho'/\rho=0.5$ ).



**Table 4.7:** List of sections and section properties; Influence of steel model in R/C beams

		Steel Model	Steel & Concrete Strengths	Tension steel ratio ( $A_s/b_w/d$ )	Steel Model	
IVA	IVA1	Keeping $\epsilon_{su} = 0.1$ Changing $\epsilon_{sp}$	S220 - C20 $\epsilon_{sy} = 0.0011$	0.0055	$\epsilon_{sp} = 2\epsilon_{sy}$	IVA1
	IVA2				$\epsilon_{sp} = 10\epsilon_{sy}$	IVA2
IVB	IVB1			0.0190	$\epsilon_{sp} = 2\epsilon_{sy}$	IVB1
	IVB2				$\epsilon_{sp} = 10\epsilon_{sy}$	IVB2
IVC	IVC1		S420 - C20 $\epsilon_{sy} = 0.0021$	0.0048	$\epsilon_{sp} = 2\epsilon_{sy}$	IVC1
	IVC2				$\epsilon_{sp} = 10\epsilon_{sy}$	IVC2
IVD	IVD1			0.0136	$\epsilon_{sp} = 2\epsilon_{sy}$	IVD1
	IVD2				$\epsilon_{sp} = 10\epsilon_{sy}$	IVD2
IVE	IVE1		S420 - C35 $\epsilon_{sy} = 0.0021$	0.0048	$\epsilon_{sp} = 2\epsilon_{sy}$	IVE1
	IVE2				$\epsilon_{sp} = 10\epsilon_{sy}$	IVE2
IVF	IVF1	0.0190		$\epsilon_{sp} = 2\epsilon_{sy}$	IVF1	
	IVF2			$\epsilon_{sp} = 10\epsilon_{sy}$	IVF2	
IVG	IVG1	Keeping $\epsilon_{sp} = 5\epsilon_{sy}$ Changing $\epsilon_{su}$	S220 - C20 $\epsilon_{sy} = 0.0011$	0.0055	$\epsilon_{su} = 0.05$	IVG1
	IVG2				$\epsilon_{su} = 0.10$	IVG2
	IVG3				$\epsilon_{su} = 0.15$	IVG3
	IVG4				$\epsilon_{su} = 0.20$	IVG4
IVH	IVH1		0.0190	$\epsilon_{su} = 0.05$	IVH1	
	IVH2			$\epsilon_{su} = 0.10$	IVH2	
	IVH3			$\epsilon_{su} = 0.15$	IVH3	
	IVH4			$\epsilon_{su} = 0.20$	IVH4	
IVJ	IVJ1		S420 - C20 $\epsilon_{sy} = 0.0021$	0.0048	$\epsilon_{su} = 0.05$	IVJ1
	IVJ2				$\epsilon_{su} = 0.10$	IVJ2
	IVJ3	$\epsilon_{su} = 0.15$			IVJ3	
	IVJ4	$\epsilon_{su} = 0.20$			IVJ4	
IVK	IVK1	0.0136	$\epsilon_{su} = 0.05$	IVK1		
	IVK2		$\epsilon_{su} = 0.10$	IVK2		
	IVK3		$\epsilon_{su} = 0.15$	IVK3		
	IVK4		$\epsilon_{su} = 0.20$	IVK4		
IVL	IVL1	S420 - C35 $\epsilon_{sy} = 0.0021$	0.0048	$\epsilon_{su} = 0.05$	IVL1	
	IVL2			$\epsilon_{su} = 0.10$	IVL2	
	IVL3			$\epsilon_{su} = 0.15$	IVL3	
	IVL4			$\epsilon_{su} = 0.20$	IVL4	
IVM	IVM1	0.0190	$\epsilon_{su} = 0.05$	IVM1		
	IVM2		$\epsilon_{su} = 0.10$	IVM2		
	IVM3		$\epsilon_{su} = 0.15$	IVM3		
	IVM4		$\epsilon_{su} = 0.20$	IVM4		

TC YÜKSEKÖĞRETİM VE ARAŞTIRMA BAKANLIĞI  
DOKÜMANİZASYON MERKEZİ

**Table 4.8: Results; Influence of steel model in R/C beams**

		Curvature (rad/m)						Curvature ductility ratio	Maximum M**	
		Yield A <sub>s</sub>	Str. Hard. A <sub>s</sub>	Cover Crush	Core Crush	Yield A <sub>s</sub> '	Str. Hard. A <sub>s</sub> '			
IVA	IVA1	0.0036	0.0053	0.0462	0.0960	0.1091	0.1271	51	0.084	IVA1
	IVA2	0.0036	0.0256	0.0472	0.0968	0.1142	*	51	0.083	IVA2
IVB	IVB1	0.0042	0.0077	0.0226	0.0299	0.0172	0.0423	71	0.229	IVB1
	IVB2	0.0042	0.0245	0.0245	0.0320	0.0214	0.1183	72	0.224	IVB2
IVC	IVC1	0.0055	0.0120	0.0328	0.0688	0.1025	0.1750	32	0.112	IVC1
	IVC2	0.0055	0.0426	0.0338	0.0703	0.1050	*	32	0.112	IVC2
IVD	IVD1	0.0064	0.0128	0.0152	0.0231	0.0313	0.0531	36	0.276	IVD1
	IVD2	0.0064	0.0483	0.0153	0.0235	0.0350	0.1377	37	0.270	IVD2
IVE	IVE1	0.0052	0.0092	0.0477	0.0856	0.1817	*	36	0.066	IVE1
	IVE2	0.0052	0.0435	0.0491	0.0893	0.1822	*	36	0.066	IVE2
IVF	IVF1	0.0077	0.0124	0.0176	0.0229	0.0365	0.0637	31	0.225	IVF1
	IVF2	0.0077	0.0464	0.0178	0.0234	0.0403	0.1476	32	0.220	IVF2
IVG	IVG1	0.0036	0.0119	0.0440	0.0825	0.0894	*	27	0.085	IVG1
	IVG2	0.0036	0.0120	0.0466	0.0963	0.1096	*	51	0.083	IVG2
	IVG3	0.0036	0.0120	0.0475	0.0990	0.1215	0.2303	81	0.083	IVG3
	IVG4	0.0036	0.0120	0.0481	0.1031	0.1342	0.2713	110	0.081	IVG4
IVH	IVH1	0.0042	0.0141	0.0222	0.0286	0.0172	0.0616	37	0.252	IVH1
	IVH2	0.0042	0.0141	0.0232	0.0306	0.0205	0.0734	72	0.228	IVH2
	IVH3	0.0042	0.0142	0.0236	0.0314	0.0208	0.0813	69	0.217	IVH3
	IVH4	0.0042	0.0142	0.0239	0.0319	0.0210	0.0841	67	0.212	IVH4
IVJ	IVJ1	0.0055	0.0245	0.0327	0.0625	0.0829	*	18	0.115	IVJ1
	IVJ2	0.0055	0.0246	0.0333	0.0692	0.1033	*	32	0.112	IVJ2
	IVJ3	0.0055	0.0246	0.0335	0.0703	0.1076	0.2720	57	0.111	IVJ3
	IVJ4	0.0055	0.0246	0.0335	0.0709	0.1098	0.2867	81	0.108	IVJ4
IVK	IVK1	0.0064	0.0263	0.0153	0.0235	0.0315	0.0923	27	0.289	IVK1
	IVK2	0.0064	0.0264	0.0153	0.0235	0.0321	0.1026	36	0.274	IVK2
	IVK3	0.0064	0.0264	0.0153	0.0235	0.0324	0.1069	37	0.268	IVK3
	IVK4	0.0064	0.0264	0.0153	0.0235	0.0325	0.1093	37	0.265	IVK4
IVL	IVL1	0.0052	0.0249	0.0466	0.0814	*	*	18	0.066	IVL1
	IVL2	0.0052	0.0251	0.0482	0.0861	0.1819	*	36	0.066	IVL2
	IVL3	0.0052	0.0251	0.0486	0.0901	0.2405	*	53	0.066	IVL3
	IVL4	0.0052	0.0251	0.0489	0.0910	0.2499	*	72	0.065	IVL4
IVM	IVM1	0.0077	0.0260	0.0178	0.0234	0.0361	0.0997	19	0.237	IVM1
	IVM2	0.0077	0.0261	0.0178	0.0234	0.0373	0.1121	31	0.223	IVM2
	IVM3	0.0077	0.0261	0.0178	0.0234	0.0394	0.1276	32	0.217	IVM3
	IVM4	0.0077	0.0262	0.0178	0.0234	0.0397	0.1313	31	0.215	IVM4

\* Tension reinforcement ruptured, before the event occurred.  
 \*\* M:  $M/b_w d^2 f_c$

#### 4.5.2 Discussion of Results

Group IVA - Beams in this group had C20 concrete and S220 steel. Tension steel ratio was 0.0055, and the ultimate steel strain was  $\epsilon_{su}=0.1$ . Beams having steel of different strain hardening strains ( $\epsilon_{sp}=2\epsilon_{sy}$  or  $10\epsilon_{sy}$ ) behaved almost the same. Their ultimate moment capacities and curvature ductility ratios were the same. Only the beam in which steel strain hardening was 10 times the yield strain (Beam IVA2) failed before strain hardening occurred in the compression steel (See Figure A.35, Appendix A).

Group IVB - Beams were identical with those of IVA, the only difference being the ratio of tension reinforcement, which was increased to 0.0190. As can be seen from Figure A.36 of Appendix A, the beams having steel of different strain hardening starting points ( $\epsilon_{sp}=2\epsilon_{sy}$ ;  $10\epsilon_{sy}$ ) had the same curvature ductility ratios and almost the same ultimate moment capacities. The behaviour of two beams were similar till the yielding. After that, till the failure, moments of the beam with strain hardening 10 times of the yield strain were a little bit greater than those of the other. Since  $\epsilon_{sp}$  in beam IVB1 was lower than that of IVB2, tension steel hardened earlier and therefore the tension force started to increase earlier. Consequently the compressive force tried to increase earlier by increasing neutral axis depth. Therefore values of moments became greater. But at the end, that is at the ultimate curvature, the moments of the two beams were almost the same.

Groups from IVC to IVF - Beams of these groups were the same as of the previous group. However different concrete and steel grades were used (S420-C20 and S420-C35). For each material combination low and high tension reinforcement ratios were investigated. The discussions made for the beams of the previous group were also valid for beams of these groups (See Figures from A.37 to A.40, Appendix A).

Group IVG - Beams having C20 concrete and S220 steel were investigated. Tension steel ratio was 0.0055, and strain hardening was assumed to start at  $5\epsilon_{sy}$ . Beams with different ultimate strain capacity of steel ( $\epsilon_{su}=0.05; 0.10; 0.15; 0.20$ ) behaved almost the same until tension steel started strain hardening. After this point increase in the ultimate strain capacity of steel used had a significant influence on ductility. The curvature ductility ratio of IVG2 ( $\epsilon_{su} = 0.1$ ) was 89% greater than that of IVG1 ( $\epsilon_{su} = 0.05$ ), the curvature ductility ratio of IVG3 ( $\epsilon_{su} = 0.15$ ) was 59% greater than that of IVG2 ( $\epsilon_{su} = 0.1$ ). The curvature ductility ratio of IVG4 ( $\epsilon_{su} = 0.2$ ) was 36% greater than that of IVG3 ( $\epsilon_{su} = 0.15$ ). The ultimate moment capacities of these four beams were almost the same. Also the cause of failure of all beams was the rupturing of the tension steel (See Figure A.41, Appendix A).

Group IVH - Beams of this group were identical with those of IVG, the only difference being that the ratio of tension reinforcement which was increased to 0.0190. It was observed that increase in the ultimate strain capacity of steel used caused a decrease in the ultimate moment capacity of the beam. The ultimate moment of IVH2 ( $\epsilon_{su} = 0.1$ ) was 10% less than that of IVH1 ( $\epsilon_{su} = 0.05$ ) and the ultimate moment of IVH3 ( $\epsilon_{su} = 0.15$ ) was 5% less than that of IVH2. The ultimate moment of IVH4 ( $\epsilon_{su} = 0.2$ ) was 2% less than that of IVH3 ( $\epsilon_{su} = 0.15$ ). Keeping strain hardening starting point, yield and ultimate strengths identical and decreasing only ultimate strain of steel, increased the slope of the strain hardening portion for steel. As a result, after the yielding, gain in force (therefore in ultimate moment capacities) in beams which are reinforced with steel having smaller ultimate strains was greater.

Failure of beams IVH2, IVH3, IVH4 were not due to rupturing of tension steel, but due to the crushing of confined concrete. Therefore the ultimate curvatures of these beams were almost the same. Bearing in mind that their concrete strengths were same, this result is not unexpected. However the failure of IVH1 was due to rupturing of tension steel, and its curvature ductility ratio was approximately half of the others (See Figure A.42, Appendix A).

Groups from IVJ to IVM - In these groups materials used were either C20 & S420 or C35 & S420. For each material combination, two different tension reinforcement ratios were considered.  $\epsilon_{sp}$  was always taken equal to  $5\epsilon_{sy}$ . In each case the influence of the steel ultimate strain was studied. As can be seen in Figures from A.43 to A.46 of Appendix A, the behaviour was not different from the ones of Group IVG & IVH.

#### 4.5.3 Conclusions

Whether strain hardening of bars used as tension reinforcement starts at twice the yield strain, or at 10 times the yield strain, does not effect the beam behaviour.

The ultimate moment capacities of beams with bars in tension which start strain hardening very late, were just a little bit lower than those of the others in which steel with higher strain hardening strains have been used.

For low tensile reinforcement ratios, when the failure of beam is controlled by the rupturing of tension steel, ultimate strain capacity of steels used in tensile reinforcement, affect the behaviour and the ductility of the beam. The moment-curvature diagrams of such beams resemble to the shapes of the stress-strain diagram of the steel used. The ductility of the beam seemed to increase when steel with higher ultimate strain is used.

For high tensile reinforcement ratios, beams reinforced with steel having ultimate strain capacity of 0.1, behaved much better than the beams reinforced with steel having ultimate strain capacity of 0.05. Ductility of beams reinforced with steel having  $\epsilon_{su}=0.1$  was much higher than the ones with  $\epsilon_{su}=0.05$ . But when the ultimate strain capacity of steel was over 0.1, ductility did not improve due to the fact that the

failure of these beams was controlled not by rupturing of tension steels, but by crushing of core concrete.

Although whether strain hardening of steels start at 2, 5 or 10 times of yield strains is not so important, ultimate strain capacities of steels are very important. It is recommended that ultimate strain capacities of these steels should be at least 0.1.

#### **4.6 Case Study V: Influence of Tension Reinforcement Ratio in R/C Beams**

This study aims to investigate the influence of the amount of tension reinforcement on the beam behaviour. For this purpose 40 moment-curvature diagrams for rectangular and 'T' sections were drawn. The main variables investigated were concrete and steel strengths, ultimate strain of steel, tension and compression reinforcement ratios and "d'/d" ratios. The list of all 40 sections with their properties are given in Table 4.9. The results are presented in Table 4.10.

##### **4.6.1 Assumptions**

- Web reinforcement ratio ( $\rho_w$ ) for all beams was equal to 0.0044 ( $\phi 10/120$  mm).
- For T-beams flange width was 1500 mm, and flange height was 150 mm.

**Table 4.9:** List of sections and section properties; Influence of tension reinforcement ratio in R/C beams

		Beam Cross Section	d'/d	Comp. st. ratio ( $A_s'/A_s$ )	Steel & Conc. Strengths	Ult. Strain of Steel	Tension St. Ratio	
VA	VA1	Rectangular 60x30 cm	d'/d = 0.071 d' = 40 mm d = 560 mm	$A_s'/A_s = 0.5$	S220 - C20	0.1	0.0055	VA1
	VA2						0.0108	VA2
	VA3						0.0147	VA3
	VA4						0.0190	VA4
VB	VB1					0.18	0.0055	VB1
	VB2						0.0108	VB2
	VB3						0.0147	VB3
	VB4						0.0190	VB4
VC	VC1				S420 - C20	0.1	0.0027	VC1
	VC2						0.0061	VC2
	VC3						0.0096	VC3
	VC4						0.0136	VC4
VD	VD1					0.18	0.0027	VD1
	VD2						0.0061	VD2
	VD3						0.0096	VD3
	VD4						0.0136	VD4
VE	VE1				S420 - C40	0.18	0.0040	VE1
	VE2						0.0091	VE2
	VE3						0.0147	VE3
	VE4						0.0190	VE4
VF	VF1			$A_s'/A_s = 1.0$	S220 - C20	0.1	0.0055	VF1
	VF2						0.0108	VF2
	VF3						0.0147	VF3
	VF4						0.0190	VF4
VG	VG1					0.18	0.0055	VG1
	VG2						0.0108	VG2
	VG3						0.0147	VG3
	VG4						0.0190	VG4
VH	VH1		d'/d = 0.101 d' = 55 mm d = 545 mm	$A_s'/A_s = 0.5$	S220 - C20	0.18	0.0055	VH1
	VH2						0.0108	VH2
	VH3						0.0147	VH3
	VH4						0.0190	VH4
VJ	VJ1	T-beam $b_f = 150$ cm $h_f = 15$ cm	d'/d = 0.071 d' = 40 mm d = 560 mm	$A_s'/A_s = 0.5$	S420 - C20	0.1	0.0037	VJ1
	VJ2						0.0121	VJ2
	VJ3						0.0215	VJ3
	VJ4						0.0287	VJ4
VK	VK1					0.18	0.0037	VK1
	VK2						0.0121	VK2
	VK3						0.0215	VK3
	VK4						0.0287	VK4



**Table 4.10: Results; Influence of tension reinforcement ratio in R/C beams**

		Curvature (rad/m)						Curvature ductility ratio	Maximum M**	
		Yield A <sub>s</sub>	Str. Hard. A <sub>s</sub>	Cover Crush	Core Crush	Yield A <sub>s</sub> '	Str. Hard. A <sub>s</sub> '			
VA	VA1	0.0036	0.0120	0.0466	0.0963	0.1096	*	51	0.083	VA1
	VA2	0.0040	0.0122	0.0332	0.0539	0.0613	0.1354	58	0.150	VA2
	VA3	0.0041	0.0131	0.0285	0.0408	0.0324	0.0949	81	0.188	VA3
	VA4	0.0042	0.0141	0.0232	0.0306	0.0205	0.0734	72	0.228	VA4
VB	VB1	0.0036	0.0120	0.0479	0.1026	0.1343	0.2658	104	0.082	VB1
	VB2	0.0040	0.0122	0.0340	0.0600	0.0737	0.1528	105	0.136	VB2
	VB3	0.0041	0.0131	0.0290	0.0432	0.0371	0.1086	85	0.174	VB3
	VB4	0.0042	0.0142	0.0238	0.0318	0.0209	0.0831	67	0.214	VB4
VC	VC1	0.0053	0.0254	0.0489	0.1049	0.1925	*	37	0.066	VC1
	VC2	0.0056	0.0244	0.0283	0.0544	0.0803	*	34	0.141	VC2
	VC3	0.0065	0.0233	0.0202	0.0359	0.0513	0.1406	47	0.204	VC3
	VC4	0.0064	0.0235	0.0153	0.0235	0.0321	0.1026	36	0.274	VC4
VD	VD1	0.0053	0.0255	0.0495	0.1158	0.2515	*	62	0.065	VD1
	VD2	0.0056	0.0244	0.0284	0.0553	0.0837	0.2278	80	0.133	VD2
	VD3	0.0065	0.0233	0.0202	0.0363	0.0528	0.1524	48	0.195	VD3
	VD4	0.0064	0.0235	0.0153	0.0235	0.0324	0.1084	37	0.266	VD4
VE	VE1	0.0048	0.0248	0.0597	0.1097	0.3150	*	65	0.048	VE1
	VE2	0.0057	0.0208	0.0340	0.0555	0.1064	0.2490	73	0.102	VE2
	VE3	0.0057	0.0240	0.0240	0.0336	0.0606	0.1730	57	0.153	VE3
	VE4	0.0064	0.0225	0.0196	0.0282	0.0443	0.1414	41	0.191	VE4
VF	VF1	0.0043	0.0138	0.0491	0.1062	0.1813	*	44	0.086	VF1
	VF2	0.0037	0.0158	0.0399	0.0720	0.1262	*	45	0.159	VF2
	VF3	0.0041	0.0137	0.0367	0.0595	0.1043	0.1665	45	0.220	VF3
	VF4	0.0034	0.0121	0.0345	0.0571	0.0892	0.1486	63	0.285	VF4
VG	VG1	0.0043	0.0138	0.0500	0.1136	0.2820	*	74	0.084	VG1
	VG2	0.0037	0.0159	0.0406	0.0738	0.1849	0.2793	100	0.166	VG2
	VG3	0.0041	0.0137	0.0374	0.0610	0.1526	0.2288	91	0.219	VG3
	VG4	0.0034	0.0121	0.0352	0.0632	0.1160	0.2037	126	0.280	VG4
VH	VH1	0.0035	0.0134	0.0415	0.1056	0.1326	0.2483	117	0.079	VH1
	VH2	0.0039	0.0148	0.0294	0.0635	0.0738	0.1508	103	0.132	VH2
	VH3	0.0039	0.0151	0.0251	0.0538	0.0558	0.1119	85	0.169	VH3
	VH4	0.0040	0.0158	0.0220	0.0405	0.0341	0.0793	67	0.208	VH4
VJ	VJ1	0.0076	0.0226	0.1074	*	*	*	24	0.096	VJ1
	VJ2	0.0058	0.0214	0.0521	0.1051	0.1579	*	29	0.283	VJ2
	VJ3	0.0061	0.0218	0.0354	0.0642	0.0997	0.1370	24	0.466	VJ3
	VJ4	0.0059	0.0212	0.0290	0.0440	0.0773	0.1068	18	0.602	VJ4
VK	VK1	0.0076	0.0227	0.1129	0.2360	*	*	42	0.090	VK1
	VK2	0.0058	0.0214	0.0530	0.1078	0.1868	0.2407	49	0.266	VK2
	VK3	0.0061	0.0218	0.0357	0.0655	0.1050	0.1477	26	0.447	VK3
	VK4	0.0059	0.0212	0.0291	0.0446	0.0808	0.1141	20	0.586	VK4

\* Tension reinforcement ruptured, before the event occurred.  
\*\* M:  $M/b_w d^2 f_c$



#### 4.6.2 Discussion of Results

Group VA - These were rectangular beams reinforced with S220 grade steel. Ultimate strain capacity for steel was 0.1. Concrete strength was 20 MPa. Compression reinforcement ratio was  $\rho'/\rho=0.5$  and  $d'/d$  was 0.071. Moment-curvature diagrams obtained by changing the tension steel ratio ( $\rho=0.0055$ ; 0.0108; 0.0147; 0.0190) are presented in Figure A.47 of Appendix A.

It can be said that, increasing the amount of tension steel in beams delays the yielding and strain hardening. However this delay is not very significant. Increasing the tension steel results in yielding and strain hardening of compression reinforcement at earlier stages. Also core crushing occurs at earlier stages. As can be seen in Table 4.10, curvatures corresponding to yielding and strain hardening of compression reinforcement and core crushing are significantly smaller in beams with higher tension reinforcement ratios. Since the neutral axis depth increases with increasing tension steel ratio, strains in compression steel also increase.

Increasing the tension steel in the beam delays the yield of the tension reinforcement. After the yielding, more steel leads to greater tensile force. To satisfy the force equilibrium, the stresses in compressed concrete increase faster. After reaching the ultimate stress, concrete starts to crush and the capacity drops. Therefore the compression steel is forced to take this force. This leads to yielding of compression steel faster.

Ultimate moment capacities of beams in Group VA were approximately proportional with their tension steel ratios. Maximum dimensionless moment ( $M/b_w d^2 f_c$ ) of beam VA2 ( $\rho = 0.0108$ ) was 1.81 times greater than that of the beam VA1 ( $\rho = 0.0055$ ). The maximum moment of VA3 ( $\rho = 0.0147$ ) was 1.25 times greater than that of VA2 and the maximum moment of VA4 ( $\rho = 0.0190$ ) was 1.21 times greater than that of VA3. The highest curvature ductility ratio was for VA3

whose tensile reinforcement ratio was about the limiting value specified in TS500. The failures of beams VA1 and VA2 were due to the rupturing of the tension reinforcement, while the others failed by crushing of core concrete.

Group VB - Beams of this group were identical with those of VA, the only difference being the strain capacity of reinforcing steel was increased to 0.18. It was observed that the ones with low tensile reinforcement ratios (VB1:  $\rho=0.0055$  and VB2:  $\rho=0.0108$ ) behaved much more ductile than those of the identical beams in Group VA (reinforcing steel with ultimate strain of 0.1). The behaviour of other beams (VB3:  $\rho=0.0147$  and VB4:  $\rho=0.0190$ ) was not significantly influenced by the strain capacity of steel. In such beams, the slope of the strain hardening portion of the steel was more important than the ultimate strain capacity. The curvature ductility ratios of VB3 and VB4 were almost identical with those of VA3 and VA4 respectively. In beams of Group VB, the beam with tensile reinforcement ratio of 0.0108 had the highest curvature ductility ratio. This ratio was 19% greater than the curvature ductility ratio of VB3 ( $\rho=0.0147$ ) whose tensile reinforcement ratio was about the limiting value. However the ductility ratio of all beams in this group was adequate, lowest ratio being 67 (See Figure A.48, Appendix A).

Groups from VC to VE - Instead of S220-C20 material combination as in Group VA or VB, for beams of these groups had S420-C20 (Groups VC & VD) and S420-C40 (Group VE). Moment-curvature diagrams obtained for different tension steel ratios are presented in Figures from A.49 to A.51. In general the behaviour of beams of these groups behaved similar to the ones of Groups VA & VB. For beams with ultimate strain capacity of reinforcing steel as 0.1 (Group VC), most ductile behaviour was observed in the beam whose tensile reinforcement ratio was about  $\rho_1$ . When ultimate strain capacity was 0.18 (Groups VD & VE), beam having about 25% less reinforcement than the balanced, behaved more ductile than the others.

Groups VF - Rectangular beams made of S220 steel were investigated. Ultimate strain capacity for steel was 0.1 and the concrete strength was 20 MPa. Compression reinforcement ratio was 1.0 and  $d'/d$  ratio was 0.071. The moment-curvature diagrams obtained for different tension steel ratios ( $\rho=0.0055$ ; 0.0108; 0.0147; 0.0190) are presented in Figure A.52 of Appendix A. The main difference of this group was in the compression reinforcement ratio (which was  $\rho'/\rho=1.0$ ). This caused all beams to fail due to the rupturing of tension steels. (The reason is explained in the case study named "Influence of Compression Reinforcement in R/C Beams" - Section 4.2) In this group, the curvature ductility ratios of beams with tensile reinforcement ratios of 0.0055 (VF1), 0.0108 (VF2) and 0.0147 (VF3), were almost the same. However the curvature ductility ratio of the beam which had tensile reinforcement ratio of 0.0190 (VF4) was 40% greater than those of the others.

Group VG - Beams of this group were identical with those of VF, the only difference being the strain capacity of reinforcing steel, which was increased to 0.18. For the beams of this group rupturing of tension steel did not occur easily, due to high ultimate strain capacity of reinforcing steel. Therefore both ultimate moment capacities and ductilities increased with the increasing tensile reinforcement ratio (See Figure A.53, Appendix A).

Group VH - These were rectangular beams reinforced with S220 steel. Ultimate strain capacity for steel was 0.18 and concrete strength was 20 MPa. Compression reinforcement ratio was  $\rho'/\rho=0.5$  and  $d'/d$  ratio was 0.101. The moment-curvature diagrams obtained for different tension steel ratios ( $\rho=0.0055$ ; 0.0108; 0.0147; 0.0190) are presented in Figure A.54 of Appendix A. The main difference of this group from others was the effective depth (it was decreased from 560 mm to 545 mm). This caused a decrease in the ultimate moment capacities of all beams. Moreover, it was seen from the figure that by increasing the tension reinforcement, the beam behaved in a less ductile manner.

Group VJ - These were T-beams reinforced with S420 steel. Ultimate strain capacity of steel was 0.1 and the concrete strength was 20 MPa. Compression reinforcement ratio was  $\rho'/\rho=0.5$  and  $d'/d$  ratio was 0.071. Moment-curvature diagrams of beams with different tensile reinforcement ratios ( $\rho=0.0037$ ; 0.0121; 0.0215; 0.0287) are presented in Figure A.55. The least ductile behaviour belongs to the beam whose tensile reinforcement ratio was 0.0287. It had a curvature ductility ratio 38% less than the one whose with reinforcement ratio of 0.0121 which exhibited the most ductile behaviour in this group.

Group VK - These T-beams were identical with those of Group VJ, only strain capacity of steel was increased to 0.18. Comparing the beams of this group with the identical ones of the previous group (Group VJ), it is seen that, increasing ultimate strain capacity of reinforcing steel to 0.18 did not change the behaviour of beams having tensile reinforcement ratios of 0.0287 and 0.0215, but increased the curvature ductility ratios of beams having tensile reinforcement ratios of 0.0121 & 0.0037. The curvature ductility ratio of these beams were 1.7 times greater than those of the identicals with 0.1 ultimate strain capacity of steel (See Figure A.56, Appendix A).

#### 4.6.3 Conclusions

Yield capacity and ultimate strength of beams were almost directly proportional with the tensile reinforcement ratios.

It is not possible to say that ductility of beams increases or decreases by increasing tensile steel ratio. Ductility depends not only on the tension steel ratio, but other variables. However in general limiting value specified in TS500 ( $\rho_s$ ) makes the beam to behave most ductile, especially if the ultimate strain capacity of reinforcement steels is about 0.1. If the ultimate strain capacity of steel is higher than 0.15 the

tension steel ratio which corresponds to maximum ductility becomes less than  $\rho_1$ . Maximum tensile reinforcement ratio specified in TS500 ( $\rho_m$ ) leads to less ductile behaviour.

Beams whose tensile reinforcement ratios are low ( $\rho_t$  or less) fail by rupturing of tensile steel. However beams with high tensile reinforcement ratios (above  $\rho_t$ ) fail by crushing of the core concrete.

To get the most ductile behaviour for a beam, it should be designed in such a manner that the tensile steel does not rupture before the moment capacity drops 15% in the descending portion of the moment-curvature diagram.

#### **4.7 Case Study VI: Influence of Confined Concrete Models on Moment Curvature Diagrams of R/C Beams**

This study aims to investigate the influence of confined concrete model on moment-curvature diagrams of beams. For this purpose 16 moment-curvature diagrams for rectangular sections were drawn. The main variables investigated were the ultimate strains of steel and the web reinforcement ratios (tie ratios). There are 4 groups. In each group, moment-curvature diagrams of a beam drawn according to different confinement models ("Saatcioglu", "Sheikh & Uzumeri", "Modified Kent & Park", "Modified Kent & Park, with linear ascending part") are presented and discussed. The list of the sections with the properties are given in Table 4.11. The results are presented in Table 4.12.

**Table 4.11: List of sections and section properties; Influence of confined concrete models on moment-curvature diagrams of R/C beams**

		Ties	Ultimate Strain of Steel	Confined Concrete Model	
VIA	VIA1	Φ10/90 mm	0.1	Saatçioğlu	VIA1
	VIA2			Sheikh & Üzimeri	VIA2
	VIA3			Mod. Kent & Park	VIA3
	VIA4			MKP, with linear ascen.	VIA4
VIB	VIB1	Φ10/90 mm	0.18	Saatçioğlu	VIB1
	VIB2			Sheikh & Üzimeri	VIB2
	VIB3			Mod. Kent & Park	VIB3
	VIB4			MKP, with linear ascen.	VIB4
VIC	VIC1	Φ8/120 mm	0.1	Saatçioğlu	VIC1
	VIC2			Sheikh & Üzimeri	VIC2
	VIC3			Mod. Kent & Park	VIC3
	VIC4			MKP, with linear ascen.	VIC4
VID	VID1	Φ8/120 mm	0.18	Saatçioğlu	VID1
	VID2			Sheikh & Üzimeri	VID2
	VID3			Mod. Kent & Park	VID3
	VID4			MKP, with linear ascen.	VID4

**Table 4.12: Results; Influence of confined concrete models on moment-curvature diagrams of R/C beams**

		Curvature (rad/m)						Curvature ductility ratio	Maximum M**	
		Yield A <sub>s</sub>	Str. Hard. A <sub>s</sub>	Cover Crush	Core Crush	Yield A <sub>s</sub> '	Str. Hard. A <sub>s</sub> '			
VIA	VIA1	0.0075	0.0227	0.0144	0.0598	0.0412	0.1422	40	0.246	VIA1
	VIA2	0.0063	0.0246	0.0160	0.1429	0.0464	0.1429	38	0.251	VIA2
	VIA3	0.0076	0.0239	0.0180	0.0331	0.0451	0.1398	40	0.242	VIA3
	VIA4	0.0068	0.0232	0.0142	0.0263	0.0353	0.1219	45	0.241	VIA4
VIB	VIB1	0.0075	0.0227	0.0144	0.0614	0.0421	0.1531	72	0.233	VIB1
	VIB2	0.0063	0.0246	0.0160	0.1536	0.0485	0.1536	92	0.237	VIB2
	VIB3	0.0076	0.0239	0.0180	0.0333	0.0461	0.1510	49	0.230	VIB3
	VIB4	0.0068	0.0232	0.0142	0.0264	0.0359	0.1468	55	0.230	VIB4
VIC	VIC1	0.0073	0.0254	0.0142	0.0491	0.0408	0.1095	36	0.229	VIC1
	VIC2	0.0062	0.0244	0.0158	0.0819	0.0458	0.1151	43	0.232	VIC2
	VIC3	0.0075	0.0234	0.0177	0.0293	0.0412	0.1041	26	0.227	VIC3
	VIC4	0.0068	0.0231	0.0142	0.0231	0.0322	0.1003	29	0.225	VIC4
VID	VID1	0.0073	0.0255	0.0142	0.0500	0.0416	0.1166	37	0.222	VID1
	VID2	0.0062	0.0244	0.0158	0.0894	0.0469	0.1227	44	0.224	VID2
	VID3	0.0075	0.0235	0.0177	0.0295	0.0420	0.1103	27	0.222	VID3
	VID4	0.0068	0.0231	0.0142	0.0231	0.0348	0.1060	29	0.221	VID4

\* Tension reinforcement ruptured, before the event occurred.

\*\* M:  $M/b_w d^2 f_c$

#### 4.7.1 Assumptions

- Unconfined concrete strength ( $f_c$ ) for all sections is equal to 20 MPa.
- Tensile reinforcement ratio ( $A_s/b_w/d$ ) for all beams is 0.0112 ( $6\Phi 20$ ).
- Compression steel ratio is 0.5.
- S420 steel is used as reinforcements (both longitudinal bars and ties).
- Ties:  $\Phi 8/120$  mm;  $\Phi 10/90$  mm which correspond to  $\rho_w = 0.0028$ ; 0.0058 respectively.

#### 4.7.2 Discussion of Results

Group VIA - Beams were confined with  $\Phi 10/90$  mm ties. Ultimate strain capacity of longitudinal reinforcement was 0.1. Moment-curvature diagrams drawn by using different confined concrete models are presented in Figure A.57 of Appendix A. As can be seen from this figure all beams exhibited similar behaviour till the curvature reached the value of 0.14. This point is the point where strain hardening of compression reinforcements starts. From this point on, in general the diagram of the beam drawn by using Sheikh & Uzumeri Model rise.

Comparing the stress-strain diagrams drawn for different confined concrete models, it was observed that, after a certain strain value, all the diagrams have a horizontal portion with a highly reduced slope. Highest moment capacity was obtained using the model of Sheikh & Uzumeri (See Figure A.61, Appendix A).. But since the compressive force carried by confined concrete in this beam will correspond to a smaller neutral axis depth, the ultimate strain in the tension reinforcement will be reached faster. Therefore moment-curvature diagram drawn using Sheikh & Uzumeri Model had a smaller curvature capacity.



Group VIB - These beams were also confined with  $\Phi 10/90$  mm ties. The ultimate strain capacity of longitudinal reinforcement was increased to 0.18. Since the strain capacity of steel so high, the discussion made at the last sentence of the previous paragraph loses its validity. Therefore the diagram drawn by using Sheikh & Uzumeri Model had not only the highest moment capacity but also the highest curvature ductility ratio. A similar discussion can be made in order to explain the behaviour of the beam whose diagram is obtained by using Saatcioglu Model (See Figure A.58, Appendix A).

Groups VIC & VID - These beams were confined with  $\Phi 8/120$  mm ties. Ultimate strain capacity of longitudinal reinforcement was 0.1 for Group VIC, and 0.18 for Group VID. Above discussions were also valid for beams of these groups. In other words, if the failures are due to the crushing of core concrete, diagrams drawn by using Sheikh & Uzumeri models have the highest moment capacities and curvature ductility ratios. Then comes diagrams drawn by using Saatcioglu Model. It should be noted that although the confinement in Groups VIC & VID was much less as compared to VIA & VIB, the moment-curvature diagrams were almost identical. This can be seen by comparing Figures A.59 & A.60 of Appendix A. This is not surprising since all beams were underreinforced.

#### **4.7.3 Conclusions**

Diagrams of various beams drawn by using different confined concrete models are similar till the strain hardenings of the compression steel. From this point on diagrams drawn by using Sheikh & Uzumeri and Saatcioglu models show higher performances (greater moment and greater curvature capacity).



Constant stress level at the ends of the stress-strain diagrams based on various confinement models correspond to different strains. This difference is observed on the moment-curvature diagrams at high curvature values.

The differences between the diagrams drawn by using different models are only observable if the failures of beams are due to crushing of core concrete. The magnitude of these differences are related to the amount of web reinforcement. The differences become more visible when high confinement ratios are used.

There is absolutely no difference in the diagrams drawn by using Modified Kent & Park Model and the same model with linear ascending part (Roy & Sozen).

#### **4.8 Case Study VII: Influence of Flange Width in T-Beams**

This study is aimed to investigate the influence of flange width on T-beam behaviour. For this purpose 30 moment-curvature diagrams for different sections were drawn. The main variables investigated were the concrete strength, flange height, ultimate strains of steel, and tension steel ratio. In each group 3 beams having 3 different flange widths ( $b_f=8b_w$ ;  $4b_w$ ;  $b_w$ ) were investigated. The list of all 30 sections with their properties are given in Table 4.13. The results are presented in Table 4.14.

##### **4.8.1 Assumptions**

- S420 steel is used as reinforcement.
- Web reinforcement ratio ( $\rho_w$ ) for all beams is equal to 0.0044 ( $\Phi$  10/120 mm).
- Compression steel ratio is  $\rho'/\rho=0.5$  for all sections.
- Three common flange widths, 8 times, 4 times & 1 time of web width correspond to 2400, 1200 & 300 millimeters respectively.

**Table 4.13: List of sections and section properties; Influence flange width in T-beams**

		Concrete Strength	Flange Heights	Ult. Strain of Steel	Tension Steel Ratio	Flange Width	
VIIA	VIIA1	C25	$h_f = h/4$ 150 mm	0.1	$\rho = 0.0096$ (8 $\Phi$ 16)	$b_f = 8b_w$	VIIA1
	VIIA2					$b_f = 4b_w$	VIIA2
	VIIA3					$b_f = b_w$	VIIA3
VIIB	VIIB1				$\rho = 0.0190$ (6 $\Phi$ 26)	$b_f = 8b_w$	VIIB1
	VIIB2					$b_f = 4b_w$	VIIB2
	VIIB3					$b_f = b_w$	VIIB3
VIIC	VIIC1		0.18		$\rho = 0.0096$ (8 $\Phi$ 16)	$b_f = 8b_w$	VIIC1
	VIIC2					$b_f = 4b_w$	VIIC2
	VIIC3					$b_f = b_w$	VIIC3
VIID	VIID1				$\rho = 0.0190$ (6 $\Phi$ 26)	$b_f = 8b_w$	VIID1
	VIID2					$b_f = 4b_w$	VIID2
	VIID3					$b_f = b_w$	VIID3
VIIE	VIIE1	$h_f = h/2$ 300 mm	0.1	$\rho = 0.0096$ (8 $\Phi$ 16)	$b_f = 8b_w$	VIIE1	
	VIIE2				$b_f = 4b_w$	VIIE2	
	VIIE3				$b_f = b_w$	VIIE3	
VIIF	VIIF1			$\rho = 0.0190$ (6 $\Phi$ 26)	$b_f = 8b_w$	VIIF1	
	VIIF2				$b_f = 4b_w$	VIIF2	
	VIIF3				$b_f = b_w$	VIIF3	
VIIG	VIIG1		0.18		$\rho = 0.0096$ (8 $\Phi$ 16)	$b_f = 8b_w$	VIIG1
	VIIG2					$b_f = 4b_w$	VIIG2
	VIIG3					$b_f = b_w$	VIIG3
VIIH	VIIH1				$\rho = 0.0190$ (6 $\Phi$ 26)	$b_f = 8b_w$	VIIH1
	VIIH2					$b_f = 4b_w$	VIIH2
	VIIH3					$b_f = b_w$	VIIH3
VIIJ	VIIJ1	C40	$h_f = h/4$ 150 mm	0.18	$\rho = 0.0096$ (8 $\Phi$ 16)	$b_f = 8b_w$	VIIJ1
	VIIJ2					$b_f = 4b_w$	VIIJ2
	VIIJ3					$b_f = b_w$	VIIJ3
VIIK	VIIK1				$\rho = 0.0190$ (6 $\Phi$ 26)	$b_f = 8b_w$	VIIK1
	VIIK2					$b_f = 4b_w$	VIIK2
	VIIK3					$b_f = b_w$	VIIK3

**Table 4.14: Results; Influence of flange width in T-beams**

		Curvature (rad/m)						Curvature ductility ratio	Maximum M**	
		Yield A <sub>s</sub>	Str. Hard. A <sub>s</sub>	Cover Crush	Core Crush	Yield A <sub>s</sub> '	Str. Hard. A <sub>s</sub> '			
VIIA	VIIA1	0.0060	0.0230	0.0925	0.1799	*	*	31	0.192	VIIA1
	VIIA2	0.0050	0.0258	0.0607	0.1176	0.1937	*	39	0.186	VIIA2
	VIIA3	0.0079	0.0236	0.0236	0.0401	0.0595	0.1573	34	0.168	VIIA3
VIIB	VIIB1	0.0051	0.0261	0.0611	0.1086	0.1840	*	37	0.365	VIIB1
	VIIB2	0.0053	0.0241	0.0386	0.0637	0.1072	0.1543	32	0.332	VIIB2
	VIIB3	0.0075	0.0240	0.0138	0.0187	0.0265	0.0919	26	0.299	VIIB3
VIIC	VIIC1	0.0060	0.0230	0.0943	0.1906	*	*	55	0.185	VIIC1
	VIIC2	0.0050	0.0259	0.0616	0.1283	0.2342	0.2937	76	0.174	VIIC2
	VIIC3	0.0079	0.0237	0.0237	0.0406	0.0626	0.1714	44	0.160	VIIC3
VIID	VIID1	0.0051	0.0262	0.0620	0.1134	0.2216	0.2552	58	0.338	VIID1
	VIID2	0.0053	0.0241	0.0390	0.0689	0.1180	0.1679	36	0.317	VIID2
	VIID3	0.0075	0.0241	0.0138	0.0187	0.0266	0.0964	26	0.293	VIID3
VIIE	VIIE1	0.0060	0.0230	0.0925	0.1799	*	*	31	0.192	VIIE1
	VIIE2	0.0050	0.0258	0.0607	0.1176	0.1937	*	39	0.186	VIIE2
	VIIE3	0.0079	0.0236	0.0236	0.0401	0.0595	0.1573	34	0.168	VIIE3
VIIF	VIIF1	0.0051	0.0261	0.0611	0.1086	0.1840	*	37	0.365	VIIF1
	VIIF2	0.0052	0.0241	0.0386	0.0637	0.1072	0.1543	48	0.332	VIIF2
	VIIF3	0.0075	0.0240	0.0138	0.0187	0.0265	0.0919	26	0.299	VIIF3
VIIG	VIIG1	0.0060	0.0230	0.0943	0.1906	*	*	55	0.185	VIIG1
	VIIG2	0.0050	0.0259	0.0616	0.1283	0.2342	0.2937	83	0.174	VIIG2
	VIIG3	0.0079	0.0237	0.0237	0.0406	0.0626	0.1714	44	0.160	VIIG3
VIIH	VIIH1	0.0051	0.0262	0.0620	0.1134	0.2216	0.2552	68	0.338	VIIH1
	VIIH2	0.0052	0.0241	0.0390	0.0689	0.1180	0.1679	51	0.317	VIIH2
	VIIH3	0.0075	0.0241	0.0138	0.0187	0.0266	0.0964	26	0.293	VIIH3
VIIJ	VIIJ1	0.0051	0.0208	0.1368	0.2249	*	*	61	0.116	VIIJ1
	VIIJ2	0.0050	0.0236	0.0822	0.1525	0.3097	*	62	0.114	VIIJ2
	VIIJ3	0.0054	0.0242	0.0327	0.0568	0.0942	0.2384	72	0.106	VIIJ3
VIIK	VIIK1	0.0050	0.0195	0.0827	0.1346	0.2882	0.3287	72	0.221	VIIK1
	VIIK2	0.0060	0.0218	0.0537	0.0867	0.1659	0.2264	47	0.206	VIIK2
	VIIK3	0.0064	0.0225	0.0196	0.0282	0.0443	0.1414	41	0.191	VIIK3

\* Tension reinforcement ruptured, before the event occurred.  
 \*\* M:  $M/b_w d^2 f_c$

#### 4.8.2 Discussion of Results

Group VIIA - Beams were made of C25 concrete. Tension reinforcement ratio was 0.0096 ( $8\Phi 16$ ). Ultimate strain capacity for steel was 0.1. Flange height was 150 mm ( $h/4$ ), for T-beams. Moment-curvature diagrams of beams with different flange widths ( $b=8b_w$ ;  $4b_w$ ;  $b_w$ ) are presented in Figure A.63 of Appendix A. Moment-curvature diagram of the rectangular section had an ultimate curvature capacity of 0.2678 rad/m. Changing this cross section into a "T" shape with a flange height of  $1/4$  of the total height and flange width of four times of web width, resulted in a decrease in the ultimate curvature. (Ultimate curvature dropped to 0.1937 rad/m). However for the T-section the curvature ductility ratio was a little bit greater, since yield curvature of this beam was almost half of that of the rectangular one. However when the flange width was increased to 8 times of web width, curvature ductility ratio decreased even below the value obtained for the rectangular section. On the other hand, ultimate moment capacity of beam VIIA1 ( $b_f=8b_w$ ) was 14%, and ultimate moment capacity of beam VIIA2 ( $b_f=4b_w$ ) was 11% greater than that of VIIA3 ( $b_f=b_w$ , rectangular section).

Group VIIB - Increasing tensile reinforcement ratio to 0.0190 ( $6\Phi 26$ ) for the same examples discussed above, both the curvature ductility ratios and the ultimate moment capacities of beams decreased by reducing the flange width from 8 times of web width to first 4 times then 1 time of web width (rectangular). This time ultimate moment capacity of beam VIIB1 ( $b_f=8b_w$ ) is 22%, and ultimate moment capacity of beam VIIB2 ( $b_f=4b_w$ ) is 11% greater than that of VIIB3 ( $b_f=b_w$ , rectangular) (See Figure A.64, Appendix A).

No significant difference was observed in the ultimate curvature of two flanged and one rectangular sections. However curvature ductility ratios of T-beams were higher than that of the rectangular beams.

Groups VIIC & VIID - Beams in Groups VIIC & VIID were identical with those of Groups VIIA & VIIB respectively. However the strain capacity of reinforcing steel was increased to 0.18 in the examples of these groups. Increasing ultimate strain capacity of longitudinal steel to 0.18, for beams whose tensile reinforcement ratio was 0.0096 resulted in a more ductile behaviour. Beams with tensile reinforcement ratio of 0.0190 behave slightly more ductile as compared with the behaviour of those in which steel with lower ultimate strain capacity was used. Other than that, no different observations from the ones discussed in the previous two paragraphs were made (See Figure A.65 & Figure A.66, Appendix A).

Groups from VIIE to VIIH - Beams in Groups VIIE, VIIF, VIIG & VIIH were identical with those in Groups VIIA, VIIB, VIIC & VIID respectively. However the flange height of all T-beams was increased to 300 mm ( $h/2$ ). Increasing flange height from  $1/4$  of the total heights to  $1/2$  did not change the behaviour of beams having flange widths 8 times of web width. However it made the behaviour of beams with  $b=4b_w$  a little bit more ductile. Ultimate moment capacities of all beams whose flange heights were  $1/4$  of the total height, were the same with the ones which had twice the flange height (See Figures from A.67 to A.70, Appendix A).

Group VIIJ - Beams (either 'T' or rectangular) were made of C40 concrete. Tension reinforcement ratio was 0.0096 ( $8\Phi 16$ ). Ultimate strain capacity for steel was 0.18. Flange height was 150 mm ( $h/4$ ), for all T-beams. Moment-curvature diagrams of beams with different flange widths ( $b_f=8b_w$ ;  $4b_w$ ;  $b_w$ ) are presented in Figure A.71 of Appendix A. It is observed that lowering the width of flange from 8 times of web width to first 4 and then 1, resulted in small decreases in ultimate moment capacities and small increases in curvature ductility ratios.

Group VIIK - Increasing tensile reinforcement ratio to 0.0190 ( $6\Phi 26$ ) for the same examples discussed in Group VIIJ, the beams of Group VIIK were obtained. They were also identical with those of Group VIID, but the concrete strength was

increased from 25 MPa to 40 MPa. Whether the characteristic concrete strength was 40 MPa or 25 MPa did not seem to be so important for the beams whose tensile reinforcement ratio was 0.019. Increasing the characteristic strength of concrete to 40 MPa for such beams, resulted in no significant differences in the behaviour (See Figure A.72, Appendix A). Although the dimensionless moment capacity of beams in Group VIIK were considerable lower than those of VIID, when these moments are multiplied with respective concrete strength, moments were almost identical.

#### 4.8.3 Conclusions

In general to change the cross section of a beam from rectangular to "T" shape makes it to behave more ductile (greater ductility ratio) and to have greater maximum moment capacity. However at some ranges of flange width and height it is possible to have T-beams with smaller ductility ratios as compared to rectangular sections.

To increase the width of flange from 4 times to 8 times of the web width resulted in greater ultimate moment capacities, but it is not possible to give a general judgement about the curvature ductility ratios. It can be said that for high tensile reinforcement ratios ( $\rho \geq 0.019$ ), the curvature ductility ratios of T-beams whose flange widths are 8 times of web widths tend to behave more ductile than those whose flange widths are 4 times of web widths. However for low tensile reinforcement ratios, ductility can decrease as the flange width increases.

To increase the heights of the flanges from quarter of total height to half of the total height did not change neither the capacity nor the behaviour, except for the beams which had high ratios of tension reinforcement and the reinforcing steels had high ultimate strain capacities ( $\epsilon_{su} = 0.18$ ).

## **CHAPTER V**

### **NUMERICAL APPLICATIONS OF THE PROGRAM STUDIES ON R/C COLUMNS**

#### **5.1 General**

In this chapter the column examples will be presented and discussed. There are eight main case studies (listed in the first chapter). Each case study consists of some examples where related moment-curvature diagrams are drawn and presented in the appendix. The examples and related diagrams are grouped for an easier comparison. The grouping system is similar to that described at the beginning of the previous chapter. The case study numbers are shown by Roman numerals, beginning with VIII, and ending at XV.

In order to simplify the presentation and the discussions, types of reinforcement configuration for columns are numbered. Different longitudinal and transverse reinforcement configurations considered and their numbering were given in Figure 3.15, in Chapter 3.

Again to avoid the repetition of general assumptions valid for all columns, the common assumptions are presented prior to discussion of individual groups. The common assumptions are:

- Concrete carries tension. The mathematical model for concrete in tension was presented previously (Section 3.2.3)

- The axial load which corresponds to zero moment capacity in the interaction diagram ( $N_0$ ) is determined by the following formula:

$$N_0 = 0.85 f_{ck} A_c + f_{yk} A_s$$

- The transverse reinforcement volumetric ratio (named as  $\rho_s$ ) is assumed as defined in the Sheikh & Uzumeri Analytical Model for Concrete Confinement in Tied Columns [2]:  $\rho_s$  = the ratio of the volume of total lateral reinforcement to the volume of core. In order to standardize it, the core is assumed to be bounded by the centerlines of the perimeter ties, in all examples. However, while calculating the forces according to the model proposed by Kent & Park, it is certainly born in mind that the core is bounded by the perimeter measured from outside to outside of ties.

- Strain hardening of reinforcing steel starts generally at a strain of five times the yield strain. The exception to this is for the group where the "Influence of Concrete Strength in R/C Columns" is investigated (Section 5.5).

- In general the reinforcing steel of type S420 is used in the examples. However in investigating "Influence of Ratio of Longitudinal Bars ( $\rho_t = A_{st}/A_c$ ) in R/C Columns" (Section 5.6) and "Influence of Axial Load Level ( $'N/f_{ck}A_c'$  Ratio) in R/C Columns" (Section 5.8), S220 steel is also used.

- Cross sectional dimensions for all columns were taken as 500 by 500 mm. However for the groups where "Influence of Axial Load Level ( $'N/f_{ck}A_c'$  Ratio) in R/C Columns" is investigated (Section 5.8), rectangular sections (300 by 600 mm) were also considered.



- One of the most difficult things in investigating the column behaviour, is determining the yielding point on the moment-curvature diagram of a column. Yield curvature was defined as the point where the slope of the moment-curvature diagram changes significantly.

- Interaction diagrams using unconfined concrete and elasto-plastic models for steel for the column sections investigated are given in Appendix B. Load levels are also marked on these interaction diagrams.

## **5.2 Case Study VIII: Influence of Lateral Reinforcement Configuration in R/C Columns**

This study aims to investigate the influence of lateral reinforcement configuration on the column behaviour. For this purpose 25 moment-curvature diagrams for 50 cm square sections were drawn. The main variables investigated were ratio of longitudinal reinforcement, concrete strength and models, ultimate strain of steel, axial load level, and ( $d''/h$ ) ratio. The list of all 25 sections with their properties are given in Table 5.1. The results are presented in Table 5.2.

### **5.2.1 Assumptions**

- Volumetric ratio for the transverse reinforcement ( $\rho_s$ ) for all columns was taken as 0.015. Spacing was also same for all sections and was 100 mm. Diameter of transverse bars and clear covers were so arranged that the lateral reinforcement ratios and spacings remained unchanged.

**Table 5.1:** List of sections and section properties; Influence of lateral reinforcement configuration in R/C columns.

		$d^2 / h$	N (Axial Load)	$\epsilon_{su}$	Conc. Strength and Model	$\rho_t$ ( $A_{st} / A_c$ )	Configur. Number*									
VIII A	VIII A1	0.84 $A_c / A_{ck} = 1.2$	$0.5 f_{ck} A_c$	0.1	C20 Saatcioglu	0.017	2	VIII A1								
	VIII A2						3	VIII A2								
	VIII A3						4	VIII A3								
VIII B	VIII B1					0.84 $A_c / A_{ck} = 1.2$	$0.5 f_{ck} A_c$	0.1	C20 Saatcioglu	0.025	5	VIII B1				
	VIII B2										6	VIII B2				
	VIII B3										7	VIII B3				
VIII C	VIII C1									0.84 $A_c / A_{ck} = 1.2$	$0.5 f_{ck} A_c$	0.1	C20 Saatcioglu	0.034	8	VIII C1
	VIII C2														9	VIII C2
VIII D	VIII D1													0.84 $A_c / A_{ck} = 1.2$	$0.5 f_{ck} A_c$	0.1
	VIII D2	6	VIII D2													
	VIII D3	7	VIII D3													
VIII E	VIII E1	0.84 $A_c / A_{ck} = 1.2$	$0.5 f_{ck} A_c$	0.1	C20 MKP											
	VIII E2					6	VIII E2									
	VIII E3					7	VIII E3									
VIII F	VIII F1				0.84 $A_c / A_{ck} = 1.2$	$0.5 f_{ck} A_c$	0.1	C40 Saatcioglu	0.025							
	VIII F2									6	VIII F2					
	VIII F3									7	VIII F3					
VIII G	VIII G1							0.84 $A_c / A_{ck} = 1.2$	$0.5 f_{ck} A_c$	0.18	C20 Sh. & Uz.	0.025	5	VIII G1		
	VIII G2									6			VIII G2			
	VIII G3									7			VIII G3			
VIII H	VIII H1	0.84 $A_c / A_{ck} = 1.2$	$0.25 f_{ck} A_c$	0.1						C20 Sh. & Uz.	0.025	5	VIII H1			
	VIII H2		6	VIII H2												
	VIII H3		7	VIII H3												
VIII J	VIII J1		0.77	$0.5 f_{ck} A_c$	0.1	C20 Saatcioglu	0.034			8	VIII J1					
	VIII J2		$A_c / A_{ck} = 1.4$							9	VIII J2					

\* Refer to Figure 3.15

**Table 5.2: Results; Influence of lateral reinforcement configuration in R/C columns**

		Curvature (rad/m)						Curvature ductility ratio	Maximum M**	
		Cover Crush	Yield A <sub>s</sub> '	Yield A <sub>s</sub>	Core Crush	Str. Hard. A <sub>s</sub> '	Str. Hard. A <sub>s</sub>			
VIII A	VIII A1	0.0061	0.0086	0.0133	0.0223	0.0496	0.0496	12	0.239	VIII A1
	VIII A2	0.0063	0.0089	0.0127	0.0296	0.0512	0.0512	18	0.242	VIII A2
	VIII A3	0.0063	0.0089	0.0127	0.0296	0.0511	0.0511	16	0.241	VIII A3
VIII B	VIII B1	0.0064	0.0089	0.0127	0.0226	0.0486	0.0583	12	0.295	VIII B1
	VIII B2	0.0067	0.0092	0.0123	0.0346	0.0532	0.0532	18	0.306	VIII B2
	VIII B3	0.0067	0.0092	0.0122	0.0317	0.0521	0.0521	15	0.302	VIII B3
VIII C	VIII C1	0.0066	0.0091	0.0128	0.0223	0.0490	0.0490	17	0.344	VIII C1
	VIII C2	0.0069	0.0094	0.0116	0.0343	0.0516	0.0516	20	0.355	VIII C2
VIII D	VIII D1	0.0071	0.0098	0.0114	0.0158	0.0481	0.0569	10	0.301	VIII D1
	VIII D2	0.0073	0.0101	0.0111	0.0328	0.0574	0.0427	15	0.319	VIII D2
	VIII D3	0.0072	0.0099	0.0107	0.0220	0.0510	0.0510	11	0.307	VIII D3
VIII E	VIII E1	0.0077	0.0094	0.0118	0.0102	0.0491	0.0491	10	0.300	VIII E1
	VIII E2	0.0076	0.0094	0.0117	0.0102	0.0481	0.0571	9	0.297	VIII E2
	VIII E3	0.0076	0.0094	0.0117	0.0102	0.0478	0.0567	9	0.296	VIII E3
VIII F	VIII F1	0.0082	0.0074	0.0137	0.0140	0.0438	0.0674	9	0.203	VIII F1
	VIII F2	0.0082	0.0074	0.0129	0.0194	0.0454	0.0626	10	0.204	VIII F2
	VIII F3	0.0082	0.0074	0.0129	0.0172	0.0448	0.0611	9	0.203	VIII F3
VIII G	VIII G1	0.0071	0.0098	0.0114	0.0158	0.0480	0.0568	9	0.301	VIII G1
	VIII G2	0.0073	0.0101	0.0111	0.0328	0.0575	0.0428	14	0.319	VIII G2
	VIII G3	0.0072	0.0099	0.0107	0.0220	0.0510	0.0510	11	0.307	VIII G3
VIII H	VIII H1	0.0096	0.0150	0.0096	0.0234	0.0820	0.0359	44	0.279	VIII H1
	VIII H2	0.0099	0.0158	0.0099	0.0449	0.0879	0.0357	41	0.286	VIII H2
	VIII H3	0.0097	0.0152	0.0097	0.0338	0.0839	0.0368	53	0.281	VIII H3
VIII J	VIII J1	0.0066	0.0099	0.0135	0.0232	0.0557	0.0652	17	0.313	VIII J1
	VIII J2	0.0069	0.0102	0.0131	0.0338	0.0583	0.0583	22	0.318	VIII J2

\* Ultimate curvature was reached, before the event occurred.  
\*\* M: M / bh<sup>2</sup>f<sub>c</sub>

### 5.2.2 Discussion of Results

Group VIIIA - Columns were reinforced with 8 $\Phi$ 26 longitudinal bars ( $\rho_t=0.017$ ) having an ultimate strain of 0.1. Characteristic strength of concrete was 20 MPa. Axial load level was  $0.5f_{ck}A_c$  (maximum permitted in the Turkish Seismic Code) and  $d''/h$  ratio was 0.84. Saatcioglu confinement model was used to calculate the core concrete stresses. Configurations 2, 3 & 4 of Figure 3.15 were investigated. The moment-curvature curves obtained are presented in Figure A.73, Appendix A. For this group, the lateral reinforcement configurations did not influence the moment-curvature relationships so much. Moment-curvature diagrams and curvature ductility ratios of the columns with configuration numbers 3 & 4 were exactly same and they behaved somewhat more ductile than that of the column with configuration number 2.

Group VIIIB - These were identical columns with those of Group VIIIA. However the ratio of longitudinal was increased from 0.017 to 0.025 (12 $\Phi$ 26). Configurations 5, 6 & 7 were investigated. The moment-curvature curves obtained are presented in Figure A.74 of Appendix A. It is observed that the column with transverse reinforcement configuration number 6, behaved somewhat more ductile than the others. Although the confinement ratios and spacings of all three columns were kept the same by arranging the diameters of transverse reinforcement, the poorest behaviour, curvature ductility ratio, and maximum moment capacity belonged to the one with the configuration number of 5. Then comes 7. The contribution of the configuration type on the behaviour appears clearly by comparing the columns with configuration number of 6 (VIIIB2) with the others (VIIIB1 & VIIIB3). This may be due to the fact that the configuration type number 6 resembles the circular or spiral which is the most effective configuration in confining.

Group VIIC - These were identical columns with those of Group VIIIA & VIIIB. However the ratio of longitudinal bars was increased to 0.034 (16 $\Phi$ 26). Configurations 8 & 9 were investigated. The moment-curvature curves obtained are

presented in Figure A.75. It was aimed to compare two examples which represent two extreme confinement configurations, one with one tie, the other one five ties. (VIIIIC1, configuration number 8) and (VIIIIC2, configuration number 9). Looking at the diagrams it is observed that, although the column VIIIIC2 seems to behave better (considering ductility and maximum moment capacity) than the other, the curvature ductility ratios and maximum moment capacities of these two examples were almost the same. Also the curvature values that correspond to crushing of clear cover, tension steels yielding point, etc. are almost the same. Only crushing of core concrete starting point in VIIIIC2 took place later than that of column VIIIIC1 (See Table A.16, Appendix A).

Group VI IID - Columns were reinforced with  $12\Phi 26$  longitudinal bars ( $\rho_t = 0.025$ ) with ultimate strain of 0.1. Characteristic strength of concrete was 20 MPa. Axial load level was  $0.5f_{ck}A_c$  and  $d''/h$  ratio was 0.84. Sheikh & Uzumeri confinement model was used to calculate the core concrete stresses. Configurations 5, 6 & 7 were investigated. Changing only the confinement model, keeping all other variables same as in the examples of Group VI IIB, the discussions made for the examples of group VI IIB seemed to be valid. However change in behaviour and in maximum moment capacity at the column with configuration number of 6, was more visible in Sheikh & Uzumeri model (See Figure A.76, Appendix A). Sheikh & Uzumeri model considers the confinement configuration. It should also be noted that Sheikh & Uzumeri models results in smaller curvature capacities as compared to Saatcioglu model (Compare Figures A.74 & A.76).

Group VI IIE - These were identical columns with those of Group VI IIB or VI IID. However the confinement model was Modified Kent & Park this time. For the same columns (configurations 5, 6 & 7), with Modified Kent & Park model, it is seen that all columns behave exactly the same with less curvature ductility capacities than of Group VI IIB & VI IID. This is probably due to the fact that Modified Kent & Park model does not take into account the transverse steel configuration type (See Figure

A.77, Appendix A). Similar behaviour of these three columns raises some doubts about the modified Kent & Park model which does not take into account confinement configuration.

Group VIII F - These were identical columns with those of Group VIII B. However the concrete strength was increased to 40 MPa. Saatcioglu model was used for confined concrete. It was observed that although the start of crushing of core concrete in columns VIII F2 (conf. no: 6) and VIII F3 (conf. no: 7) occurred later as compared to that of column VIII F1 (conf. no: 5), this did not influence the behaviour and all columns had similar moment-curvature diagrams (See Figure A.78, Appendix A). When Figures A.74 & A.78 are compared, it will be seen that curvature capacity decreased considerably with increasing concrete strength.

Group VIII G - Identical columns with those of Group VIII D. However ultimate strain of longitudinal steel was increased to 0.18. Columns with steel having  $\epsilon_{su}=0.18$  had similar moment-curvature diagrams with those of with  $\epsilon_{su}=0.1$  (See Figure A.79, Appendix A).

Group VIII H - These were identical columns with those of Group VIII D. However the level of the axial load was reduced to " $0.25f_{ck}A_c$ ". It was observed that for all columns maximum moment capacities decreased a little and behaviour became much more ductile as compared with those of the examples of group VIII D. Such a behaviour was expected. However, different from the examples with the axial load of " $0.5f_{ck}A_c$ ", there was no significant differences in the behaviour of columns with various configuration types. More important than that, the column with configuration number of 6 (VIII H2) had the lowest curvature capacity (See Figure A.80, Appendix A). This is because neutral axis heights of that column reduced more rapidly and always remained less than those of the others (VIII H1 & VIII H3) since the core of that column was confined most effectively, therefore tension reinforcements strains reached their ultimate values earlier and ruptured.

Group VIIIJ - These were identical columns with those of Group VIIC. However the ratio of ' $d/h$ ' was decreased from 0.84 to 0.77 (that is, the ratio of ' $A_s/A_{ck}$ ' was increased from 1.2 to 1.4). The discussions made for the examples of Group VIIC were valid for this group also. Moreover, although maximum moment capacities of both VIIIJ1 and VIIIJ2 were a little less than those of the VIIC1 & VIIC2 respectively, this was not due to the influence of lateral reinforcement configuration type, but due to the influence of the ratio of ' $A_s/A_{ck}$ ' (See Figure A.81, Appendix A).

### 5.2.3 Conclusions

Transverse steel configuration seemed to influence the behaviour. Confinement configuration influenced ductility and maximum moment capacity of the column.

The influence of lateral reinforcement configuration was very clear when the ratio of longitudinal bars was about 0.025, more clear when this ratio was about 0.034. It seems that the confinement configuration becomes more distinct as the ratio of longitudinal reinforcement increases.

When configurations 5, 6 and 7 are compared, number 6 seems to be more effective than the others.

When the axial load level was decreased from  $0.5f_{ck}A_c$  to  $0.25f_{ck}A_c$  and when the characteristic concrete strength was increased from 20 MPa to 40 MPa, the effect of confinement configuration seemed to be less important.

Modified Kent & Park model does not take into account the transverse steel configuration type in defining the confined concrete stress-strain relationship. On the

other hand, Sheikh & Uzumeri and Saatcioglu models take into account the confinement configuration. Therefore for different reinforcement configuration types, Sheikh & Uzumeri and Saatcioglu models yield more realistic results.

### **5.3 Case Study IX: Influence of Lateral Reinforcement Ratio " $\rho_s$ " in R/C Columns**

This study aims to investigate the influence of volumetric ratio of lateral reinforcement, " $\rho_s$ " on column behaviour. For this purpose 27 moment-curvature diagrams for 50 cm square sections were drawn. The main variables investigated were confinement configuration types, ratios of longitudinal reinforcement, concrete strength and concrete models, ultimate strain of steel, axial load level, and 'd'/h' ratio. In each group, columns having different confinement ratios ( $\rho_s=0.010$ ; 0.015; 0.020) were investigated. The list of all 27 sections with their properties are given in Table 5.3. The results are presented in Table 5.4.

#### **5.3.1 Assumptions**

•In each group, three examples with three different levels of transverse reinforcement ratios were investigated. These ratios were  $\rho_s = 0.010$ , 0.015 & 0.020. Spacing of ties was same for all sections and was 100 mm. Transverse steel diameter and clear cover were so arranged that spacings remained unchanged.



**Table 5.3: List of sections and section properties; Influence of lateral reinforcement ratio " $\rho_s$ " in R/C columns**

		$d'' / h$	N (Axial Load)	$\epsilon_{su}$	Conc. Strength and Model	$\rho_t$ ( $A_{st} / A_c$ )	Configur. Number*	Confinement Ratio									
IXA	IXA1	0.83 $A_c / A_{ck} = 1.2$	$0.5 f_{ck} A_c$	0.1	C20 Sh. & Uz.	0.013	1	0.010	IXA1								
	IXA2							0.015	IXA2								
	IXA3							0.020	IXA3								
IXB	IXB1					$0.83$ $A_c / A_{ck} = 1.2$	$0.5 f_{ck} A_c$	0.1	C20 Sh. & Uz.	0.026	4	0.010	IXB1				
	IXB2											0.015	IXB2				
	IXB3											0.020	IXB3				
IXC	IXC1									$0.83$ $A_c / A_{ck} = 1.2$	$0.5 f_{ck} A_c$	0.1	C20 Sh. & Uz.	0.039	7	0.010	IXC1
	IXC2															0.015	IXC2
	IXC3															0.020	IXC3
IXD	IXD1	$0.83$ $A_c / A_{ck} = 1.2$	$0.5 f_{ck} A_c$	0.1	C20 Saatcioglu									0.026	4	0.010	IXD1
	IXD2															0.015	IXD2
	IXD3															0.020	IXD3
IXE	IXE1				$0.83$ $A_c / A_{ck} = 1.2$	$0.5 f_{ck} A_c$	0.1	C20 MKP	0.026					4	0.010	IXE1	
	IXE2														0.015	IXE2	
	IXE3														0.020	IXE3	
IXF	IXF1							$0.83$ $A_c / A_{ck} = 1.2$	$0.5 f_{ck} A_c$	0.1	C40 Sh. & Uz.	0.026	4	0.010	IXF1		
	IXF2													0.015	IXF2		
	IXF3													0.020	IXF3		
IXG	IXG1	$0.83$ $A_c / A_{ck} = 1.2$	$0.5 f_{ck} A_c$	0.18							C20 Sh. & Uz.	0.026	4	0.010	IXG1		
	IXG2			0.015										IXG2			
	IXG3			0.020										IXG3			
IXH	IXH1			$0.83$ $A_c / A_{ck} = 1.2$	$0.25 f_{ck} A_c$	0.1	C20 Sh. & Uz.				0.026	4	0.010	IXH1			
	IXH2				0.015	IXH2											
	IXH3				0.020	IXH3											
IXJ	IXJ1				0.76 $A_c / A_{ck} = 1.4$	$0.5 f_{ck} A_c$	0.1	C20 Sh. & Uz.	0.026	4	0.010	IXJ1					
	IXJ2										0.015	IXJ2					
	IXJ3										0.020	IXJ3					

\* Refer to Figure 3.15

**Table 5.4: Results; Influence of lateral reinforcement ratio " $\rho_s$ " in R/C columns**

		Curvature (rad/m)						Curvature ductility ratio	Maximum M**	
		Cover Crush	Yield $A_s'$	Yield $A_s$	Core Crush	Str. Hard. $A_s'$	Str. Hard. $A_s$			
IXA	IXA1	0.0068	0.0095	0.0119	0.0137	0.0450	*	5	0.248	IXA1
	IXA2	0.0069	0.0097	0.0112	0.0160	0.0490	0.0580	7	0.252	IXA2
	IXA3	0.0070	0.0098	0.0115	0.0183	0.0519	0.0519	12	0.255	IXA3
IXB	IXB1	0.0071	0.0099	0.0115	0.0182	0.0499	0.0499	7	0.313	IXB1
	IXB2	0.0072	0.0100	0.0108	0.0249	0.0519	0.0519	13	0.319	IXB2
	IXB3	0.0073	0.0101	0.0110	0.0300	0.0533	0.0533	20	0.324	IXB3
IXC	IXC1	0.0073	0.0099	0.0114	0.0178	0.0467	0.0549	9	0.380	IXC1
	IXC2	0.0073	0.0100	0.0116	0.0240	0.0507	0.0507	15	0.385	IXC2
	IXC3	0.0073	0.0100	0.0108	0.0286	0.0535	0.0535	19	0.390	IXC3
IXD	IXD1	0.0064	0.0089	0.0133	0.0243	0.0490	0.0588	14	0.293	IXD1
	IXD2	0.0065	0.0090	0.0126	0.0292	0.0504	0.0504	31	0.295	IXD2
	IXD3	0.0066	0.0091	0.0129	0.0319	0.0512	0.0512	45	0.302	IXD3
IXE	IXE1	0.0075	0.0092	0.0128	0.0092	0.0468	0.0561	9	0.295	IXE1
	IXE2	0.0076	0.0093	0.0124	0.0101	0.0490	0.0587	12	0.303	IXE2
	IXE3	0.0077	0.0095	0.0119	0.0110	0.0509	0.0509	19	0.310	IXE3
IXF	IXF1	0.0076	0.0068	0.0154	0.0130	0.0445	*	7	0.202	IXF1
	IXF2	0.0076	0.0068	0.0149	0.0149	0.0465	0.0560	14	0.206	IXF2
	IXF3	0.0077	0.0068	0.0143	0.0190	0.0479	0.0578	19	0.208	IXF3
IXG	IXG1	0.0071	0.0099	0.0115	0.0182	0.0499	0.0499	8	0.313	IXG1
	IXG2	0.0072	0.0100	0.0108	0.0249	0.0519	0.0519	12	0.319	IXG2
	IXG3	0.0073	0.0101	0.0110	0.0300	0.0533	0.0533	18	0.324	IXG3
IXH	IXH1	0.0096	0.0157	0.0096	0.0256	0.0734	0.0385	16	0.291	IXH1
	IXH2	0.0097	0.0160	0.0097	0.0323	0.0810	0.0381	27	0.295	IXH2
	IXH3	0.0098	0.0162	0.0098	0.0398	0.0864	0.0366	58	0.298	IXH3
IXJ	IXJ1	0.0070	0.0106	0.0121	0.0186	0.0567	0.0659	4	0.291	IXJ1
	IXJ2	0.0071	0.0107	0.0124	0.0253	0.0589	0.0589	7	0.296	IXJ2
	IXJ3	0.0071	0.0108	0.0126	0.0301	0.0604	0.0604	11	0.299	IXJ3

\* Ultimate curvature was reached, before the event occurred.  
\*\* M:  $M / bh^2f_c$

### 5.3.2 Discussion of Results

Group IXA - Columns of this group were reinforced with 4 $\Phi$ 32 longitudinal bars ( $\rho_t = 0.013$ ) having ultimate strain of 0.1. Characteristic strength of concrete was 20 MPa. Axial load level was  $0.5f_{ck}A_c$  and  $d''/h$  ratio was 0.83. Configuration type was 1, as shown in Figure 3.15. Sheikh & Uzumeri confinement model was used for the core concrete. The moment-curvature curves of columns having different confinement ratios are presented in Figure A.82 of Appendix A. From the figure it is observed that, when the lateral reinforcement ratio " $\rho_s$ " is increased from 0.010 to first 0.015 and then 0.020 changed the behaviour and ductility, but did not change the moment capacities so much. Curvature ductility ratio of IXA3 ( $\rho_s=0.020$ ) was 2.5 times and IXA2 ( $\rho_s=0.015$ ) was 1.5 times greater than that of the IXA1 ( $\rho_s=0.010$ ). The curvature values which correspond to initiation of crushing of clear cover, yielding of tension steel, etc. were not influenced by the changing confinement ratios. Only the starting point of crushing of core concrete was delayed a little with the increase in confining, as expected.

Group IXB - Columns were reinforced with 8 $\Phi$ 32 longitudinal bars ( $\rho_t=0.026$ ) having ultimate strain of 0.1. Characteristic strength of concrete was 20 MPa. Axial load level was  $0.5f_{ck}A_c$  and  $d''/h$  ratio was 0.83. Configuration type was 4, in Figure 3.15. Sheikh & Uzumeri confinement model was used to calculate the core concrete stresses. The examples of this group were identical with those of Group IXA, but the ratio of longitudinal bars was increased to 0.026, and the confinement configuration was 4 instead of 1. The discussions made in the previous paragraph were valid for this group also. For this group the curvature ductility ratio of IXB3 ( $\rho_s=0.020$ ) was 3 times and IXB2 ( $\rho_s=0.015$ ) was 2 times greater than that of the IXB1 ( $\rho_s=0.010$ ) (See Figure A.83, Appendix A). It should be noted that curvature capacity increased significantly with increasing ratio of longitudinal reinforcement (Compare Figures A.82 & A.83).

Group IXC - These were identical columns as those of Group IXA or IXB. However the ratio of longitudinal bars was increased to 0.039 ( $12\Phi32$ ), and confinement configuration was 7 of Figure 3.15. The only difference with previous groups was that there was a gain in moment capacity after the clear cover crushing, since more steel means better compensation of strength loss due to crushing of cover concrete. This gain becomes more distinct as  $\rho_s$  increases (See Figure A.84, Appendix A). Also curvature capacity of columns in this group were somewhat higher than those of Group IXB.

Groups IXD & IXE - All the variables of the examples in Group IXB were kept same, only the confined concrete model was changed from Sheikh and Uzumeri to first Saatcioglu (Group IXD) and then to Modified Kent & Park (Group IXE). Therefore, nine examples were grouped in three figures (Figure A.83: Sheikh & Uzumeri; Figure A.85: Saatcioglu; Figure A.86: Modified Kent & Park). Although in general discussions for the examples of Group IXB were valid for the examples of Groups IXD & IXE, there were differences between these three cases. For example, curvature capacities calculated by using Saatcioglu model were almost twice as much as those calculated by using other models. Curves obtained by Sheikh & Uzumeri (Figure A.83) are not too different from those obtained by Modified Kent & Park Model (Figure A.86).

Groups IXF & IXG - When characteristic concrete strengths of columns were increased from 20 MPa to 40 MPa (Group IXF) or when the strain capacities of longitudinal steel used in columns were raised from 0.1 to 0.18 (Group IXG), keeping other variables same as in the examples of Group IXB, no significant differences in behaviour were observed (See Figure A.87 & Figure A.88, Appendix A). However changing the concrete strength from 20 MPa to 40 MPa decreased both the dimensionless moment capacity and the curvature capacity. It should be noted that the axial load  $N=0.5f_{ck}A_c$  for the column with C40 is twice that of column made with

C20. Therefore in reality the moment capacity increased due to increasing concrete strength.

Group IXH - Columns of this group were identical with those of IXB, the only difference being the level of axial load, which was decreased to " $0.25f_{ck}A_c$ ". It was observed that for all columns dimensionless moment capacities decreased a little and behaviours become much more ductile as compared with those of the examples of group IXB (See Figure A.89, Appendix A). Curvature ductility ratios of IXH3 ( $\rho_s=0.020$ ) was about 3.5 times and IXH2 ( $\rho_s=0.015$ ) was about 1.5 times greater than that of the IXH1 ( $\rho_s=0.010$ ). The axial load levels considered are also marked on the interaction diagram B3 in Appendix B.

Group IXJ - Reducing the ratio of ' $d/h$ ' from 0.83 to 0.76 (that is, increasing the ratio of ' $A_c/A_{ck}$ ' from 1.2 to 1.4), and keeping all other variables same as in the examples of Group IXB, it is seen that the discussions made in the paragraph for the examples of Group IXB were valid also for the examples of Group IXJ (See Figure A.90, Appendix A).

### 5.3.3 Conclusions

For the columns having the same types of transverse steel configurations and same spacing, increase in confinement ratio (only by arranging diameters of lateral steels) resulted in more ductility and slightly higher moment capacities.

The curvature ductility ratios of the columns with a confinement ratio of 0.015, were 1.5-2.0 times greater than those of columns with  $\rho_s=0.01$ . The curvature ductility ratios of the columns with a confinement ratio of 0.020 were 2.0-3.5 (these numbers depend on the other variables) times greater than those of the columns with confinement ratios of 0.010.

The ductility of the columns seemed to be insensitive to variables such as, 'd"/h' ratio and the ultimate strain capacity of longitudinal steel, because comparing all the figures obtained by changing any of these variables, discussions made remained the same. The behaviour changed with changing concrete strength.

Increase in confinement delayed the starting of core concrete crushing, but does not change the order of other observations, such as starting of clear cover crushing, starting of tension steels yielding, etc.

#### **5.4 Case Study X: Influence of Lateral Reinforcement Spacing in R/C Columns**

This study aims to investigate the influence of lateral reinforcement spacing on column behaviour. For this purpose 27 moment-curvature diagrams for 50 cm square sections were drawn. The main variables investigated were lateral reinforcement configuration types, ratios of longitudinal bars, concrete strength, confined concrete models, ultimate strain of steel, axial load level, and d"/h ratios. In each group, columns having different tie spacings (spacing: 70, 100, 130 mm) were investigated. Volumetric ratio of ties i.e  $\rho_s$  was kept the same in all columns. The list of all 27 sections with their properties are given in Table 5.5. The results are presented in Table 5.6.

##### **5.4.1 Assumptions**

•In each group, three examples with three different transverse reinforcement spacings were investigated. These spacings were 70, 100 & 130 mm. Lateral reinforcement ratio " $\rho_s$ " was kept the same for all cases ( $\rho_s=0.015$ ). Transverse steel diameters and clear covers were so arranged that lateral reinforcement ratio remained unchanged.

**Table 5.5: List of Sections and section properties; Influence of lateral reinforcement spacing in R/C columns**

		$d'' / h$	N (Axial Load)	$\epsilon_{su}$	Conc. Strength and Model	$\rho_t$ ( $A_{st} / A_c$ )	Configur. Number*	Tie Spacing	
XA	XA1	0.83 $A_c / A_{ck} = 1.2$	$0.5 f_{ck} A_c$	0.1	C20 Sh. & Uz.	0.013	1	70 mm	XA1
	XA2							100 mm	XA2
	XA3							130 mm	XA3
XB	XB1	0.83 $A_c / A_{ck} = 1.2$	$0.5 f_{ck} A_c$	0.1	C20 Sh. & Uz.	0.026	4	70 mm	XB1
	XB2							100 mm	XB2
	XB3							130 mm	XB3
XC	XC1	0.83 $A_c / A_{ck} = 1.2$	$0.5 f_{ck} A_c$	0.1	C20 Sh. & Uz.	0.039	7	70 mm	XC1
	XC2							100 mm	XC2
	XC3							130 mm	XC3
XD	XD1	0.83 $A_c / A_{ck} = 1.2$	$0.5 f_{ck} A_c$	0.1	C20 Saatcioglu	0.026	4	70 mm	XD1
	XD2							100 mm	XD2
	XD3							130 mm	XD3
XE	XE1	0.83 $A_c / A_{ck} = 1.2$	$0.5 f_{ck} A_c$	0.1	C20 MKP	0.026	4	70 mm	XE1
	XE2							100 mm	XE2
	XE3							130 mm	XE3
XF	XF1	0.83 $A_c / A_{ck} = 1.2$	$0.5 f_{ck} A_c$	0.1	C40 Sh. & Uz.	0.026	4	70 mm	XF1
	XF2							100 mm	XF2
	XF3							130 mm	XF3
XG	XG1	0.83 $A_c / A_{ck} = 1.2$	$0.5 f_{ck} A_c$	0.18	C20 Sh. & Uz.	0.026	4	70 mm	XG1
	XG2							100 mm	XG2
	XG3							130 mm	XG3
XH	XH1	0.83 $A_c / A_{ck} = 1.2$	$0.25 f_{ck} A_c$	0.1	C20 Sh. & Uz.	0.026	4	70 mm	XH1
	XH2							100 mm	XH2
	XH3							130 mm	XH3
XJ	XJ1	0.76 $A_c / A_{ck} = 1.4$	$0.5 f_{ck} A_c$	0.1	C20 Sh. & Uz.	0.026	4	70 mm	XJ1
	XJ2							100 mm	XJ2
	XJ3							130 mm	XJ3

\* Refer to Figure 3.15

**Table 5.6: Results; Influence of lateral reinforcement spacing in R/C columns**

		Curvature (rad/m)						Curvature ductility ratio	Maximum M**	
		Cover Crush	Yield A <sub>s</sub> '	Yield A <sub>s</sub>	Core Crush	Str. Hard. A <sub>s</sub> '	Str. Hard. A <sub>s</sub>			
XA	XA1	0.0069	0.0097	0.0113	0.0164	0.0498	0.0498	9	0.253	XA1
	XA2	0.0069	0.0097	0.0112	0.0160	0.0490	0.0580	7	0.252	XA2
	XA3	0.0069	0.0096	0.0112	0.0140	0.0481	0.0567	6	0.251	XA3
XB	XB1	0.0072	0.0100	0.0109	0.0273	0.0524	0.0524	15	0.320	XB1
	XB2	0.0072	0.0100	0.0108	0.0249	0.0519	0.0519	12	0.319	XB2
	XB3	0.0072	0.0100	0.0108	0.0204	0.0513	0.0513	11	0.317	XB3
XC	XC1	0.0073	0.0100	0.0117	0.0262	0.0517	0.0517	18	0.387	XC1
	XC2	0.0073	0.0100	0.0116	0.0240	0.0507	0.0507	15	0.385	XC2
	XC3	0.0073	0.0099	0.0115	0.0197	0.0495	0.0495	12	0.384	XC3
XD	XD1	0.0066	0.0092	0.0129	0.0340	0.0510	0.0510	33	0.299	XD1
	XD2	0.0065	0.0090	0.0126	0.0292	0.0504	0.0504	31	0.295	XD2
	XD3	0.0064	0.0089	0.0125	0.0268	0.0499	0.0499	28	0.294	XD3
XE	XE1	0.0076	0.0093	0.0124	0.0101	0.0491	0.0588	16	0.302	XE1
	XE2	0.0076	0.0093	0.0124	0.0101	0.0490	0.0587	12	0.303	XE2
	XE3	0.0076	0.0093	0.0124	0.0101	0.0490	0.0586	12	0.304	XE3
XF	XF1	0.0076	0.0068	0.0149	0.0166	0.0470	0.0567	12	0.206	XF1
	XF2	0.0076	0.0068	0.0149	0.0149	0.0465	0.0560	11	0.206	XF2
	XF3	0.0076	0.0048	0.0149	0.0135	0.0460	0.0553	9	0.205	XF3
XG	XG1	0.0072	0.0100	0.0109	0.0273	0.0524	0.0524	15	0.320	XG1
	XG2	0.0072	0.0100	0.0108	0.0249	0.0519	0.0519	12	0.319	XG2
	XG3	0.0072	0.0100	0.0108	0.0204	0.0513	0.0513	10	0.317	XG3
XH	XH1	0.0098	0.0160	0.0098	0.0355	0.0828	0.0384	58	0.295	XH1
	XH2	0.0097	0.0160	0.0097	0.0323	0.0810	0.0381	27	0.295	XH2
	XH3	0.0097	0.0159	0.0097	0.0297	0.0788	0.0375	22	0.294	XH3
XJ	XJ1	0.0071	0.0107	0.0124	0.0276	0.0596	0.0596	8	0.297	XJ1
	XJ2	0.0071	0.0107	0.0124	0.0253	0.0589	0.0589	7	0.296	XJ2
	XJ3	0.0070	0.0107	0.0123	0.0211	0.0582	0.0582	5	0.294	XJ3

\* Ultimate curvature was reached, before the event occurred.  
\*\* M: M / bh<sup>2</sup>f<sub>c</sub>



## 5.4.2 Discussion of Results

In all groups it is observed that, when the lateral reinforcement spacing was increased, keeping the confinement ratio and configuration same, curvature ductility ratios decreased, but the moment capacities remained unchanged. The curvature ductility ratios of columns having 130 mm spacings for lateral reinforcements were 10-15%, and columns having 100 mm spacings were 20-30% less than those of with  $s=70$  mm. The differences changed when the axial load level was reduced from  $0.5f_{ck}A_c$  to  $0.25f_{ck}A_c$ . Reduction in curvature ductility ratio, when the spacing was increased from 70 mm to 130 mm for the axial load of  $0.25f_{ck}A_c$ , was not 20-30%, but was 60% (See Figures from A.91 to A.99, Appendix A).

The influence of tie spacing was not different when Sheikh & Uzumeri model and Kent & Park models were used. When Figures A.92 & A.95 are compared it will be seen that the behaviour was almost the same, except Sheikh & Uzumeri model resulted in greater moment capacities.

The behaviour observed changed considerably when Saatcioglu model was used (Figure A.94). Curvature capacities were significantly greater using Saatcioglu model

The curvature values that corresponding to clear cover crushing, tension steel yielding, etc. were not influenced by changing lateral steel spacings. However, starting point of core concrete crushing occurred a little earlier with the increase in spacings of lateral steels, as it was expected.

### 5.4.3 Conclusions

For the columns having the same type of transverse steel configurations and same ratios of transverse reinforcements, increase in spacing of lateral steel resulted in less ductile behaviour. This was true for all confined concrete models used.

For designers, it is recommended to use smaller spacings with smaller tie diameter, instead of larger spacings with larger tie diameters.

### 5.5 Case Study XI: Influence of Concrete Strength in R/C Columns

This study aims to investigate the influence of concrete strength on the column behaviour. For this purpose 39 moment-curvature diagrams for 50 cm square sections were drawn. The main variables investigated were ratios of longitudinal bars, transverse steel ratios and configuration types, confined concrete models, axial load levels, and steel models. In each group, columns having different concrete strengths ( $f_{ck}=20; 30; 40$  MPa) were investigated. The list of all 39 sections with their properties are given in Table 5.7. The results are presented in Table 5.8.

#### 5.5.1 Assumptions

- Clear cover in all cases was 23 mm. Diameters of longitudinal and transverse reinforcements were 32 and 10 mm respectively. Therefore the ratio of 'd'/h' is same for all columns.
- For all groups, three different concrete strength were used; C20, C30 & C40. The numbers 20, 30 & 40 represents the characteristic strengths (in MPa) of unconfined concrete used in columns.

**Table 5.7: List of sections and section properties; Influence of concrete strength in R/C columns**

		Steel Model	N (Axial Load)	Concrete Model	Ties	Configur. Number*	$\rho_t$ ( $A_{st} / A_c$ )	Concrete Strength							
XIA	XIA1	$\epsilon_{sp} = 5\epsilon_{sy}$ $\epsilon_{su} = 0.1$	$0.5 f_{ck} A_c$	Saatcioglu	$\Phi 10/150$	1	0.013	C20	XIA1						
	XIA2							C30	XIA2						
	XIA3							C40	XIA3						
XIB	XIB1				$\epsilon_{sp} = 5\epsilon_{sy}$ $\epsilon_{su} = 0.1$	$0.5 f_{ck} A_c$	Saatcioglu	$\Phi 10/100$	1	0.013	C20	XIB1			
	XIB2										C30	XIB2			
	XIB3										C40	XIB3			
XIC	XIC1							$\epsilon_{sp} = 5\epsilon_{sy}$ $\epsilon_{su} = 0.1$	$0.5 f_{ck} A_c$	Saatcioglu	$\Phi 10/100$	2	0.026	C20	XIC1
	XIC2													C30	XIC2
	XIC3													C40	XIC3
XID	XID1	$\epsilon_{sp} = 5\epsilon_{sy}$ $\epsilon_{su} = 0.1$	$0.5 f_{ck} A_c$	Saatcioglu							$\Phi 10/150$	4	0.026	C20	XID1
	XID2													C30	XID2
	XID3													C40	XID3
XIE	XIE1				$\epsilon_{sp} = 5\epsilon_{sy}$ $\epsilon_{su} = 0.1$	$0.5 f_{ck} A_c$	Saatcioglu				$\Phi 10/100$	4	0.026	C20	XIE1
	XIE2													C30	XIE2
	XIE3													C40	XIE3
XIF	XIF1							$\epsilon_{sp} = 5\epsilon_{sy}$ $\epsilon_{su} = 0.1$	$0.5 f_{ck} A_c$	Saatcioglu	$\Phi 10/100$	7	0.039	C20	XIF1
	XIF2													C30	XIF2
	XIF3													C40	XIF3
XIG	XIG1	$\epsilon_{sp} = 5\epsilon_{sy}$ $\epsilon_{su} = 0.1$	$0.25 f_{ck} A_c$	Sh. & Uz.							$\Phi 10/100$	4	0.026	C20	XIG1
	XIG2													C30	XIG2
	XIG3													C40	XIG3
XIH	XIH1			$\epsilon_{sp} = 5\epsilon_{sy}$ $\epsilon_{su} = 0.1$	$0.25 f_{ck} A_c$	MKP	$\Phi 10/100$				4	0.026	C20	XIH1	
	XIH2												C30	XIH2	
	XIH3												C40	XIH3	
XIJ	XIJ1					$\epsilon_{sp} = 5\epsilon_{sy}$ $\epsilon_{su} = 0.1$	$0.25 f_{ck} A_c$	Saatcioglu	$\Phi 10/100$	4	0.026	C20	XIJ1		
	XIJ2											C30	XIJ2		
	XIJ3											C40	XIJ3		
XIK	XIK1	$\epsilon_{sp} = 5\epsilon_{sy}$ $\epsilon_{su} = 0.1$	$0.25 f_{ck} A_c$						Saatcioglu	$\Phi 10/100$	7	0.039	C20	XIK1	
	XIK2												C30	XIK2	
	XIK3												C40	XIK3	
XIL	XIL1			$\epsilon_{sp} = 5\epsilon_{sy}$ $\epsilon_{su} = 0.18$	$0.5 f_{ck} A_c$					Saatcioglu	$\Phi 10/100$	4	0.026	C20	XIL1
	XIL2													C30	XIL2
	XIL3													C40	XIL3
XIM	XIM1			$\epsilon_{sp} = 2\epsilon_{sy}$ $\epsilon_{su} = 0.1$	$0.5 f_{ck} A_c$	Sh. & Uz.	$\Phi 10/100$	3		0.026	C20	XIM1			
	XIM2										C30	XIM2			
	XIM3										C40	XIM3			
XIN	XIN1	$\epsilon_{sp} = 10\epsilon_{sy}$ $\epsilon_{su} = 0.1$	$0.5 f_{ck} A_c$	Sh. & Uz.	$\Phi 10/100$	3	0.026	C20	XIN1						
	XIN2							C30	XIN2						
	XIN3							C40	XIN3						

\* Refer to Figure 3.15

**Table 5.8: Results; Influence of concrete strength in R/C columns**

		Curvature (rad/m)						Curvature ductility ratio	Maximum M**	
		Cover Crush	Yield A <sub>s</sub> '	Yield A <sub>s</sub>	Core Crush	Str. Hard. A <sub>s</sub> '	Str. Hard. A <sub>s</sub>			
XIA	XIA1	0.0058	0.0083	0.0158	0.0136	*	*	4	569.5	XIA1
	XIA2	0.0072	0.0080	0.0170	0.0118	*	*	3	712.0	XIA2
	XIA3	0.0078	0.0078	*	0.0102	*	*	2	851.2	XIA3
XIB	XIB1	0.0058	0.0083	0.0153	0.0161	0.0416	*	6	573.9	XIB1
	XIB2	0.0072	0.0080	0.0174	0.0135	*	*	3	718.9	XIB2
	XIB3	0.0078	0.0078	0.0171	0.0116	*	*	2	862.2	XIB3
XIC	XIC1	0.0063	0.0088	0.0139	0.0193	0.0461	0.0642	7	709.2	XIC1
	XIC2	0.0076	0.0084	0.0136	0.0139	*	*	4	857.5	XIC2
	XIC3	0.0082	0.0082	0.0154	0.0127	32.0000	16.0000	3	997.1	XIC3
XID	XID1	0.0063	0.0089	0.0131	0.0215	0.0470	0.0564	8	710.8	XID1
	XID2	0.0076	0.0084	0.0136	0.0151	0.0444	*	5	858.9	XID2
	XID3	0.0082	0.0082	0.0155	0.0134	*	*	4	1001.3	XID3
XIE	XIE1	0.0065	0.0091	0.0135	0.0263	0.0490	0.0590	19	716.9	XIE1
	XIE2	0.0077	0.0085	0.0137	0.0190	0.0466	0.0561	11	862.3	XIE2
	XIE3	0.0082	0.0082	0.0149	0.0149	0.0447	*	5	1007.8	XIE3
XIF	XIF1	0.0069	0.0095	0.0123	0.0330	0.0499	0.0499	24	930.2	XIF1
	XIF2	0.0081	0.0089	0.0133	0.0239	0.0457	0.0632	15	1033.8	XIF2
	XIF3	0.0085	0.0085	0.0138	0.0191	0.0442	0.0685	10	1176.5	XIF3
XIG	XIG1	0.0072	0.0100	0.0117	0.0220	0.0503	0.0503	9	768.0	XIG1
	XIG2	0.0079	0.0087	0.0126	0.0161	0.0471	0.0564	8	899.0	XIG2
	XIG3	0.0076	0.0076	0.0160	0.0139	0.0444	0.0624	8	989.9	XIG3
XIH	XIH1	0.0076	0.0093	0.0122	0.0101	0.0474	0.0568	9	727.5	XIH1
	XIH2	0.0072	0.0089	0.0131	0.0089	0.0451	0.0632	8	844.0	XIH2
	XIH3	0.0070	0.0086	0.0145	0.0086	0.0435	*	9	928.8	XIH3
XIJ	XIJ1	0.0088	0.0141	0.0099	0.0365	0.0714	0.0412	27	674.5	XIJ1
	XIJ2	0.0113	0.0141	0.0098	0.0297	0.0724	0.0417	17	790.8	XIJ2
	XIJ3	0.0128	0.0143	0.0099	0.0239	0.0731	0.0421	13	907.4	XIJ3
XIK	XIK1	0.0087	0.0134	0.0096	0.0463	0.0794	0.0406	47	902.4	XIK1
	XIK2	0.0109	0.0134	0.0095	0.0324	0.0791	0.0410	45	992.5	XIK2
	XIK3	0.0122	0.0135	0.0095	0.0270	0.0788	0.0412	25	1106.1	XIK3
XIL	XIL1	0.0065	0.0091	0.0135	0.0263	0.0490	0.0590	16	716.9	XIL1
	XIL2	0.0077	0.0085	0.0137	0.0190	0.0466	0.0560	11	862.3	XIL2
	XIL3	0.0082	0.0082	0.0149	0.0149	0.0447	*	6	1007.8	XIL3
XIM	XIM1	0.0072	0.0100	0.0116	0.0189	0.0218	0.0218	8	763.9	XIM1
	XIM2	0.0078	0.0087	0.0135	0.0151	0.0196	0.0256	6	895.1	XIM2
	XIM3	0.0076	0.0076	0.0159	0.0134	0.0159	0.0274	6	985.4	XIM3
XIN	XIN1	0.0072	0.0100	0.0116	0.0189	*	*	7	763.9	XIN1
	XIN2	0.0078	0.0087	0.0135	0.0151	*	*	5	895.1	XIN2
	XIN3	0.0076	0.0076	0.0159	0.0134	*	*	5	985.4	XIN3

\* Ultimate curvature was reached, before the event occurred.  
\*\* M (in kN.m)

### 5.5.2 Discussion of Results

Group XIA - Columns were reinforced with  $4\Phi 32$  longitudinal bars ( $\rho_t=0.013$ ) having strain hardening and ultimate strain of 0.01 & 0.1 respectively. Axial load level was  $0.5f_{ck}A_c$ . Ties were  $\Phi 10/150$  mm, and configuration was number 1, of Figure 3.15. Saatcioglu confined concrete model was used to calculate the core concrete stresses. The moment-curvature curves of the examples having different concrete strengths are presented in Figure A.100 of Appendix A. Increasing the characteristic strength of concrete from 20 MPa to first 30 MPa and then 40 MPa did not give an idea about the influence of concrete strength on ductility of columns in this group, because the behaviour of the columns XIA1, XIA2 & XIA3 ( $f_{ck} = 20, 30$  & 40 MPa) was very brittle indicating that the confinement used was inadequate. Columns of this group reached their ultimate curvatures just after the clear cover crushed. Especially the behaviour of XIA3 was so brittle that its tension steels could not start to yield before ultimate curvature was reached.

Group XIB - Columns of this group were identical with those of XIA, the only difference being that the ties were increased to  $\Phi 10/100$  mm. Reducing tie spacing from 150 mm to 100 mm, resulted a little more ductile behaviour, but again the behaviour was brittle (See Figure A.101, Appendix A). However, it is clear that, increasing the characteristic strength of concrete resulted in greater moment capacity. Moment capacity of XIB2 ( $f_{ck}=30$  MPa) was 1.25 times and of XIB3 ( $f_{ck}=40$  MPa) was 1.5 times as much as that of XIB1 ( $f_{ck}=20$  MPa).

Group XIC & XID - Columns of the Group XIC were identical with those of XIB, the only difference being that the longitudinal reinforcement ratio was increased to 0.026 ( $8\Phi 32$ ). Configuration type was 2 of Figure 3.15. Columns of the Group XID were identical with those of XIA, the only differences being that the longitudinal reinforcement ratio was increased to 0.026 ( $8\Phi 32$ ), and the configuration number was taken as 4. More ductile diagrams were obtained in these groups as compared to

those of the previous groups, but still the limited ductility made it difficult for discussions (See Figure A.102 & Figure A.103, Appendix A).

Group XIE - Columns were reinforced with  $8\Phi 32$  longitudinal bars ( $\rho_t=0.026$ ) having strain hardening and ultimate strain of 0.01 & 0.1 respectively. Axial load level was ' $0.5f_{ck}A_c$ '. Ties were  $\Phi 10/100$  mm, and configuration number was 4. Saatcioglu confinement model was used to calculate the core concrete stresses. The moment-curvature curves of the examples having different concrete strengths are presented in Figure A.104 of Appendix A. Increasing characteristic strength of concrete from 20 MPa to first 30 MPa and then 40 MPa made the columns to behave less ductile. Curvature ductility ratio of XIE2 ( $f_{ck}=30$  MPa) was approximately twice and that of XIE1 ( $f_{ck}=20$  MPa) was approximately 4 times as much as that of XIE3 ( $f_{ck}=40$  MPa). The reason for this can be explained as following:

It was stated that axial load level was kept the same and was equal to  $0.5f_{ck}A_c$ ; In reality since ' $f_{ck}$ ' differs from sample to sample, the axial load level increased with the increasing concrete strength. The level of ' $N/N_0$ ' depended not on the concrete strength but also on the ratio of the longitudinal reinforcement. Therefore, increasing the concrete strength pushes the column to higher axial load levels and thus to less ductile behaviour.

Group XIF - Columns of the Group XIF were identical with those of XIE, the only differences being that the longitudinal reinforcement ratio was increased to 0.039 ( $12\Phi 32$ ), and the configuration number was taken as 7. More ductile behaviour was obtained as compared to those in Group XIE, but the rate of decrease in ductility with increasing strength of concrete was a little less than that of discussed in the paragraph of the examples of Group XIE. Also there were gains in moment capacities of the columns after their clear covers spalled, since more steel meant more compensation of strength loss due to crushing of cover concrete. This becomes very clear in XIE1 ( $f_{ck}=20$  MPa) (See Figure A105, Appendix A).

Groups XIG & XIH - Columns of the Groups XIG & XIH were identical with those of XIE, the only difference was the confinement model. Sheikh & Uzumeri was used in Group XIG and Modified Kent & Park was used in Group XIH instead of Saatcioglu as in XIE. The discussions about influence of concrete strength on column behaviour from confinement model point of view lead to the result that the diagrams drawn by using Sheikh & Uzumeri model or Modified Kent & Park model were generally less ductile than those drawn by using Saatcioglu confinement model. Unlike discussions made for the examples of Group XIE (diagrams drawn by using Saatcioglu model) there was no decrease in curvature ductility ratios with increasing concrete strength. Also, after the clear cover crushed, there were sharp drops in the moment capacities of the diagrams drawn by using Saatcioglu and Sheikh & Uzumeri models, especially when the characteristic strengths of concrete is 40 MPa. However this was not the case when Modified Kent & Park model was used. When Kent & Park model was used, the decrease in moment capacity after clear cover crushing was less in XIH3 which had the highest concrete strength ( $f_{ck}=40$  MPa). The moment-curvature diagrams of these groups are presented in Figures A.106 & A.107 of Appendix A.

Groups XIJ & XIK - Columns in Groups XIJ & XIK were identical with those columns in Groups XIE & XIF respectively. However the level of the axial load was reduced to  $0.25f_{ck}A_c$ . Reducing the axial load level from  $0.5f_{ck}A_c$  to  $0.25f_{ck}A_c$ , made the behaviours of all columns more ductile (1.5 to 2.5 times more ductile), but did not change the rate of decrease in curvature ductility with increasing concrete strength so much (See Figure A.108 & Figure A.109, Appendix A).

Group from XII to XIN - Columns of the Group XII were identical with those of XIE, the only difference being that the strain capacity of steel which was increased to 0.18. Columns of Group XIM were reinforced with  $8\Phi 32$  longitudinal bars ( $\rho_t = 0.026$ ) with strain hardening and ultimate strains of 0.0042 & 0.1 respectively. Axial load level was  $0.5f_{ck}A_c$ . Ties were  $\Phi 10/100$  mm, and configuration



number was 3. Sheikh & Uzumeri confinement model was used to calculate the core concrete stresses. Columns of Group XIN were identical with those of XIM, the only difference being that the strain hardening strain of steel was increased to 0.021. Playing with the model of longitudinal steel, either by increasing ultimate strain capacity from 0.1 to 0.18 or by changing strain hardening starting point ( $\epsilon_{sp}=2\epsilon_{sy}$  or  $\epsilon_{sp}=10\epsilon_{sy}$ ) did not change the behaviour of the columns (See Figures from A.110 to A.112, Appendix A).

### 5.5.3 Conclusions

For the columns having same level of axial load in terms of ' $f_{ck}A_c$ ', that is when ' $N/f_{ck}A_c$ ' ratio is stable, increase in the characteristic strength of concrete resulted in less ductile behaviour.

The curvature ductility ratio was in general inversely proportional with the concrete strength, if Saatcioglu confinement model is used for confined concrete. However if Modified Kent & Park or Sheikh & Uzumeri confinement models are used instead of Saatcioglu model, although ultimate curvatures of columns tend to decrease with increasing concrete strength, curvature ductility ratios remain almost the same.

The changes in the model of longitudinal reinforcements, such as the ultimate strain capacity or the strain hardening starting point, did not influence the behaviour significantly for the axial load levels considered.

If columns have low ratios of longitudinal reinforcement ( $\rho_t=0.013$ ) and insufficient amounts of transverse reinforcements ( $\Phi 10/150$  mm, conf. no: 1), whatever the other variables are very poor behaviour, that is brittle behaviour was observed.



## 5.6 Case Study XII: Influence of Ratio of Longitudinal Bars ( $\rho_t=A_{st}/A_c$ ) in R/C Columns

This study aims to investigate the influence of the ratio of longitudinal reinforcement ( $\rho_t=A_{st}/A_c$ ) on the column behaviour. For this purpose 33 moment-curvature diagrams for 50 cm square sections were drawn. The main variables investigated were the volumetric ratio of ties and configuration type, steel strength, 'd"/h' ratio and the ultimate strains of steel. The list of all 33 sections with their properties are given in Table 5.9. The results are presented in Table 5.10.

### 5.6.1 Assumptions

- For the confined concrete in the core, Saatcioglu confinement model was used in all cases.
- For all samples characteristic concrete strength is 20 MPa; and the axial load level is  $0.5f_{ck}A_c$ .
- Five different ratios of longitudinal bars were investigated. These are 0.01, 0.02, 0.029, 0.03, 0.04, and correspond to  $8\Phi 20$ ,  $8\Phi 28$ ,  $8\Phi 34$ ,  $12\Phi 28$ ,  $16\Phi 28$  respectively.

### 5.6.2 Discussion of Results

Groups XIIA & XIIB - Columns were reinforced with 8 longitudinal S420 bars having ultimate strain of 0.1. Tie configuration was number 2. 'd"/h' ratio was 0.824. Ties in columns of Group XIIA and Group XIIB were  $\Phi 10/100$  and  $\Phi 8/110$  mm respectively. Different longitudinal bar diameters (20; 28; 34 mm) were investigated. To increase the diameter of longitudinal bars from 20 mm ( $\rho_t=0.01$ ) to first 28 mm ( $\rho_t=0.02$ ) and then 34 mm ( $\rho_t=0.029$ ), changed the behaviour of columns

**Table 5.9: List of sections and section properties; Influence of ratio of longitudinal bars ( $\rho_l = A_{st}/A_c$ ) in R/C columns**

		$\epsilon_{su}$	$d^*/h$	Steel Strength	Ties	Configur. Number*	$\rho_l$ ( $A_{st} / A_c$ )		
XIIA	XIIA1	0.1	0.824	S420 $\epsilon_{sp} = 0.01$	$\Phi 10/100$	2	0.01	XIIA1	
	XIIA2						0.02	XIIA2	
	XIIA3						0.029	XIIA3	
XIIB	XIIB1				$\Phi 8/110$	2	0.01	XIIB1	
	XIIB2						0.02	XIIB2	
	XIIB3						0.029	XIIB3	
XIIC	XIIC1			$\Phi 10/100$	2	0.02	XIIC1		
	XIIC2				5	0.03	XIIC2		
	XIIC3				8	0.04	XIIC3		
XIID	XIID1	$\Phi 10/100$	4	0.02	XIID1				
	XIID2		6	0.03	XIID2				
	XIID3		9	0.04	XIID3				
XIIE	XIIE1	$\Phi 8/110$	4	0.02	XIIE1				
	XIIE2		6	0.03	XIIE2				
	XIIE3		9	0.04	XIIE3				
XIIF	XIIF1	S220 $\epsilon_{sp} = 0.0055$	$\phi 10/100$	2	0.01	XIIF1			
	XIIF2				0.02	XIIF2			
	XIIF3				0.029	XIIF3			
XIIG	XIIG1		$\phi 10/100$	4	0.02	XIIG1			
	XIIG2			6	0.03	XIIG2			
	XIIG3			9	0.04	XIIG3			
XIIH	XIIH1		0.18	0.824	S420 $\epsilon_{sp} = 0.01$	$\Phi 10/100$	2	0.01	XIIH1
	XIIH2							0.02	XIIH2
	XIIH3							0.029	XIIH3
XIIJ	XIIJ1	$\Phi 10/100$				4	0.02	XIIJ1	
	XIIJ2					6	0.03	XIIJ2	
	XIIJ3					9	0.04	XIIJ3	
XIIK	XIIK1	S420 $\epsilon_{sp} = 0.01$			$\Phi 10/100$	2	0.01	XIIK1	
	XIIK2						0.02	XIIK2	
	XIIK3						0.029	XIIK3	
XII L	XII L1	$\Phi 10/100$	4	0.02	XII L1				
	XII L2		6	0.03	XII L2				
	XII L3		9	0.04	XII L3				

\* Refer to Figure 3.15



a little bit from ductility point of view, but increased the moment capacities. That is, ultimate moment capacities of these columns were approximately proportional with the ratio of longitudinal steel used (See Figure A.113 & Figure A.114, Appendix A).

Group XIIC - Columns had S420 longitudinal bars with ultimate strains of 0.1. Ties were  $\Phi 10/100$  mm. 'd"/h' ratio was 0.824. Columns reinforced with 8 $\Phi 28$  bars ( $\rho_t=0.02$ ; conf. no: 2), 12 $\Phi 28$  ( $\rho_t=0.03$ ; conf. no: 5), and 16 $\Phi 28$  ( $\rho_t=0.04$ ; conf. no: 8) were investigated. It was observed that changing the longitudinal reinforcement did not cause any significant changes in ductility (See Figure A.115, Appendix A).

Group XIID - Columns in this group were identical with those of Group XIIC. However the confinement configuration was changed. Columns reinforced with 8 $\Phi 28$  ( $\rho_t=0.02$ ; conf. no: 4), 12 $\Phi 28$  ( $\rho_t=0.03$ ; conf. no: 6), and 16 $\Phi 28$  ( $\rho_t=0.04$ ; conf. no: 9) bars were investigated. Although there was no significant difference between columns having 8 and 12 bars, column XIID3 (16 bars) had a curvature ductility ratio of almost 3 times as much as those of the others (See Figure A.116, Appendix A). Comparing this with the discussions of the above paragraph, it can be said that it is not the number of longitudinal bars but the confinement configuration which affects the ductility of columns. Configuration number 9 is very effective, from the ductility point of view.

Group XIIE - Changing the ties from  $\Phi 10/100$  mm to  $\Phi 8/110$  mm, decreased the ductility significantly. However the effect of the ratio of longitudinal bars on the behaviour was almost the same (See Figure A.117, Appendix A).

Groups XIIF & XIIG - Columns in Groups XIIF & XIIG were identical with those in Groups XIIA & XIID respectively. However the steel used to reinforce the columns longitudinally was S220 in the examples of these groups. Behaviour was less ductile than those reinforced with S420 steel. No different observation or discussion

from explained for the samples reinforced longitudinally by S420 steel, is made (See Figure A.118 & Figure A.119, Appendix A).

Groups XIIIH & XIIIJ - Columns in Groups XIIIH & XIIIJ were identical again with those in Groups XIIIA & XIID respectively. However the ratio of 'd"/h' was taken 0.704, instead of 0.824. Columns with 8 longitudinal bars, whatever their diameters were (Group XIIIH; See Figure A.120, Appendix A) showed very poor behaviour from the ductility point of view. Increase in the diameter of longitudinal bars used only raised the moment capacities. However when the number of longitudinal bars were increased from 8 ( $\rho_t=0.02$ ; conf. no: 4) to first 12 ( $\rho_t=0.03$ ; conf. no: 6), then 16 ( $\rho_t=0.04$ ; conf. no: 9), keeping the steel diameter same (Group XIIIJ; See Figure A.121, Appendix A), a very significant change in ductility was observed. This change in behaviour is related to the confinement configuration.

Groups XIIIK & XIIIL - Columns in Groups XIIIK & XIIIL were identical with those in Groups XIIIA & XIID respectively. However the strain capacity of reinforcing steels was 0.18 in the examples of these groups. Increasing only the ultimate strain capacities of steels from 0.1 to 0.18 did not change the behaviour, neither the curvature ductility ratios, nor the moment capacities of columns (See Figure A.122 & Figure A.123, Appendix A).

### 5.6.3 Conclusions

For the columns which had 8 longitudinal bars, increasing the diameter, keeping other variables same, resulted an increase in moment capacities. On the other hand, the increase in the curvature ductility ratios of these columns with increasing bar diameters was not significant.

For the columns having same diameter of longitudinal steel and a single tie ( $\Phi 10/100$  mm) around these bars, increasing the number of longitudinal bars from 8 to first 12, then 16, keeping other variables same, increased the moment capacities of columns, but did not influence curvature ductility ratios so much.

For the columns having same diameter of longitudinal steel, increasing the number of longitudinal bars from 8 to first 12, then 16, as well as to change the transverse reinforcement configuration type from 4, to first 6, then 9, changed the ductility significantly, especially when the columns in which there are 8 (conf. no: 4) or 12 (conf. no: 6) steels are compared with the ones in which there are 16 (conf. no: 9) bars.

Changing the yield strength of longitudinal steel used from 420 MPa to 220 MPa, decreased the moment capacities by approximately 25-30%, but did not influence the curvature ductility ratios so much. Columns reinforced with steel having different ultimate strain capacities behaved almost similarly.

### **5.7 Case Study XIII: Influence of Confined Concrete Models on Moment Curvature Diagrams of R/C Columns**

This study aims to investigate the influence of confined concrete model on moment-curvature diagrams of R/C columns. For this purpose 38 moment-curvature diagrams for 50 cm square sections were drawn. The main variables investigated were transverse steel configuration types and amount, ratio of longitudinal bars, axial load level, concrete strength, ultimate strain of reinforcing steel, and  $d''/h$  ratios. For the Groups from XIII A to XIII E, in each group, four columns whose diagrams are drawn according to different confinement models were investigated. These models were Saatcioglu, Sheikh & Uzumeri, Modified Kent & Park, and Mod. Kent & Park with linear ascending part (Roy & Sozen). For the other groups (from XIII F to XIII L), in

each group, three columns were investigated. Mod. Kent & Park model with linear ascending part was eliminated. The list of all 38 sections with their properties are given in Table 5.11. The results are presented in Table 5.12.

### 5.7.1 Discussion of Results

Group XIII A - Columns were reinforced with  $8\Phi 32$  longitudinal bars ( $\rho_t=0.026$ ) with ultimate strains of 0.1. Concrete strength was 20 MPa. Axial load level was  $0.5f_{ck}A_c$  and  $d''/h$  ratio was 0.72. Ties were  $\Phi 10/150$  mm and configuration was number 2. Diagrams obtained by changing the confinement models used, are presented in Figure A.124 of Appendix A. They are on top of each other, and they all show so brittle behaviours that, it is not possible to compare them and make a discussion.

Group XIII B - Columns of this group were identical with those of XIII A, the only difference being that the ties were increased to  $\Phi 12/100$  mm. Although behaviour of all columns became a little more ductile than those of Group XIII A, a sound discussion was not possible, because differences between the diagrams were still hardly perceptible (See Figure A.125, Appendix A).

Group XIII C - Columns were reinforced with  $12\Phi 26$  longitudinal bars ( $\rho_t=0.025$ ) with ultimate strain of 0.1. Concrete strength was 20 MPa. Axial load level was  $0.5f_{ck}A_c$  and  $d''/h$  ratio was 0.82. Ties were  $\Phi 10/150$  mm and configuration number was 7. Diagrams obtained by changing the confinement models, are presented in Figure A.126 of Appendix A. It is observed that the columns whose moment-curvatures diagrams are drawn by using the confinement models proposed by Sheikh & Uzumeri, Modified Kent & Park, and Roy & Sozen (that is, Modified Kent & Park, with linear ascending part) behaved almost the same. The column whose moment-curvature diagram was drawn by using the Saatcioglu model was much more ductile

**Table 5.11: List of sections and section properties; Influence of confined concrete models on moment-curvature diagrams of R/C columns**

		$d^*/h$	$\epsilon_{su}$	Conc. Strength	N (Axial Load) $0.5 f_{ck} A_c$	$\rho_t$ ( $A_{st} / A_c$ )	Ties	Conf. No*	Concrete Model	
XIIIA	XIIIA1	0.72	0.1	C20	$0.5 f_{ck} A_c$	0.026	$\Phi 10/150$	2	Saatcioglu	XIIIA1
	XIIIA2								Sh. & Uz.	XIIIA2
	XIIIA3								MKP	XIIIA3
	XIIIA4								MKPLA	XIIIA4
XIIIB	XIIIB1							2	Saatcioglu	XIIIB1
	XIIIB2								Sh. & Uz.	XIIIB2
	XIIIB3								MKP	XIIIB3
	XIIIB4								MKPLA	XIIIB4
XIIIC	XIIIC1	0.82	0.1	C20	$0.5 f_{ck} A_c$	0.025	$\Phi 10/150$	7	Saatcioglu	XIIIC1
	XIIIC2								Sh. & Uz.	XIIIC2
	XIIIC3								MKP	XIIIC3
	XIIIC4								MKPLA	XIIIC4
XIID	XIID1							7	Saatcioglu	XIID1
	XIID2								Sh. & Uz.	XIID2
	XIID3								MKP	XIID3
	XIID4								MKPLA	XIID4
XIIIE	XIIIE1							6	Saatcioglu	XIIIE1
	XIIIE2								Sh. & Uz.	XIIIE2
	XIIIE3								MKP	XIIIE3
	XIIIE4								MKPLA	XIIIE4
XIIIF	XIIIF1							8	Saatcioglu	XIIIF1
	XIIIF2								Sh. & Uz.	XIIIF2
	XIIIF3								MKP	XIIIF3
XIIIG	XIIIG1							9	Saatcioglu	XIIIG1
	XIIIG2								Sh. & Uz.	XIIIG2
	XIIIG3								MKP	XIIIG3
XIIIH	XIIIH1							4	Saatcioglu	XIIIH1
	XIIIH2								Sh. & Uz.	XIIIH2
	XIIIH3								MKP	XIIIH3
XIIIJ	XIIIJ1				$0.25 f_{ck} A_c$	0.026	$\Phi 10/100$	4	Saatcioglu	XIIIJ1
	XIIIJ2								Sh. & Uz.	XIIIJ2
	XIIIJ3								MKP	XIIIJ3
XIIIK	XIIIK1			C40	$0.5 f_{ck} A_c$	0.026	$\Phi 10/100$	4	Saatcioglu	XIIIK1
	XIIIK2								Sh. & Uz.	XIIIK2
	XIIIK3								MKP	XIIIK3
XIIIL	XIIIL1	0.18		C20	$0.5 f_{ck} A_c$	0.026	$\Phi 10/100$	4	Saatcioglu	XIIIL1
	XIIIL2								Sh. & Uz.	XIIIL2
	XIIIL3								MKP	XIIIL3

\* Refer to Figure 3.15

TC YÜKSEKÖĞRETİM KURULU  
DÖNÜMANTARZI



**Table 5.12: Results; Influence of confined concrete models on moment-curvature diagrams of R/C columns**

		Curvature (rad/m)						Curvature ductility ratio	Maximum M**	
		Cover Crush	Yield A <sub>s</sub> '	Yield A <sub>s</sub>	Core Crush	Str. Hard. A <sub>s</sub> '	Str. Hard. A <sub>s</sub>			
XIIIA	XIIIA1	0.0063	0.0097	0.0178	0.0152	*	*	3	0.256	XIIIA1
	XIIIA2	0.0068	0.0110	0.0137	0.0117	*	*	2	0.267	XIIIA2
	XIIIA3	0.0074	0.0100	0.0178	0.0100	*	*	2	0.251	XIIIA3
	XIIIA4	0.0065	0.0091	0.0202	0.0083	*	*	4	0.237	XIIIA4
XIIIB	XIIIB1	0.0064	0.0098	0.0182	0.0201	0.0543	*	6	0.258	XIIIB1
	XIIIB2	0.0069	0.0112	0.0134	0.0155	*	*	3	0.273	XIIIB2
	XIIIB3	0.0075	0.0108	0.0142	0.0108	*	*	3	0.263	XIIIB3
	XIIIB4	0.0065	0.0092	0.0177	0.0099	0.0531	0.0716	9	0.247	XIIIB4
XIIIC	XIIIC1	0.0064	0.0090	0.0126	0.0243	0.0462	0.0550	12	0.281	XIIIC1
	XIIIC2	0.0071	0.0097	0.0113	0.0157	0.0451	*	7	0.294	XIIIC2
	XIIIC3	0.0076	0.0093	0.0123	0.0100	0.0442	0.0666	8	0.284	XIIIC3
	XIIIC4	0.0065	0.0083	0.0136	0.0091	0.0433	*	7	0.278	XIIIC4
XIID	XIID1	0.0069	0.0094	0.0125	0.0393	0.0536	0.0536	43	0.302	XIID1
	XIID2	0.0072	0.0100	0.0108	0.0335	0.0538	0.0538	20	0.307	XIID2
	XIID3	0.0078	0.0096	0.0121	0.0131	0.0533	0.0533	22	0.302	XIID3
	XIID4	0.0065	0.0083	0.0133	0.0108	0.0509	0.0509	21	0.300	XIID4
XIIIE	XIIIE1	0.0068	0.0094	0.0124	0.0366	0.0530	0.0530	35	0.300	XIIIE1
	XIIIE2	0.0073	0.0102	0.0111	0.0403	0.0698	0.0453	19	0.315	XIIIE2
	XIIIE3	0.0077	0.0095	0.0119	0.0119	0.0500	0.0500	14	0.296	XIIIE3
	XIIIE4	0.0065	0.0083	0.0131	0.0100	0.0479	0.0575	15	0.291	XIIIE4
XIIF	XIIF1	0.0065	0.0090	0.0126	0.0177	0.0450	0.0624	8	0.327	XIIF1
	XIIF2	0.0071	0.0097	0.0119	0.0119	0.0441	*	6	0.337	XIIF2
	XIIF3	0.0076	0.0093	0.0121	0.0093	0.0436	*	7	0.327	XIIF3
XIIG	XIIG1	0.0071	0.0096	0.0119	0.0412	0.0522	0.0522	47	0.354	XIIG1
	XIIG2	0.0074	0.0102	0.0112	0.0555	0.0555	0.0445	43	0.372	XIIG2
	XIIG3	0.0079	0.0096	0.0121	0.0130	0.0509	0.0509	26	0.350	XIIG3
XIIH	XIIH1	0.0065	0.0090	0.0126	0.0267	0.0496	0.0496	21	0.291	XIIH1
	XIIH2	0.0072	0.0100	0.0108	0.0202	0.0508	0.0508	10	0.312	XIIH2
	XIIH3	0.0076	0.0093	0.0123	0.0101	0.0478	0.0573	10	0.296	XIIH3
XIIJ	XIIJ1	0.0088	0.0141	0.0099	0.0370	0.0735	0.0417	30	0.277	XIIJ1
	XIIJ2	0.0097	0.0171	0.0097	0.0293	0.0765	0.0393	20	0.289	XIIJ2
	XIIJ3	0.0103	0.0146	0.0103	0.0146	0.0680	0.0412	18	0.277	XIIJ3
XIIK	XIIK1	0.0082	0.0082	0.0135	0.0151	0.0454	*	7	0.205	XIIK1
	XIIK2	0.0076	0.0076	0.0155	0.0135	0.0451	0.0632	9	0.202	XIIK2
	XIIK3	0.0070	0.0086	0.0140	0.0086	0.0441	0.0614	10	0.191	XIIK3
XIIL	XIIL1	0.0065	0.0090	0.0126	0.0267	0.0496	0.0496	17	0.291	XIIL1
	XIIL2	0.0072	0.0100	0.0108	0.0202	0.0508	0.0508	10	0.312	XIIL2
	XIIL3	0.0076	0.0093	0.0123	0.0101	0.0478	0.0573	9	0.296	XIIL3

\* Ultimate curvature was reached, before the event occurred.  
\*\* M: M / bh<sup>2</sup>f<sub>c</sub>

than those of previous ones. Ultimate moment capacities of all columns resemble to each other; however column XIIC2 (Sheikh & Uzumeri model) had the highest moment capacity.

Group XIID - Columns of this group were identical with those of XIIC, the only difference was the ties which were increased to  $\Phi 12/100$  mm. No different discussion from the previous paragraph can be made. The curvature ductility ratio of column XIID1 (Saatcioglu model), was about 100% greater than the other three. Also the gain in moment capacity after the crushing of the clear cover was more distinct when Saatcioglu model was used, column XIID1 (See Figure A.127, Appendix A).

Group XIIE - Columns of this group were identical with those of XIID, the only difference was the configuration which was changed to configuration number 6 (which was stated as the most effective confinement type, in the previous sections). Most ductile behaviour was observed for the column whose diagram was drawn using Saatcioglu model, and the highest moment capacity belongs to the one whose diagram was drawn by using Sheikh & Uzumeri model. Column in which the modified Kent & Park model was used (with parabolic or linear ascending parts) behaved a little less ductile than the XIIE2 (Sheikh & Uzumeri), and their ultimate moment capacities were about 6% less than that of XIIE2 (See Figure A.128, Appendix A). Column having Sheikh & Uzumeri model behaved almost the same as the one with Saatcioglu model up to a curvature of about 0.15 rad/m.

Group XIIF - Columns were reinforced with  $16\Phi 26$  longitudinal bars ( $\rho_t=0.025$ ) with ultimate strains of 0.1. Concrete strength was 20 MPa. Axial load level was  $0.5f_{ck}A_c$  and  $d''/h$  ratio was 0.82. Ties were  $\Phi 10/100$  mm and configuration number was 8. Diagrams obtained by changing the confinement model are presented in Figure A.129 of Appendix A. It was observed that, there were no such big

differences in the diagrams drawn by using different confinement models. In all cases ductility was quite low. Number 8 is not an effective confinement configuration.

Group XIIIIG - Columns of this group were identical with those of XIIIIF, the only difference was that the configuration number was changed to 9. The diagrams drawn by using Saatcioglu and Sheikh & Uzumeri models resemble each other. They have curvatures ductility ratios approximately 75% greater than the ones drawn by using Modified Kent & Park model (See Figure A.130, Appendix A). The highest moment capacity belongs to XIIIIG2 (Sheikh & Uzumeri). The gain in the moment capacity after the clear cover has crushed realized most in XIIIIG1 (Saatcioglu)

Groups from XIIIIH to XIIIIL - Columns of the Group XIIIIH were reinforced with  $8\Phi 32$  longitudinal bars ( $\rho_t = 0.026$ ) with an ultimate strain of 0.1. Concrete strength was 20 MPa. Axial load level was  $0.5f_{ck}A_c$  and  $d''/h$  ratio was 0.82. Ties were  $\Phi 10/100$  mm and configuration number was 4. Diagrams obtained for different confinement models are presented in Figure A.131 of Appendix A. Moment-curvature diagrams drawn by using the Saatcioglu Model had the higher curvature ductility ratio, and the gain in moment capacity after the crushing of the clear cover was more distinct, than those drawn by using other models. Although the diagram drawn by using Sheikh & Uzumeri model resemble to those drawn by using Modified Kent & Park model, the moment values, calculated using Sheikh & Uzumeri model, were 5% higher than the one calculated according to Modified Kent & Park model, corresponding to the same curvatures. These discussions were also valid when the axial load level was reduced to  $0.25f_{ck}A_c$  (Group XIIIIJ), or when the ultimate strain of longitudinal steel was raised to 0.18 (Group XIIIIL). When the characteristic strength of concrete was raised to 40 MPa (Group XIIIIK), diagrams for all models were similar (See Figures from A.132 to A.134, Appendix A).

### 5.7.2 Conclusions

In general the moment-curvature diagrams drawn by using four different models were not too different from each other, for columns investigated. However for some reinforcement configurations significant differences were observed. Moment-curvature diagrams drawn by using Saatcioglu model were more ductile than those drawn by using other models. Ultimate moment capacities calculated using the Sheikh & Uzumeri model were a little bit higher than those calculated according to other models. The differences observed changed with the reinforcement configuration.

If the columns are not confined sufficiently, or if the characteristic strength of concrete is high ( $f_{ck}=40$  MPa), or if the ratio of 'd"/h' is low (0.72), the moment-curvature diagrams based on different confined concrete models resemble to each other, and they have generally low curvature ductility ratios.

Among the diagrams where columns were very effectively confined (configuration number 6 or 9), the ones drawn by using Saatcioglu and Sheikh & Uzumeri models both have more moment capacities and show more ductile behaviour than those drawn by using Modified Kent & Park model.

For the Modified Kent & Park model, whether the model has a linear or parabolic ascending part, is not important.

### 5.8 Case Study XIV: Influence of Axial Load Level ( $N/f_{ck}A_c$ Ratio) in R/C Columns

This study aims to investigate the influence axial load level ( $N/f_{ck}A_c$  ratio) on column behaviour. For this purpose 21 moment-curvature diagrams for 50 cm square sections and 9 moment-curvature diagrams for 30x60 cm rectangular sections were

drawn. The main variables investigated were, longitudinal reinforcement ratio, transverse steel configuration type, concrete and steel strengths, ultimate strain of steel, and shapes and dimensions of cross-section. In each group columns having different axial load levels ( $N/f_{ck}A_c$  ratios: 0.5; 0.3; 0.1) were investigated. The list of all 30 sections with their properties are given in Table 5.13. The results are presented in Table 5.14.

### 5.8.1 Assumptions

- For the core concrete Saatcioglu model for confined concrete was used.
- Ties were  $\Phi 10/100$  mm for all sections. Clear covers were 25 mm.
- The columns having rectangular cross sections had 12 longitudinal bars. 3 bars are placed at the bottom, 3 at the top and 6 were placed between them in three layers, 2 bars at each. Transverse reinforcement was arranged as following: Three cross ties between the middle 6 bars, and a rectangular hoop surrounding all 12 bars.

### 5.8.2 Discussion of Results

Group XIVA - These square columns were reinforced with  $8\Phi 26$  ( $\rho_t=0.017$ ) longitudinal S420 bars with an ultimate strain of 0.1. Tie configuration number was 4. Characteristic strength of concrete was 20 MPa. The ratio of  $d''/h$  was 0.808. Diagrams of columns having different axial load levels are presented in Figure A.135 of Appendix A. Reducing the level of the axial load from  $0.5f_{ck}A_c$  to  $0.3f_{ck}A_c$  and then to  $0.1f_{ck}A_c$ , resulted in a more ductile behaviour. The curvature ductility ratio of XIVA3 ( $N=0.1f_{ck}A_c$ ), was 2.5 times and the curvature ductility ratio of XIVA2 ( $N=0.3f_{ck}A_c$ ) was 1.25 times greater than that of XIVA1 ( $N=0.5f_{ck}A_c$ ). However XIVA1 had the highest ultimate moment capacity. The capacity was 7% greater than that of XIVA2, and 24% greater than that of XIVA3. This was due to the level of the

**Table 5.13:** List of sections and section properties; Influence of axial load level

( $N/f_{ck}A_c$  ratio) in R/C columns

		Section Dimensions	$\epsilon_{su}$	Conc. & St. Strengths	Conf. No*	$\rho_t$ ( $A_{st}/A_c$ )	$N/f_{ck}A_c$				
XIVA	XIVA1	50 x 50 cm $d''/h = 0.808$ $A_c/A_{ck} = 1.29$	0.1	S420 - C20 $\epsilon_{sp} = 0.01$	4	0.017	0.5	XIVA1			
	XIVA2						0.3	XIVA2			
	XIVA3						0.1	XIVA3			
XIVB	XIVB1							7	0.025	0.5	XIVB1
	XIVB2									0.3	XIVB2
	XIVB3									0.1	XIVB3
XIVC	XIVC1							9	0.034	0.5	XIVC1
	XIVC2									0.3	XIVC2
	XIVC3									0.1	XIVC3
XIVD	XIVD1				8	0.034	0.5	XIVD1			
	XIVD2						0.3	XIVD2			
	XIVD3						0.1	XIVD3			
XIVE	XIVE1			S420 - C40 $\epsilon_{sp} = 0.01$	7	0.025	0.5	XIVE1			
	XIVE2						0.3	XIVE2			
	XIVE3						0.1	XIVE3			
XIVF	XIVF1			S220 - C20 $\epsilon_{sp} = 0.0055$	7	0.025	0.5	XIVF1			
	XIVF2						0.3	XIVF2			
	XIVF3						0.1	XIVF3			
XIVG	XIVG1		0.18	S420 - C20 $\epsilon_{sp} = 0.01$	7	0.025	0.5	XIVG1			
	XIVG2						0.3	XIVG2			
	XIVG3						0.1	XIVG3			
XIVH	XIVH1	30 x 60 cm $d''/h = 0.84$ $A_c/A_{ck} = 1.39$	0.1	S420 - C20 $\epsilon_{sp} = 0.01$	10	0.035	0.5	XIVH1			
	XIVH2						0.3	XIVH2			
	XIVH3						0.1	XIVH3			
XIVJ	XIVJ1						S420 - C40 $\epsilon_{sp} = 0.01$	10	0.035	0.5	XIVJ1
	XIVJ2									0.3	XIVJ2
	XIVJ3									0.1	XIVJ3
XIVK	XIVK1					0.18	S420 - C20 $\epsilon_{sp} = 0.01$	10	0.035	0.5	XIVK1
	XIVK2									0.3	XIVK2
	XIVK3									0.1	XIVK3

\* Refer to Figure 3.15

**Table 5.14: Results; Influence of axial load level ( $N/f_{ck}A_c$  ratio) in R/C columns**

		Curvature (rad/m)						Curvature ductility ratio	Maximum M**	
		Cover Crush	Yield $A_s'$	Yield $A_s$	Core Crush	Str. Hard. $A_s'$	Str. Hard. $A_s$			
XIVA	XIVA1	0.0062	0.0088	0.0133	0.0260	0.0486	0.0586	16	0.233	XIVA1
	XIVA2	0.0084	0.0131	0.0106	0.0358	0.0704	0.0429	20	0.218	XIVA2
	XIVA3	0.0132	0.0297	0.0080	0.0664	0.1380	0.0317	41	0.188	XIVA3
XIVB	XIVB1	0.0067	0.0092	0.0130	0.0328	0.0499	0.0499	22	0.286	XIVB1
	XIVB2	0.0084	0.0129	0.0105	0.0454	0.0785	0.0426	46	0.274	XIVB2
	XIVB3	0.0118	0.0224	0.0088	0.0614	0.0955	0.0357	48	0.247	XIVB3
XIVC	XIVC1	0.0071	0.0096	0.0118	0.0407	0.0515	0.0515	46	0.346	XIVC1
	XIVC2	0.0086	0.0130	0.0106	0.0643	0.0782	0.0420	51	0.344	XIVC2
	XIVC3	0.0111	0.0204	0.0084	0.0831	0.1002	0.0375	39	0.329	XIVC3
XIVD	XIVD1	0.0065	0.0091	0.0135	0.0195	0.0446	0.0620	8	0.323	XIVD1
	XIVD2	0.0080	0.0120	0.0110	0.0245	0.0644	0.0447	11	0.319	XIVD2
	XIVD3	0.0103	0.0179	0.0089	0.0315	0.0913	0.0381	54	0.294	XIVD3
XIVE	XIVE1	0.0082	0.0082	0.0137	0.0188	0.0439	0.0681	8	0.198	XIVE1
	XIVE2	0.0114	0.0126	0.0101	0.0253	0.0752	0.0415	19	0.187	XIVE2
	XIVE3	0.0214	0.0295	0.0079	0.0433	0.1284	0.0311	46	0.146	XIVE3
XIVF	XIVF1	0.0061	0.0039	0.0083	0.0250	0.0250	0.0329	16	0.208	XIVF1
	XIVF2	0.0084	0.0053	0.0063	0.0382	0.0382	0.0239	52	0.192	XIVF2
	XIVF3	0.0148	0.0131	0.0047	0.0593	0.0674	0.0180	76	0.169	XIVF3
XIVG	XIVG1	0.0067	0.0092	0.0130	0.0328	0.0499	0.0499	20	0.286	XIVG1
	XIVG2	0.0084	0.0129	0.0105	0.0455	0.0787	0.0426	38	0.274	XIVG2
	XIVG3	0.0118	0.0224	0.0088	0.0616	0.0966	0.0357	87	0.239	XIVG3
XIVH	XIVH1	0.0057	0.0078	0.0097	0.0271	0.0407	0.0491	27	0.321	XIVH1
	XIVH2	0.0070	0.0095	0.0086	0.0330	0.0475	0.0348	47	0.317	XIVH2
	XIVH3	0.0088	0.0134	0.0067	0.0450	0.0784	0.0309	43	0.307	XIVH3
XIVJ	XIVJ1	0.0070	0.0070	0.0110	0.0158	0.0366	0.0516	9	0.215	XIVJ1
	XIVJ2	0.0093	0.0093	0.0083	0.0208	0.0468	0.0361	13	0.208	XIVJ2
	XIVJ3	0.0139	0.0165	0.0072	0.0326	0.0833	0.0297	40	0.175	XIVJ3
XIVK	XIVK1	0.0057	0.0078	0.0097	0.0271	0.0407	0.0490	25	0.321	XIVK1
	XIVK2	0.0070	0.0095	0.0086	0.0330	0.0476	0.0348	39	0.317	XIVK2
	XIVK3	0.0088	0.0134	0.0067	0.0450	0.0787	0.0309	105	0.296	XIVK3

\* Ultimate curvature was reached, before the event occurred.  
\*\* M:  $M / bh^2f_c$



axial load as can be seen in Figure B.3 of Appendix B. Another important observation was that, the column which had  $N=0.1f_{ck}A_c$  failed by rupturing of tension steel, while others failed by the crushing of the core concrete.

Group XIVB - Square columns were reinforced with  $12\Phi 26$  ( $\rho_t=0.025$ ) longitudinal S420 bars with an ultimate strain of 0.1. Tie configuration number was 7. Characteristic strength of concrete was 20 MPa. Diagrams of columns having different axial load levels are presented in Figure A.136 of Appendix A. The general discussion on the behaviour and ultimate moment capacities, made for columns of Group XIVA were valid for columns of this group also. However, the rate of increase in curvature ductility ratios and decrease in ultimate moment capacities, by reducing the level of axial load, were different. The curvature ductility ratio of XIVB2 ( $N=0.3f_{ck}A_c$ ) was almost equal to that of XIVB3 ( $N=0.1f_{ck}A_c$ ). The reason for the high curvature ductility ratio for column XIVB2 was probably due to the fact that the failure occurred by crushing of core concrete when the rupture of steel took place. Maximum moments of these three columns were not very different from each other. This is not surprising, as can be seen in Figure B.4 of Appendix B.

Group XIVC - These were identical columns with those of Group XIVA and XIVB. However the ratio of longitudinal bars was increased to 0.034 ( $16\Phi 26$ ) and the transverse steel configuration number was taken as 9. Columns to which  $0.5f_{ck}A_c$  (XIVC1) &  $0.3f_{ck}A_c$  (XIVC2) axial loads were applied had almost the same ultimate moment capacities and curvature ductility ratios. However, other column to which  $0.1f_{ck}A_c$  (XIVC3) axial load was applied, was worse than XIVC1 & XIVC2, from both the ductility and the moment capacity point of view (See Figure A.137, Appendix A). As can be seen in Figure B.5 of Appendix B, column with an axial load of  $0.1f_{ck}A_c$  has the lowest moment capacity. All columns in this group failed by the rupturing of tension steel, and therefore unlike the examples of previous groups, columns subjected to high axial loads exhibited more ductile behaviour as compared to the one subjected to  $N=0.1f_{ck}A_c$ .



Group XIVD - Columns of this group were identical with those of XIVC, the only difference being the transverse steel configuration which was changed to 8. It was observed that, the column to which  $0.1f_{ck}A_c$  axial load was applied (XIVD3) had a curvature ductility ratio of about 5-6 times greater than those of others to which  $0.3f_{ck}A_c$  (XIVD2), and  $0.5f_{ck}A_c$  (XIVD1) axial loads were applied (See Figure A.138, Appendix A). The moment capacity of the column with an axial load of  $0.1f_{ck}A_c$  was considerably lower than the other two. This can be observed on Figure B.4 of Appendix B also.

Groups XIVE & XIVF - The columns in these groups were identical with those of Group XIVB. However the concrete strength was increased to 40 MPa for the columns of Group XIVE, and the yield strength of reinforcing steels was decreased to 220 MPa for the columns of Group XIVF. It was observed that, when the characteristic strength of concrete was increased from 20 MPa to 40 MPa or when the yield strength of reinforcing steels was decreased from 420 MPa to 220 MPa, the increase in curvature ductility ratios and decrease in moment capacities changed with the level of axial load, but the general tendency of behaviours compared with those of the examples of Group XIVB did not change (See Figure A.139 & Figure A.140, Appendix A). The interaction diagrams for XIVE and XIVF are shown in Figures B.9 & B.2 of Appendix B respectively.

Group XIVG - Columns of this group were identical with those of XIVB, the only difference being that the strain capacity of reinforcement was increased to 0.18. The columns to which  $0.5f_{ck}A_c$  (XIVG1) and  $0.3f_{ck}A_c$  (XIVG2) axial loads were applied behaved similarly with their identicals in Group XIVB. That is, to change the ultimate strain capacities of longitudinal steels did not affect the behaviour of columns to which  $0.5f_{ck}A_c$  and  $0.3f_{ck}A_c$  axial loads were applied. However the curvature ductility ratio of column XIVG3 ( $0.1f_{ck}A_c$ ;  $\epsilon_{su}=0.18$ ) was 80% greater than that of XIVB3 ( $0.1f_{ck}A_c$ ;  $\epsilon_{su}=0.1$ ). This is because, the failure of these columns (XIVB3 & XIVG3) were by the rupturing of tension steel, and increased strain capacity of steels

affected the ductility directly (See Figure A.141, Appendix A). Interaction diagram for this group is given in Figure B.4 of Appendix B.

Groups from XIVH to XIVK - Columns of Group XIVH were rectangular (30\*60 cm), reinforced with 12 $\Phi$ 26 longitudinal S420 bars with an ultimate strain of 0.1. Tie configuration number was 10. Characteristic strength of concrete was 20 MPa. Diagrams of columns having different axial load levels are presented in Figure A.142. The influence of various axial load levels ( $N/f_{ck}A_c$  ratios: 0.5; 0.3; 0.1) on the behaviour was not too different from the ones discussed for 50\*50 square columns. Columns of Group XIVJ were identical with those of XIVH, the only difference being that the concrete strength which was increased to 40 MPa. Columns of Group XIVK were identical with those of XIVH, the only difference being that the strain capacity of reinforcement was increased to 0.18. When characteristic strength of concrete or ultimate strain capacity of longitudinal steels was increased, almost similar observations to those discussed for square columns were obtained (See Figure A.143 and Figure A.144, Appendix A).

### 5.8.3 Conclusions

In general columns tend to behave more ductile, if the level of axial load is reduced. However, the level of axial load is not an independent factor which affects the behaviour. The influence of it on column behaviour changes by other characteristics, such as concrete strength, ratio and model of longitudinal steel, amount and configuration of transverse steel. For some combinations of these variables, the general statements made, may no longer be valid.

Generally the columns to which  $0.1f_{ck}A_c$  axial load is applied, behave much more ductile than the columns to which  $0.3f_{ck}A_c$  and  $0.5f_{ck}A_c$  axial loads are applied. However, for such columns, there is the danger of failure by sudden rupturing of

tensile reinforcement. Curvature ductility ratios of such columns come to the same level (sometimes fall down below) with the ones which are subjected to axial load levels of  $0.3f_{ck}A_c$  or  $0.5f_{ck}A_c$ .

Ultimate strain capacity of longitudinal reinforcement is an important factor that influences the ductility of columns to which ' $0.1f_{ck}A_c$ ' axial load is applied, because of the danger of sudden failure due to the rupturing of tensile reinforcements

### **5.9 Case Study XV: Influence of Ratio of the Gross Area to the Confined Area ( $A_c/A_{ck}$ ) in R/C Columns**

This study aims to investigate the influence of the ratio of the gross area to the confined area on the column behaviour. For this purpose 24 moment-curvature diagrams for 50 cm square sections were drawn. The main variables investigated were confined concrete models, characteristic strength of concrete, transverse steel configuration types and ratios, ratio of longitudinal reinforcement, and the axial load level. In each group two columns having different ratios of the gross areas to the confined areas ( $A_c/A_{ck}=1.235; 1.644$ ) were investigated. The list of all 24 sections with their properties are given in Table 5.15. The results are presented in Table 5.16.

#### **5.9.1 Assumptions**

- S420 steel was used.
- Ultimate strain capacity of reinforcing steel was taken as 0.12 in all cases.

**Table 5.15:** List of sections and section properties; Influence of ratio of the gross area to the confined area ( $A_c/A_{ck}$ ) in R/C columns

		N (Axial Load)	$\rho_t$ ( $A_{st}/A_c$ )	Ties	Concrete Strength	Concrete Model	$A_c/A_{ck}$		
XVA	XVA1	0.5 $f_{ck} A_c$	0.039 Conf. No: 9	$\Phi 10/100$	C20	Saatcioglu	1.235	XVA1	
	XVA2						1.644	XVA2	
XVB	XVB1					Sh. & Uz.	1.235	XVB1	
	XVB2						1.644	XVB2	
XVC	XVC1					MKP	1.235	XVC1	
	XVC2						1.644	XVC2	
XVD	XVD1					C40	Saatcioglu	1.235	XVD1
	XVD2							1.644	XVD2
XVE	XVE1						Sh. & Uz.	1.235	XVE1
	XVE2		1.644	XVE2					
XVF	XVF1		MKP	1.235	XVF1				
	XVF2			1.644	XVF2				
XVG	XVG1		$\Phi 8/140$	Saatcioglu	1.235		XVG1		
	XVG2				1.644		XVG2		
XVH	XVH1			Sh. & Uz.	1.235		XVH1		
	XVH2				1.644	XVH2			
XVJ	XVJ1	0.01 Conf. No: 1		$\Phi 10/100$	C20	Saatcioglu	1.235	XVJ1	
	XVJ2						1.644	XVJ2	
XVK	XVK1			Sh. & Uz.	1.235	XVK1			
	XVK2				1.644	XVK2			
XVL	XVL1			0.25 $f_{ck} A_c$	$\Phi 10/100$	C20	Saatcioglu	1.235	XVL1
	XVL2		1.644					XVL2	
XVM	XVM1		Sh. & Uz.				1.235	XVM1	
	XVM2						1.644	XVM2	

**Table 5.16: Results; Influence of ratio of the gross area to the confined area ( $A_g/A_{ck}$ )  
in R/C columns**

		Curvature (rad/m)						Curvature ductility ratio	Maximum M**	
		Cover Crush	Yield $A_s'$	Yield $A_s$	Core Crush	Str. Hard. $A_s'$	Str. Hard. $A_s$			
XVA	XVA1	0.0072	0.0097	0.0119	0.0414	0.0523	0.0523	52	0.393	XVA1
	XVA2	0.0071	0.0113	0.0142	0.0467	0.0567	0.0668	45	0.325	XVA2
XVB	XVB1	0.0075	0.0102	0.0112	0.0554	0.0554	0.0445	50	0.408	XVB1
	XVB2	0.0073	0.0117	0.0125	0.0701	0.0600	0.0600	29	0.347	XVB2
XVC	XVC1	0.0079	0.0097	0.0112	0.0121	0.0510	0.0510	26	0.385	XVC1
	XVC2	0.0078	0.0113	0.0134	0.0151	0.0564	0.0659	21	0.328	XVC2
XVD	XVD1	0.0086	0.0086	0.0132	0.0214	0.0474	0.0572	23	0.242	XVD1
	XVD2	0.0095	0.0102	*	*	*	*	2	0.211	XVD2
XVE	XVE1	0.0081	0.0081	0.0137	0.0359	0.0484	0.0586	24	0.244	XVE1
	XVE2	0.0091	0.0091	*	*	*	*	2	0.209	XVE2
XVF	XVF1	0.0073	0.0090	0.0127	0.0098	0.0466	0.0560	17	0.237	XVF1
	XVF2	0.0072	0.0104	0.0182	0.0110	0.0497	*	14	0.192	XVF2
XVG	XVG1	0.0068	0.0093	0.0121	0.0262	0.0487	0.0584	14	0.372	XVG1
	XVG2	0.0068	0.0109	0.0145	0.0280	0.0536	0.0723	11	0.319	XVG2
XVH	XVH1	0.0073	0.0100	0.0108	0.0221	0.0503	0.0503	10	0.393	XVH1
	XVH2	0.0072	0.0115	0.0130	0.0223	0.0549	*	6	0.338	XVH2
XVJ	XVJ1	0.0056	0.0081	0.0148	0.0164	0.0422	*	6	0.210	XVJ1
	XVJ2	0.0057	0.0090	*	*	*	*	3	0.182	XVJ2
XVK	XVK1	0.0066	0.0093	0.0124	0.0116	*	*	3	0.218	XVK1
	XVK2	0.0065	0.0108	0.0144	0.0137	*	*	2	0.198	XVK2
XVL	XVL1	0.0089	0.0136	0.0100	0.0712	0.0872	0.0388	64	0.388	XVL1
	XVL2	0.0088	0.0162	0.0106	0.0576	0.0806	0.0576	61	0.317	XVL2
XVM	XVM1	0.0092	0.0148	0.0092	0.0913	0.0913	0.0363	62	0.388	XVM1
	XVM2	0.0089	0.0172	0.0109	0.1012	0.0886	0.0468	65	0.328	XVM2

\* Ultimate curvature was reached, before the event occurred.  
\*\* M:  $M / bh^2f_c$

## 5.9.2 Discussion of Results

Groups from XVA to XVC - Columns of these groups were reinforced with 16 $\Phi$ 28 longitudinal bars ( $\rho_t = 0.039$ ). Concrete strength was 20 MPa. Ties were  $\Phi$ 10/100 mm, and configuration number was 9, Axial load level was ' $0.5f_{ck}A_c$ '. The confinement model used for the confined concrete in the core was Saatcioglu for Group XVA, Sheikh & Uzumeri for XVB, and Modified Kent & Park for Group XVC. Increasing the ratio of the gross area to the confined area from 1.235 to 1.644 (that is increasing thickness of clear cover from 20 mm to 50 mm) reduced both the curvature ductility ratio and the moment capacity of all columns. The decreases in curvature ductility ratios was not so important, but the decreases in ultimate moment capacities and in moment values corresponding to the same curvatures were significant. Almost in all cases, moment values of the columns which had a clear cover of 20 mm, were about 25% greater than those of the columns which had 50 mm clear cover, if moments corresponding to the same curvatures are compared. Also the gain in moment capacity after the crushings of cover concrete for the columns whose clear covers were 20 mm, were more significant than those whose clear covers are 50 mm (See Figures from A.145 to A.147, Appendix A). Comparing figures of Groups XVA, XVB & XVC, it was observed that although the moment-curvature curves obtained using Sheikh & Uzumeri and Saatcioglu models for the confined concrete were almost the same, when Modified Kent & Park model was used, less ductile behaviour was obtained.

Groups from XVD to XVF - Columns in Groups XVD, XVE & XVF were identical with those in Groups XVA, XVB & XVC respectively. However the concrete strength was 40 MPa in the examples of these groups. It was observed that, if Saatcioglu or Sheikh & Uzumeri confinement model is used for the core concrete, the columns whose clear covers were 50 mm failed following the cover crushing, and therefore had very low curvature ductility ratios (See Figure A.148 & Figure A.149, Appendix A). However, if Modified Kent & Park confinement model is used, the drop

in the moment capacity after the crushing of cover for the column whose clear cover is 50 mm was not so drastic (See Figure A.150, Appendix A).

Groups XVG & XVH - Columns in Groups XVG & XVH were identical with those in Groups XVA & XVB respectively. However the ties were decreased to  $\Phi 8/140\text{mm}$  in the examples of these groups. The observations were not different from those of Groups XVA & XVB (See Figure A.151 & Figure A.152, Appendix A).

Groups XVJ & XVK - Columns of these groups were reinforced with  $4\Phi 28$  longitudinal bars ( $\rho_t = 0.010$ ). Concrete strength was 20 MPa. Ties were  $\Phi 10/100$  mm, and configuration number was 1, Axial load level was  $0.5f_{ck}A_c$ . The confinement model used to calculate core concrete stresses was Saatcioglu for Group XVJ, and Sheikh & Uzumeri for Group XVK. It was observed that columns showed very poor behaviour from the ductility point of view. Therefore it would not be sensible to discuss the influence of clear cover (See Figure A.153 & Figure A.154, Appendix A).

Group XVL & XVM - Columns in Groups XVL & XVM were identical with those in Groups XVA & XVB respectively. However the axial load level was reduced to  $0.25f_{ck}A_c$ . Observations made in the first paragraph of this section were valid, for the examples of these groups also (See Figure A.155 & Figure A.156, Appendix A).

### 5.9.3 Conclusions

Increasing the ratio of the gross area to the confined area of a  $50*50$  cm square column, from 1.235 to 1.644 (to increase the thickness of clear cover from 20 mm to 50 mm) made the column to behave a little less ductile and reduced its moment capacity by 20%.

If satisfactory ductilities are maintained for columns by arranging the ratios of the longitudinal bars, the characteristic strengths of concrete, and the transverse steel amounts, etc. the moment values of columns whose clear covers are 20 mm, were about 25% greater than those of the columns whose clear covers are 50 mm, comparing moments corresponding to the same curvatures.

For the columns whose clear covers were 20 mm, there was little decrease in moment capacity at the instant that cover crushing. As the curvature was increased, this decrease was recovered. For the columns with a clear cover of 50 mm, there were sharp drops when the clear cover crushed, and mostly no gain in moment capacities were observed after the spalling of the cover concrete.





## CHAPTER VI

### CONCLUSIONS AND RECOMMENDATIONS

#### 6.1 General

In this study, the effect of different variables on the behaviour of reinforced concrete sections subjected to pure bending and bending and axial compression were investigated analytically. The investigation was made by producing moment-curvature diagrams.

A comprehensive computer program was developed to produce the moment-curvature relationship of sections subjected to bending and axial compression. The computer program included the behaviour of concrete in tension and was able to consider the stress-strain relationship of both unconfined and confined concrete. Steel models consisting of a trilinear diagram to include to the strain hardening was employed. Mainly four models for confined concrete were taken into consideration. These were; (a) Saatcioglu model, (b) Sheikh & Uzumeri model, (c) Modified Kent & Park model and (d) Modified Kent & Park model with linear ascending branch.

In the trilinear diagram for the reinforcing steel, strain corresponding to strain hardening and ultimate strain were considered as variables.

## 6.2 Conclusions

The conclusions drawn from this analytical study were given at the end of each case study. In general it can be said that for beams the most important parameter was the steel model used, especially the value of ultimate strain. For columns characteristics of the confined concrete were the most important variables affecting the behaviour, i.e ductility and moment capacity.

In the following paragraphs the conclusions drawn for beams and columns will be summarized.

### 6.2.1 Beams

- When the tension reinforcement ratio is low (close to the minimum) the ratio of the compression reinforcement ( $\rho'/\rho$ ) does not influence the behaviour.
- For tension reinforcement ratios close to the limiting value of  $\rho_t$ , post yield slope of the moment-curvature diagram increases with increasing  $\rho'/\rho$  ratio. The ductility is also improved up to  $\rho'/\rho=0.5$  for steel with strain capacity of 0.1. For  $\rho'/\rho>0.5$  curvature capacity decreased. For beams reinforced with steel of  $\epsilon_{su}=0.18$ , critical  $\rho'/\rho$  ratio beyond which curvature capacity decreased was increased to 1.0.
- As expected, ductility of beams increased significantly with increasing ultimate strain of the reinforcing steel.
- As expected, in general concrete strength did not have a significant influence on the behaviour. It was observed that when the ultimate strain of steel is low ( $\epsilon_{su}=0.1$ ), ductility decreased with increasing concrete strength. When the ultimate steel strain was 0.18, ductility increased with increased concrete strength.

- The strain at which strain hardening of the reinforcing steel starts does not have a significant influence on the behaviour.
- As expected, in general the ductility increases with increasing confinement. However, since the tension reinforcement ruptures in beams with low tension reinforcement ratio, confinement in such beams does not improve the ductility. Confinement is not very effective for T-beams, whose compression zone takes place in the unconfined flange.
- As expected, the ratio of tension reinforcement affects the ductility. When  $\epsilon_{su}=0.1$ , the limiting ratio  $\rho_1$  results in the most ductile behaviour. When  $\epsilon_{su}>0.15$ , the most ductile behaviour is obtained for  $\rho<\rho_1$ . Beams in which  $\rho\leq\rho_1$  failed by the rupturing of steel. However beams having  $\rho\geq\rho_1$  failed by the crushing of concrete in the compression zone.
- As expected, in general T-beams have higher moment capacities and are more ductile as compared to rectangular beams. However at some ranges of flange width and thickness, it is possible to have T-beams which behave less ductile as compared to the rectangular ones.

### 6.2.2 Columns

- As expected, in general ductility decreases with increasing axial load level.
- As expected, the ductility of columns increases significantly with increasing volumetric tie ratio.

- In addition to the volumetric ratio of ties, reinforcement configuration has a significant influence on confinement. Influence of configuration becomes more distinct when the longitudinal steel ratio exceeds 0.025.
- When configurations 5, 6 & 7 of Figure 3.15 are compared, number 6 seems to be more effective than the others. The effectiveness of configuration number 6 is more distinct when Sheikh & Uzumeri model is used.
- Modified Kent & Park model for confined concrete does not take reinforcement configuration into account. Therefore Sheikh & Uzumeri and Saatcioglu models which consider reinforcement configuration lead to more consistent results.
- The ductility of the column seemed to be insensitive to the strain capacity of the longitudinal steel, provided that  $\epsilon_{su} \geq 0.1$ .
- For columns having the same reinforcement configuration and volumetric tie ratio, ductility decreased as the tie spacing increased.
- The influence of concrete strength on ductility differed for different confined concrete models used. While Modified Kent & Park and Sheikh & Uzumeri models indicated no change in ductility with increasing concrete strength, Saatcioglu model resulted in less ductile behaviour with increasing concrete strength.
- In general when Saatcioglu model was used for confined concrete, the ductility was higher as compared to the other models. Sheikh & Uzumeri model resulted in the highest moment capacity. However for some reinforcement configurations all the four models used yielded almost the same moment-curvature diagrams.
- As expected, increasing the ratio of gross to confined area made the column to behave in a less ductile manner.

### **6.3 Recommendations**

The results and conclusions given in this thesis are based on an analytical study. Some of these results should be checked by making laboratory tests. If good agreement is found between the analytical and experimental results then the conclusions presented can be used with confidence.

In the future studies the number of reinforcement configurations can be increased. Also, circular and triangular sections can be included.



## REFERENCES

1. Saatcioglu, M., Razvi, S. R. (1991). "Analytical Model for Confined Concrete." Res. Report No. 9101, Dept. of Civ. Engrg., Univ. of Ottawa, Ottawa, Canada.
2. Sheikh, S. A., Uzumeri, S. M., "Analytical Model for Concrete Confinement in Tied Columns", Journal of the Structural Division, Proceedings of the American Society of Civil Engineers, Vol. 108, No. ST12, December 1982, pp. 2703-2722.
3. Kent, D. C., Park, R., "Flexural Members with Confined Concrete", Journal of the Structural Division, Proceedings of the American Society of Civil Engineers, Vol. 97, No. ST7, July 1971, pp. 1969-1990.
4. Park, R., Priestley, M. J. N., Gill, W. D., "Ductility of Square-Confined Concrete Columns", Journal of the Structural Division, Proceedings of the American Society of Civil Engineers, Vol. 108, No. ST4, April 1982, pp. 929-950.
5. Saatcioglu, M., Razvi, S. R., "Strength and Ductility of Confined Concrete", Journal of the Str. Div., ASCE, V. 118, No. 6, June 1992, pp. 1590-1607.
6. Roy, H. E. M., Sozen, M. A., "A Model to Simulate the Response of Concrete to Multi-Axial Loading", Str. Res. Series, No. 268, Civ. Eng., Univ. of Illinois, 1963.
7. Ersoy, U., "Reinforced Concrete", METU, Ankara, 1991.
8. Park, R., Sampson, R. A., "Ductility of Reinforced Concrete Column Sections in Seismic Design", ACI Journal, Title No. 69-49, September 1972, pp. 543-550.
9. Sheikh, S. A., "A Comparative Study of Confinement Models", ACI Journal, Title No. 79-30, July-August 1982, pp. 296-306.
10. Park, R., "A Comparative Study of Confinement Models, Disc.79-30, From the July-August 1982 ACI Journal, p.296", ACI Jour., May-June 1983, pp. 260-265.

11. Fafitis, A., Shah, S. P., "Predictions of Ultimate Behaviour of Confined Columns Subjected to Large Deformations", ACI Journal, Title No. 82-35, July-August 1985, pp. 423-433.
12. Moehle, J. P., Cavanagh, T., "Confinement Effectiveness of Crossties in R/C", Journal of the Str. Eng., ASCE, Vol. 111, No. 10, October 1985, pp. 2105-2120.
13. Sheikh, S. A., Yeh, C. C., "Flexural Behaviour of Confined Concrete Columns", ACI Journal, Title No. 83-39, May-June 1986, pp. 389-404.
14. Sakai, K., Sheikh, A. S., "What Do We Know about Confinement in Reinforced Concrete Columns? (A Critical Review of Previous Work and Code Provisions", ACI Structural Journal, Vol. 86, No. 2, March-April 1989, pp. 192-207.
15. Park, R., Rodriguez, M., " What Do We Know about Confinement in Reinforced Concrete Columns? (A Critical Review of Previous Work and Code Provisions), Disc.86-S22, From the March-April 1989 ACI Structural Journal, p.192", ACI Structural Journal, January-February 1990, pp. 118-121.
16. Sheikh, S. A., Yeh, C. C., "Tied Concrete Columns Under Axial Load and Flexure", Journal of Structural Engineering, ASCE, Vol. 116, No. 10, October 1990, pp. 2780-2800.
17. Samra, R. M., "Ductility Analysis of Confined Columns", Journal of Structural Engineering, ASCE, Vol. 116, No. 11, November 1990, pp. 3148-3161.
18. Sheikh, S. A., Yeh, C. C., "Analytical Moment-Curvature Relations for Tied Concrete Columns", Journal of Structural Engineering, ASCE, Vol. 118, No. 2, February 1992, pp. 529-544.
19. Watson, S., Zahn, F. A., Park, R., "Confining Reinforcement for Concrete Columns", Jour. of Str. Eng., ASCE, Vol. 120, No. 6, June 1994, pp. 1798-1824.
20. Saatcioglu, M., Salamat, H., Razvi, S. R., "Confined Columns Under Eccentric Loading", Journal of Structural Engineering, ASCE, Vol. 121, No. 11, November 1995, pp. 1547-1556.
21. Park, R., Paulay, T., "Reinforced Concrete Structures", John Wiley & Sons, Inc., 1975.

22. Erol, E., "Effects of Strain Gradient and Cyclic Loading on Confined Concrete Behaviour", M. S. Thesis, Civil Eng. Dep., METU, July 1984, 90 pages.
23. TS 500: Betonarme Yapıların Hesap ve Yapım Kuralları, Türk Standardları Enstitüsü, Ankara, Nisan 1984.
24. Rüşch, H., und Hilsdorf, H., "Verformungseigenschaften von Beton Unter Zentrischen Zugspannungen", Materialprüfungsamt für das Bauwesen der Technischen Hochschule München, Rep. No. 44, 1963.
25. Hognestad, E., "A Study of Combined Bending and Axial load in R/C Members", University of Illinois Engineering Exp. Sta. Bull. No. 399, Nov. 1951.
26. Richart, F. E., Brandtzaeg, A., Brown, R. L., "A Study of the Failure of Concrete Under Combined Compressive Stresses", University of Illinois Eng. Exp. Sta. Bull. No. 185, 1928.
27. Chan, W. L., "The Ultimate Strength and Deformation of Plastic Hinges in R/C Frameworks", Magazine of Concrete Research, Vol. 7, No. 21, November 1955, pp. 121-132.
28. Soliman, M. T. M., Yu, C. W., "The Flexural Stress-Strain Relationship of Concrete Confined by Rectangular Transverse Reinforcement", Magazine of Concrete Research, Vol. 19, No. 61, December 1967, pp. 223-238.
29. Sargin, M., Ghosh, S. K., Handa, V. K., "Effects of Lateral Reinforcement upon the Strength and Deformation Properties of Concrete", Magazine of Concrete Research, Vol. 23, No. 75-76, June-September, 1971, pp. 99-110.
30. Vallenias, J., Bertero, V., Popov, E. P., "Concrete Confined by Rectangular Hoops and Subjected to Axial Loads", Report No. UCB/EERC-77/13, Earthquake Eng. Res. Cen., Univ. of California, Berkeley, August 1977.
31. Cowan, H. J., "The Strength of Plain Reinforced and Prestressed Concrete Under the Action of Combined Stresses, With Particular Reference to the Combined Bending and Torsion", Magazine of Concrete Research, V. 5, Dec. 1953.



## APPENDIX A

In Appendix A, the moment-curvature diagrams obtained for the case studies made in Chapters 4 & 5, are presented.

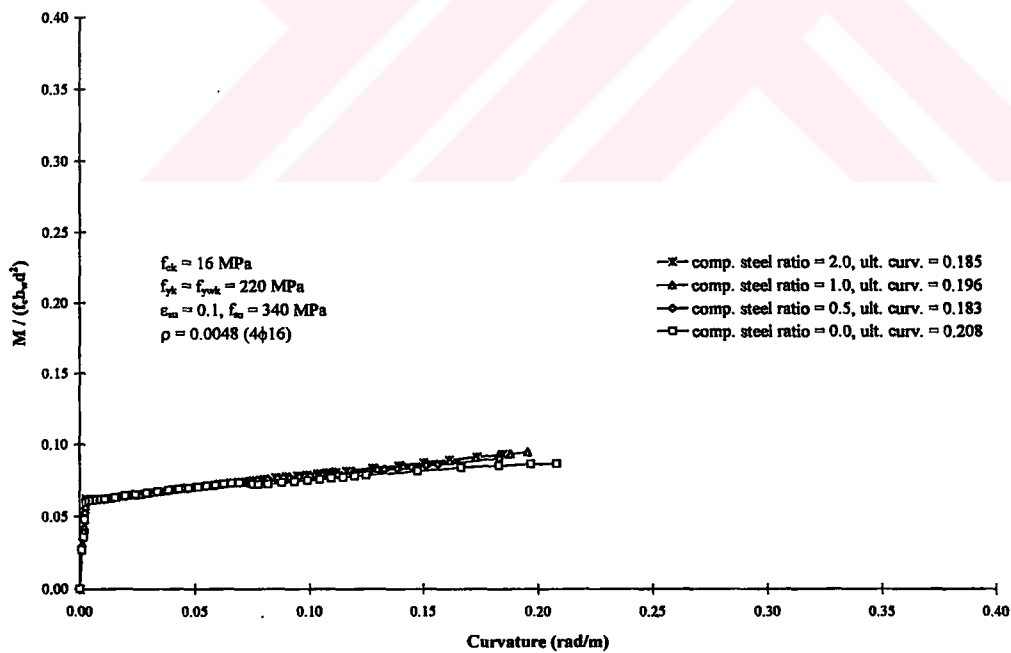


Figure A.1: Influence of compression reinforcement in R/C beams; Group IA

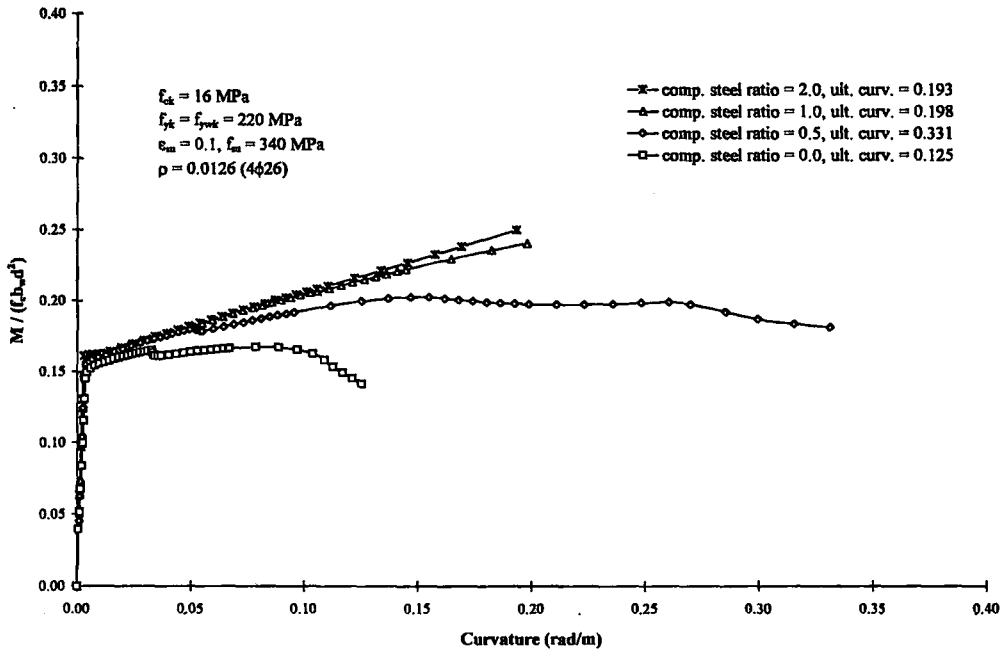


Figure A.2: Influence of compression reinforcement in R/C beams; Group IB

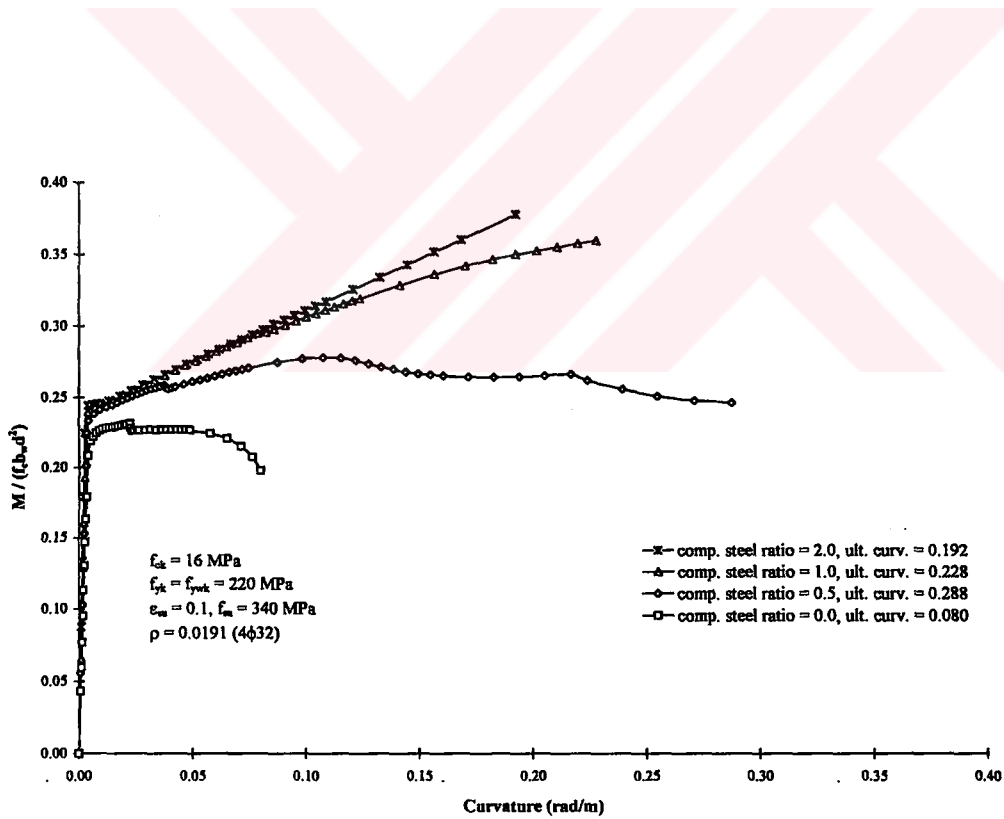


Figure A.3: Influence of compression reinforcement in R/C beams; Group IC

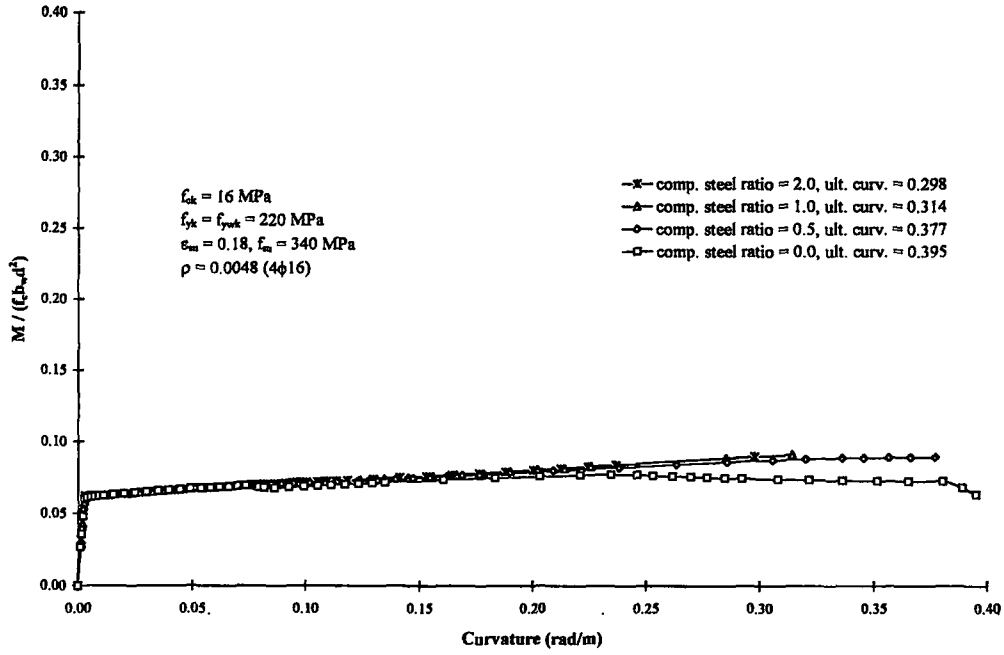


Figure A.4: Influence of compression reinforcement in R/C beams; Group ID

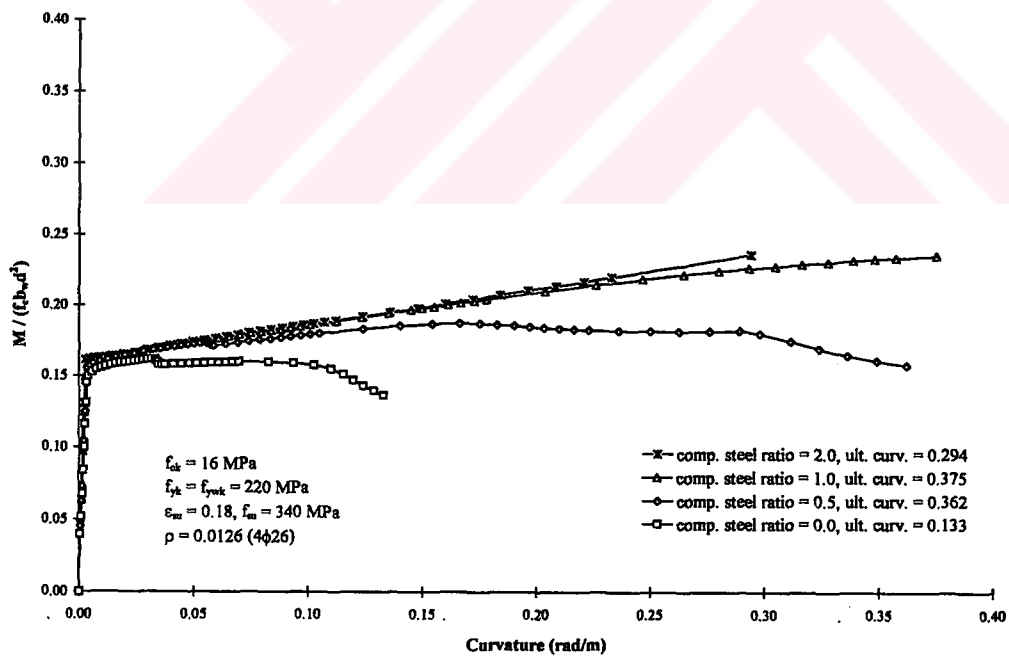


Figure A.5: Influence of compression reinforcement in R/C beams; Group IE

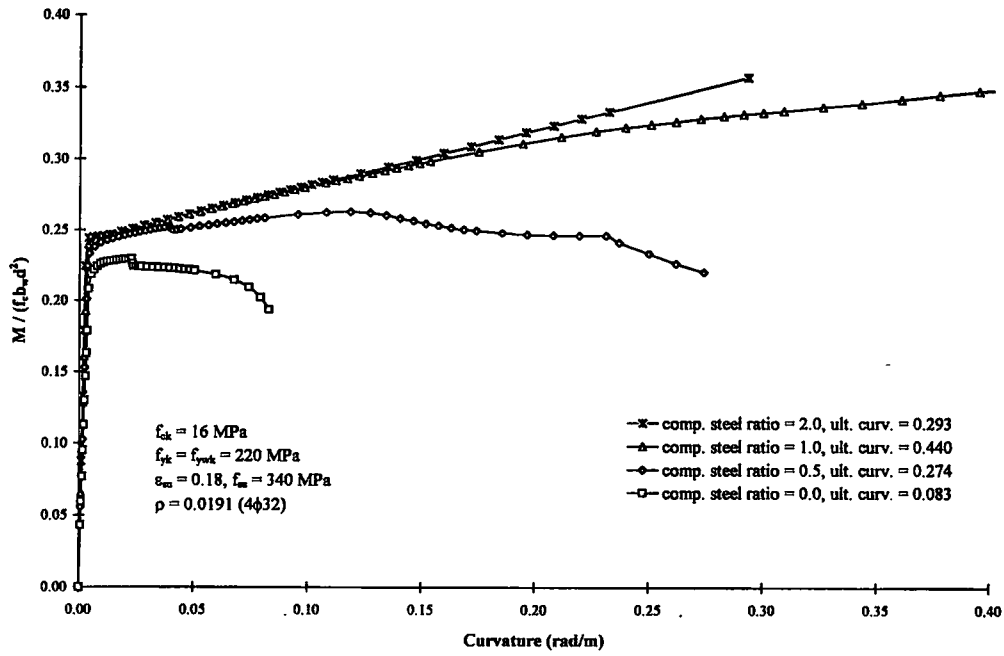


Figure A.6: Influence of compression reinforcement in R/C beams; Group IF

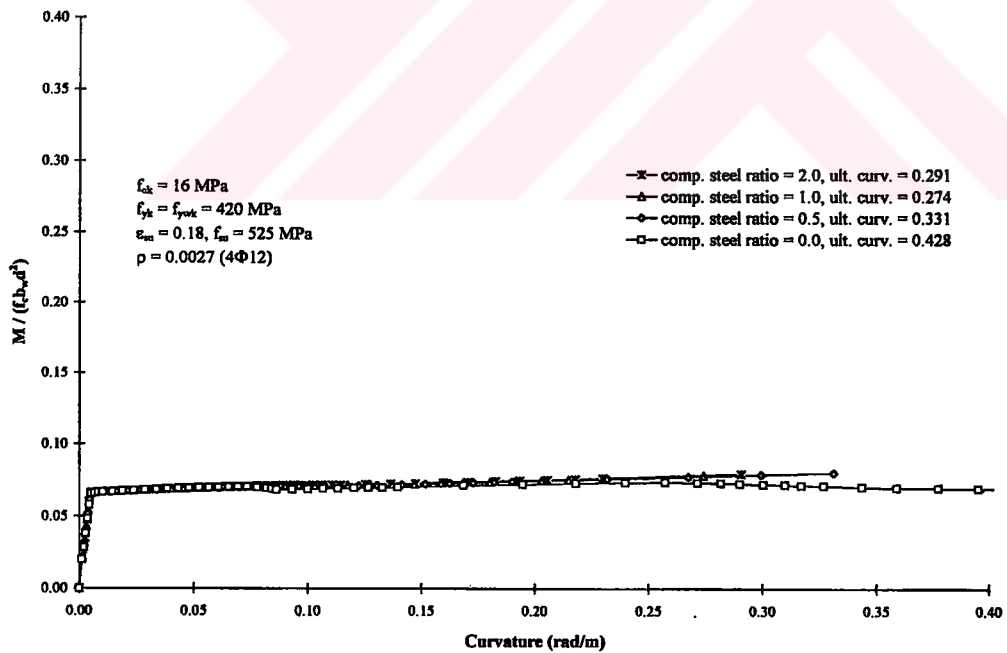


Figure A.7: Influence of compression reinforcement in R/C beams; Group IG

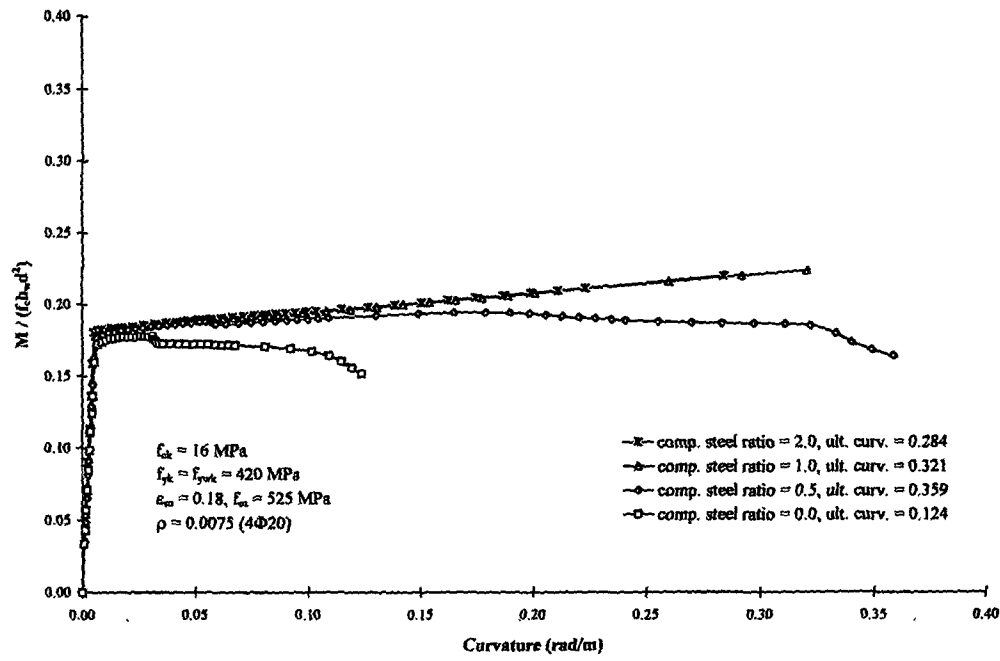


Figure A.8: Influence of compression steel in R/C beams; Group IH

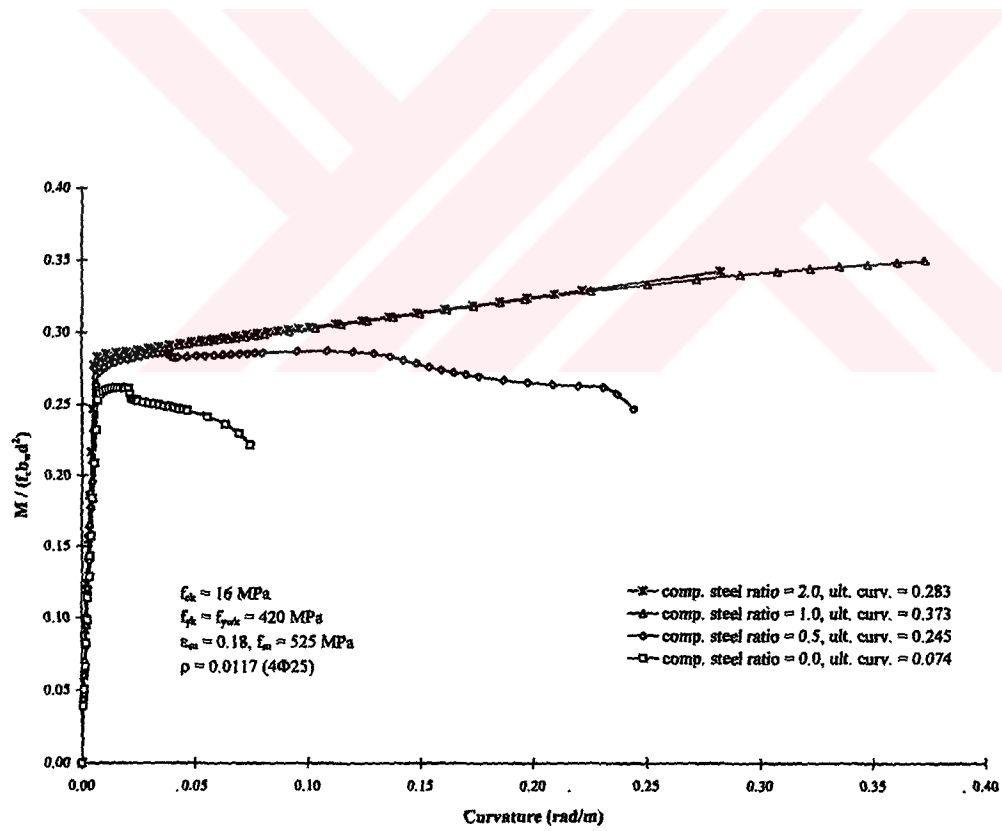


Figure A.9: Influence of compression steel in R/C beams; Group IJ

T.C. YÜKSEKÖĞRETİM KURULU  
 DOKÜMANTASYON BİRLİĞİ

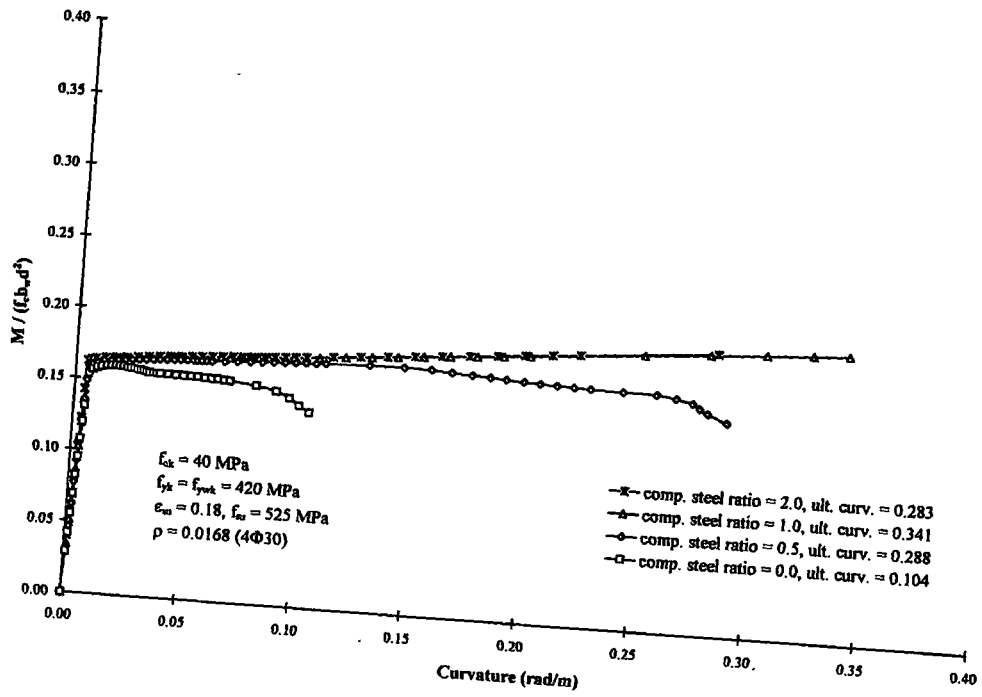


Figure A.10: Influence of compression reinforcement in R/C beams; Group IK

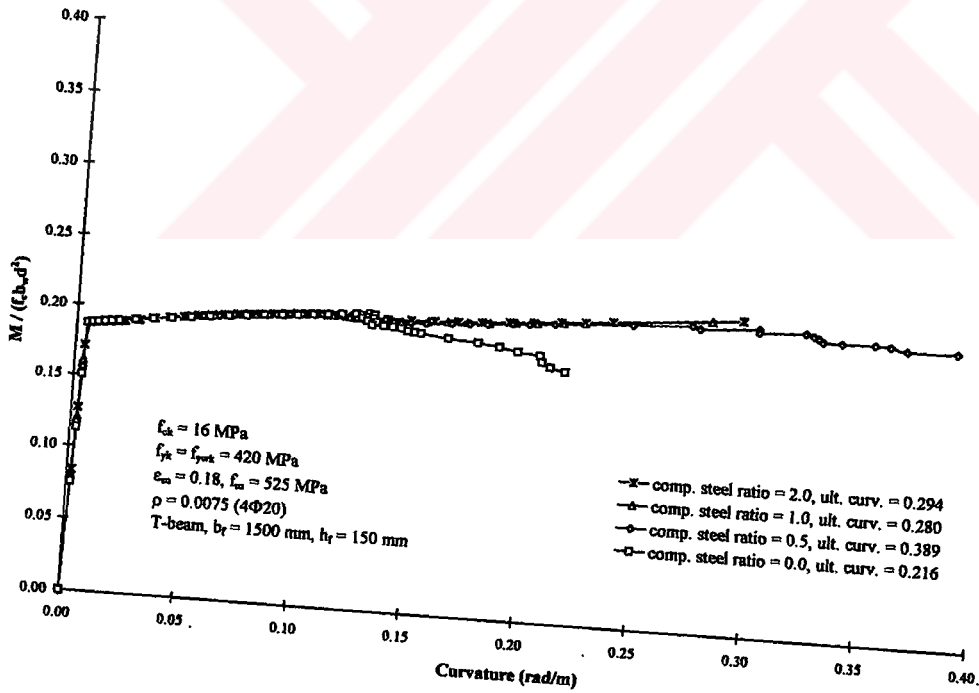


Figure A.11: Influence of compression reinforcement in R/C beams; Group II

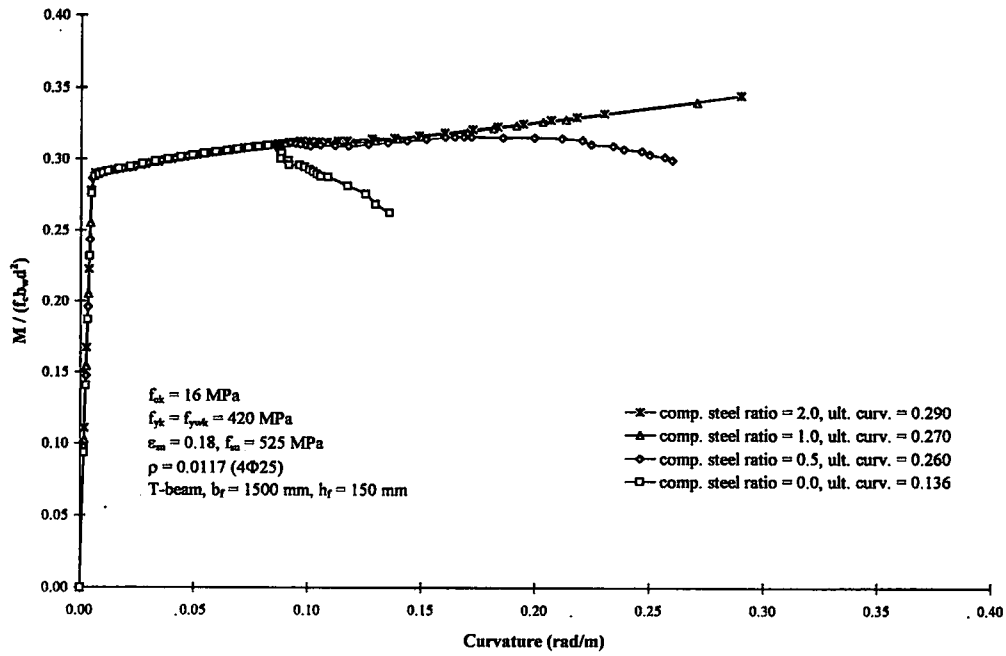


Figure A.12: Influence of compression reinforcement in R/C beams; Group IM

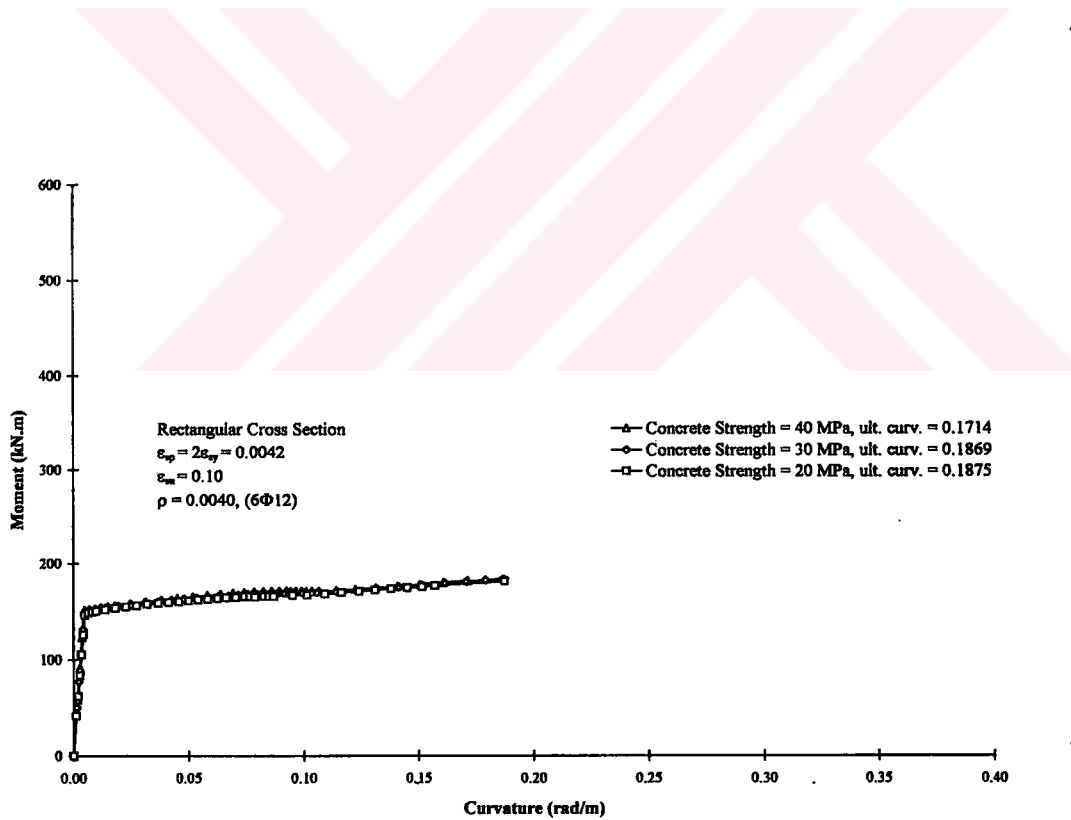


Figure A.13: Influence of concrete strength in R/C beams; Group IIA

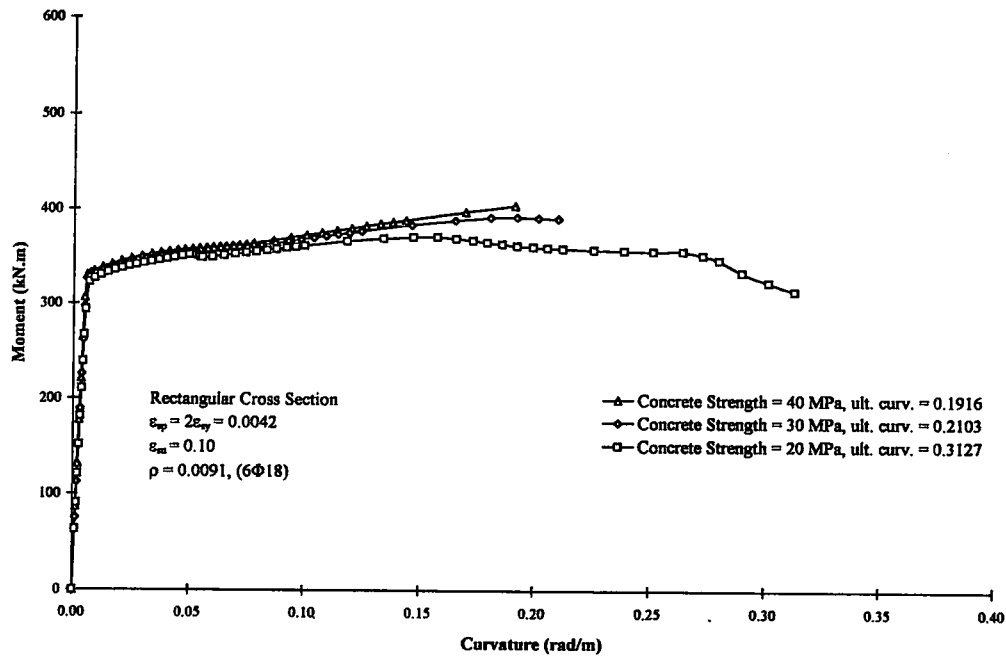


Figure A.14: Influence of concrete strength in R/C beams; Group IIB

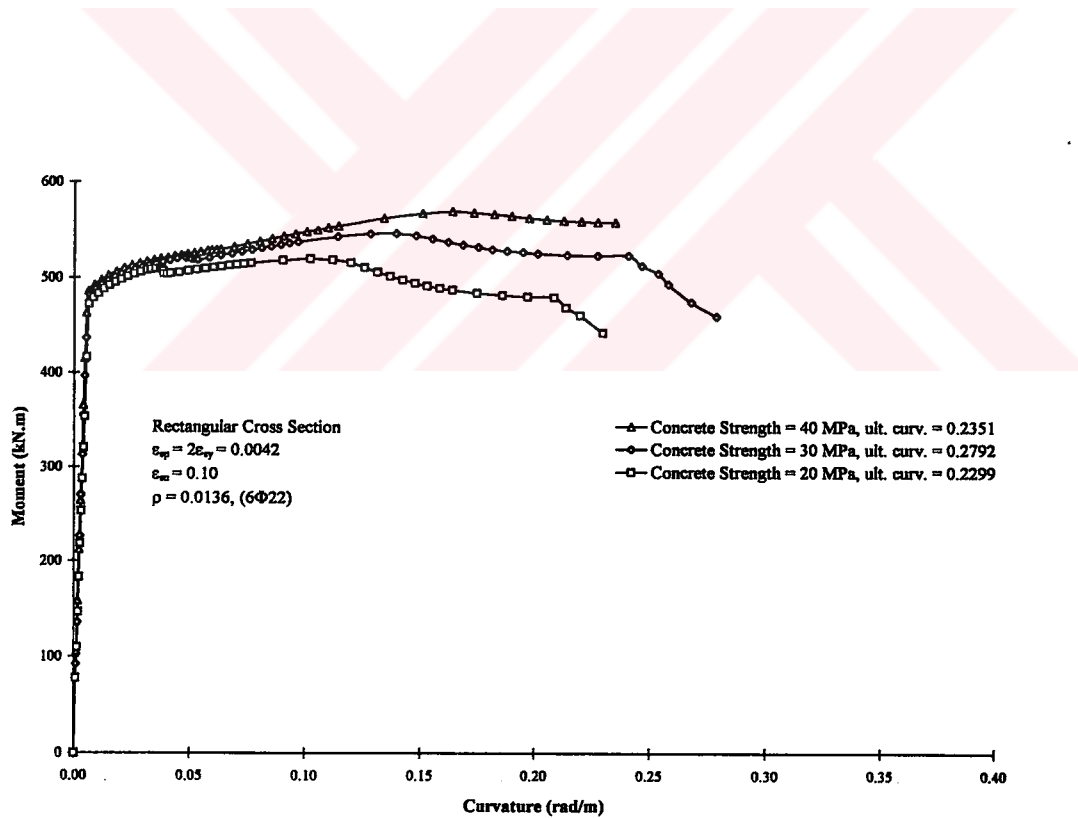


Figure A.15: Influence of concrete strength in R/C beams; Group IIC



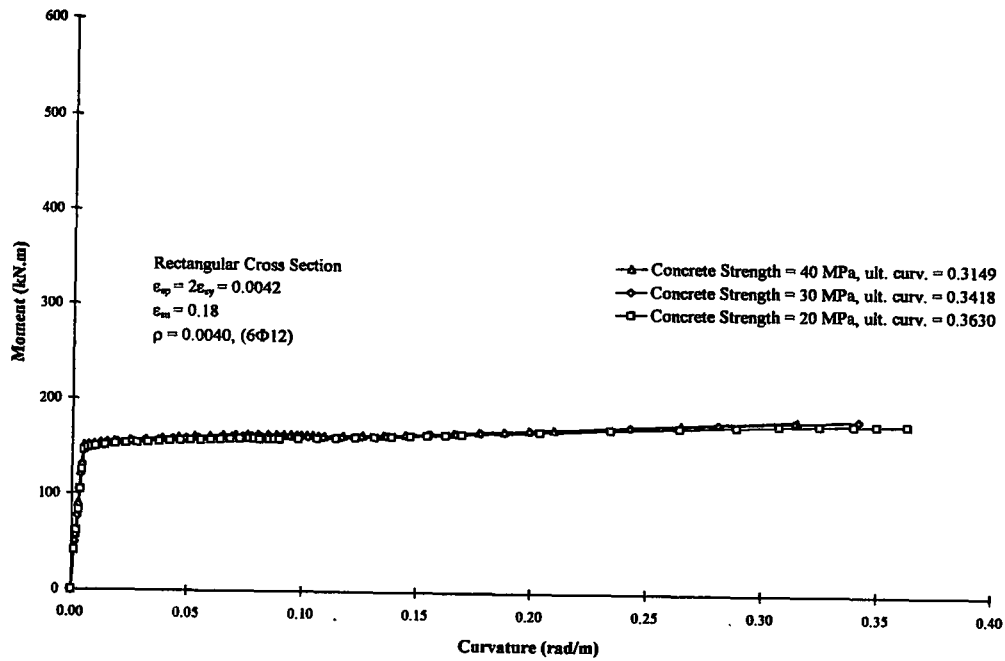


Figure A.16: Influence of concrete strength in R/C beams; Group IID

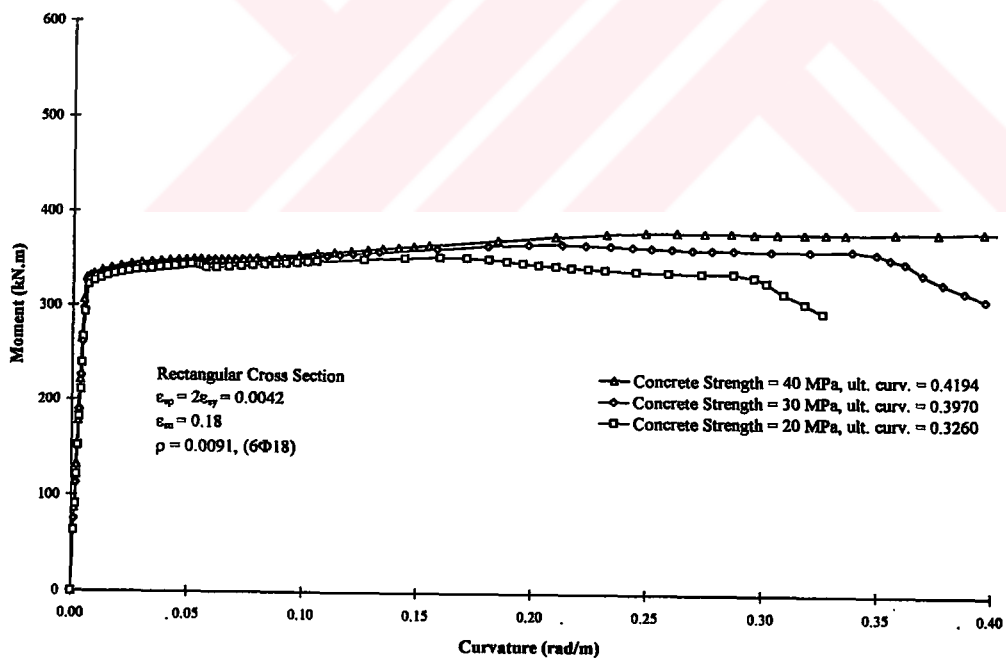


Figure A.17: Influence of concrete strength in R/C beams; Group IIE

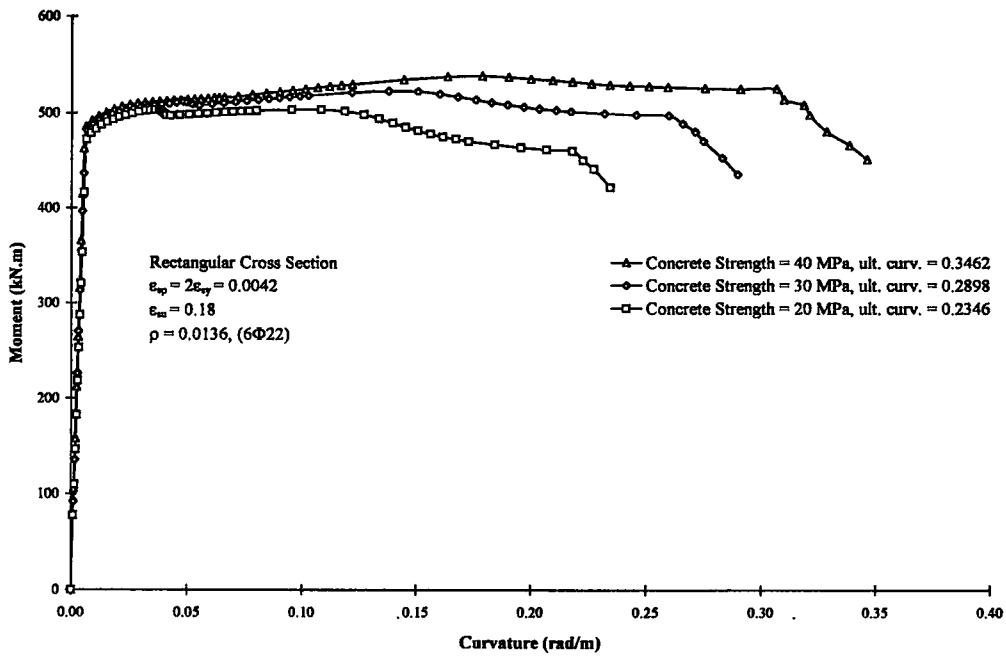


Figure A.18: Influence of concrete strength in R/C beams; Group IIF

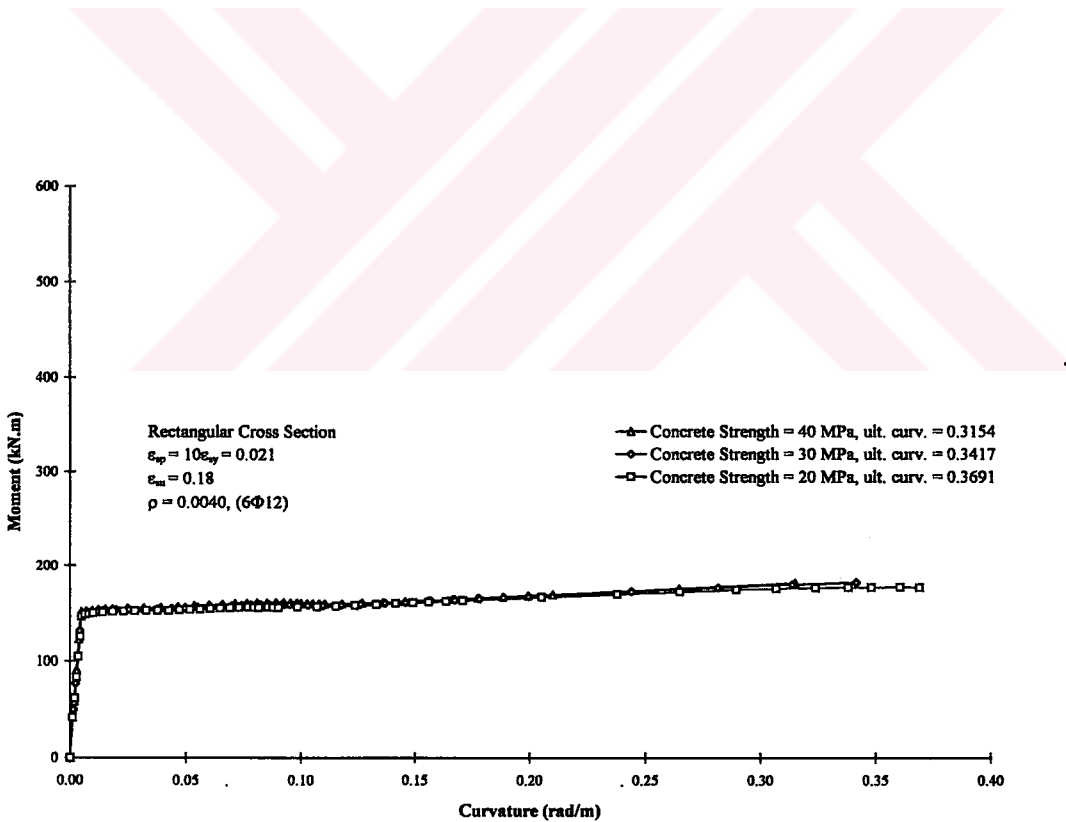


Figure A.19: Influence of concrete strength in R/C beams; Group IIG

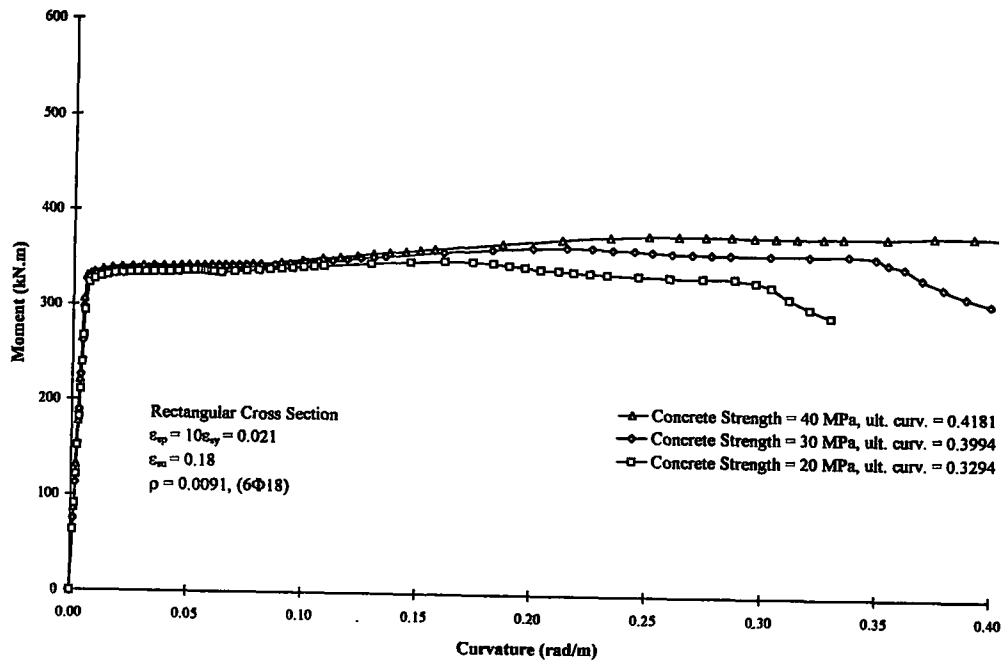


Figure A.20: Influence of concrete strength in R/C beams; Group IIIH

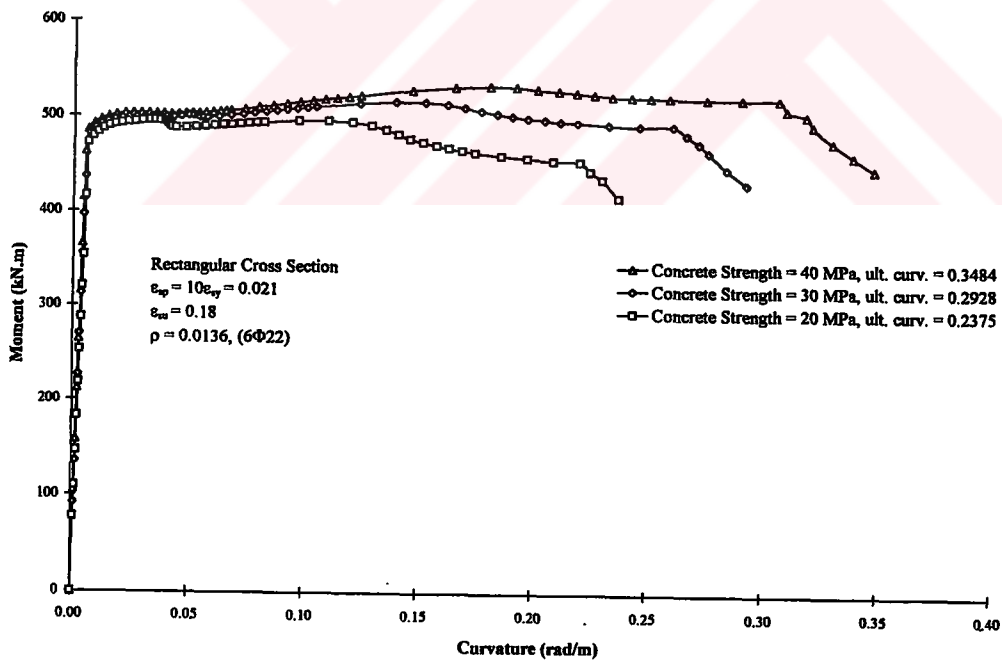


Figure A.21: Influence of concrete strength in R/C beams; Group IIIJ

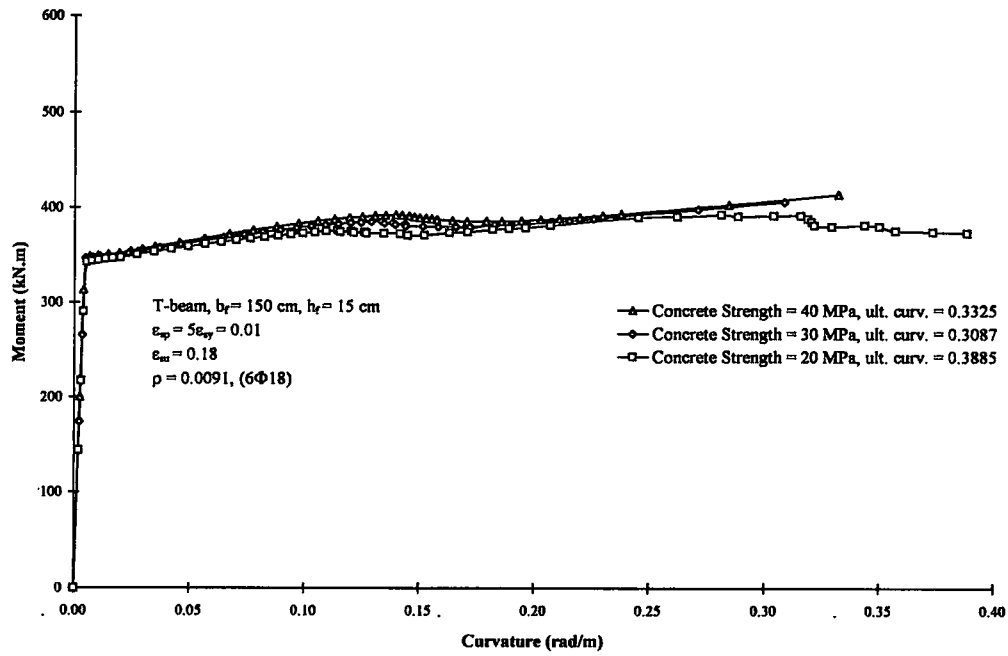


Figure A.22: Influence of concrete strength in R/C beams; Group IIIK

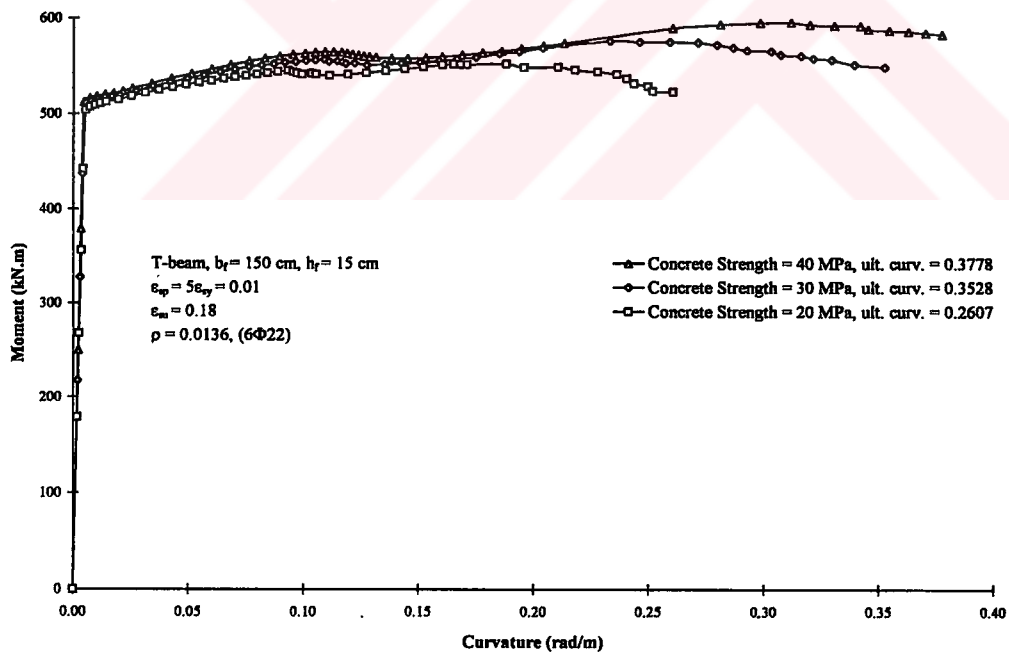


Figure A.23: Influence of concrete strength in R/C beams; Group III

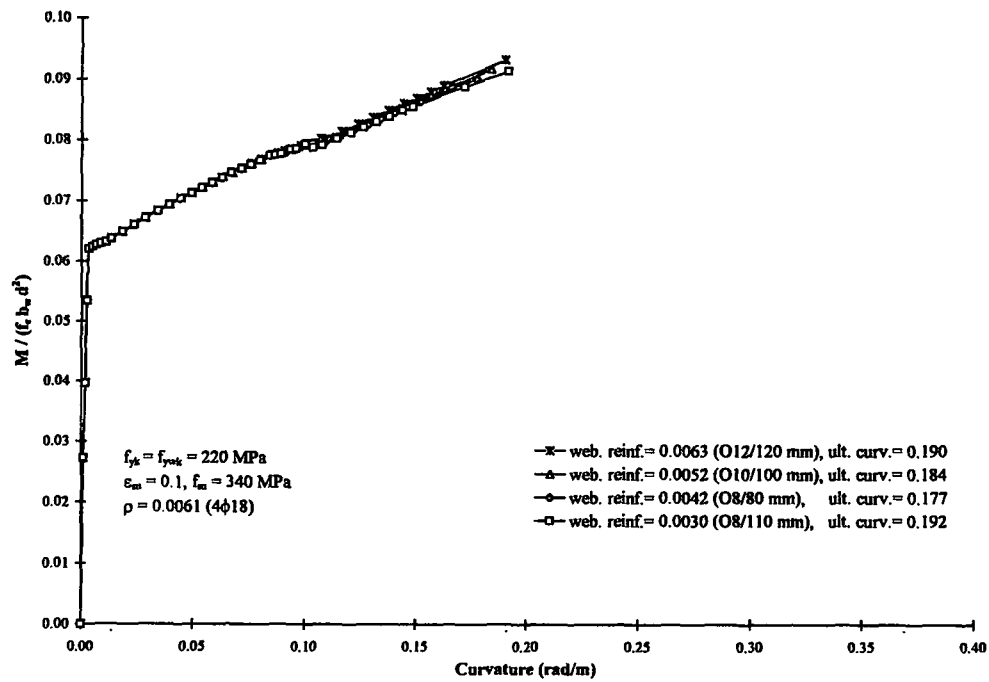


Figure A.24: Influence of confinement in R/C beams; Group IIIA

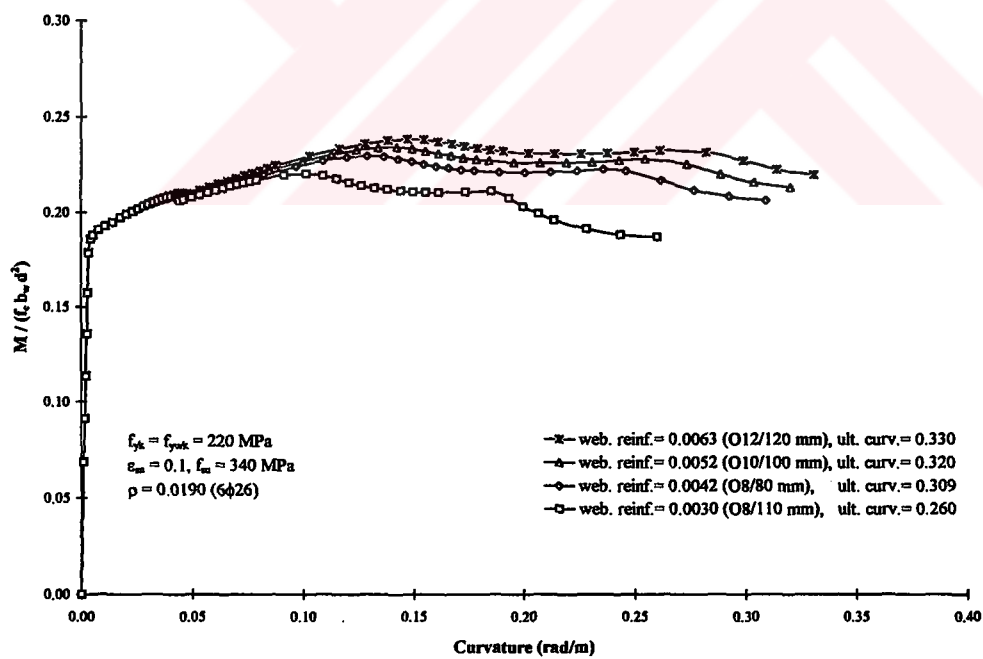


Figure A.25: Influence of confinement in R/C beams; Group IIIB

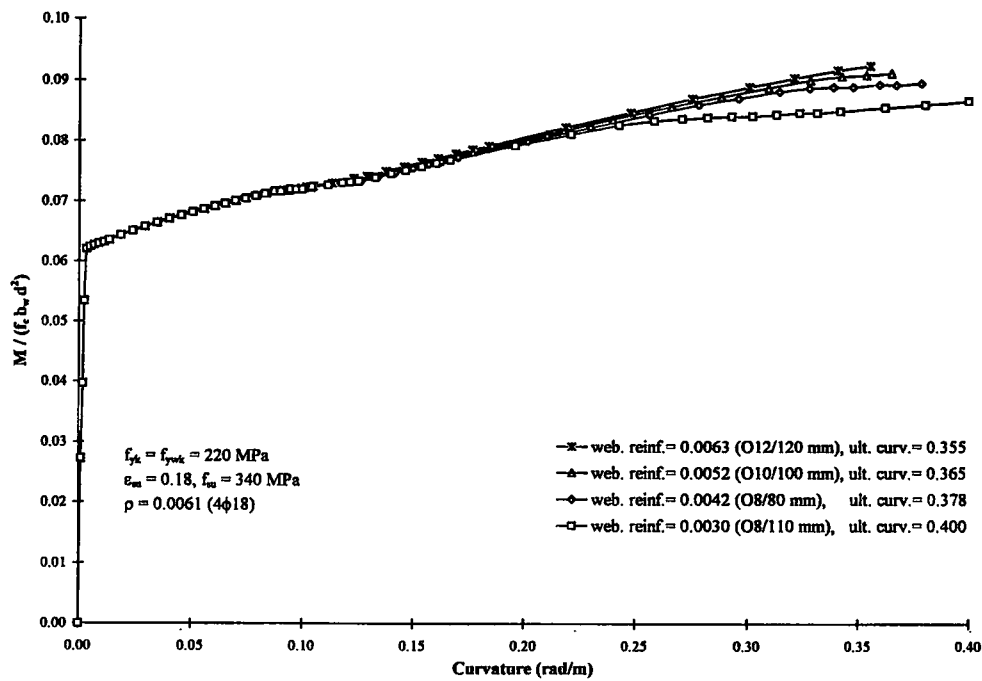


Figure A.26: Influence of confinement in R/C beams; Group IIIC

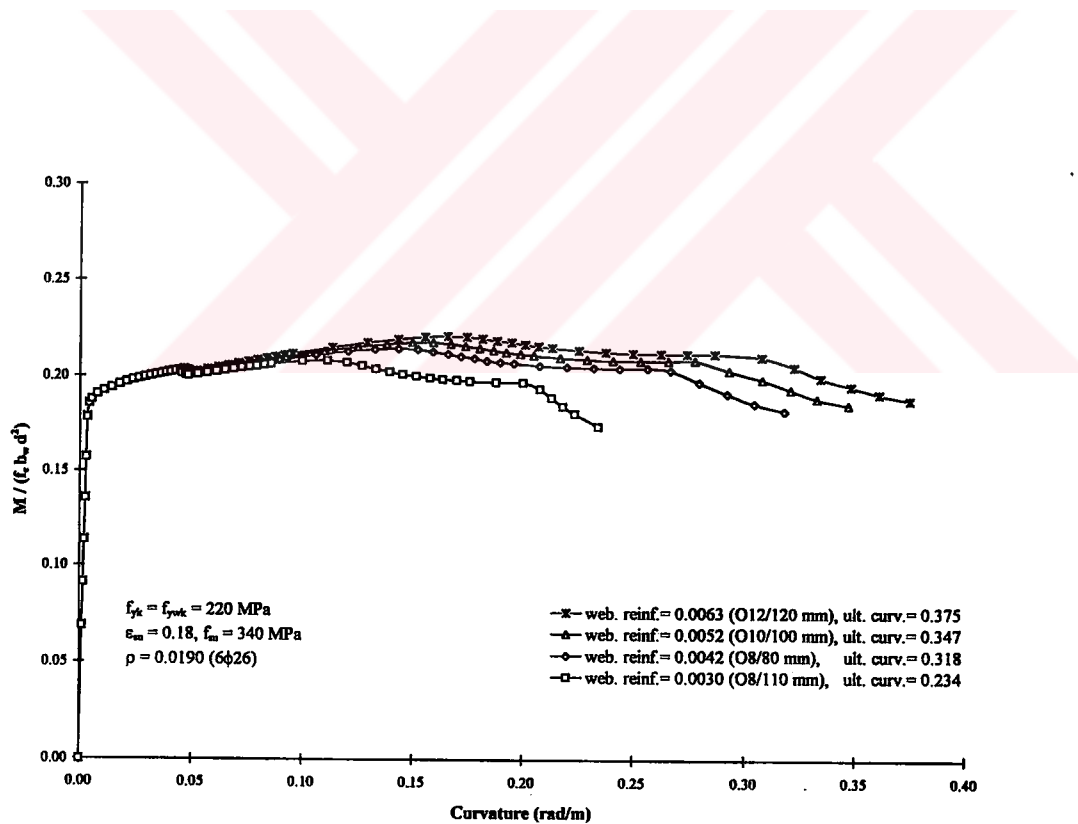


Figure A.27: Influence of confinement in R/C beams; Group IIID

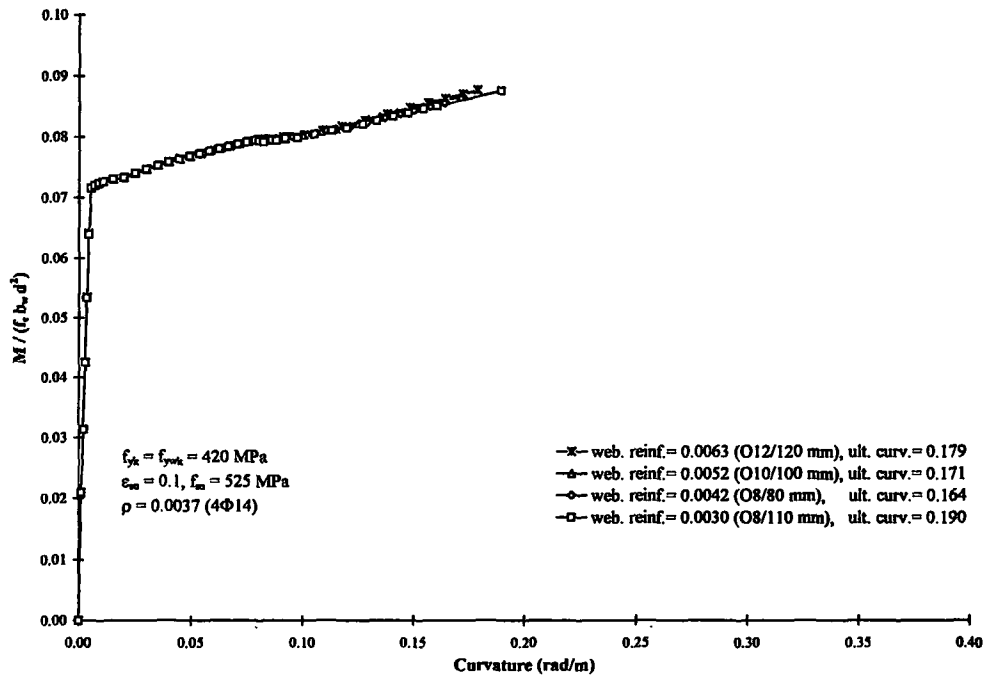


Figure A.28: Influence of confinement in R/C beams; Group III E

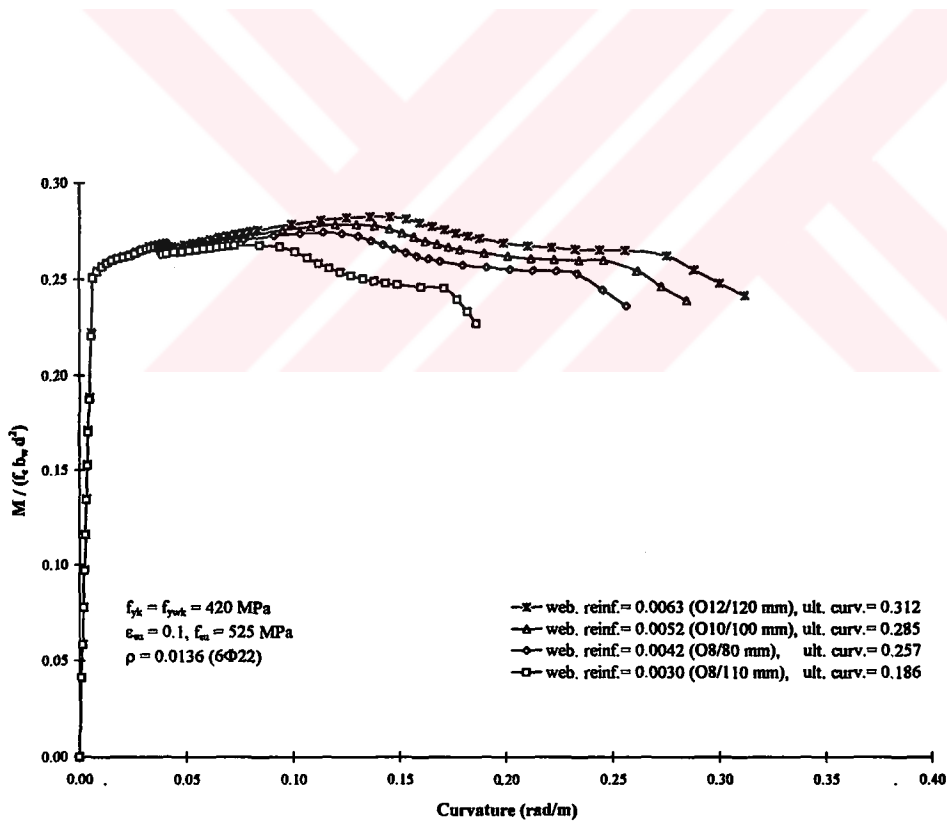


Figure A.29: Influence of confinement in R/C beams; Group III F

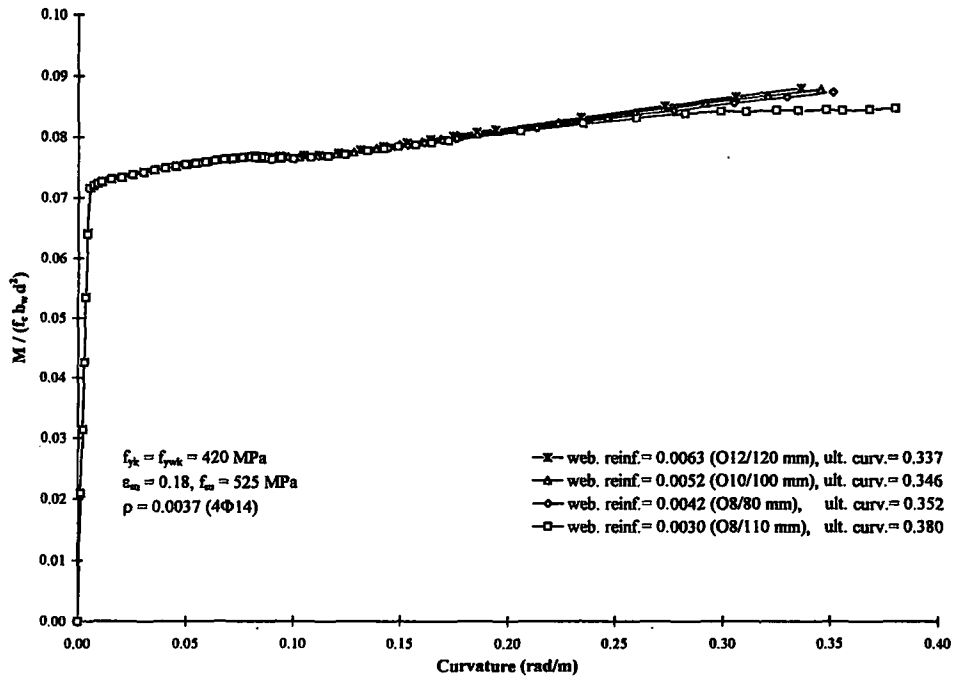


Figure A.30: Influence of confinement in R/C beams; Group III G

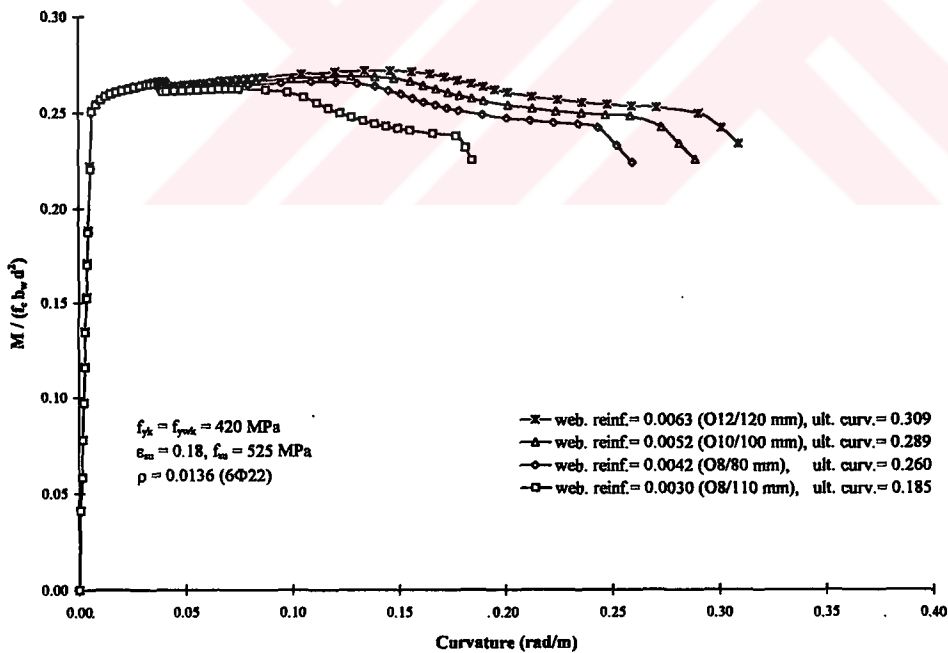


Figure A.31: Influence of confinement in R/C beams; Group III H



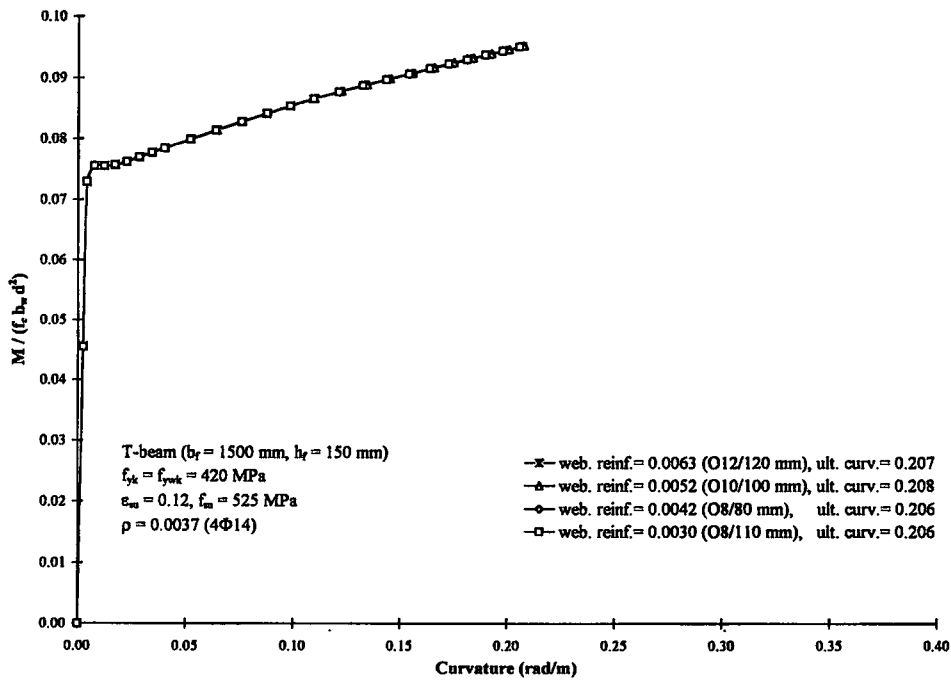


Figure A.32: Influence of confinement in R/C beams; Group IIIJ

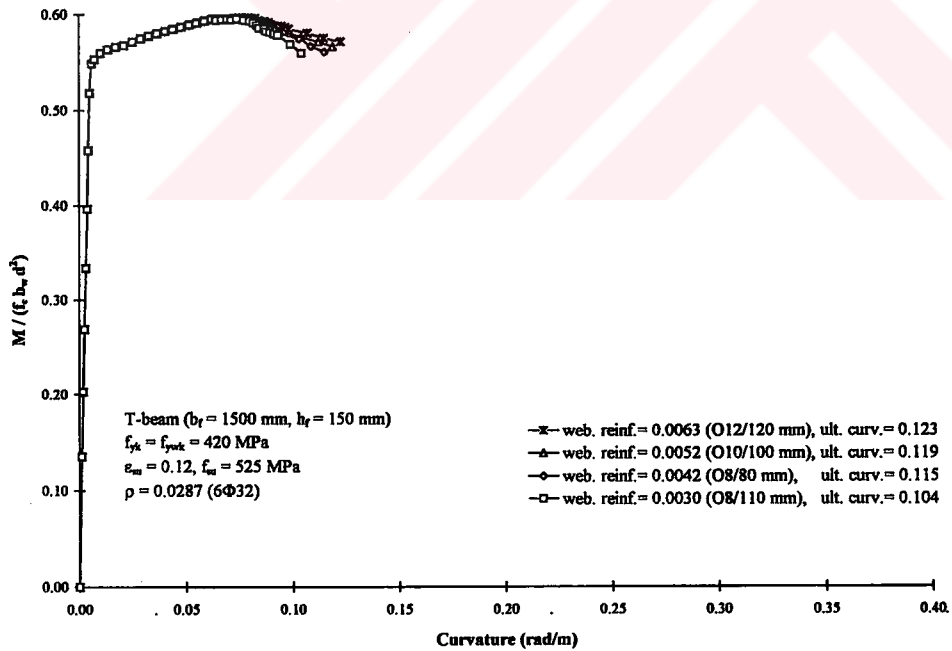


Figure A.33: Influence of confinement in R/C beams; Group IIIK

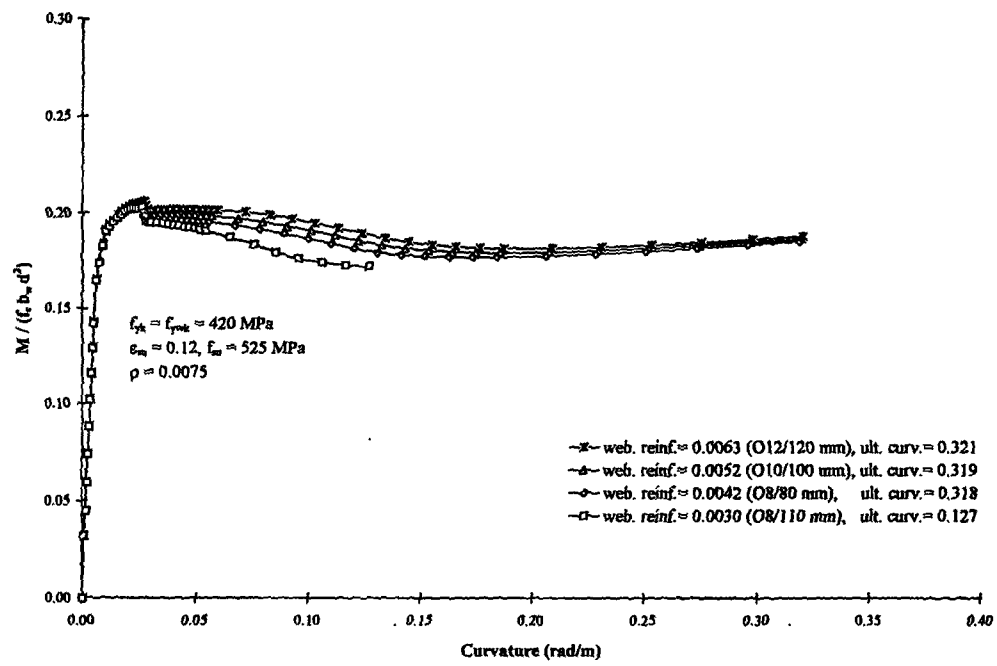


Figure A.34: Influence of confinement in R/C beams; Group III

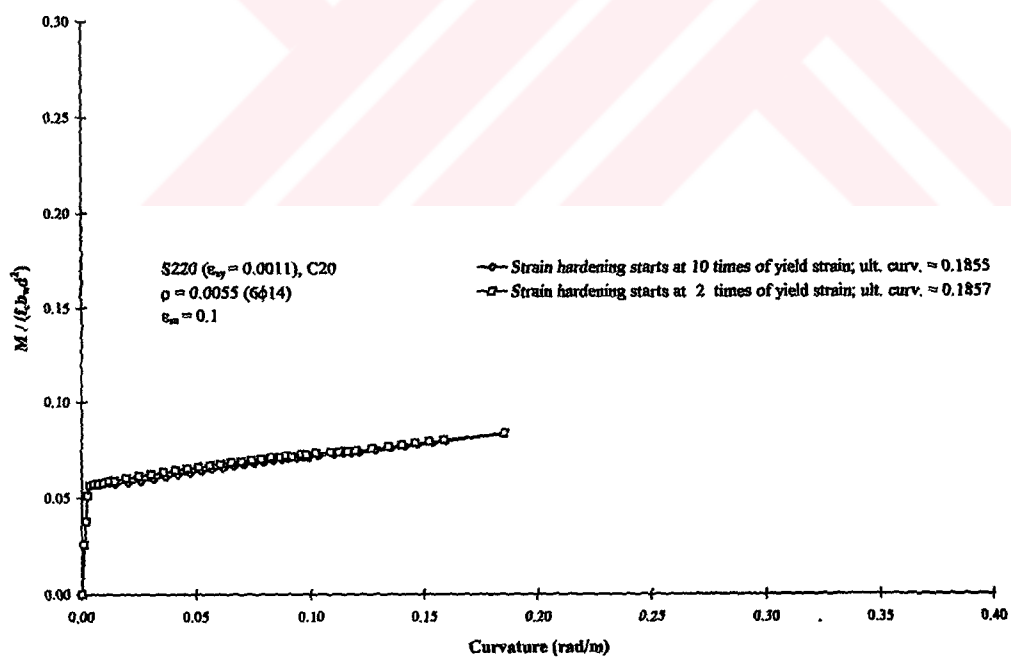


Figure A.35: Influence of the steel model in R/C beams; Group IVA

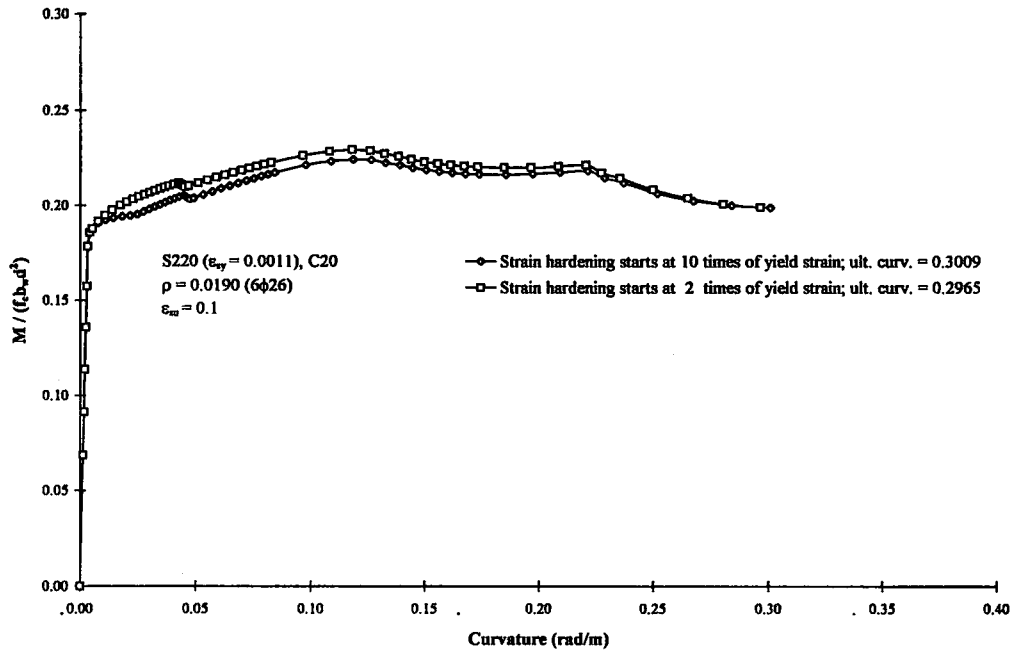


Figure A.36: Influence of the steel model in R/C beams; Group IVB

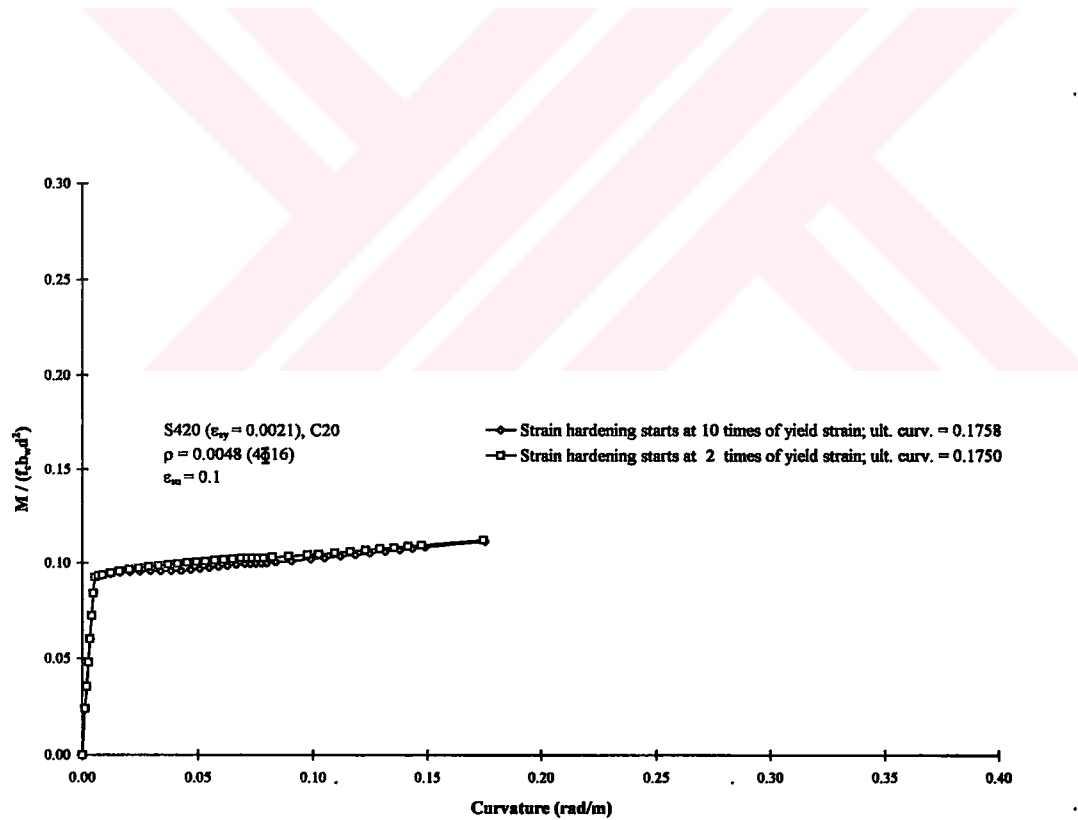


Figure A.37: Influence of the steel model in R/C beams; Group IVC

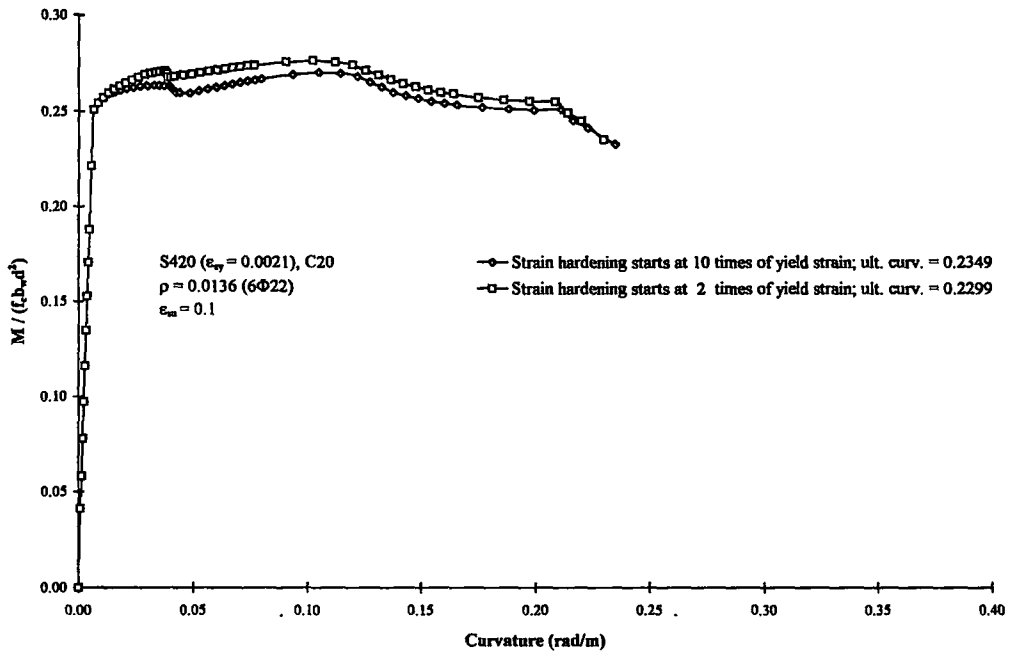


Figure A.38: Influence of the steel model in R/C beams; Group IVD

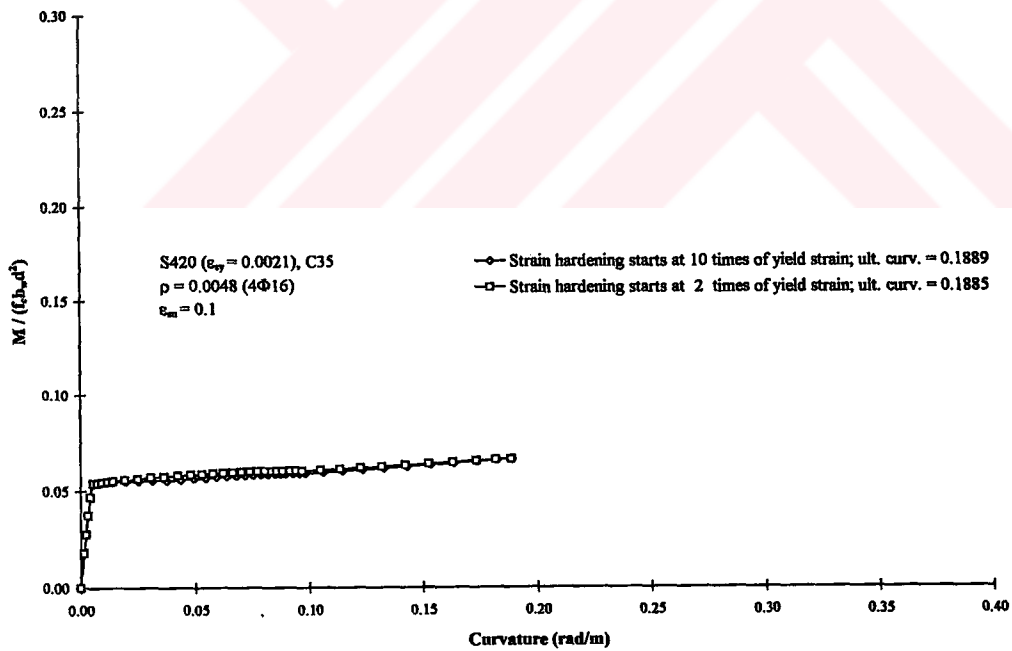


Figure A.39: Influence of the steel model in R/C beams; Group IVE

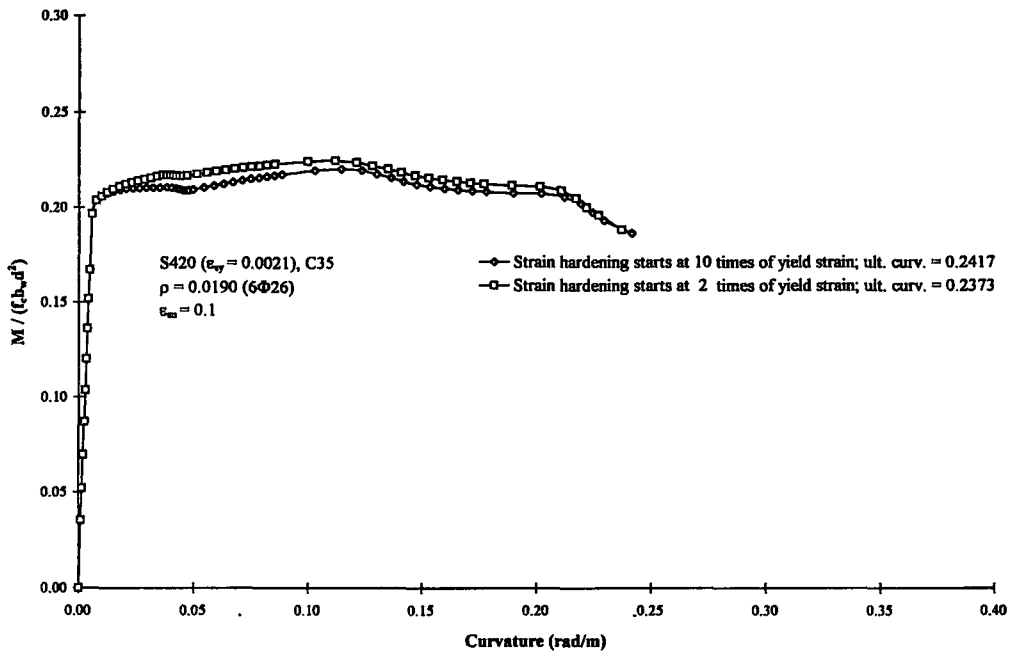


Figure A.40: Influence of the steel model in R/C beams; Group IVF

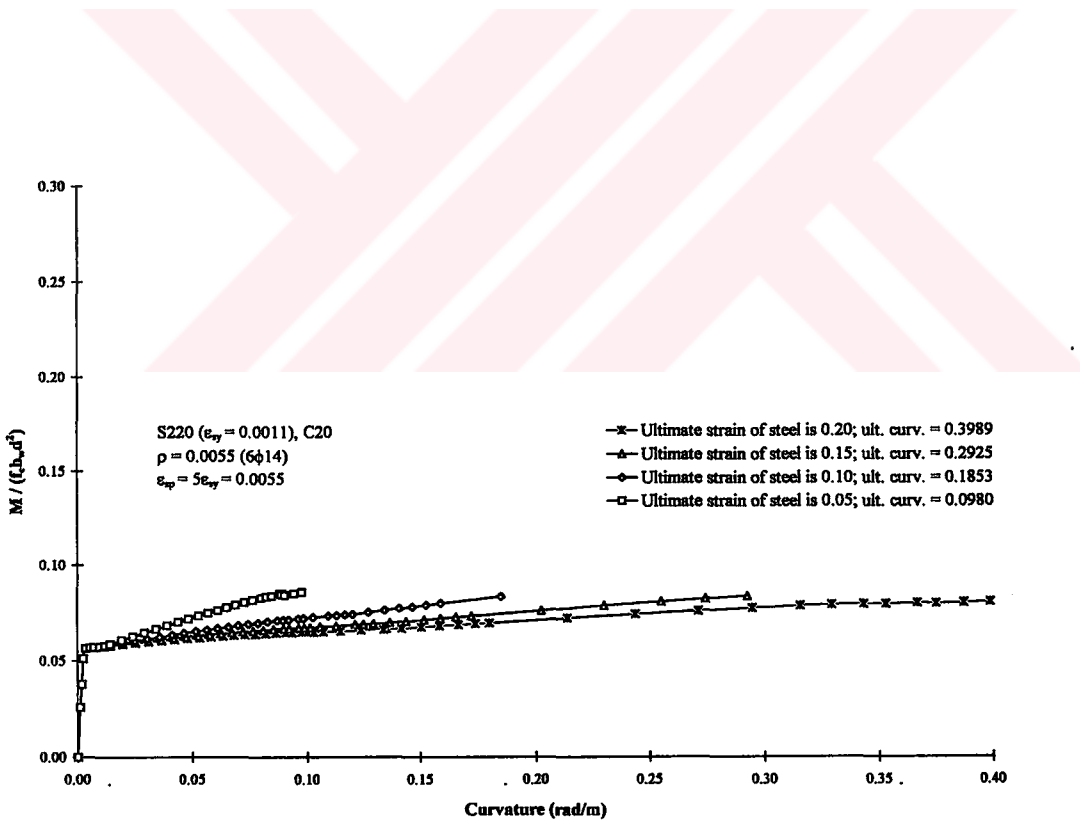


Figure A.41: Influence of the steel model in R/C beams; Group IVG

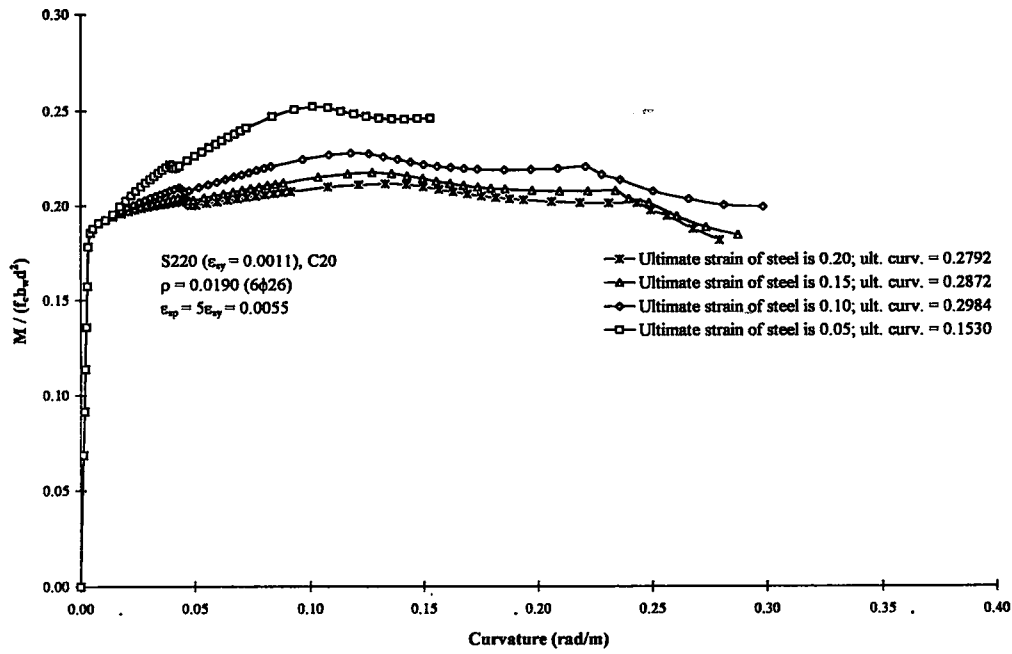


Figure A.42: Influence of the steel model in R/C beams; Group IVH

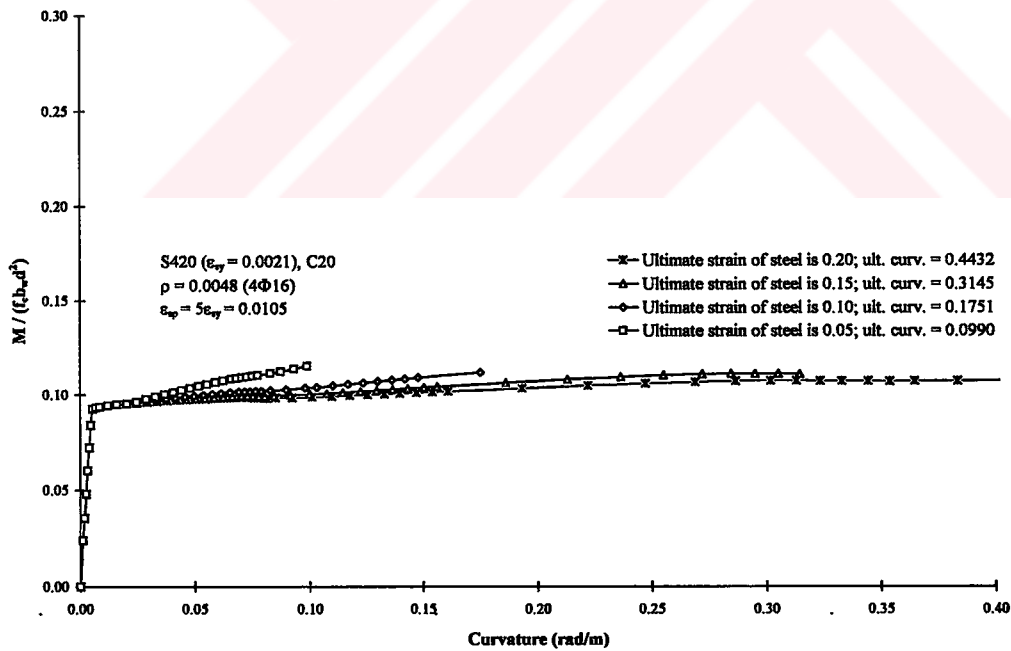


Figure A.43: Influence of the steel model in R/C beams; Group IVJ

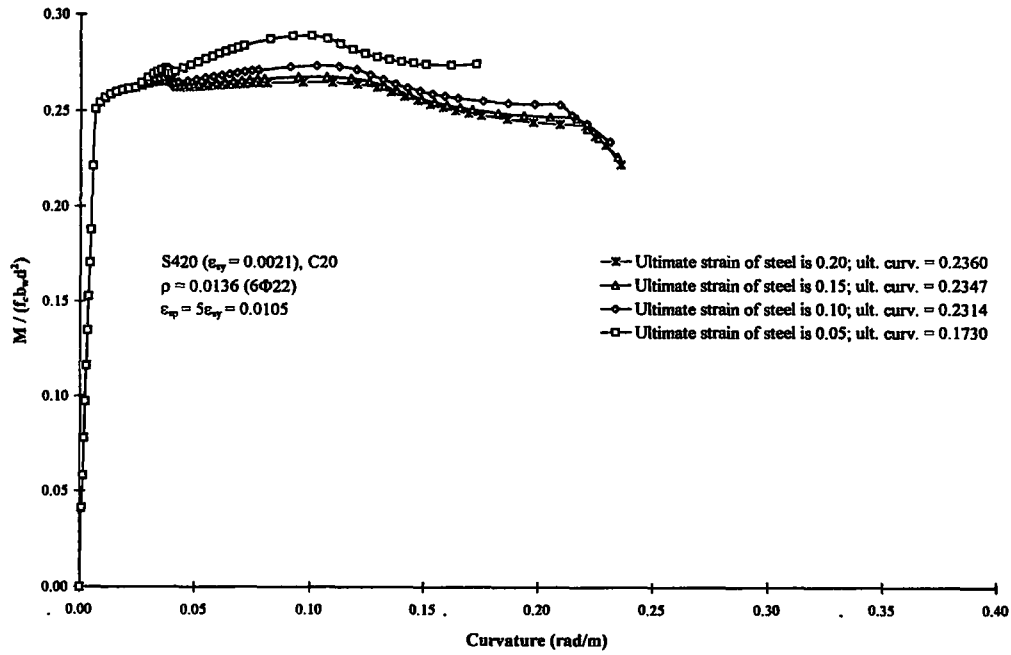


Figure A.44: Influence of the steel model in R/C beams; Group IVK

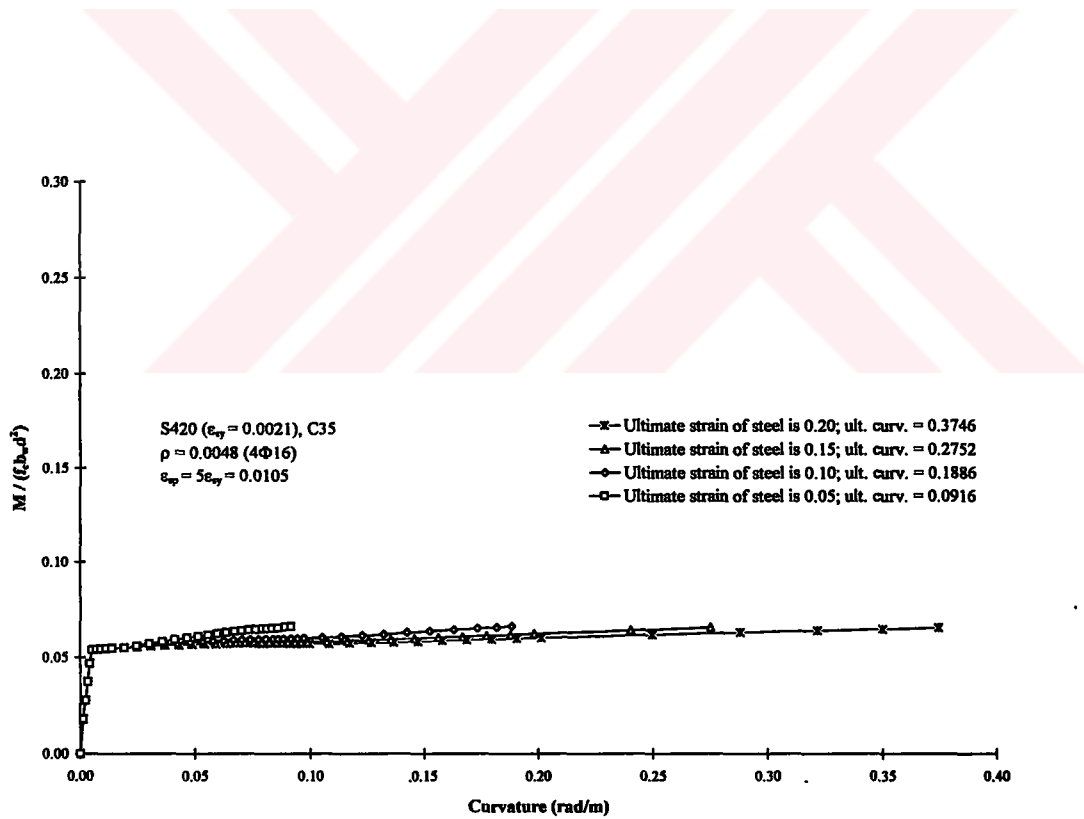


Figure A.45: Influence of the steel model in R/C beams; Group IVL

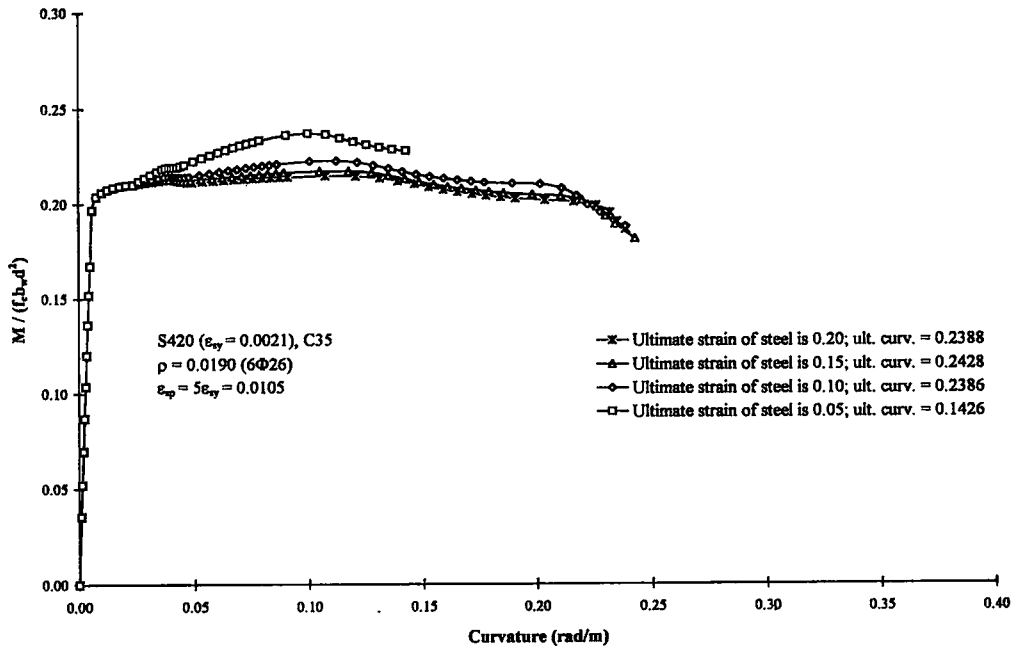


Figure A.46: Influence of the steel model in R/C beams; Group IVM

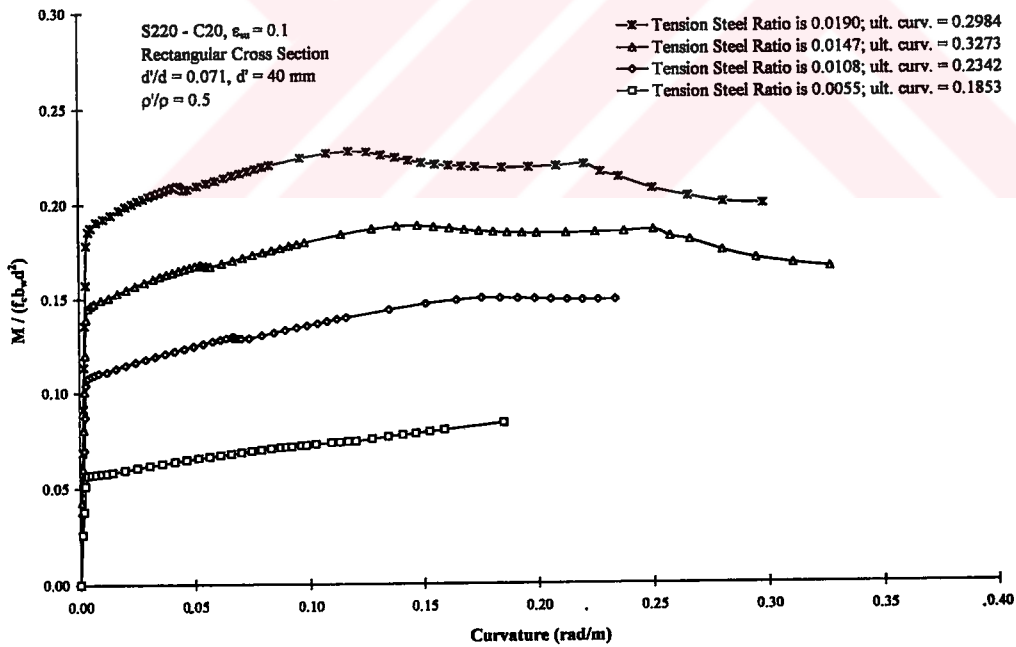


Figure A.47: Influence of tension reinforcement ratio in R/C beams; Group VA



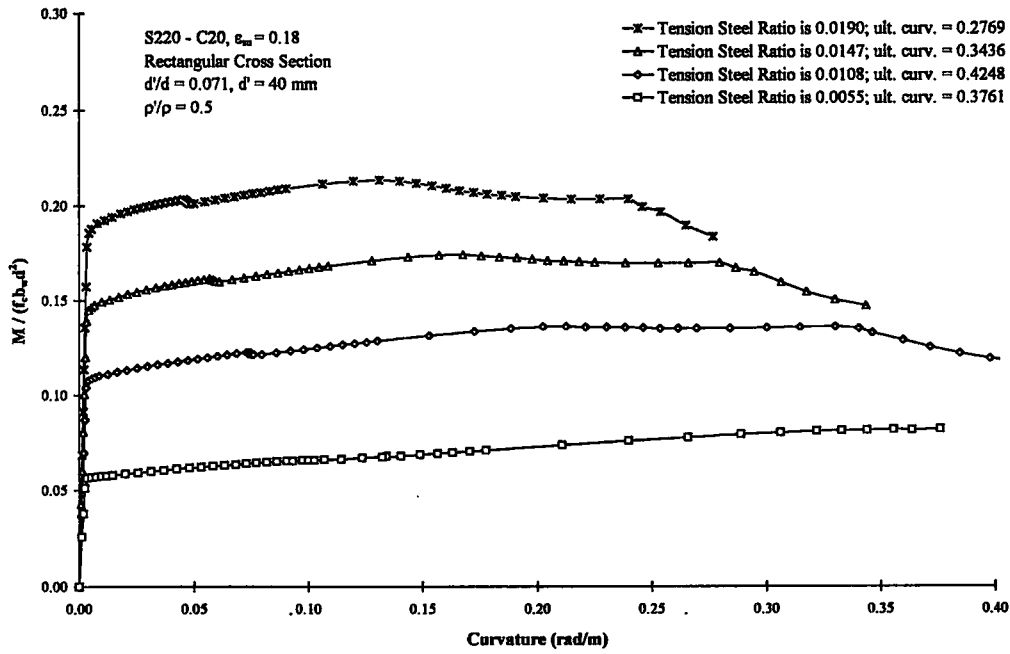


Figure A.48: Influence of tension reinforcement ratio in R/C beams; Group VB

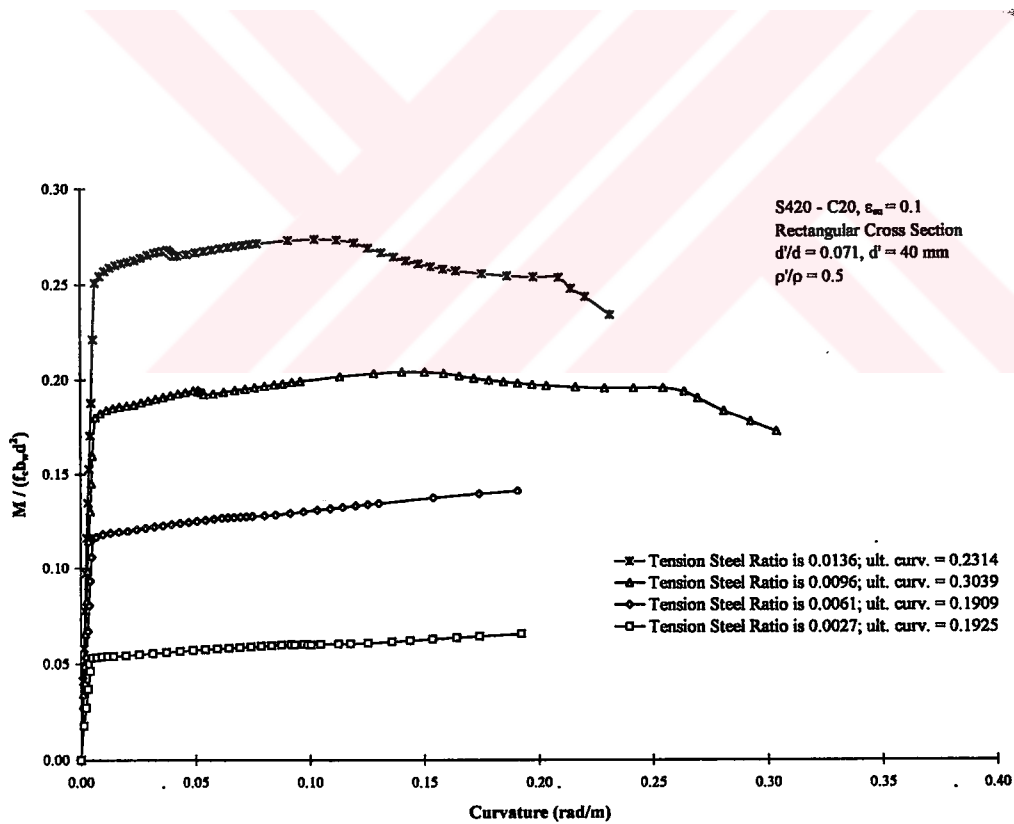


Figure A.49: Influence of tension reinforcement ratio in R/C beams; Group VC

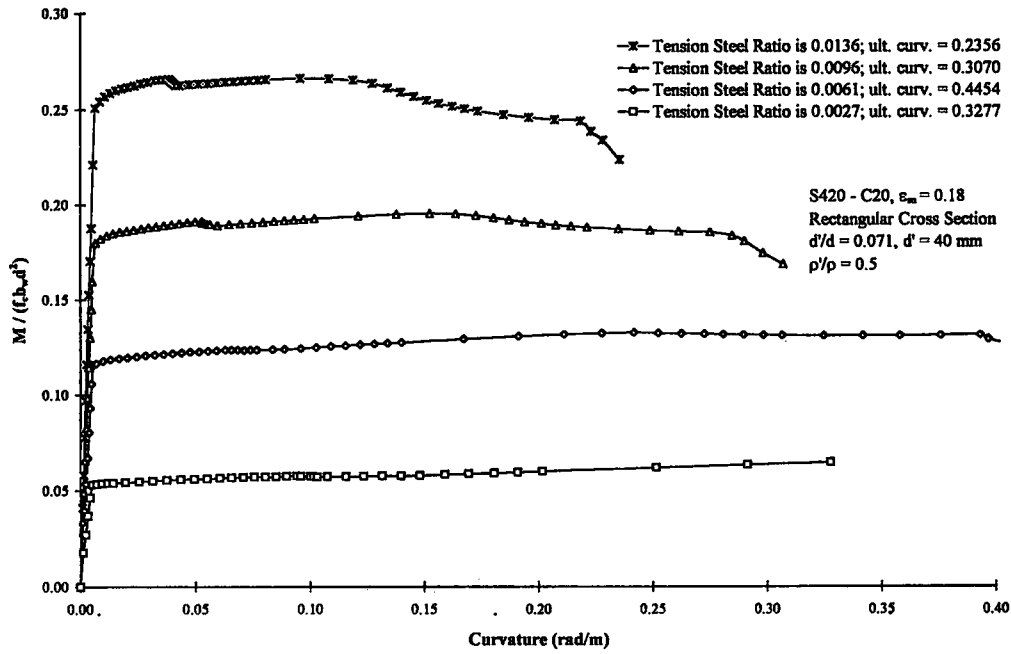


Figure A.50: Influence of tension reinforcement ratio in R/C beams; Group VD

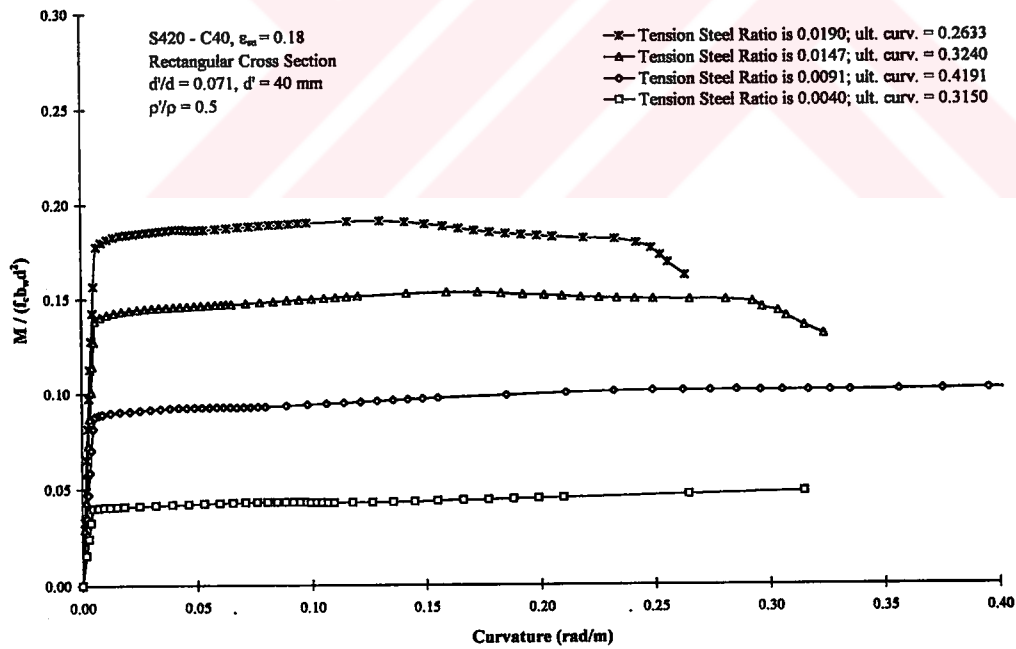


Figure A.51: Influence of tension reinforcement ratio in R/C beams; Group VE

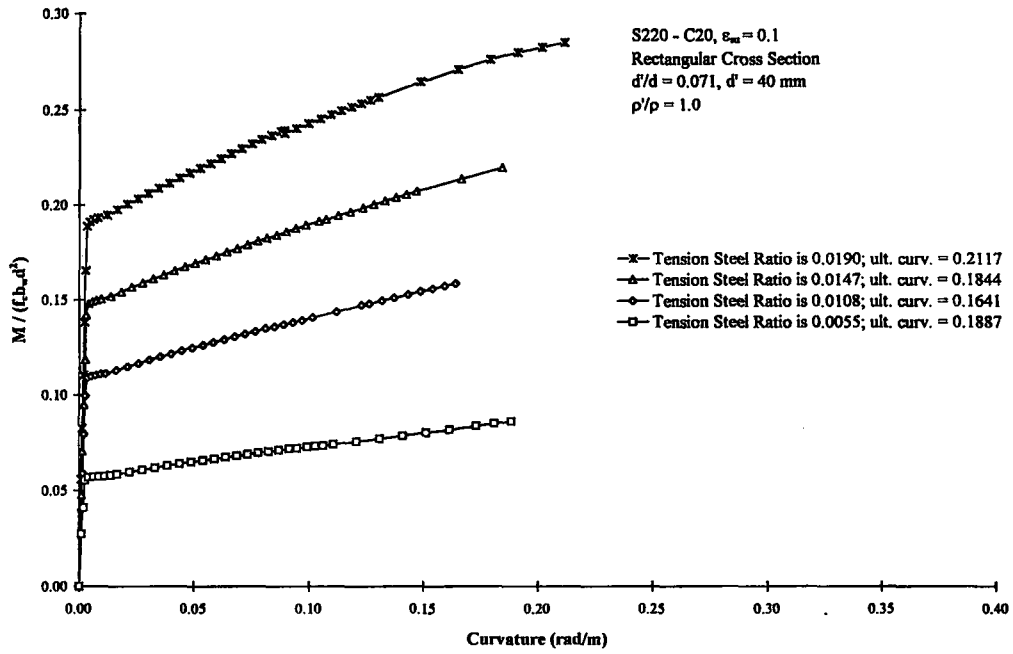


Figure A.52: Influence of tension reinforcement ratio in R/C beams; Group VF

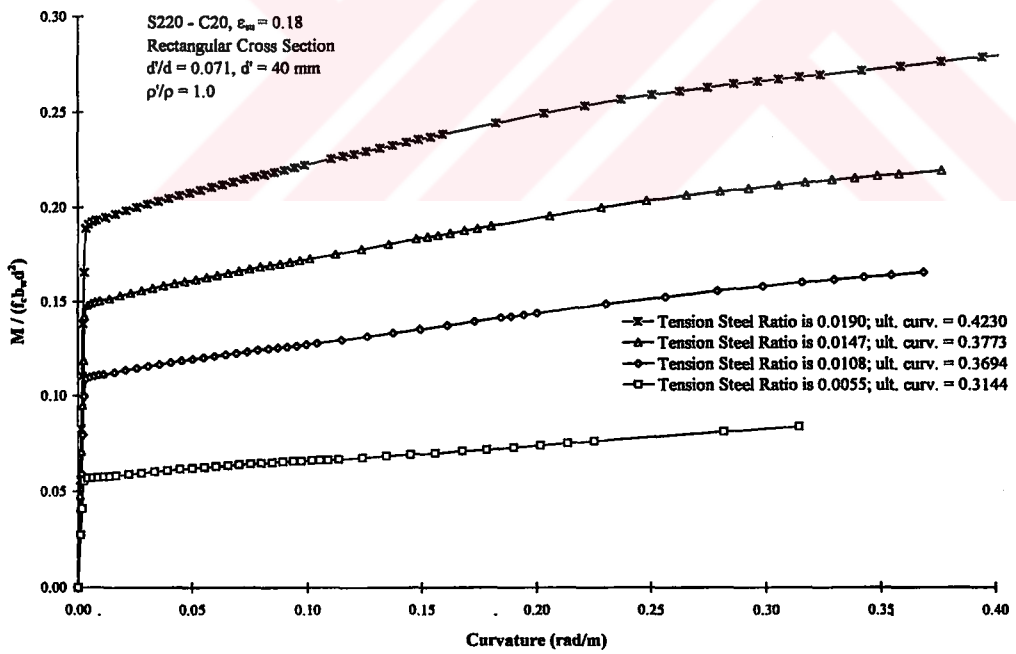


Figure A.53: Influence of tension reinforcement ratio in R/C beams; Group VG

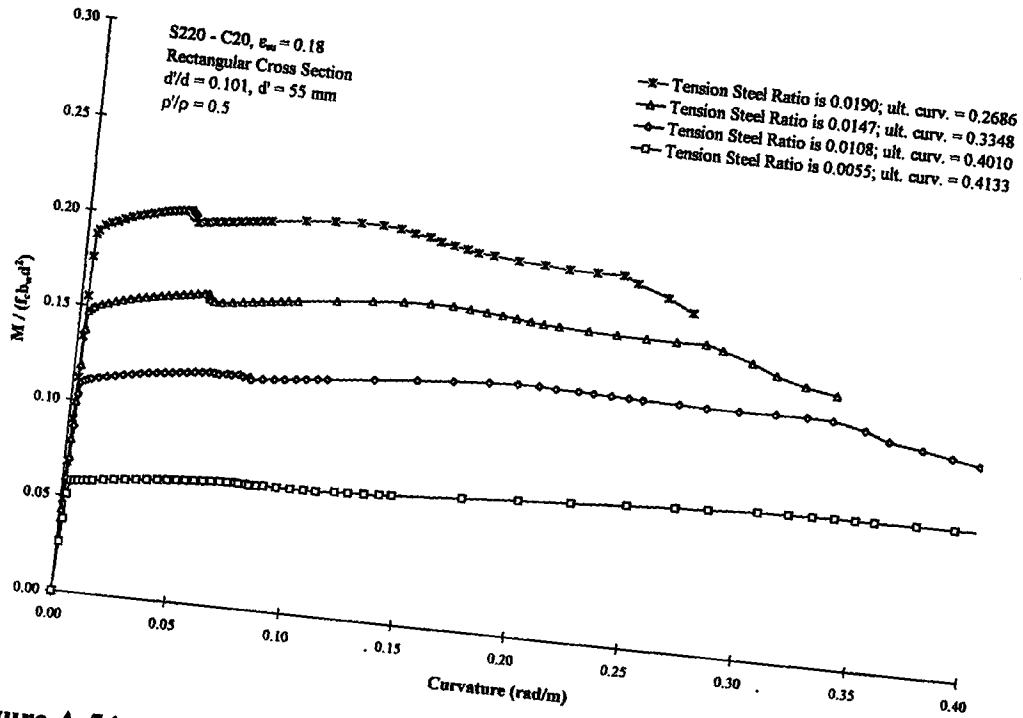


Figure A.54: Influence of tension reinforcement ratio in R/C beams; Group VH

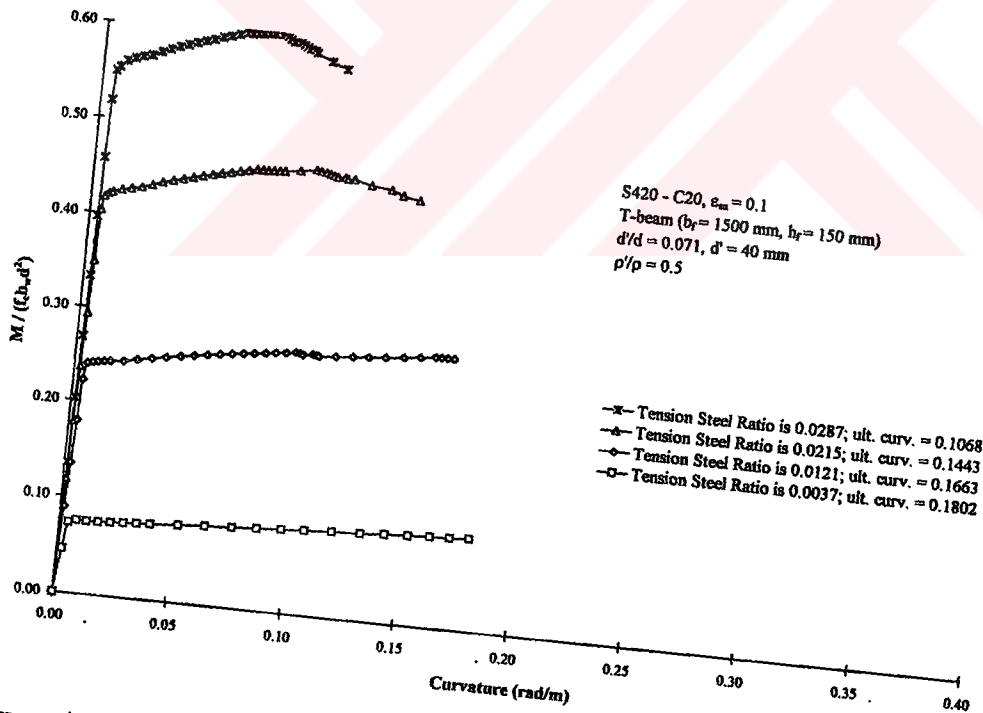


Figure A.55: Influence of tension reinforcement ratio in R/C beams; Group VJ

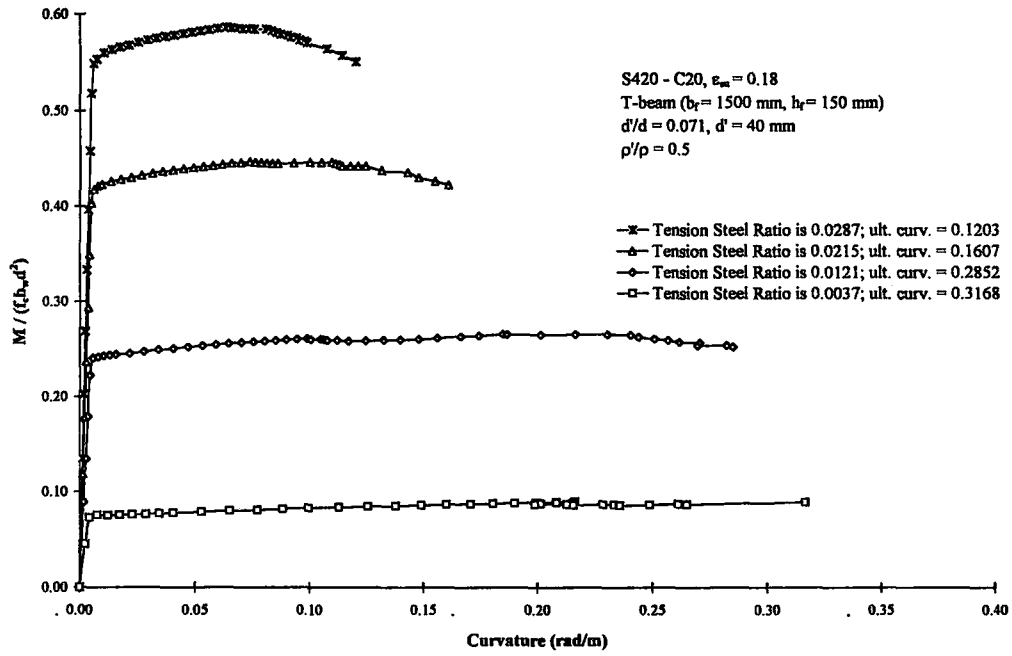


Figure A.56: Influence of tension reinforcement ratio in R/C beams; Group VK

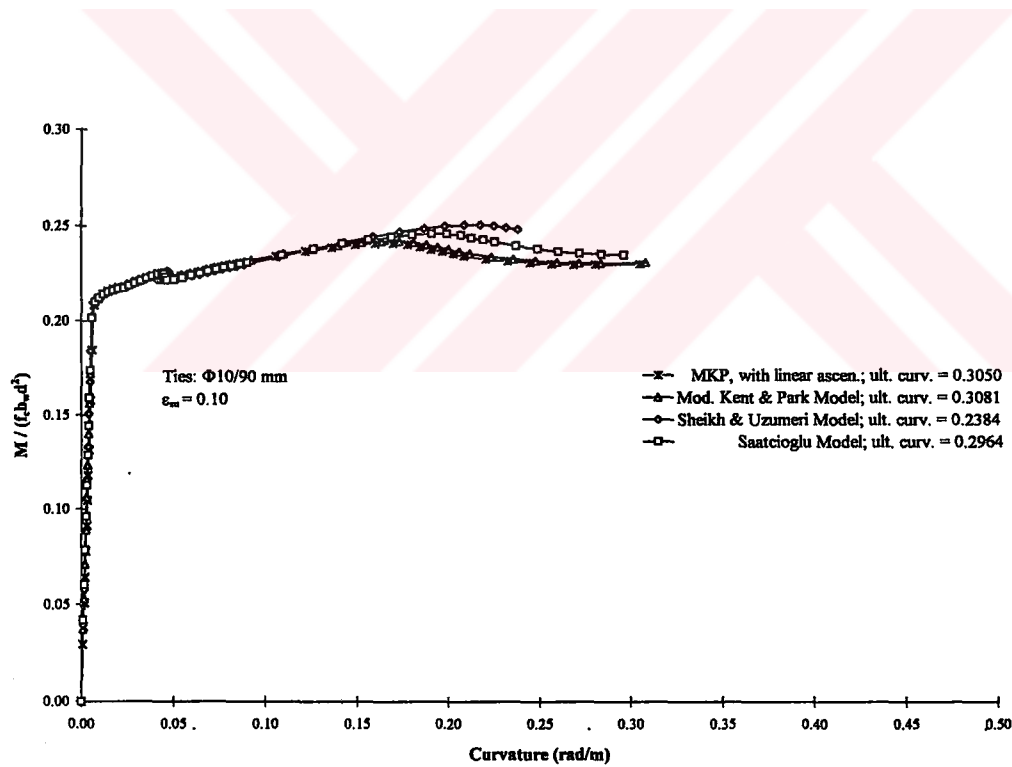
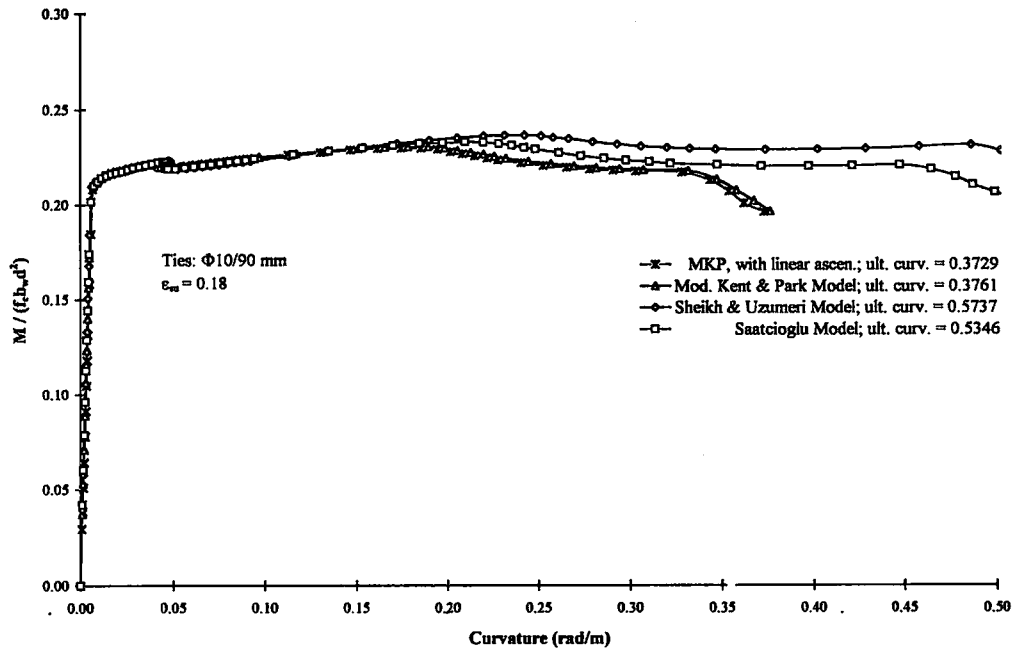
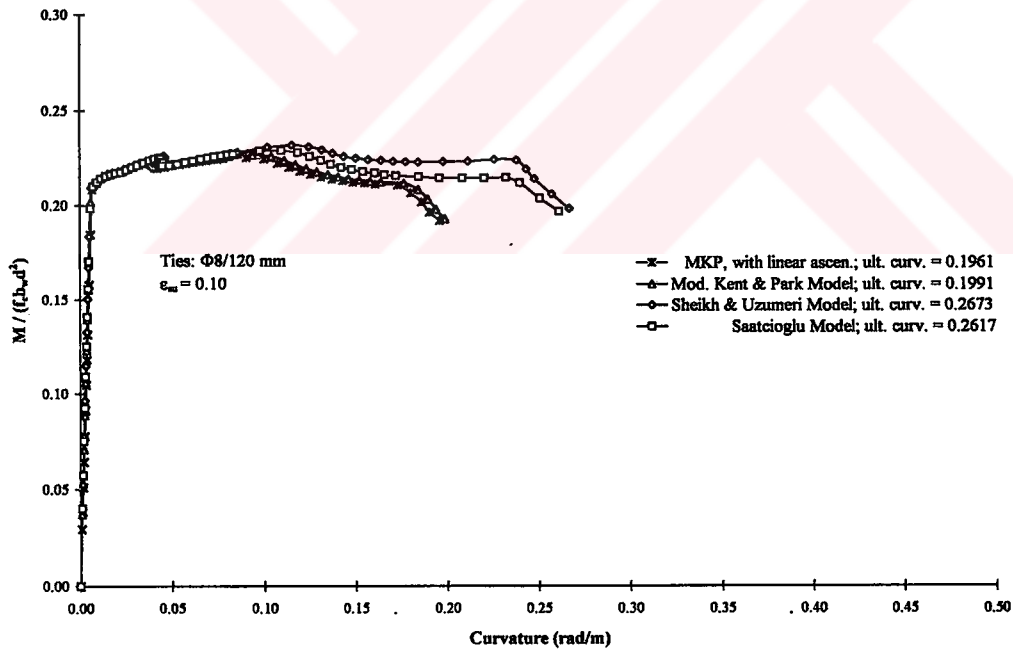


Figure A.57: Influence of confined concrete models on moment curvature diagrams of R/C beams; Group VIA



**Figure A.58:** Influence of confined concrete models on moment curvature diagrams of R/C beams; Group VIB



**Figure A.59:** Influence of confined concrete models on moment curvature diagrams of R/C beams; Group VIC

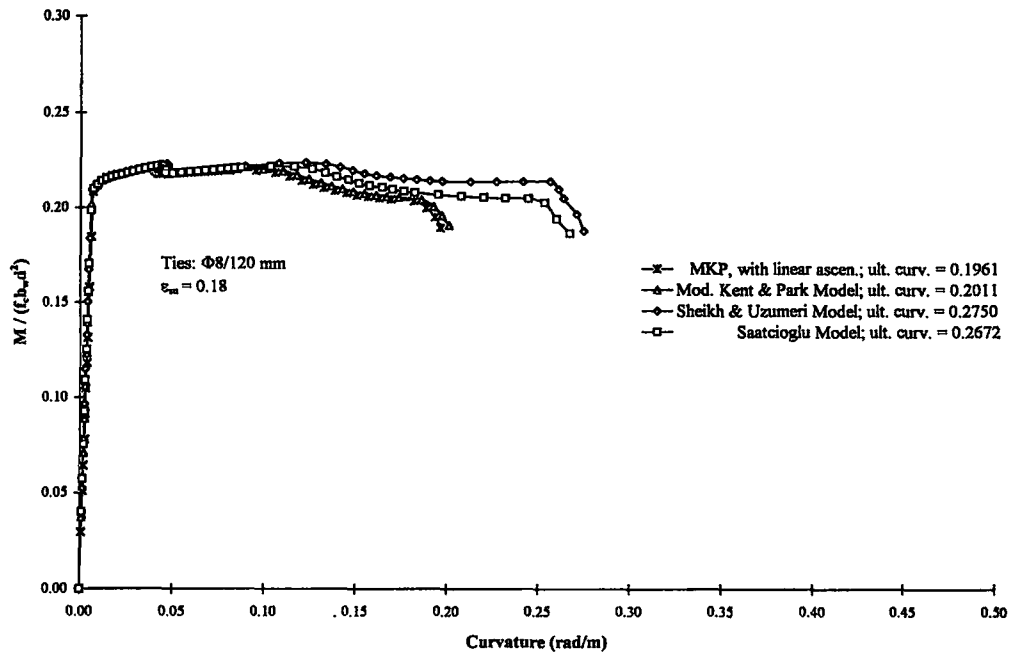


**Figure A.60:** Influence of confined concrete models on moment curvature diagrams of R/C beams; Group VID

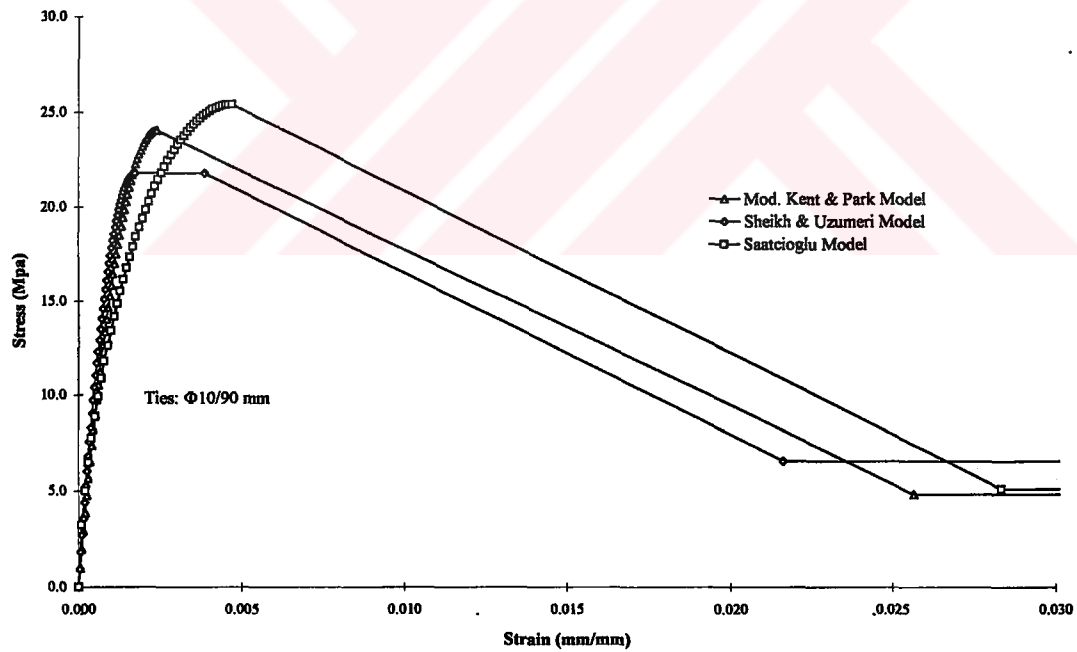


**Figure A.61:** Stress strain diagrams of concrete for different confinement models; Ties:  $\Phi 10/90$  mm

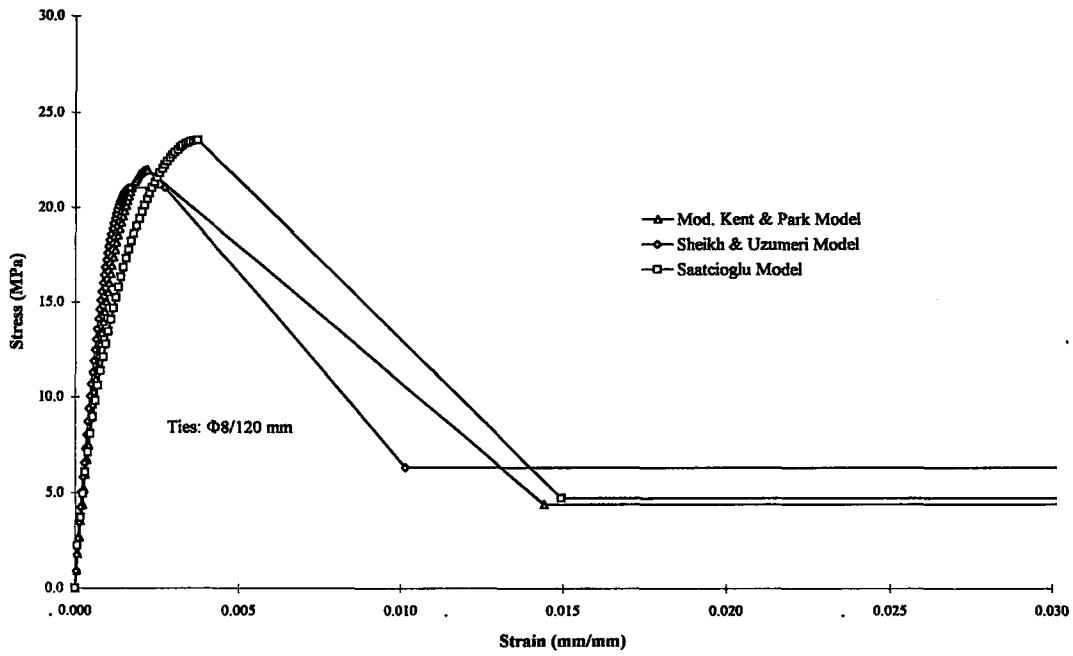


Figure A.62: Stress strain diagrams of concrete for different confinement models;

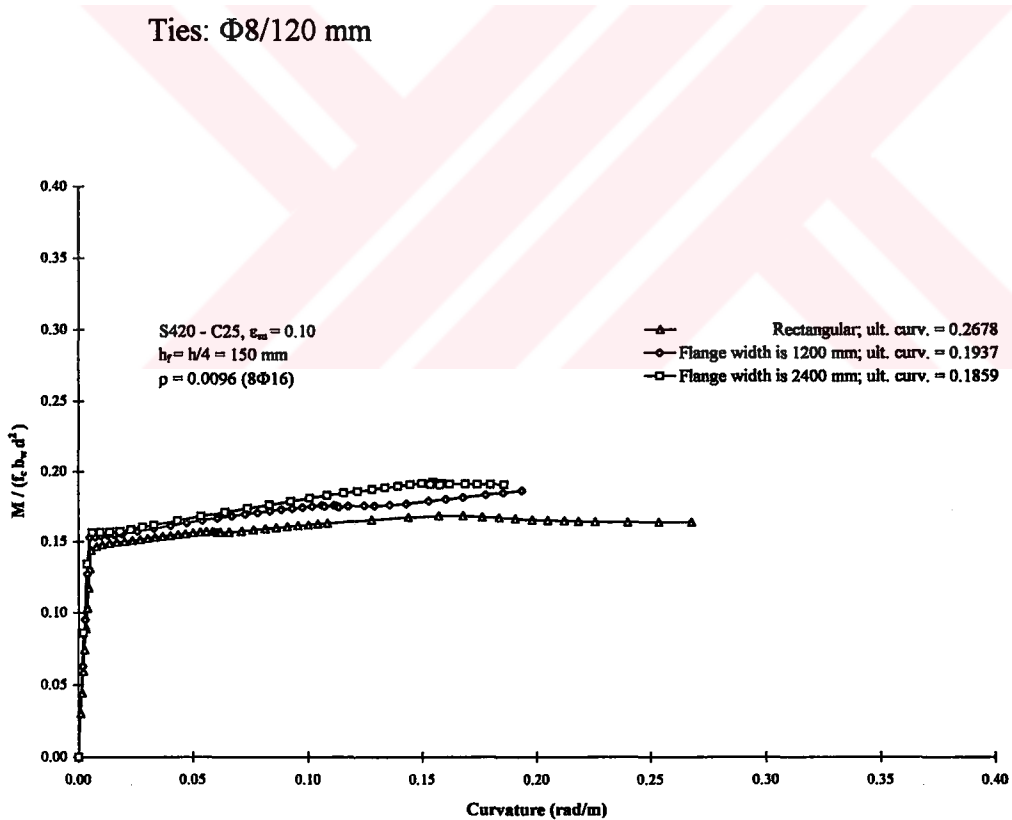


Figure A.63: Influence of flange width in T-beams; Group VIIA



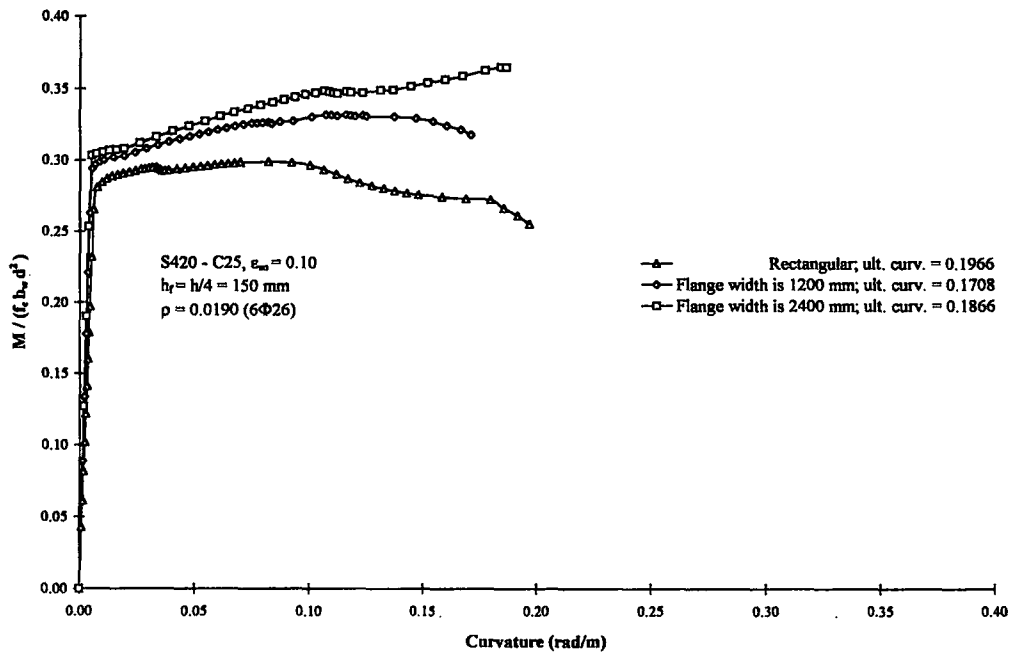


Figure A.64: Influence of flange width in T-beams; Group VIIB

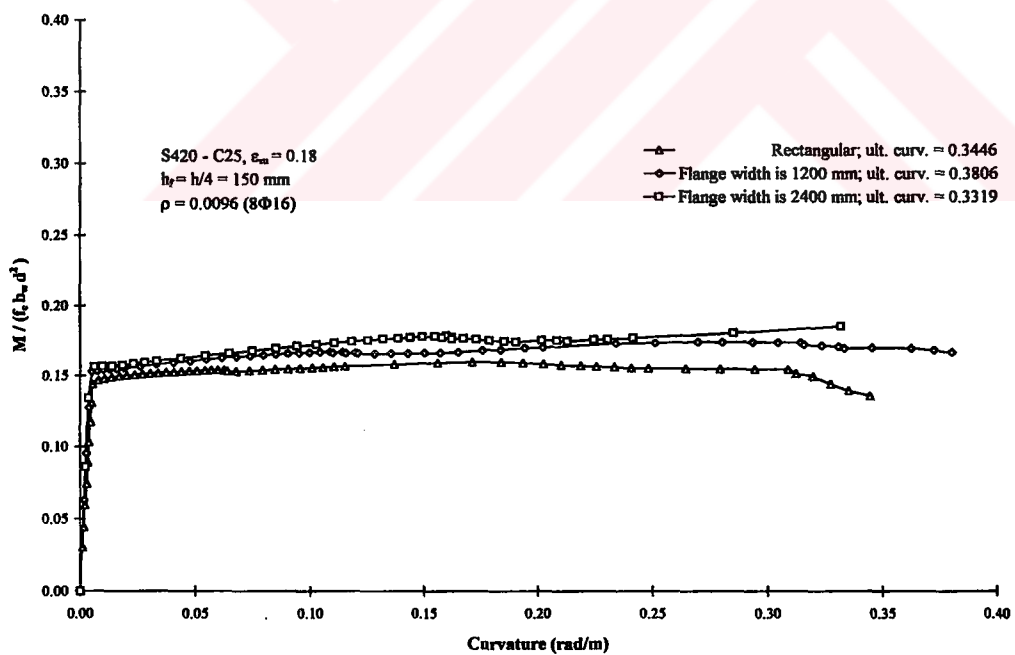


Figure A.65: Influence of flange width in T-beams; Group VIIC

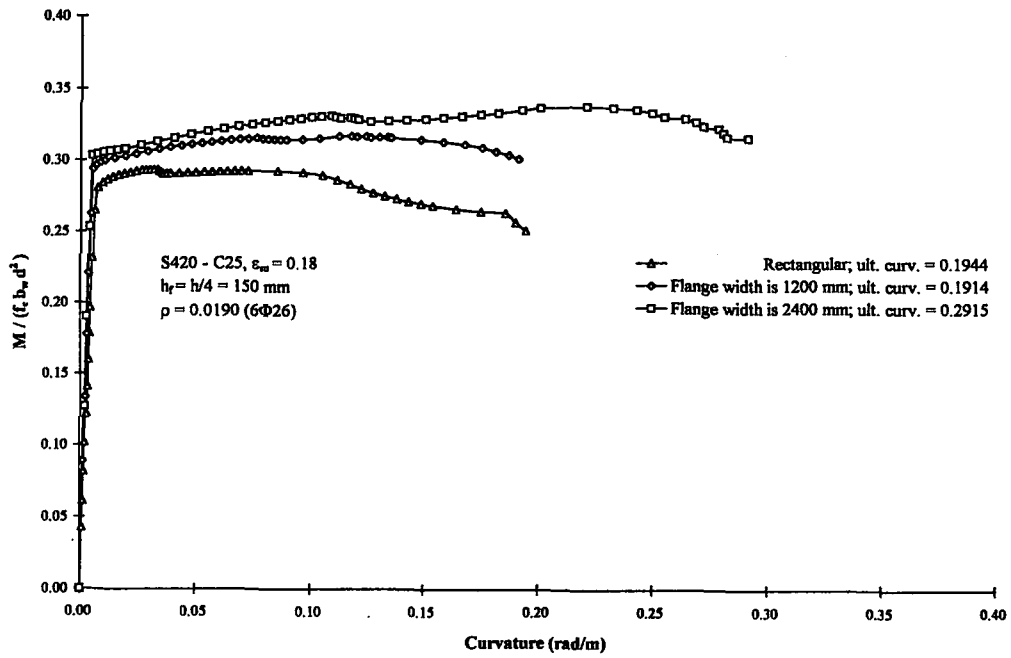


Figure A.66: Influence of flange width in T-beams; Group VIID

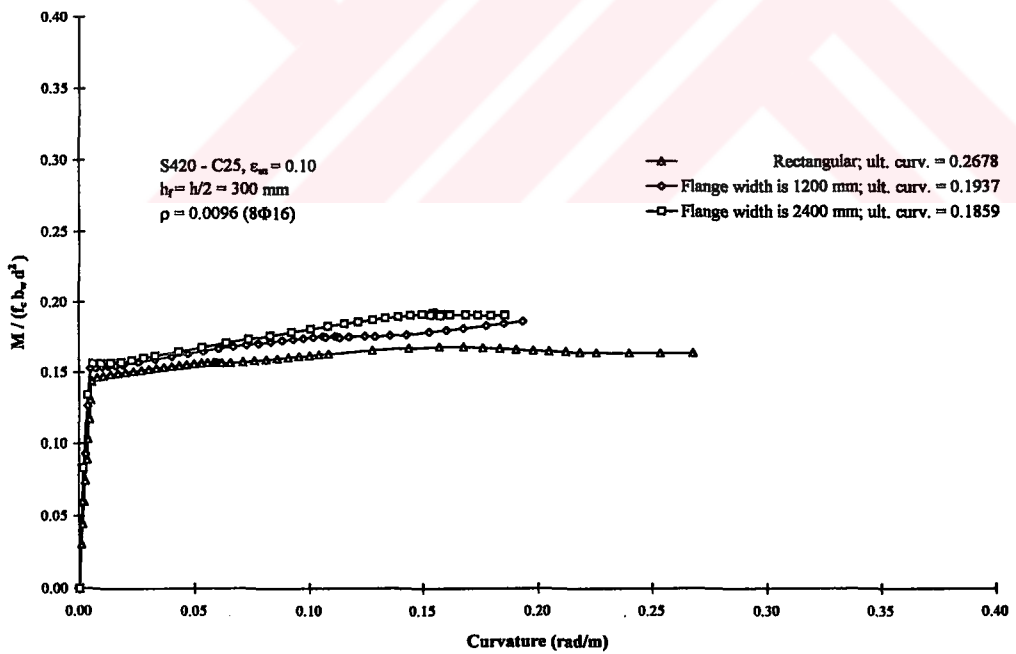


Figure A.67: Influence of flange width in T-beams; Group VIII

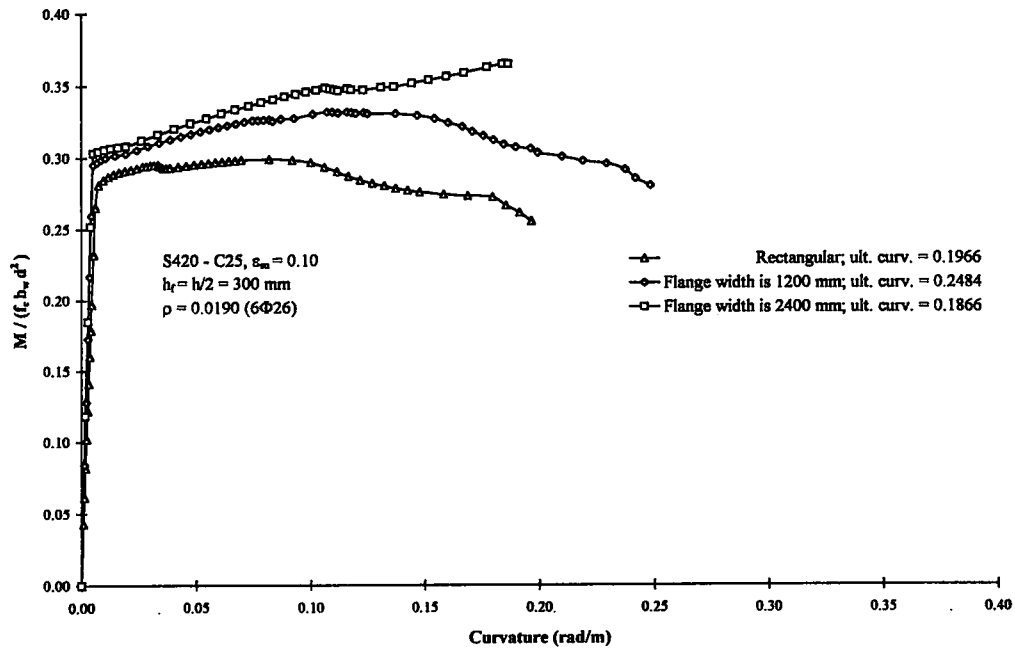


Figure A.68: Influence of flange width in T-beams; Group VIIF

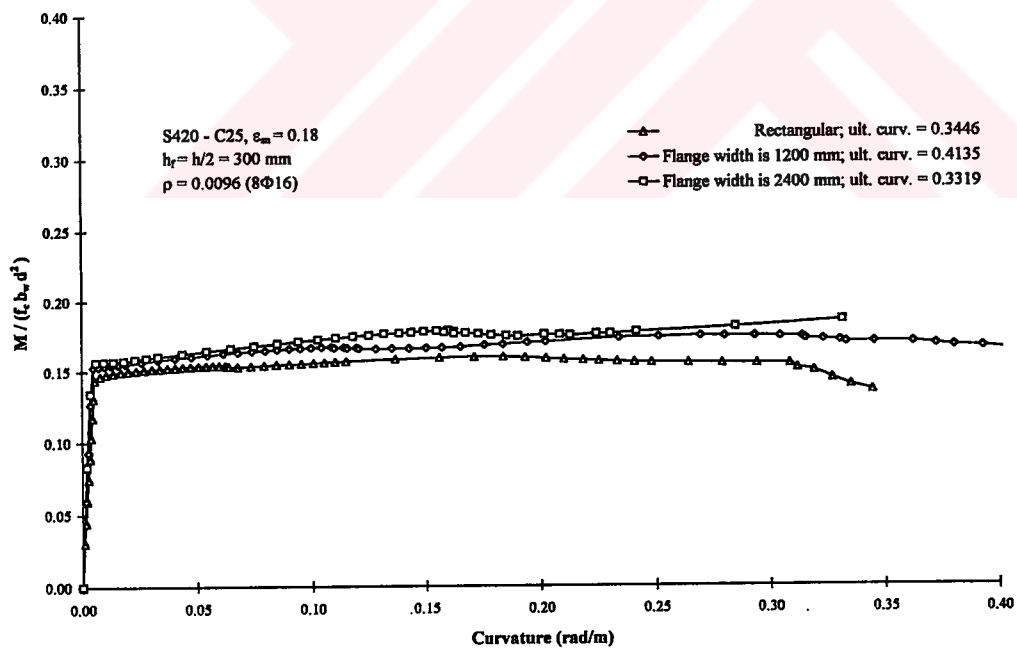


Figure A.69: Influence of flange width in T-beams; Group VIIG

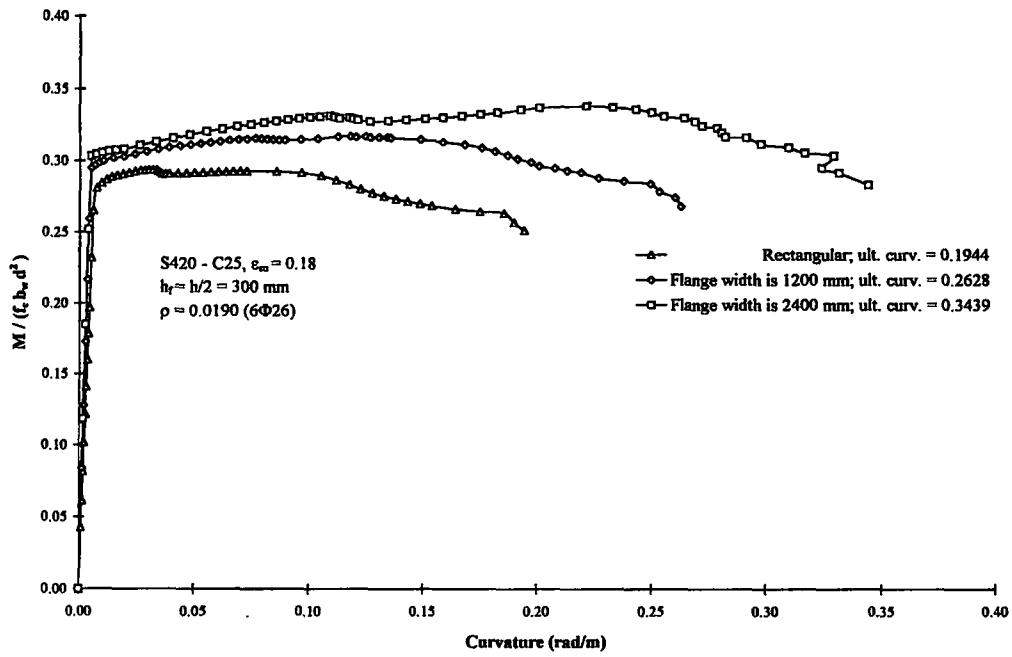


Figure A.70: Influence of flange width in T-beams; Group VIIIH

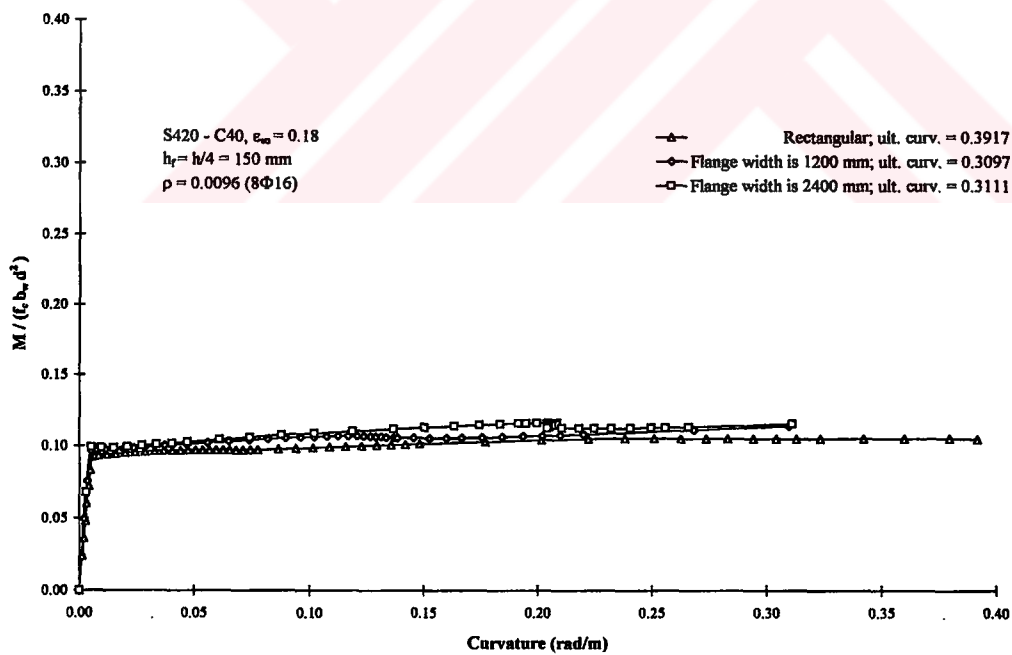


Figure A.71: Influence of flange width in T-beams; Group VIIJ

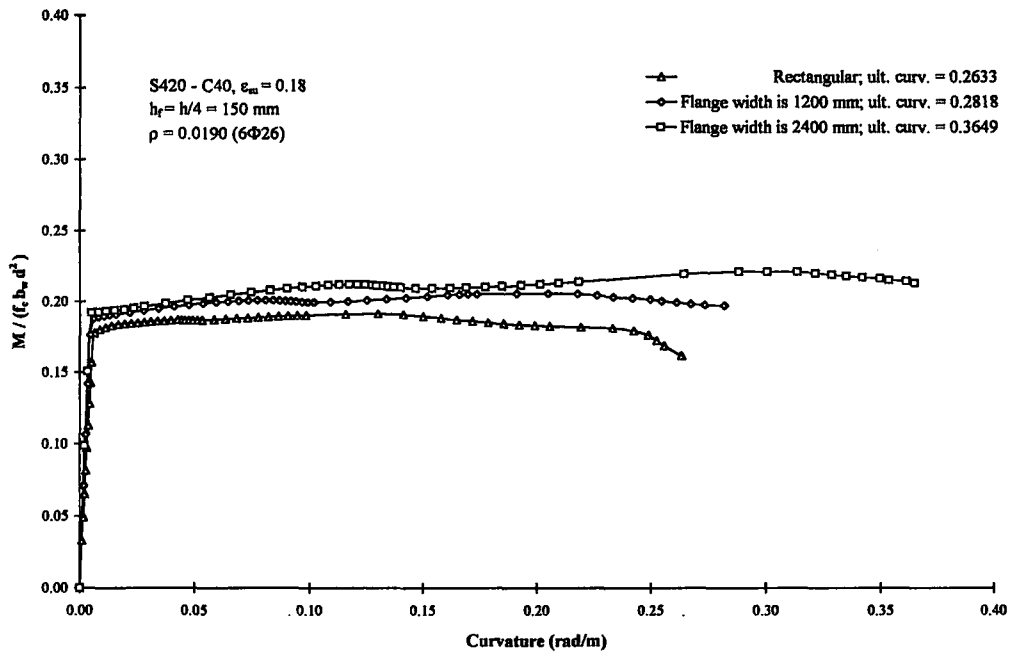


Figure A.72: Influence of flange width in T-beams; Group VIIK

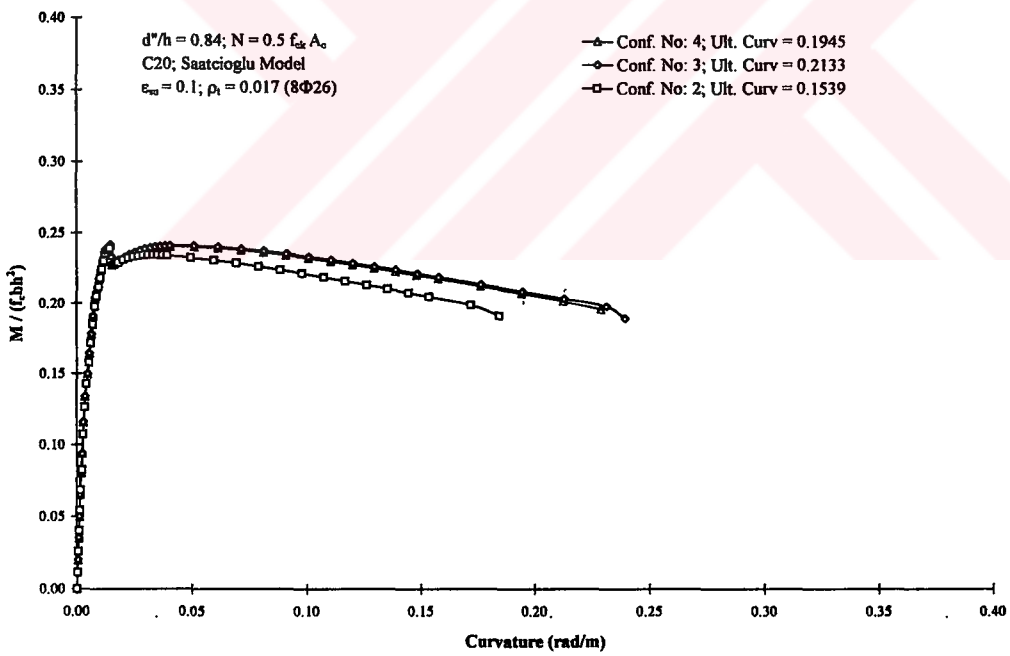


Figure A.73: Influence of lateral reinforcement configuration in R/C columns; Group VIIIA

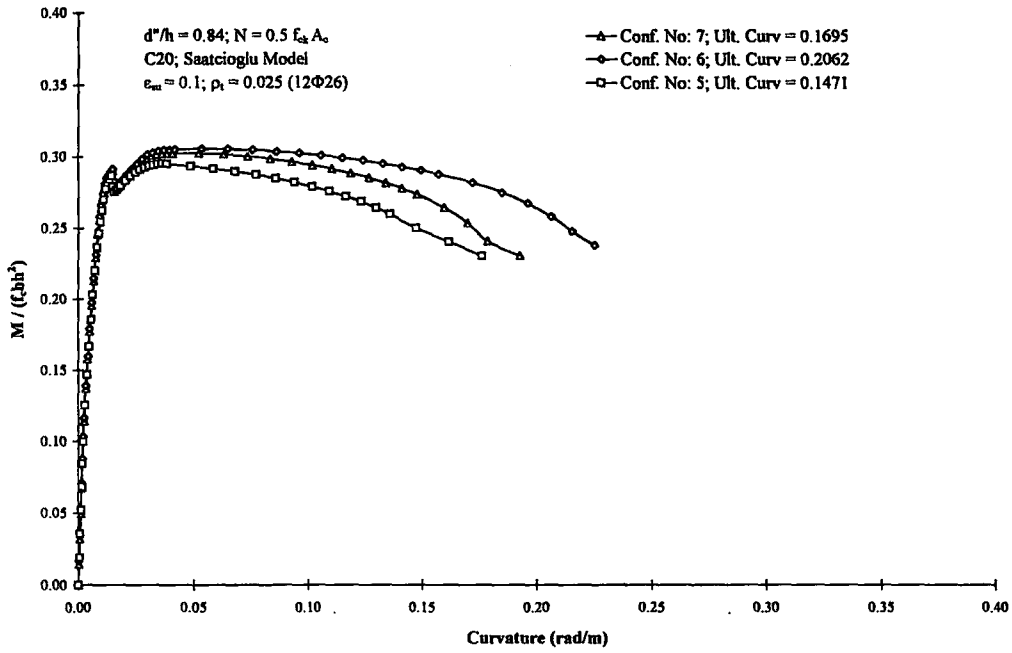


Figure A.74: Influence of lateral reinforcement configuration in R/C columns; Group

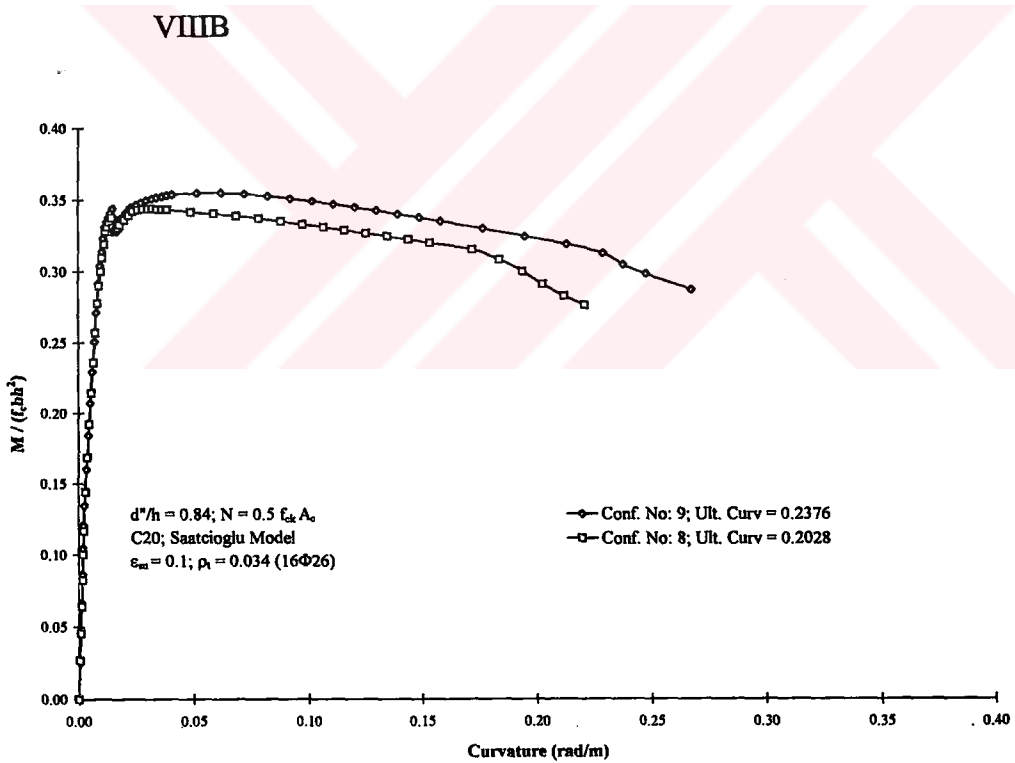


Figure A.75: Influence of lateral reinforcement configuration in R/C columns; Group

VIII C

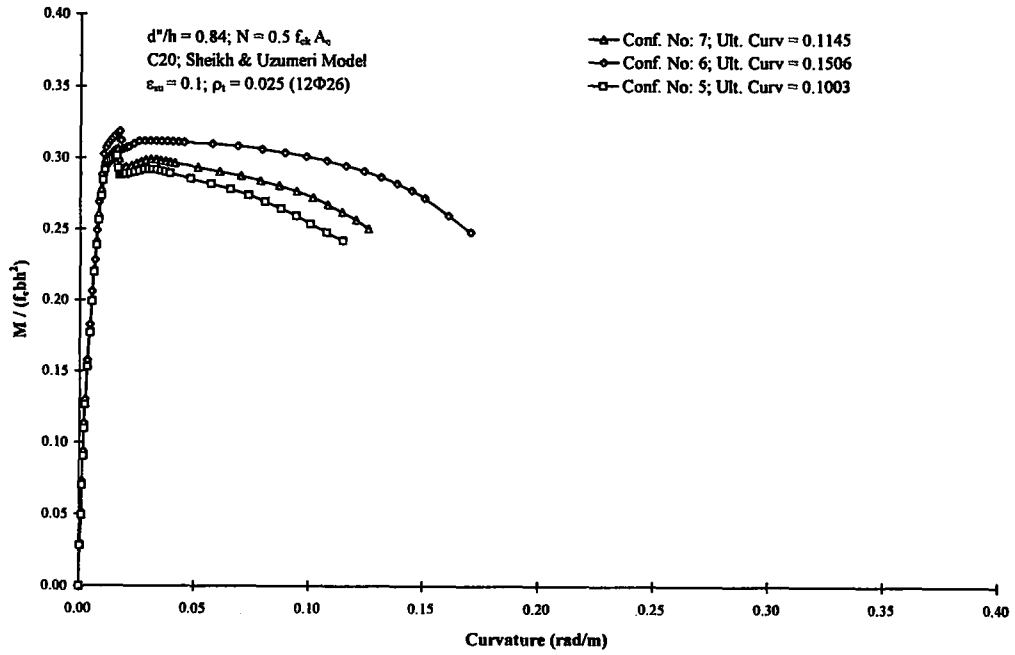


Figure A.76: Influence of lateral reinforcement configuration in R/C columns; Group

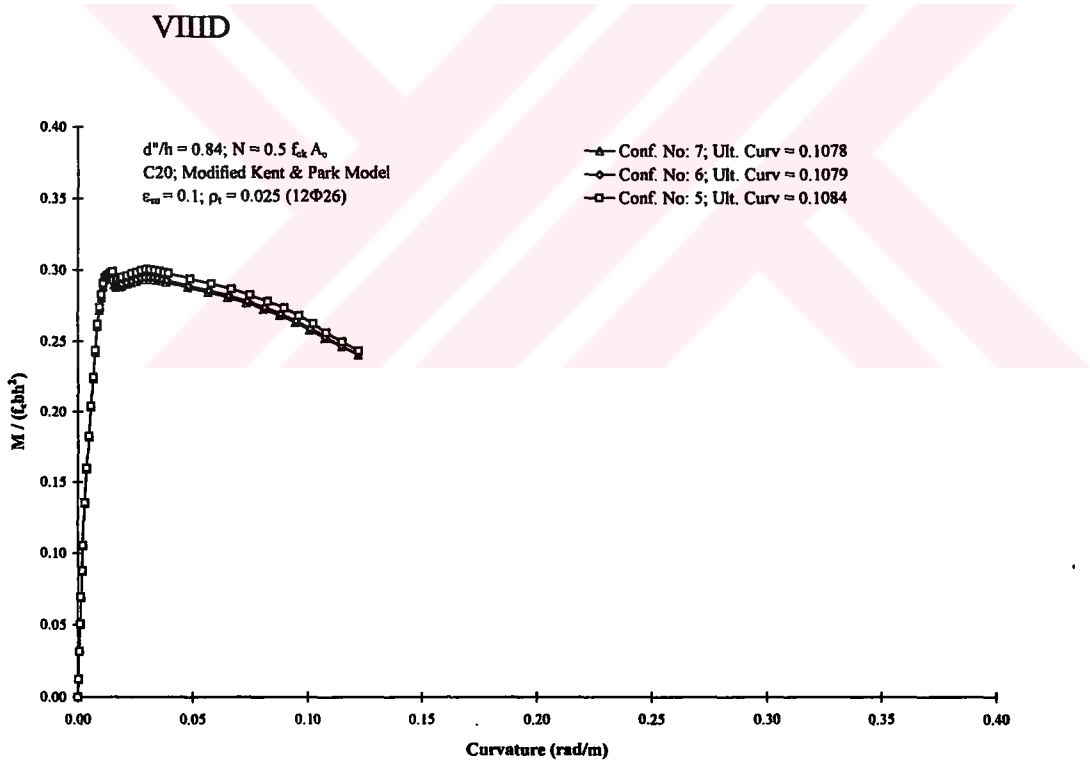


Figure A.77: Influence of lateral reinforcement configuration in R/C columns; Group

VIII E

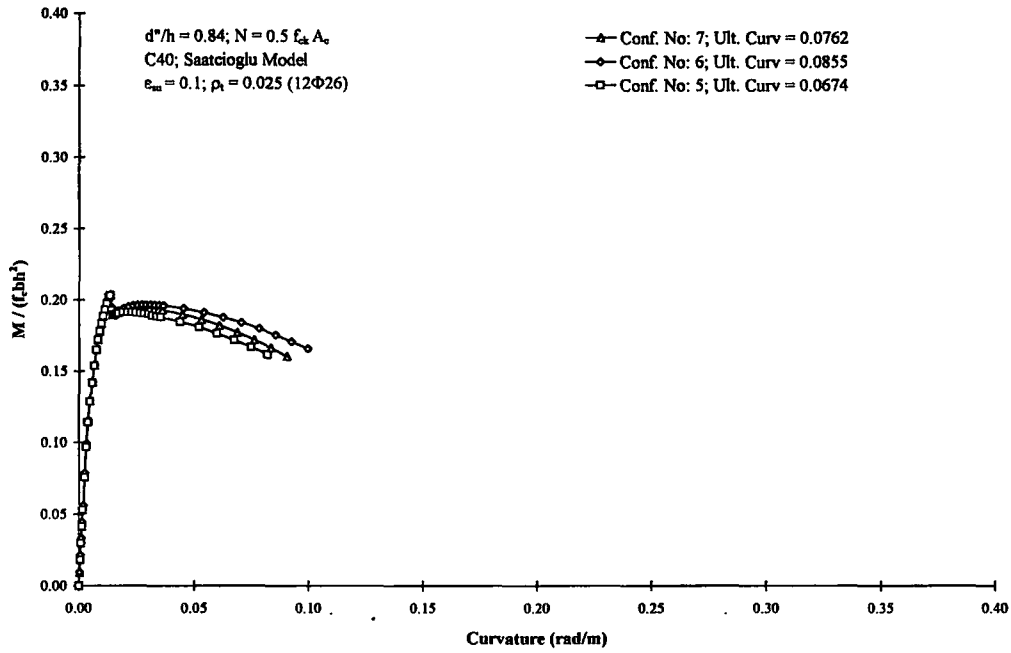


Figure A.78: Influence of lateral reinforcement configuration in R/C columns; Group

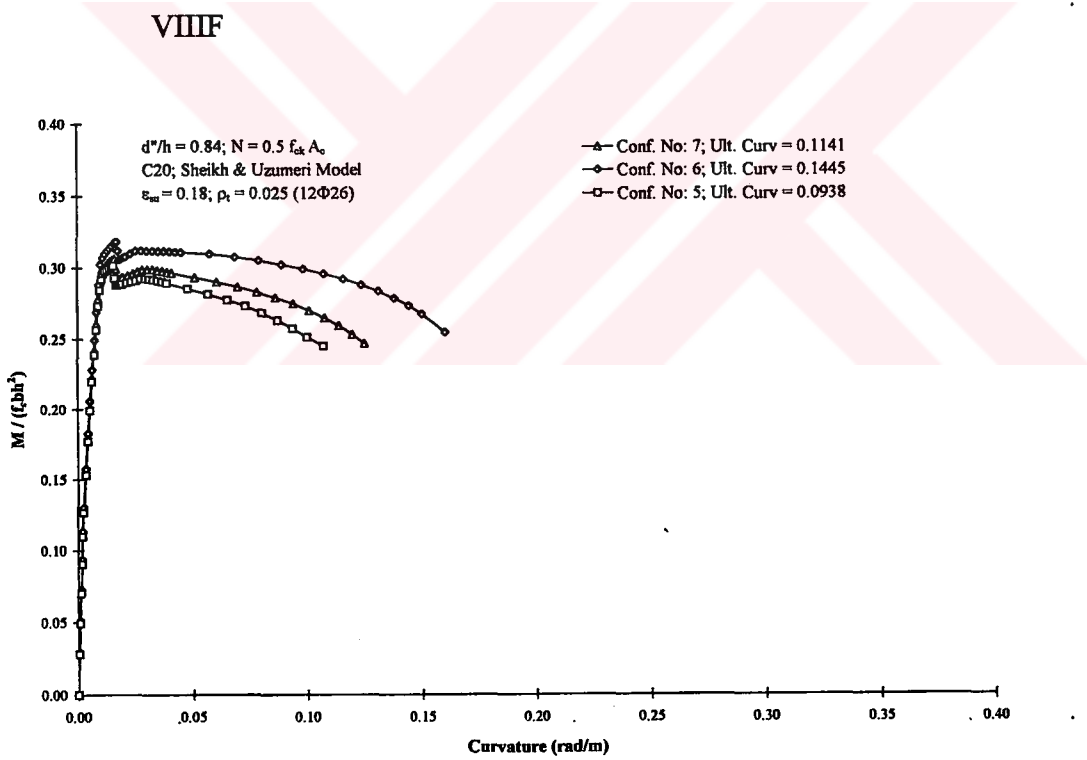
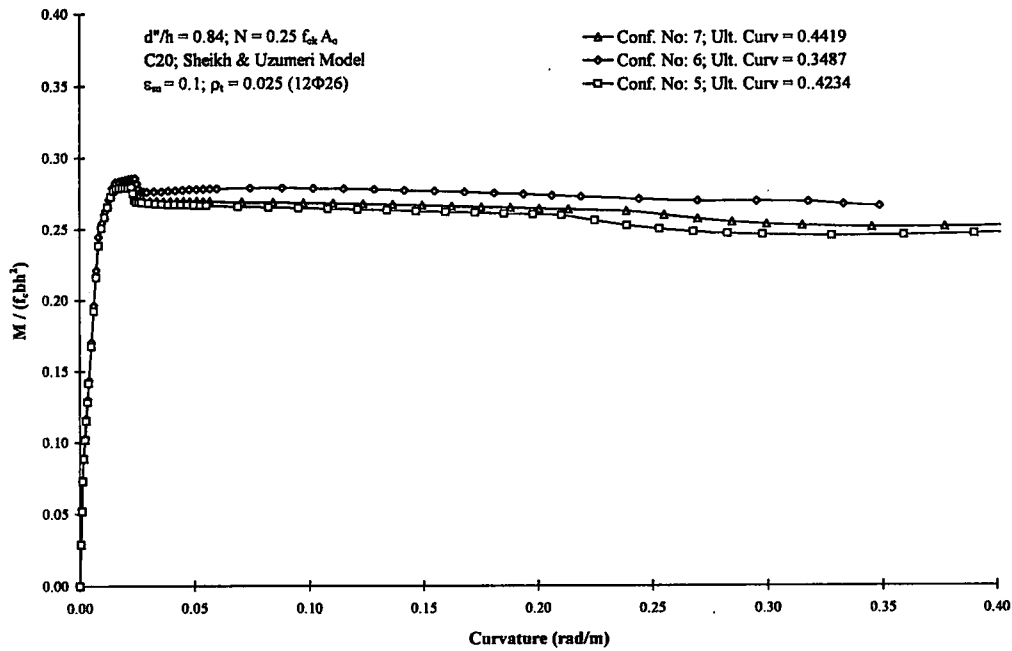


Figure A.79: Influence of lateral reinforcement configuration in R/C columns; Group

VIII G





**Figure A.80:** Influence of lateral reinforcement configuration in R/C columns; Group

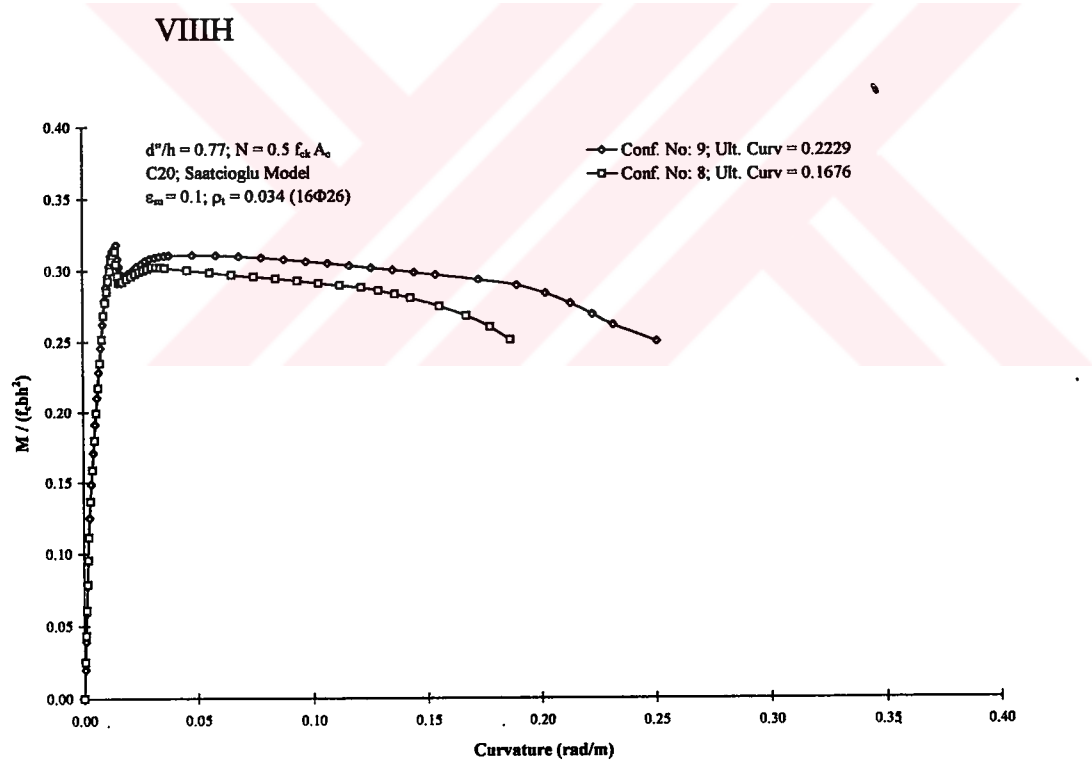


**Figure A.81:** Influence of lateral reinforcement configuration in R/C columns; Group

VIIIJ

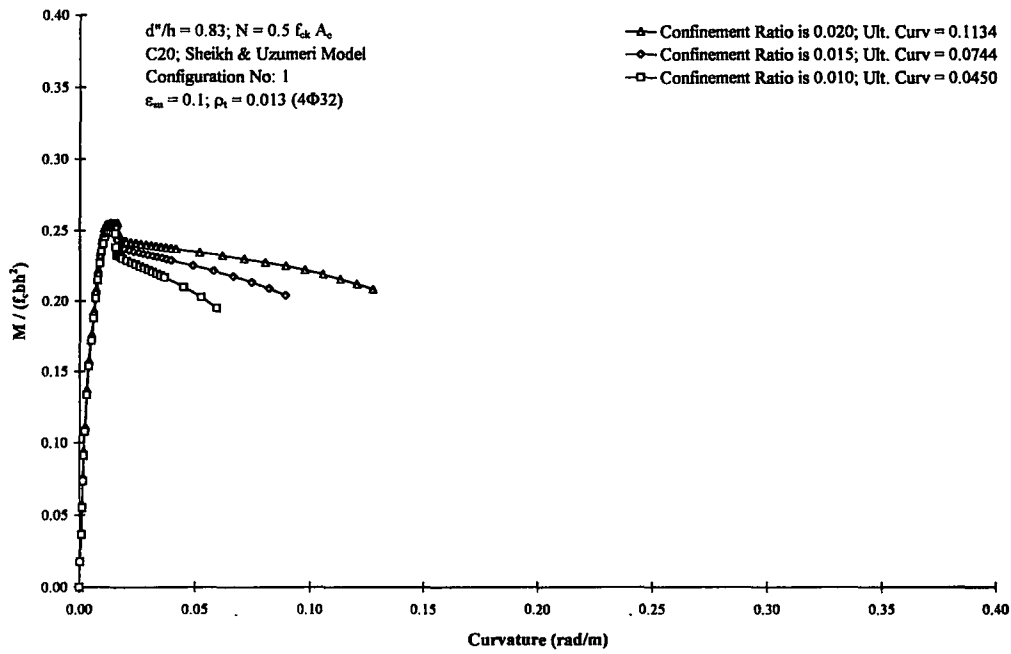


Figure A.82: Influence of lateral reinforcement ratio " $\rho_s$ " in R/C columns; Group IXA

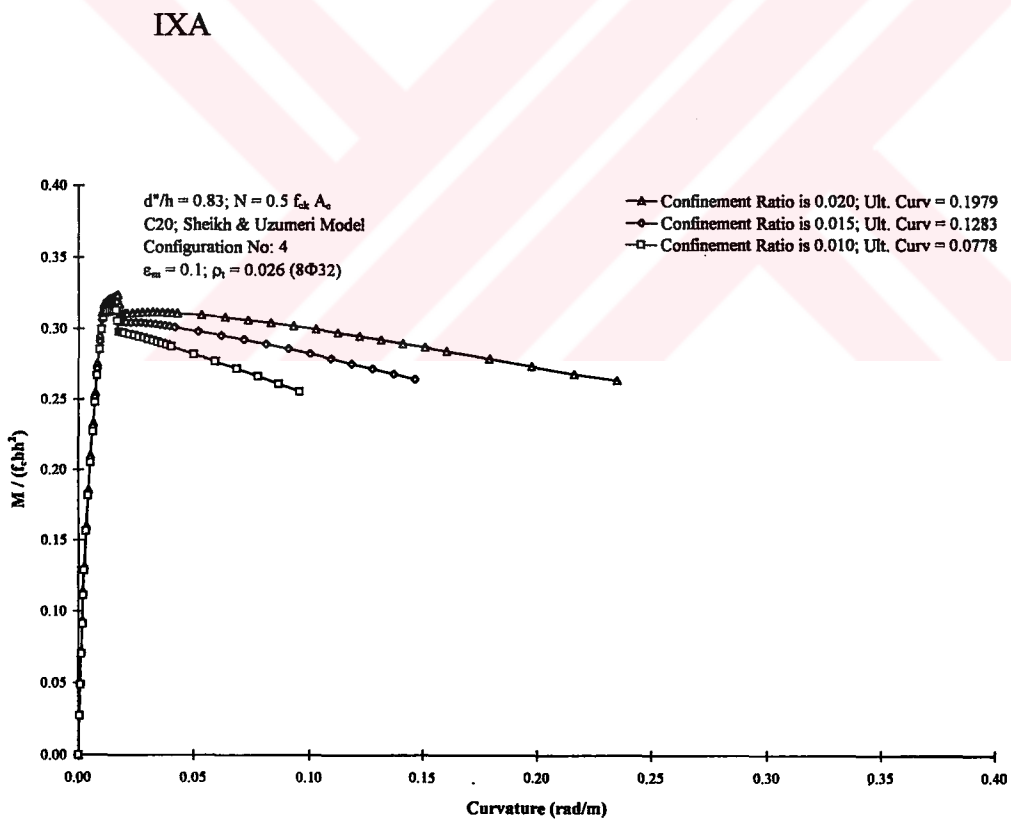


Figure A.83: Influence of lateral reinforcement ratio " $\rho_s$ " in R/C columns; Group IXB

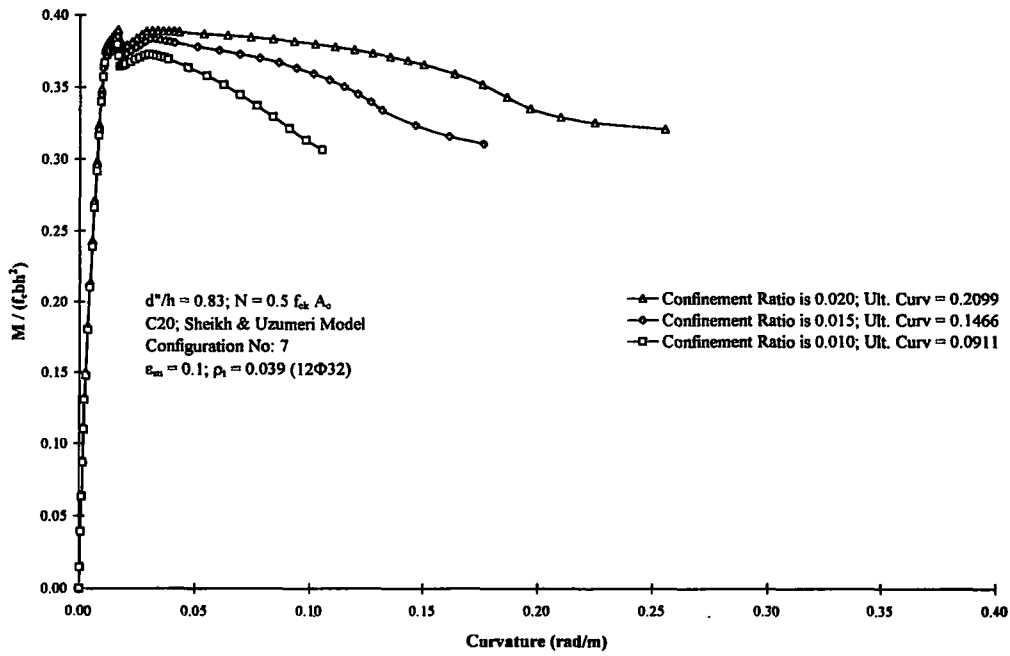


Figure A.84: Influence of lateral reinforcement ratio " $\rho_s$ " in R/C columns; Group IXC

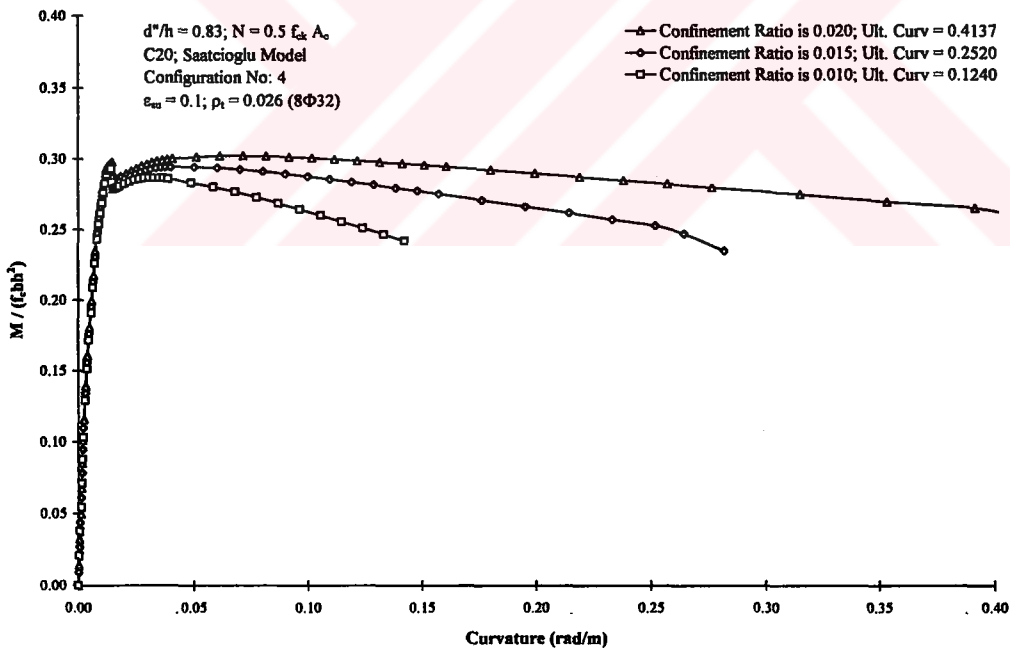


Figure A.85: Influence of lateral reinforcement ratio " $\rho_s$ " in R/C columns; Group

IXD

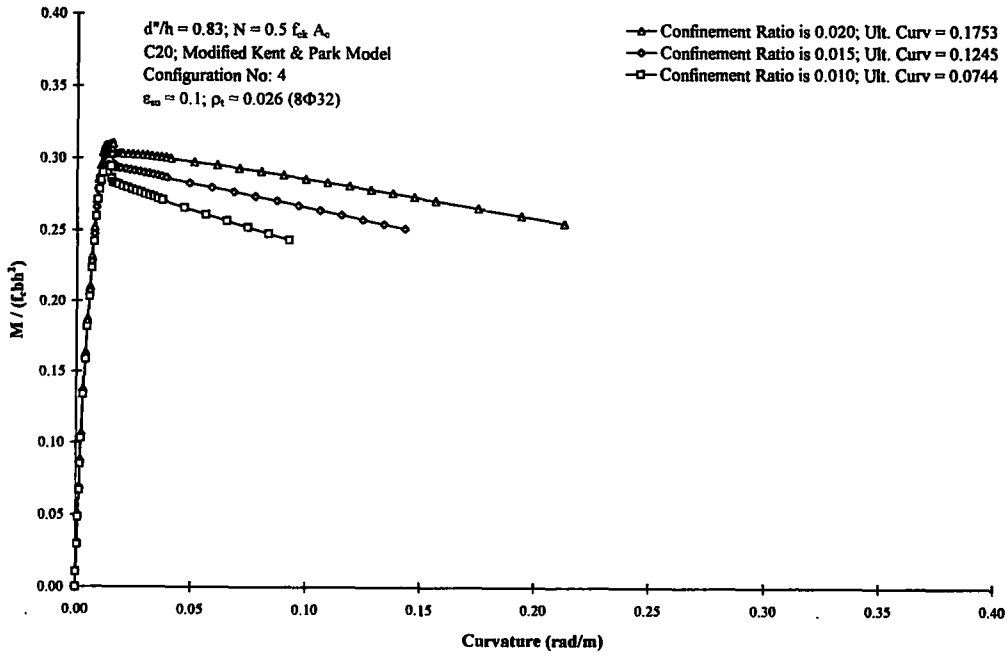


Figure A.86: Influence of lateral reinforcement ratio " $\rho_s$ " in R/C columns; Group IXE

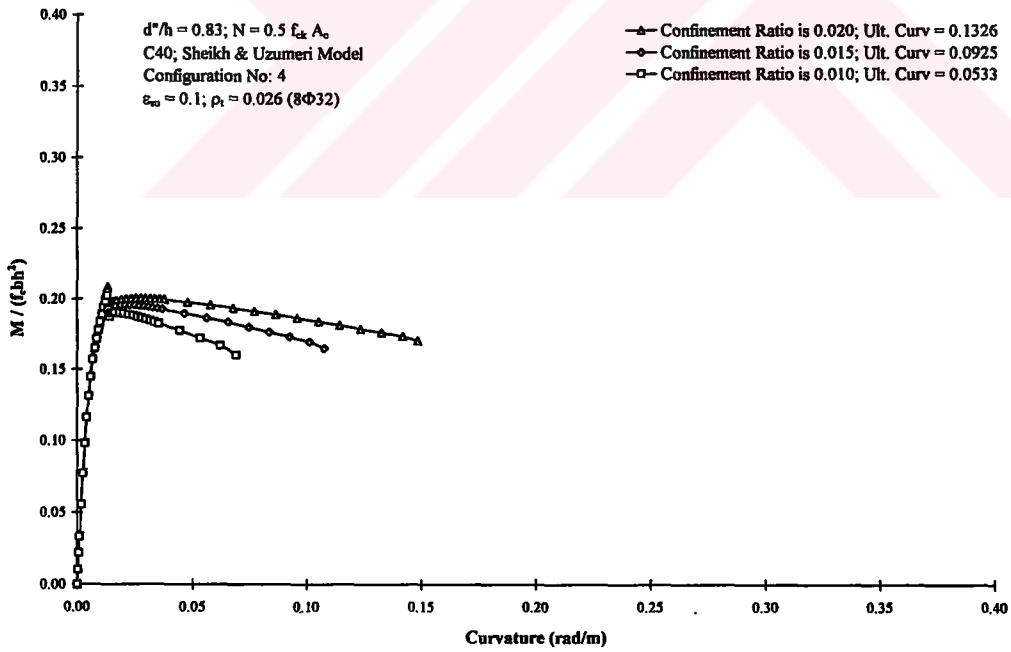


Figure A.87: Influence of lateral reinforcement ratio " $\rho_s$ " in R/C columns; Group IXF

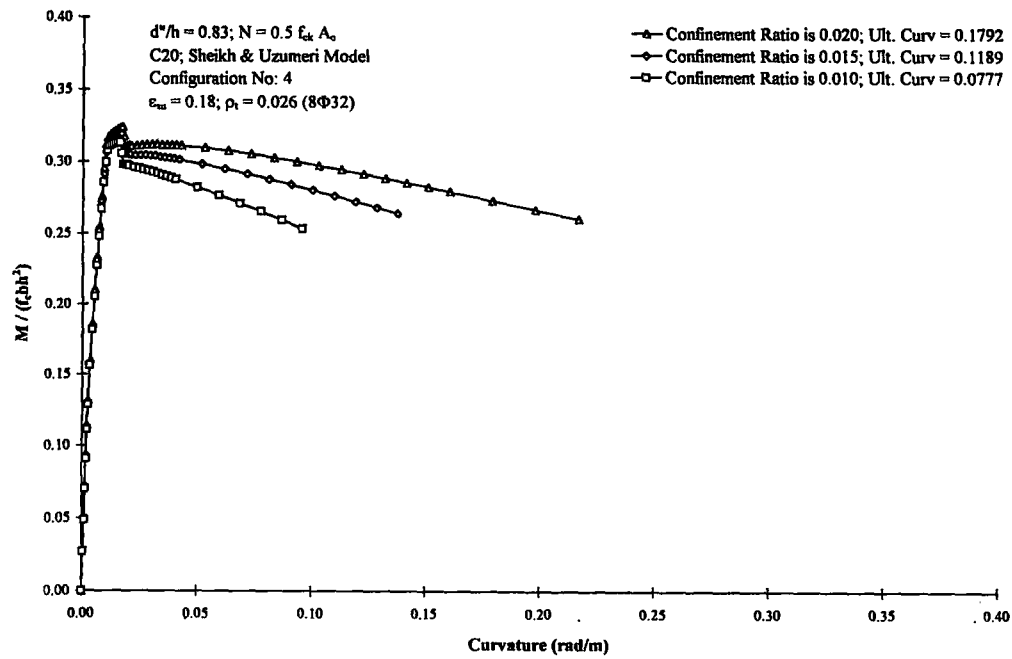


Figure A.88: Influence of lateral reinforcement ratio " $\rho_s$ " in R/C columns; Group

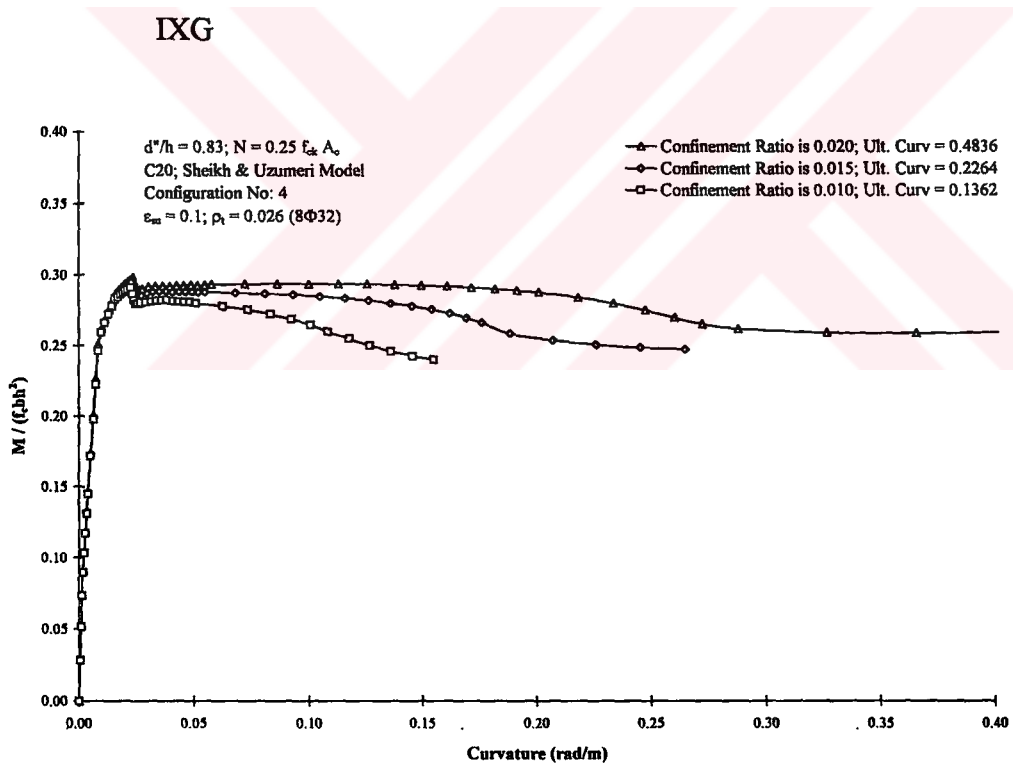
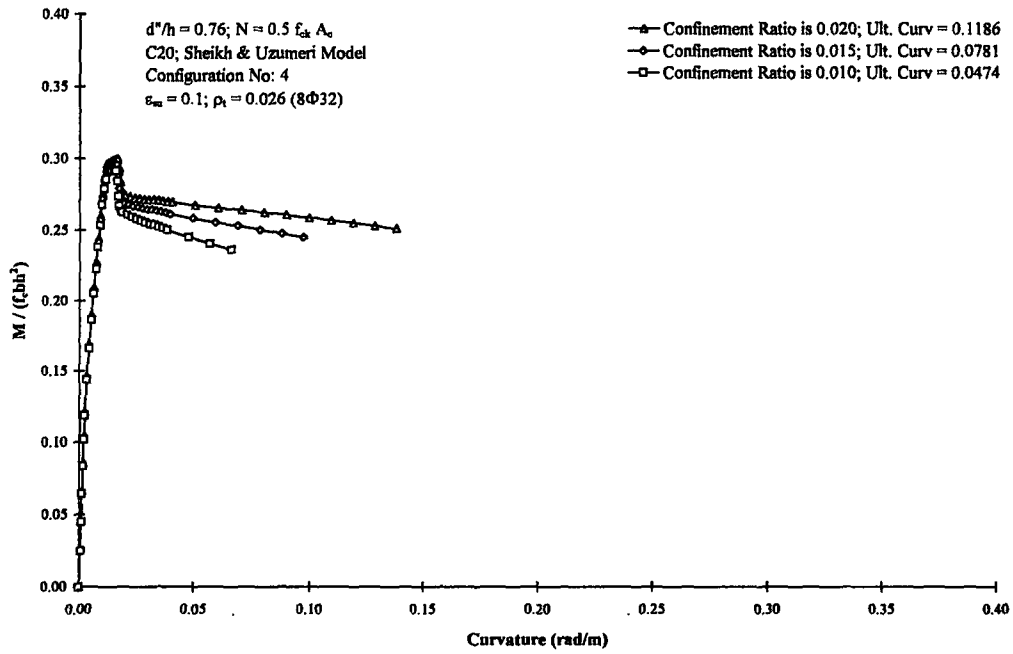
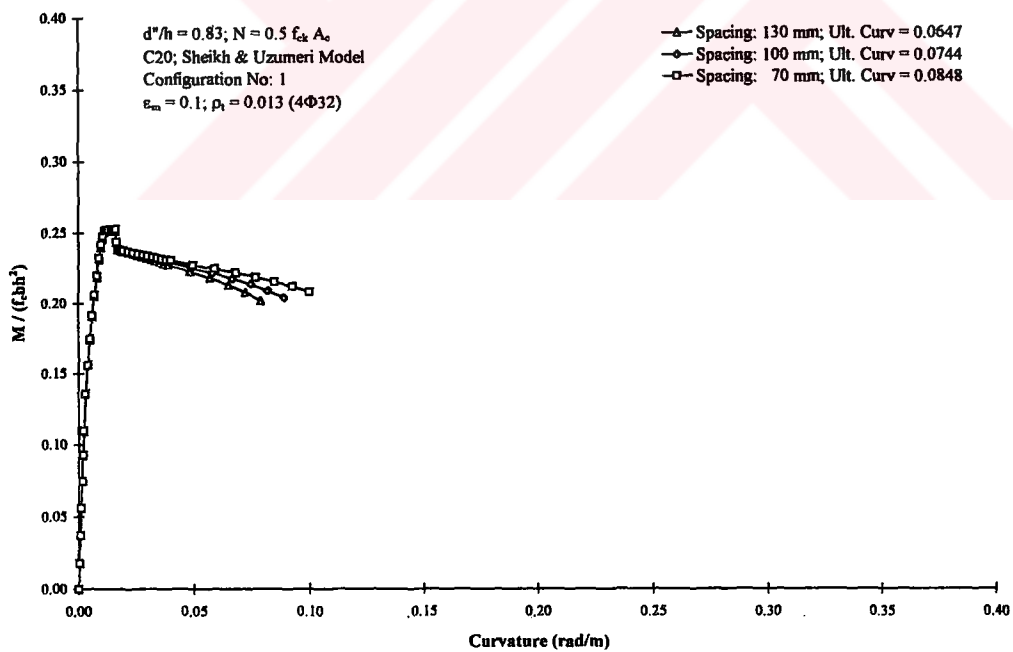


Figure A.89: Influence of lateral reinforcement ratio " $\rho_s$ " in R/C columns; Group

IXH



**Figure A.90:** Influence of lateral reinforcement ratio " $\rho_s$ " in R/C columns; Group IXJ



**Figure A.91:** Influence of lateral reinforcement spacing in R/C columns; Group XA

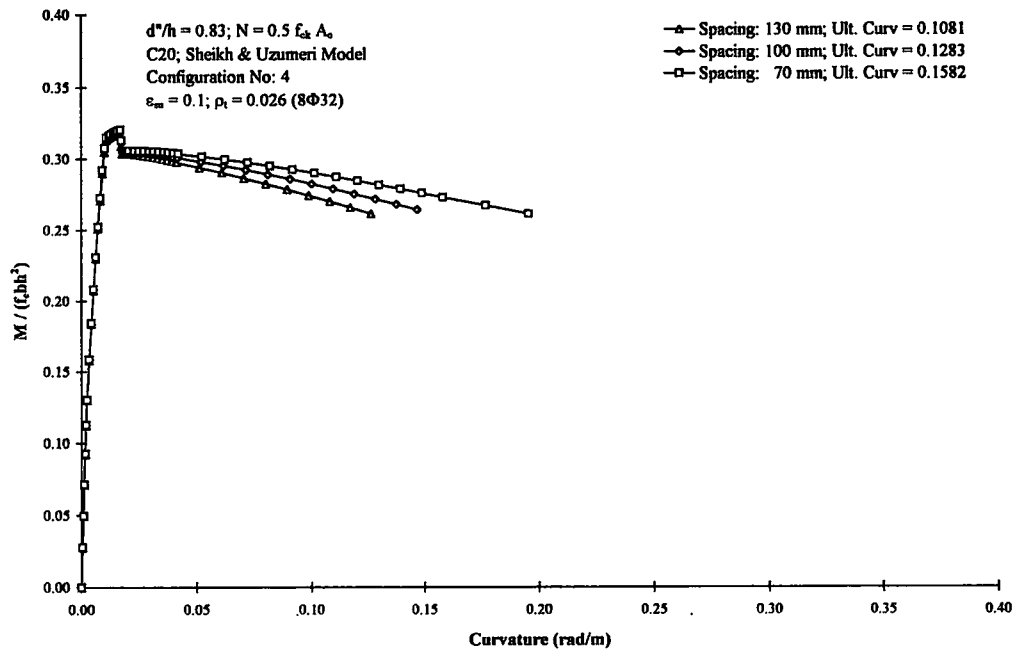


**Figure A.92:** Influence of lateral reinforcement spacing in R/C columns; Group XB

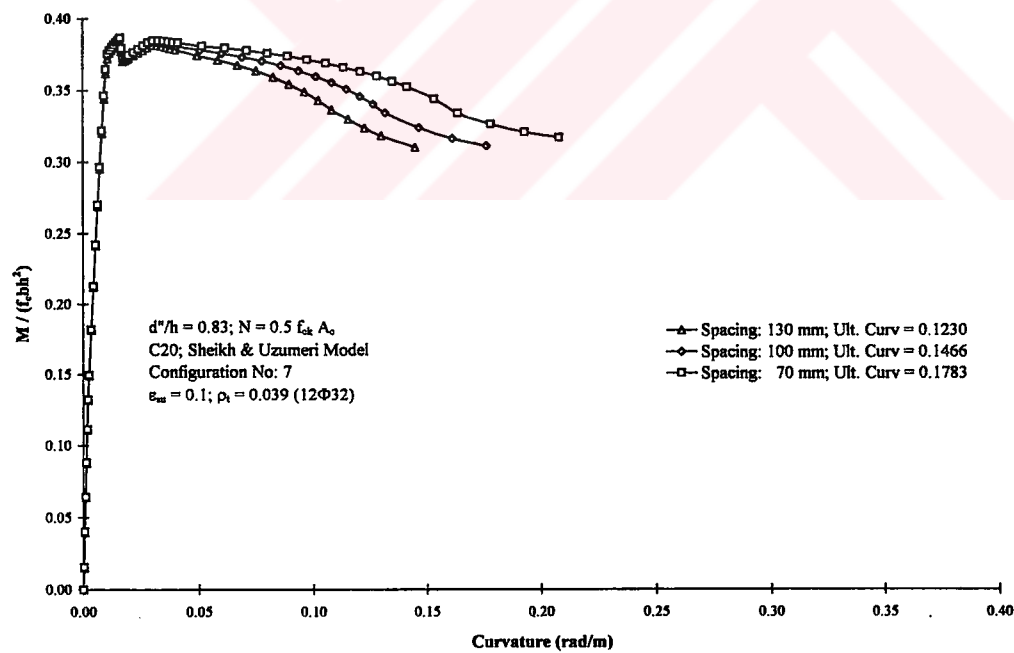


**Figure A.93:** Influence of lateral reinforcement spacing in R/C columns; Group XC

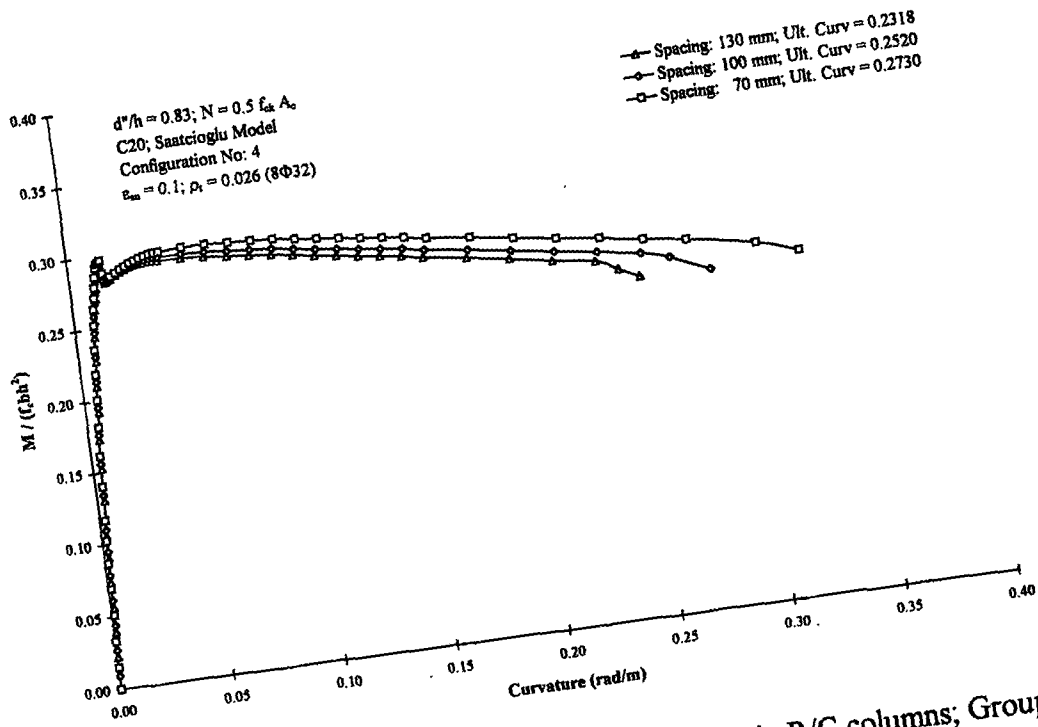


Figure A.94: Influence of lateral reinforcement spacing in R/C columns; Group XD

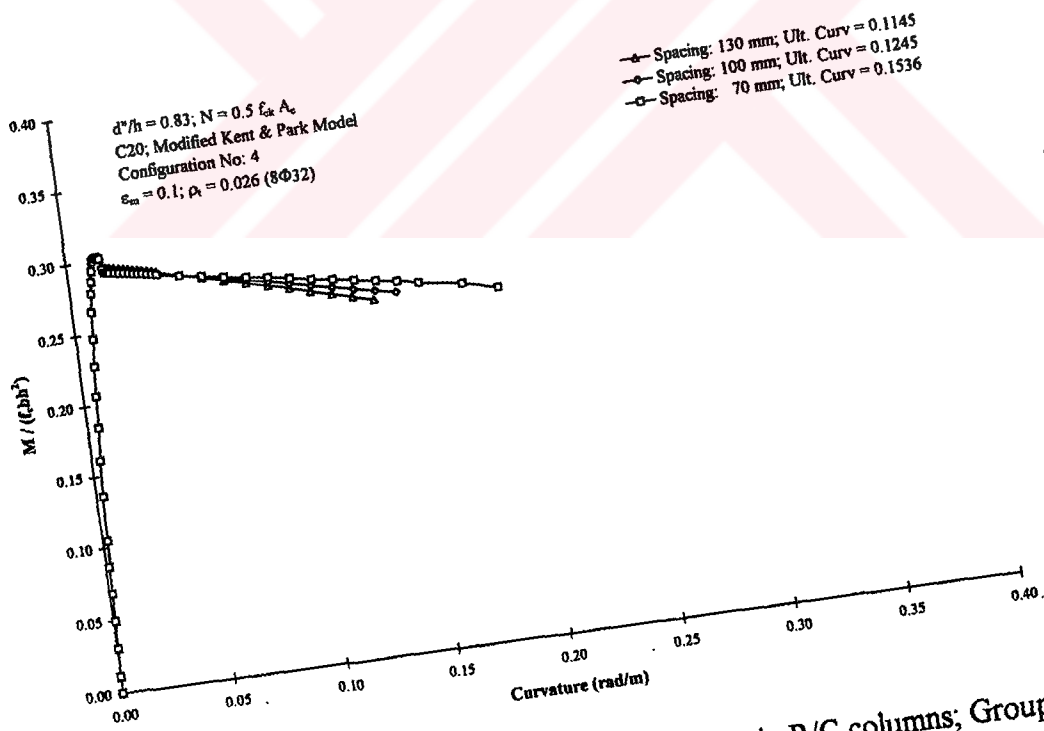


Figure A.95: Influence of lateral reinforcement spacing in R/C columns; Group XE



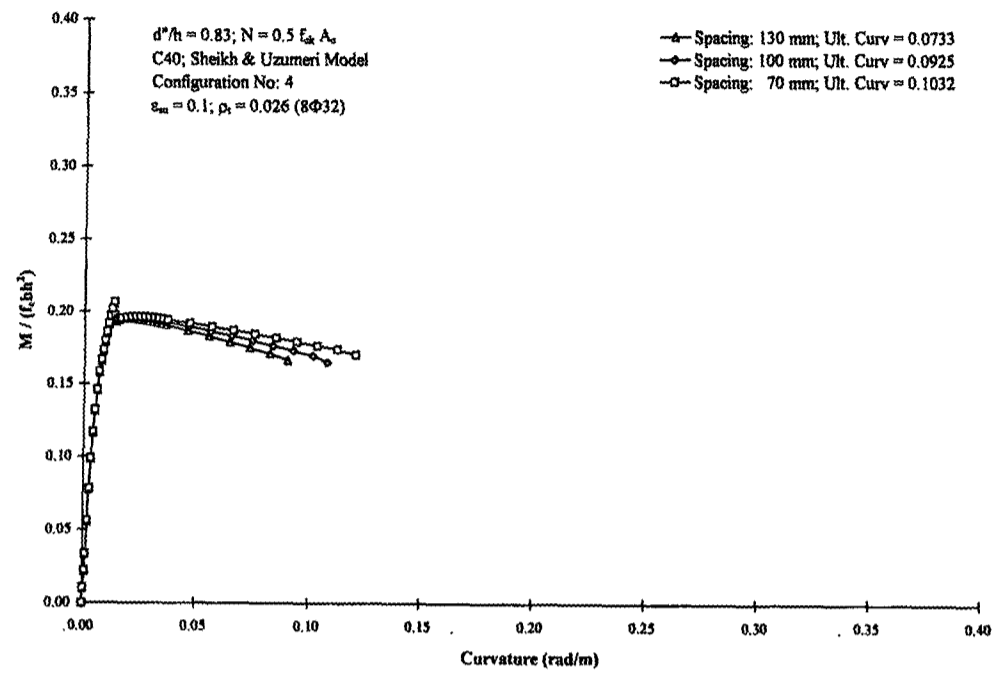


Figure A.96: Influence of lateral reinforcement spacing in R/C columns; Group XF

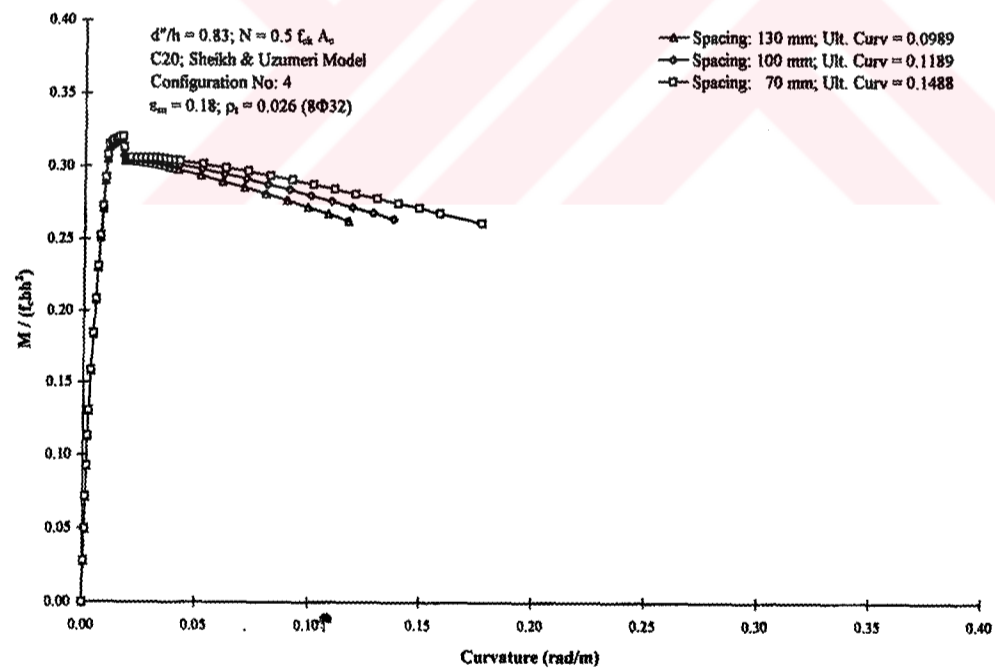
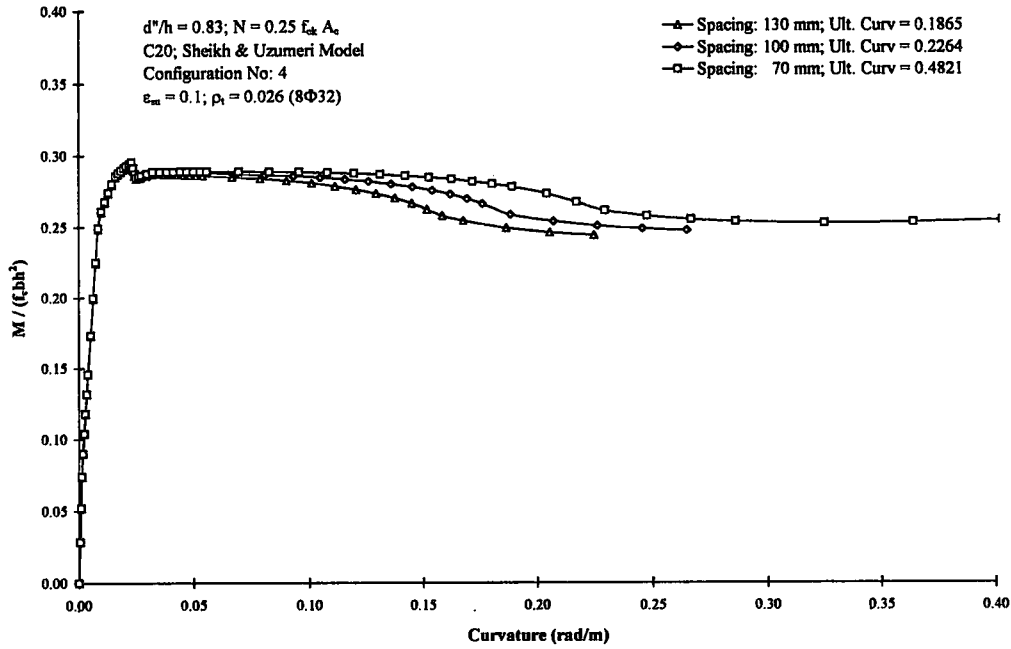
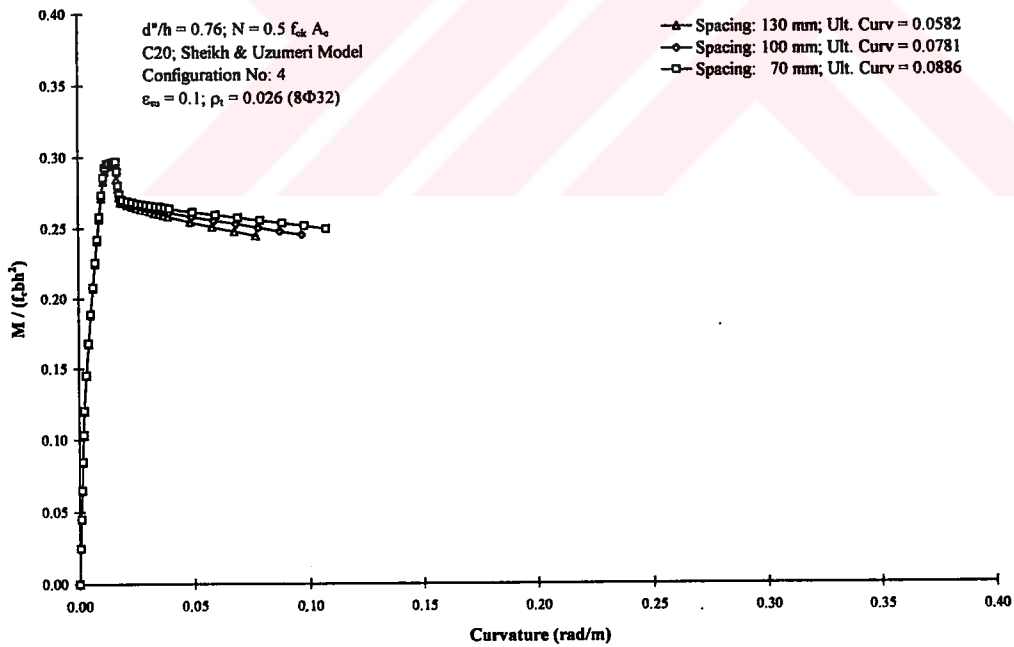


Figure A.97: Influence of lateral reinforcement spacing in R/C columns; Group XG



**Figure A.98:** Influence of lateral reinforcement spacing in R/C columns; Group XH



**Figure A.99:** Influence of lateral reinforcement spacing in R/C columns; Group XJ

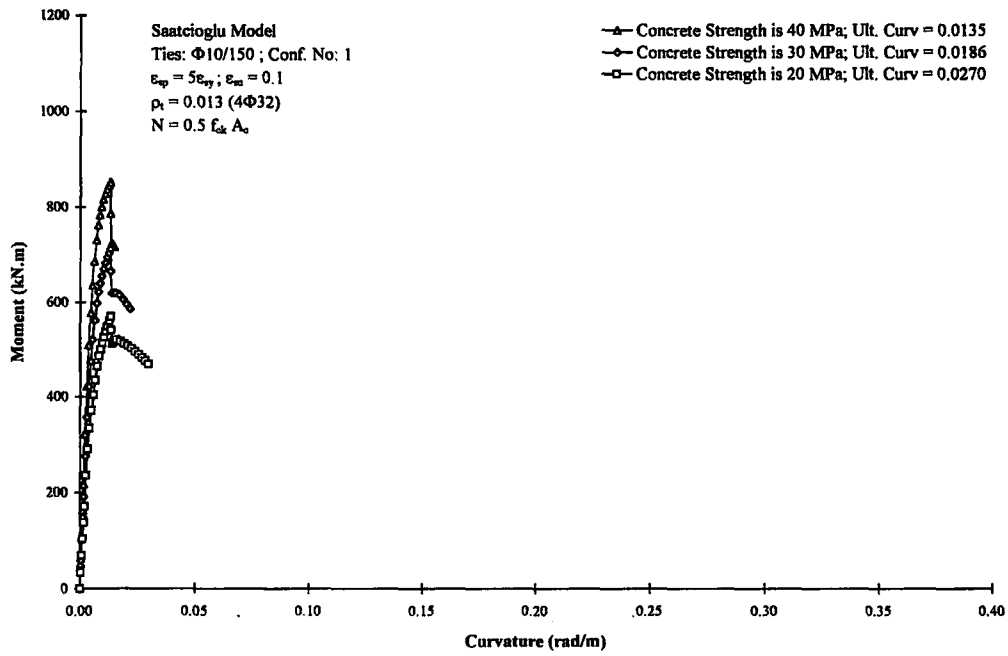


Figure A.100: Influence of concrete strength in R/C columns; Group XIA

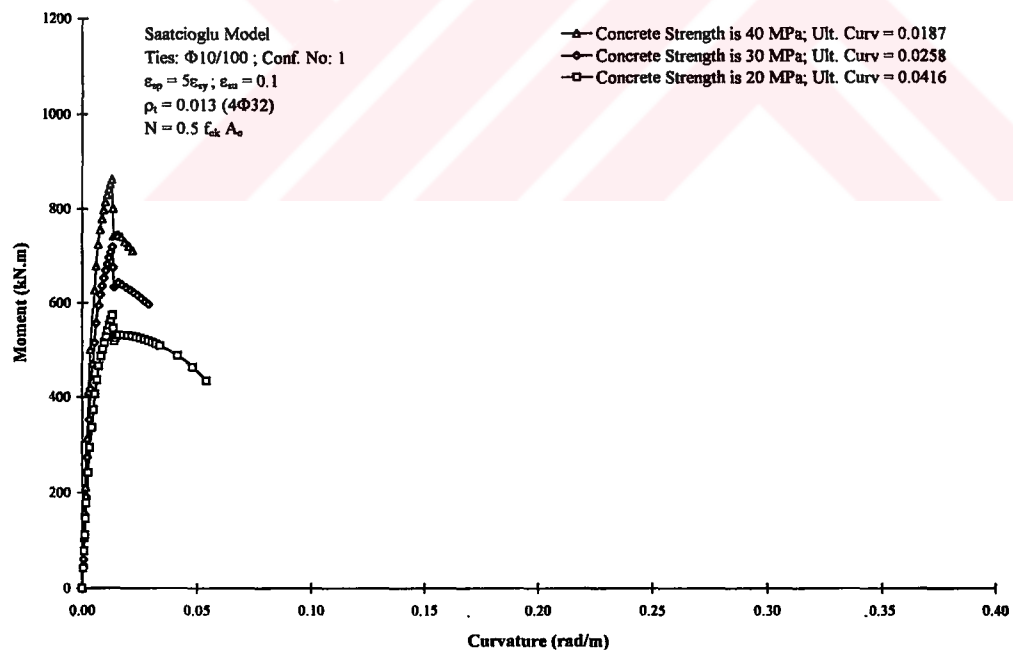


Figure A.101: Influence of concrete strength in R/C columns; Group XIB

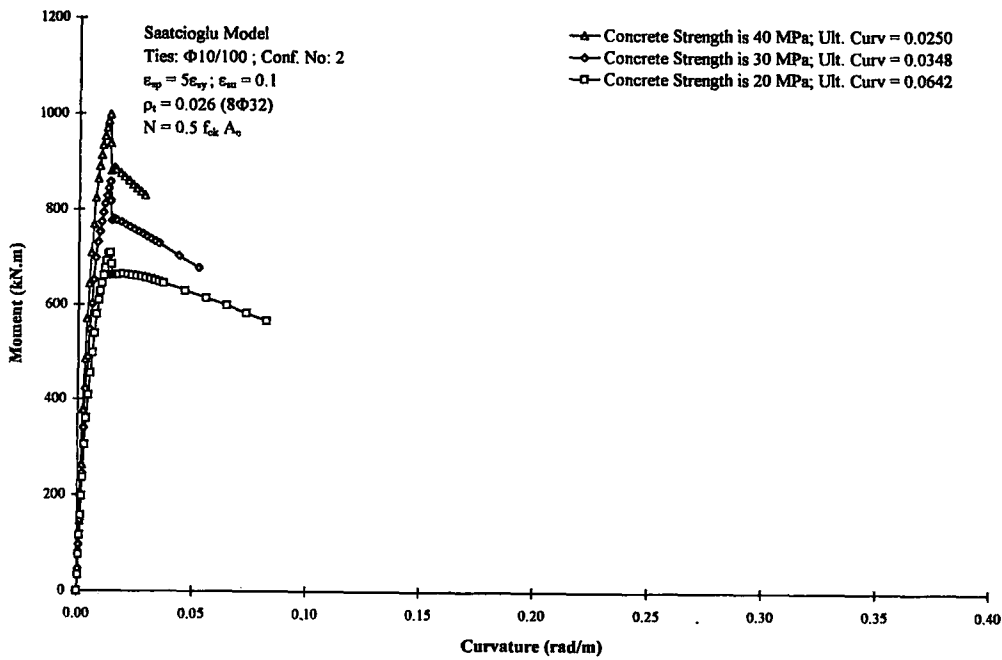


Figure A.102: Influence of concrete strength in R/C columns; Group XIC

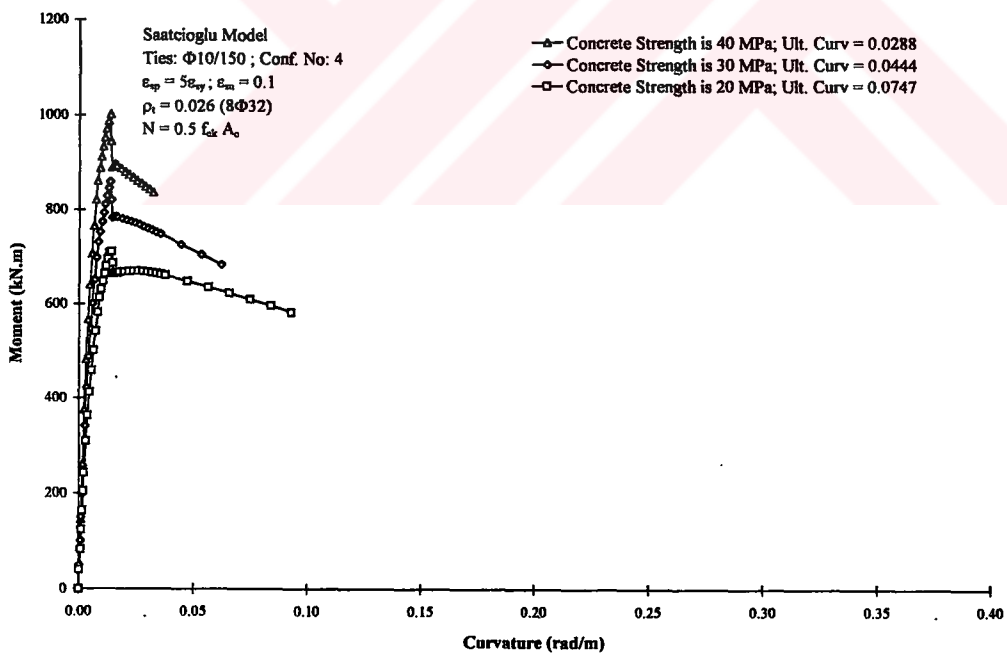


Figure A.103: Influence of concrete strength in R/C columns; Group XID

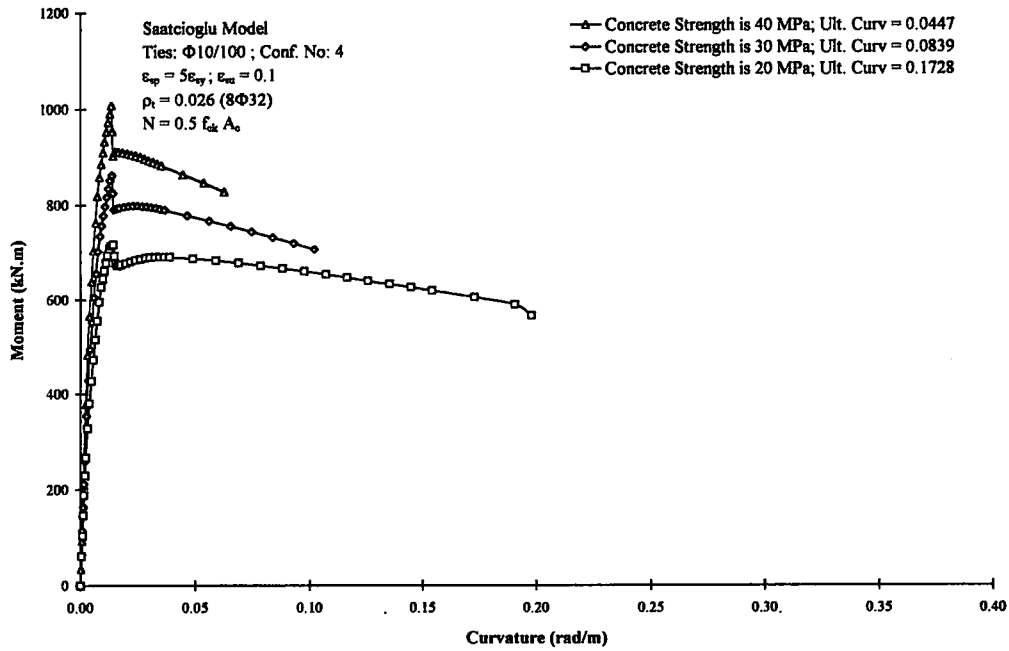


Figure A.104: Influence of concrete strength in R/C columns; Group XIE

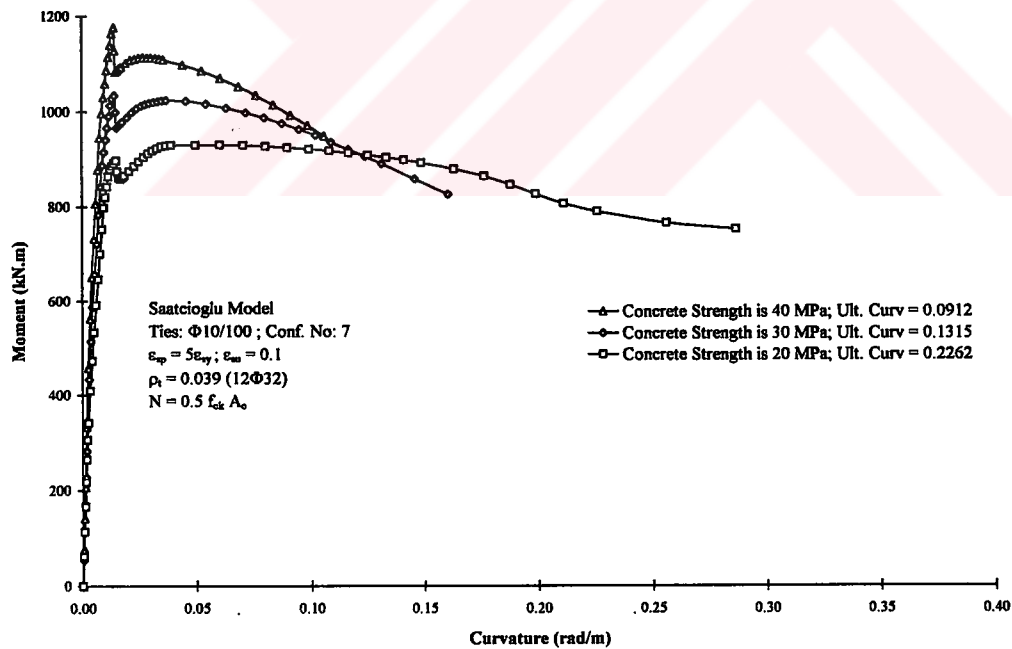


Figure A.105: Influence of concrete strength in R/C columns; Group XIF

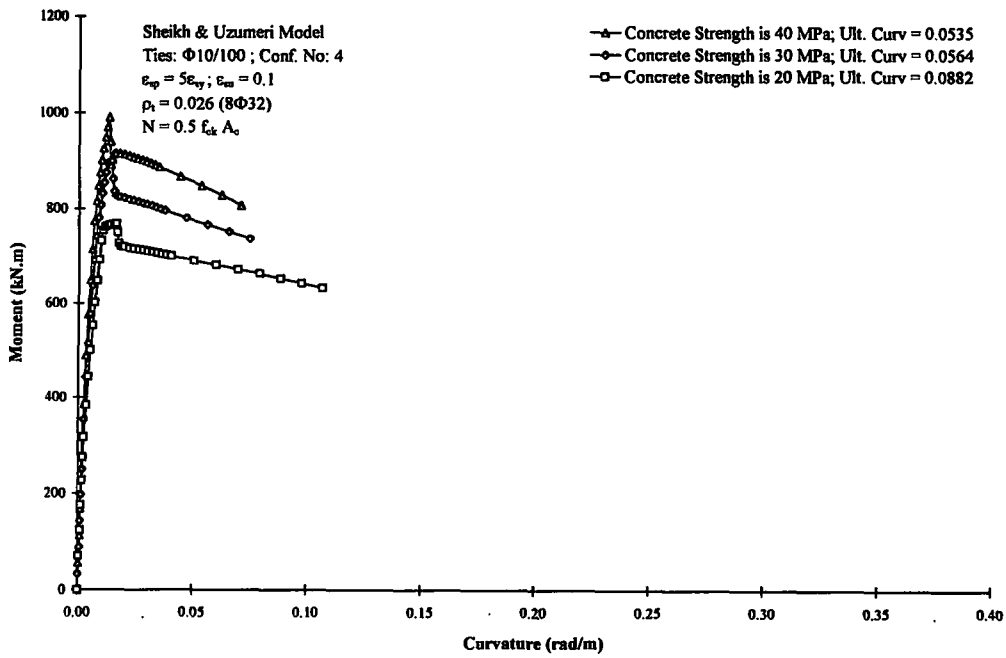


Figure A.106: Influence of concrete strength in R/C columns; Group XIX

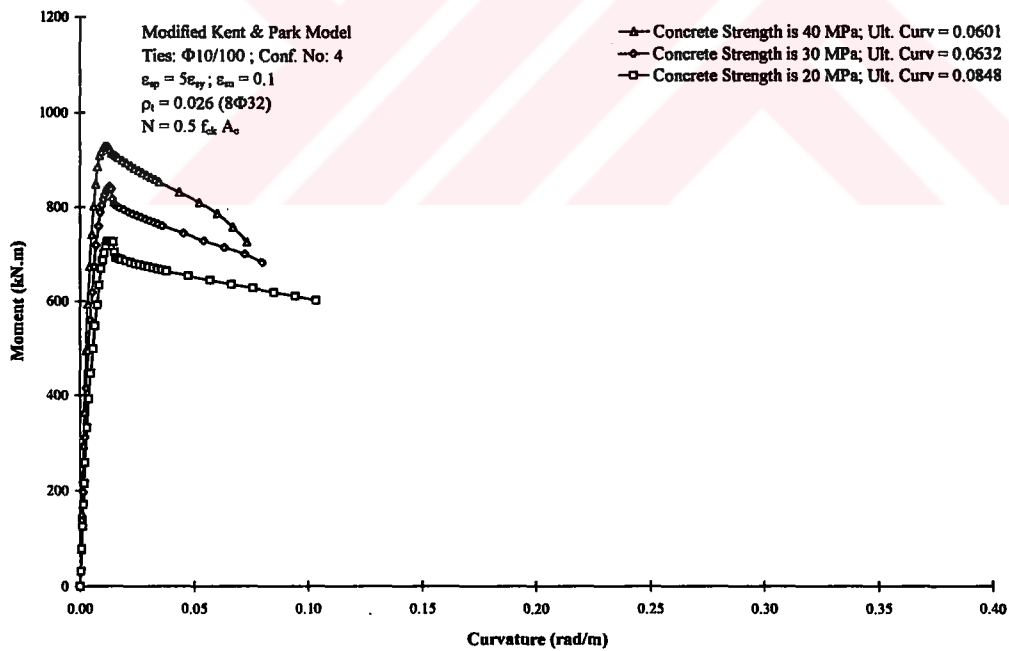
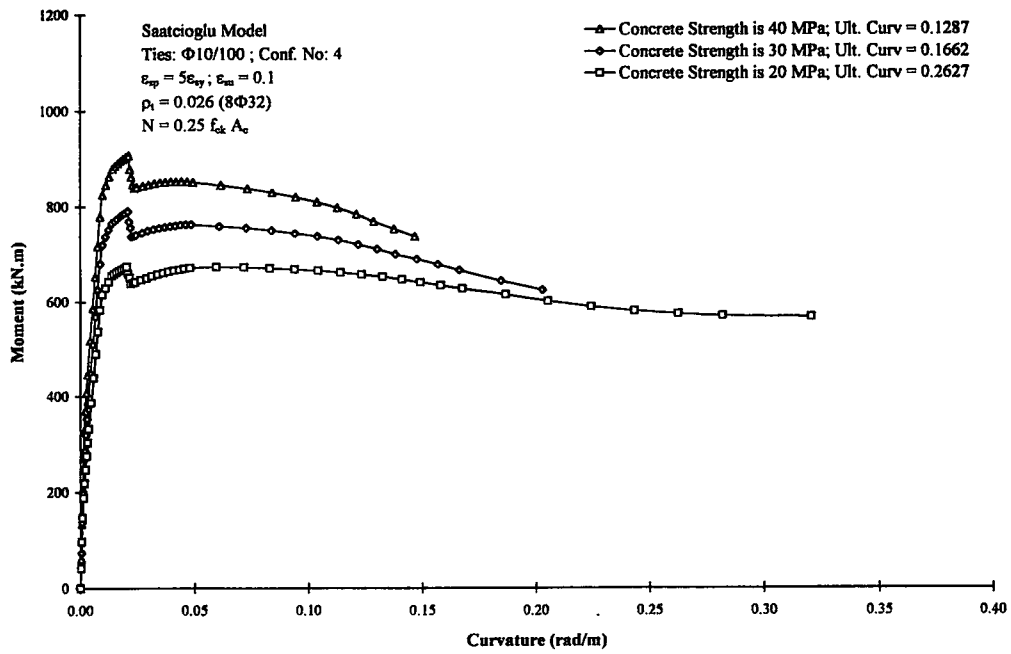
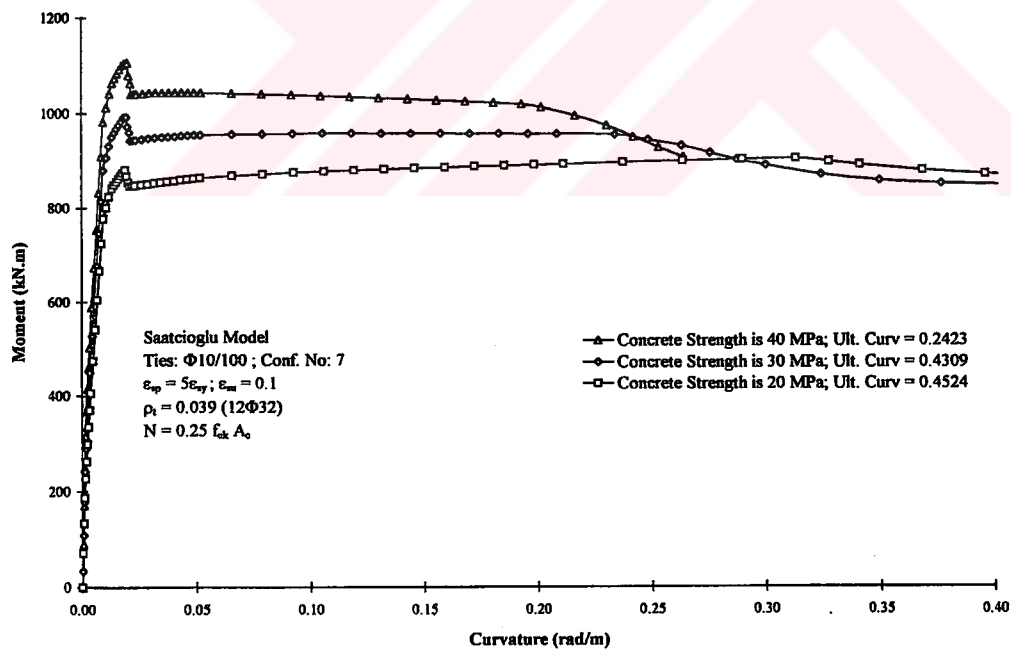


Figure A.107: Influence of concrete strength in R/C columns; Group XIII



**Figure A.108:** Influence of concrete strength in R/C columns; Group XIJ



**Figure A.109:** Influence of concrete strength in R/C columns; Group XIK

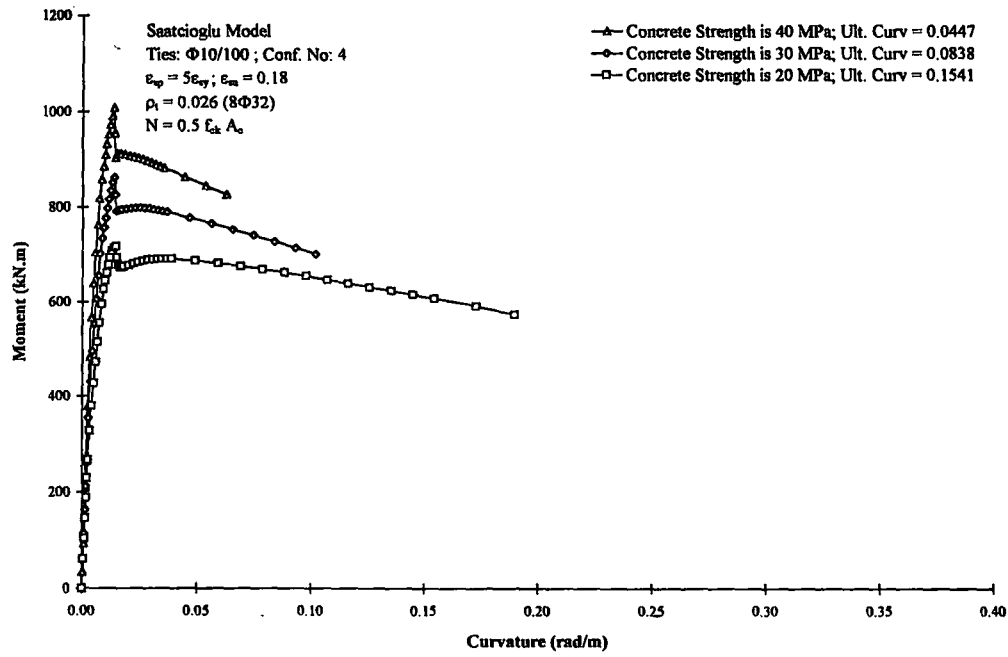


Figure A.110: Influence of concrete strength in R/C columns; Group XII

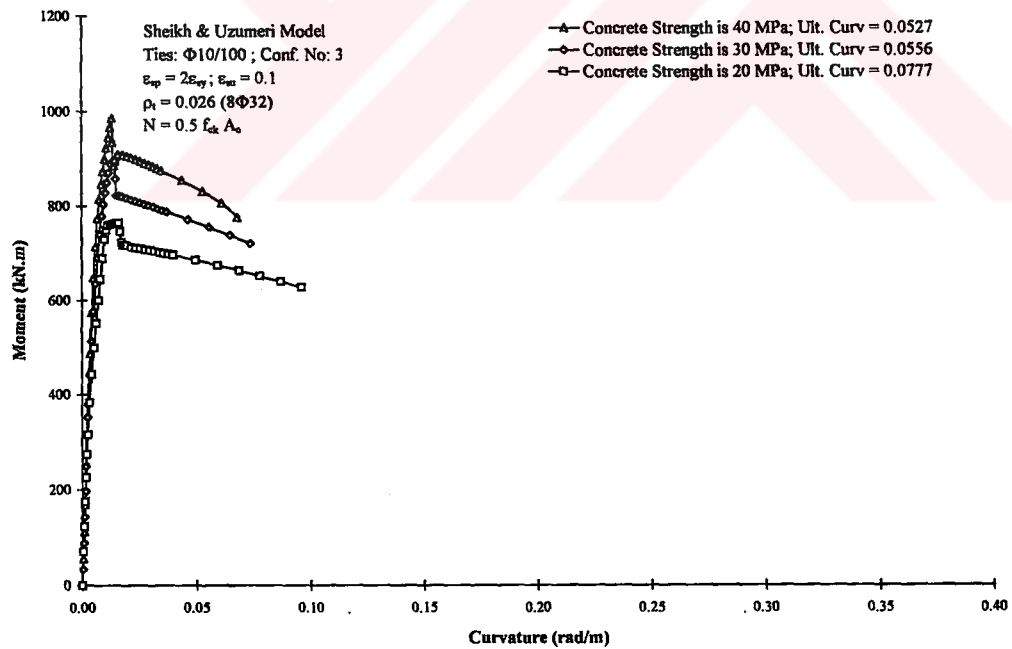


Figure A.111: Influence of concrete strength in R/C columns; Group XIM



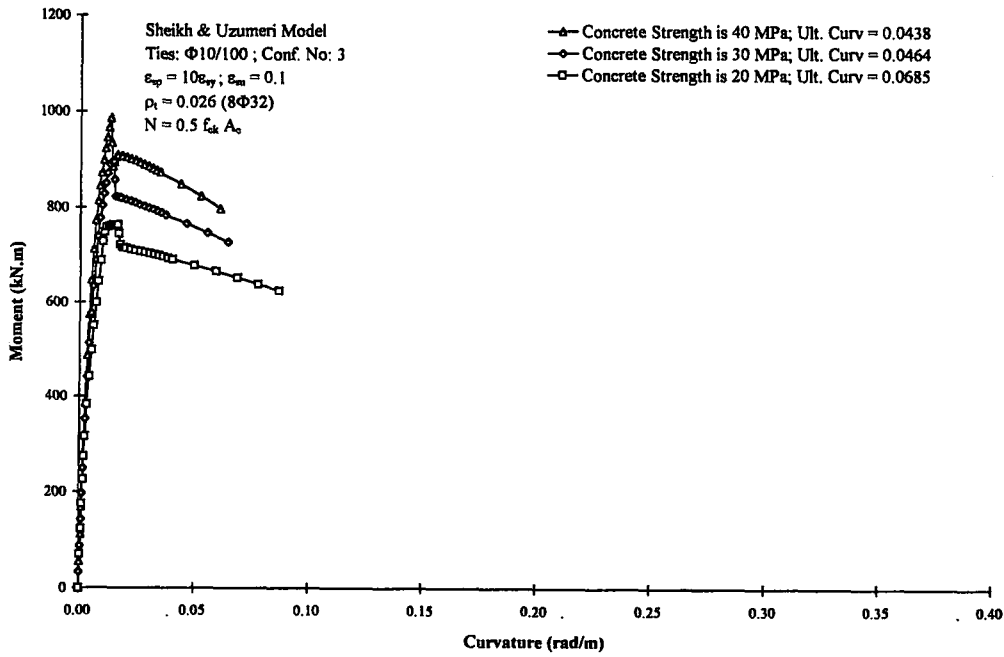


Figure A.112: Influence of concrete strength in R/C columns; Group XIN

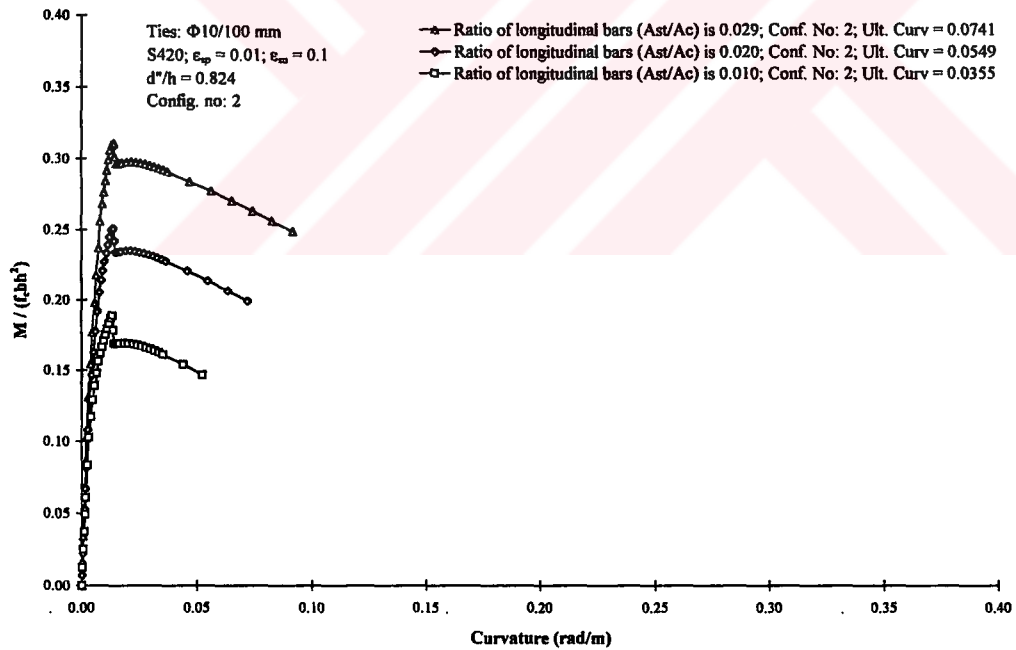


Figure A.113: Influence of ratio of longitudinal bars ( $\rho_t = A_{st}/A_c$ ) in R/C columns;  
 Group XIA

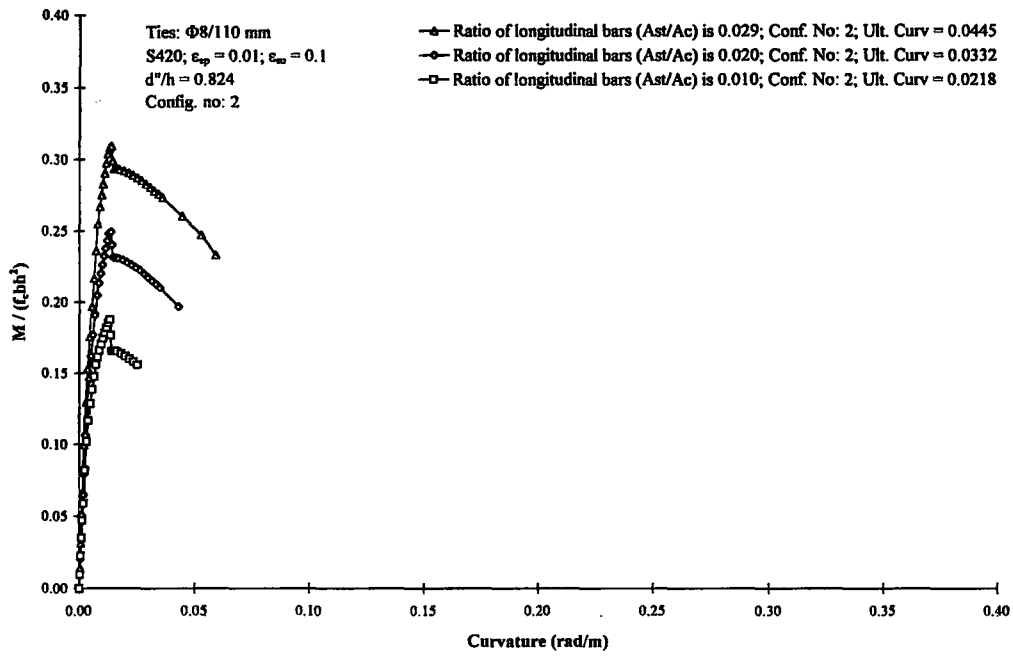


Figure A.114: Influence of ratio of longitudinal bars ( $\rho_l = A_{st}/A_c$ ) in R/C columns;

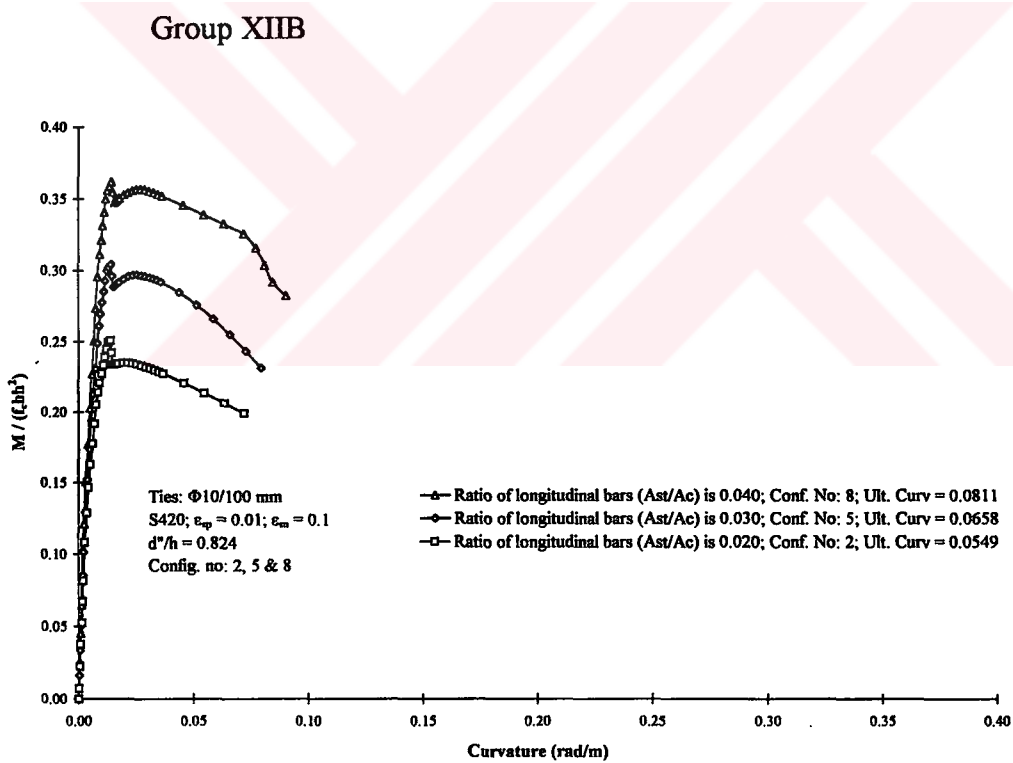


Figure A.115: Influence of ratio of longitudinal bars ( $\rho_l = A_{st}/A_c$ ) in R/C columns;

Group XIIC

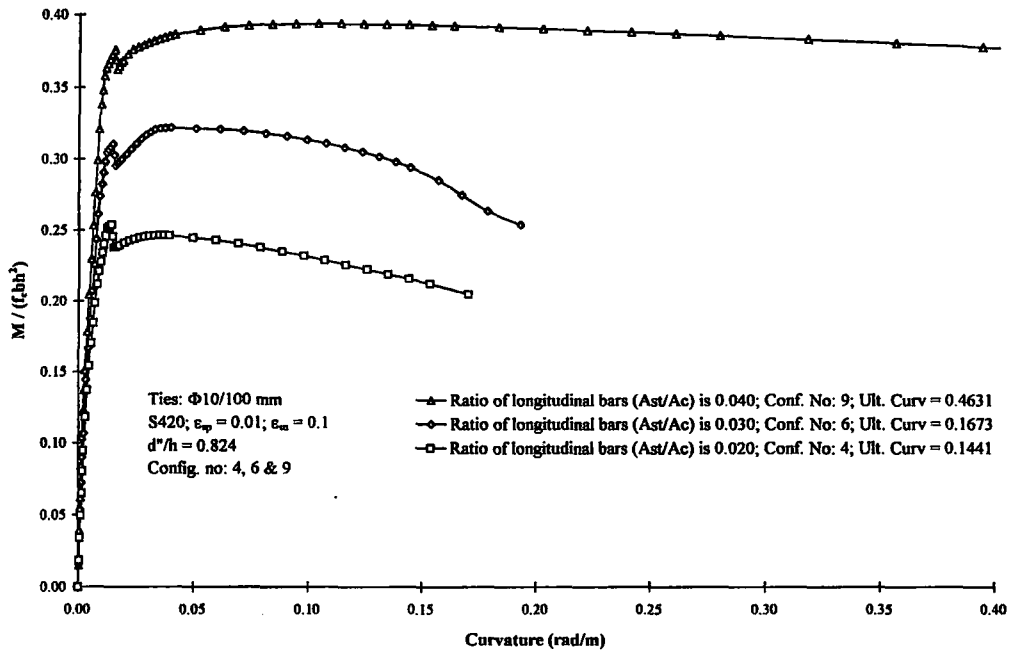


Figure A.116: Influence of ratio of longitudinal bars ( $\rho_t=A_{st}/A_c$ ) in R/C columns;

Group XIID

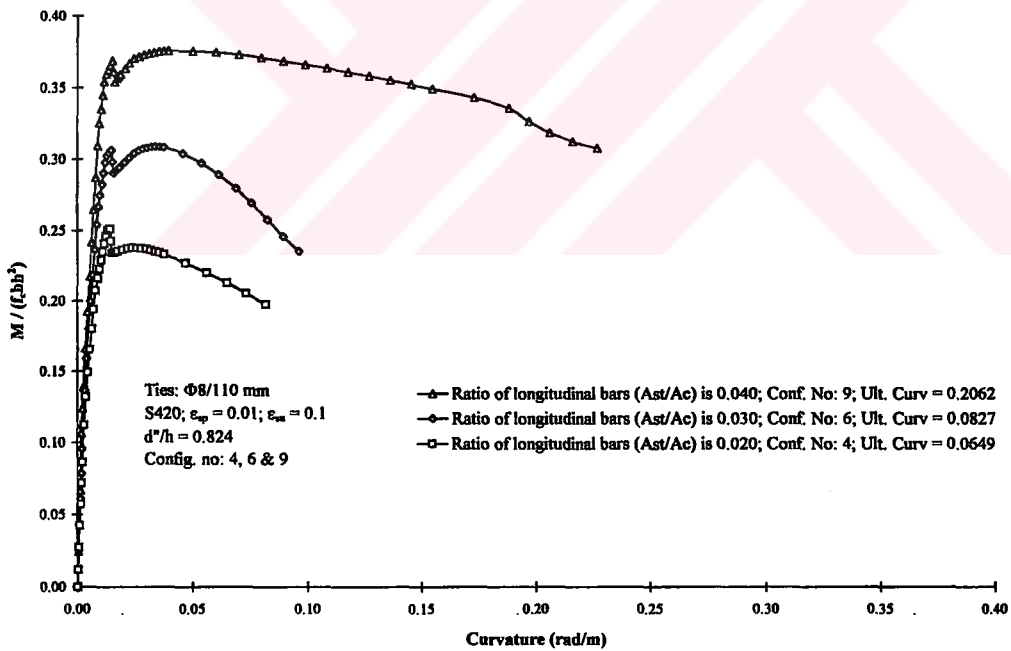


Figure A.117: Influence of ratio of longitudinal bars ( $\rho_t=A_{st}/A_c$ ) in R/C columns;

Group XIIE

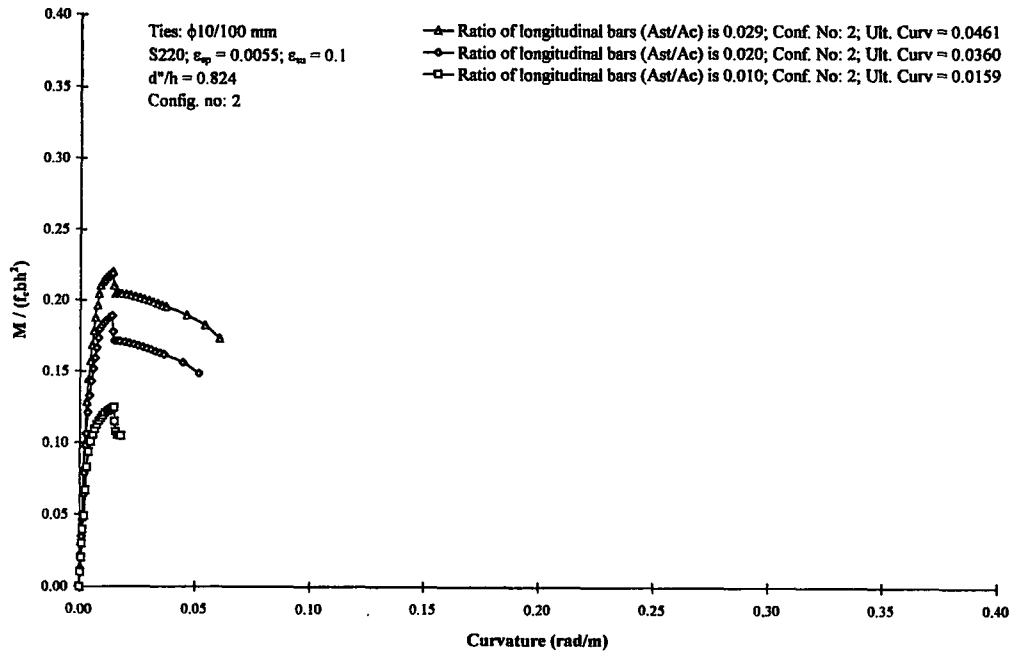


Figure A.118: Influence of ratio of longitudinal bars ( $\rho_t=A_{st}/A_c$ ) in R/C columns;

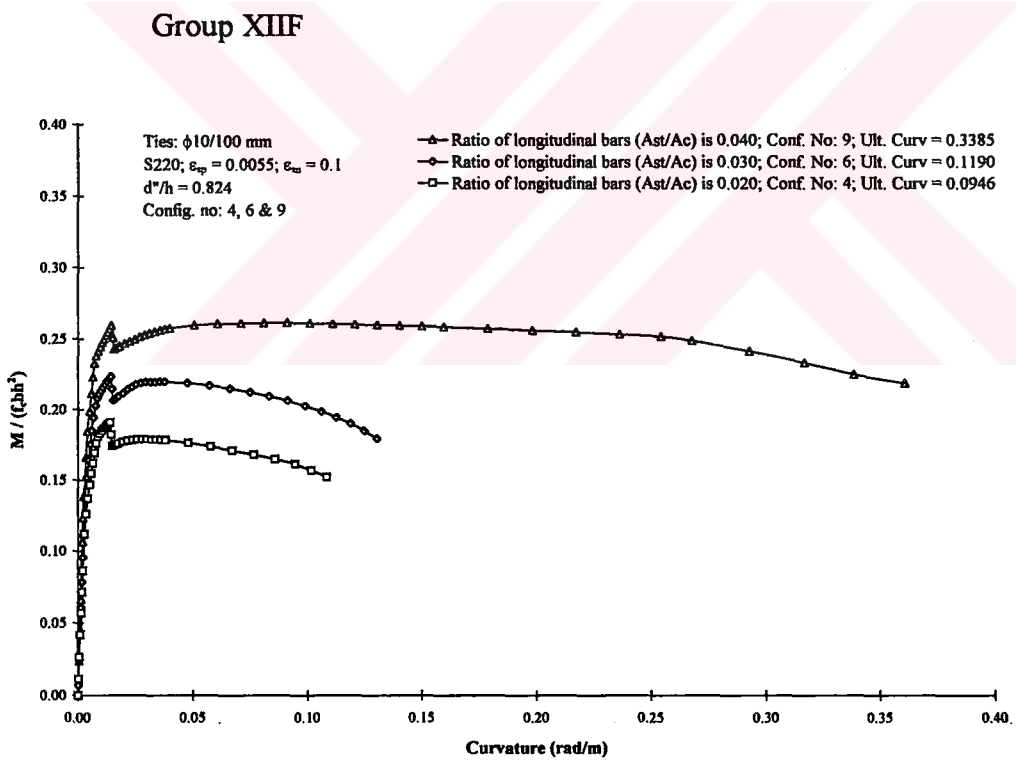


Figure A.119: Influence of ratio of longitudinal bars ( $\rho_t=A_{st}/A_c$ ) in R/C columns;

**Group XIIF**

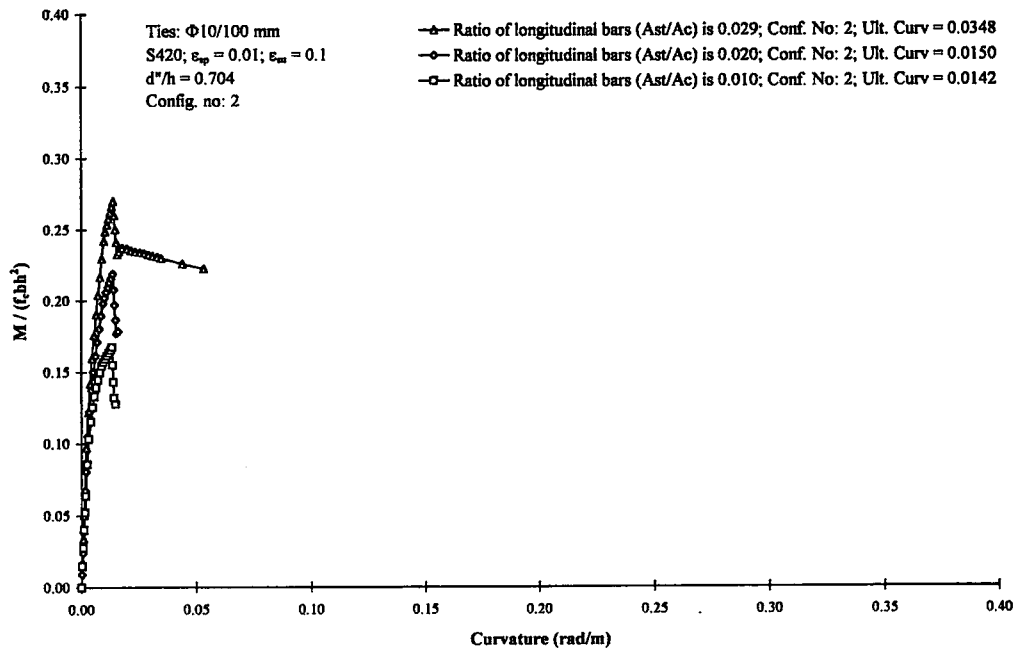


Figure A.120: Influence of ratio of longitudinal bars ( $\rho_t=A_{st}/A_c$ ) in R/C columns;

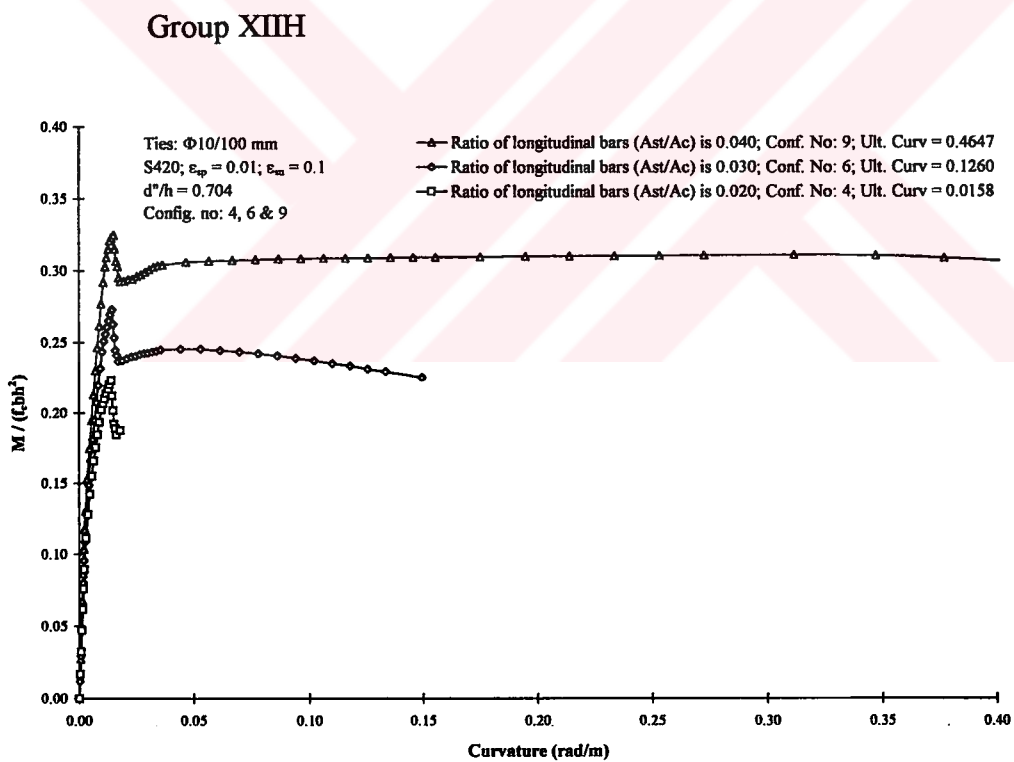


Figure A.121: Influence of ratio of longitudinal bars ( $\rho_t=A_{st}/A_c$ ) in R/C columns;

Group XIIIJ

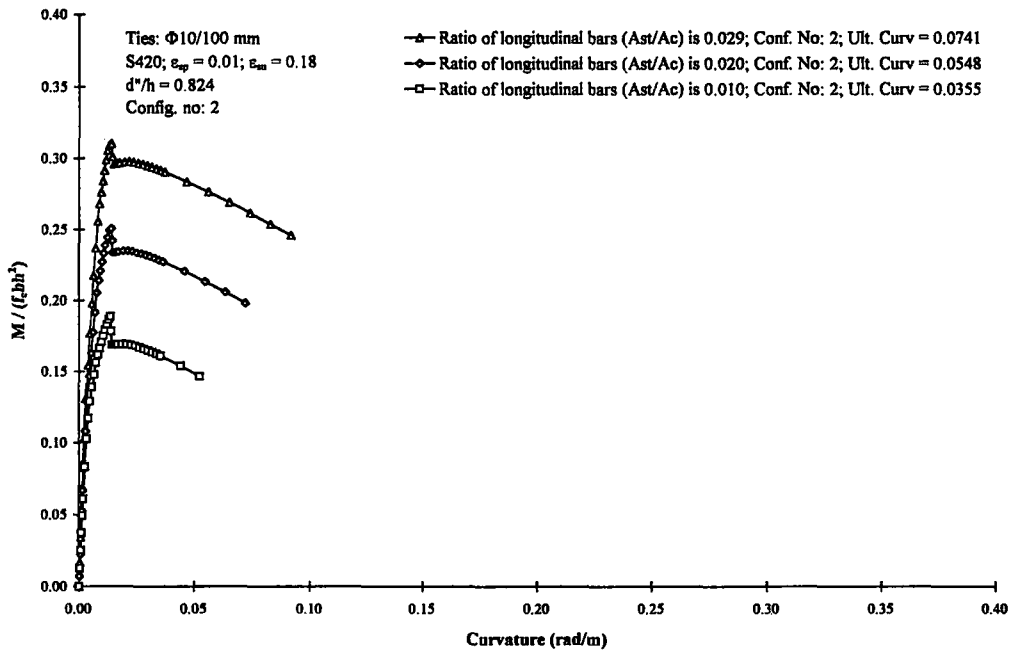


Figure A.122: Influence of ratio of longitudinal bars ( $\rho_t=A_{st}/A_c$ ) in R/C columns;

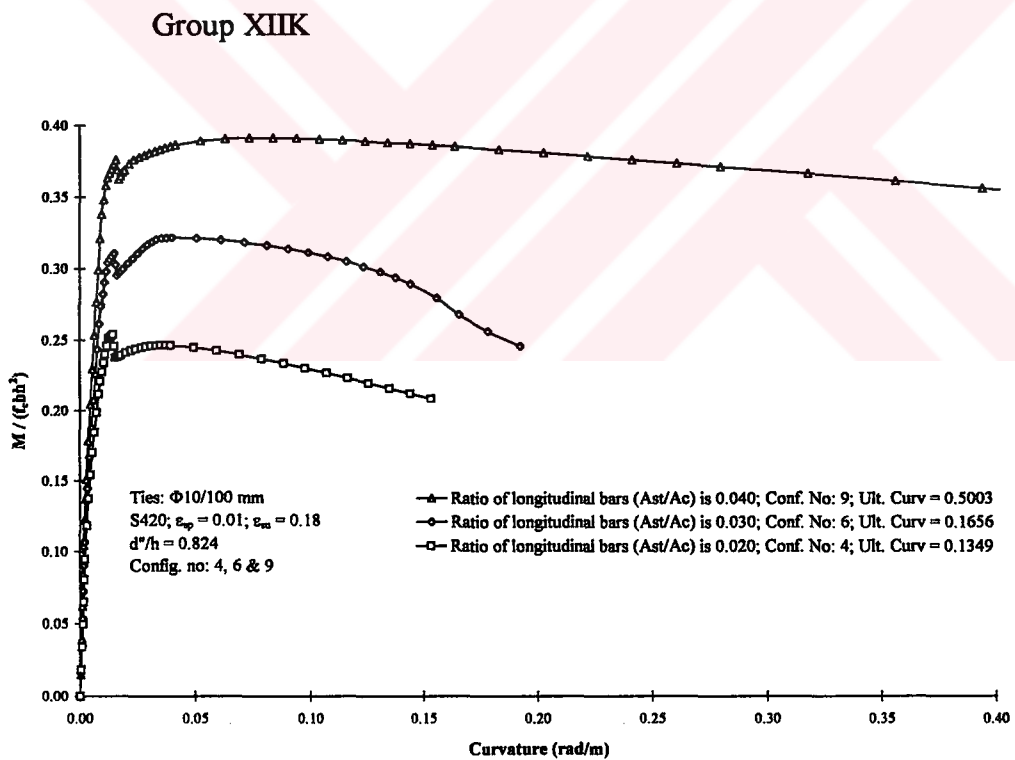
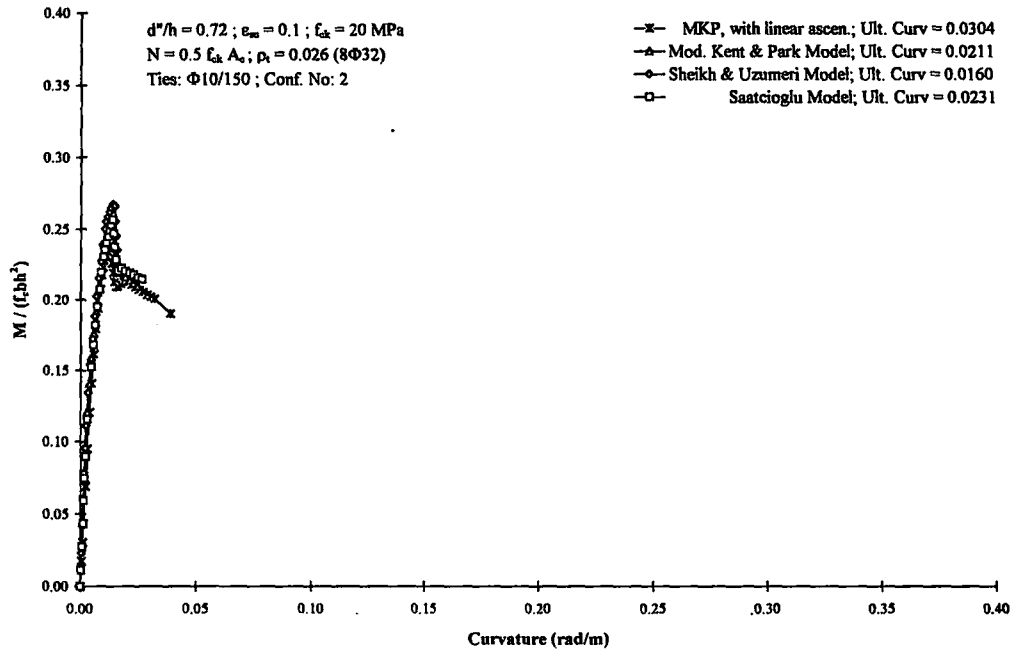
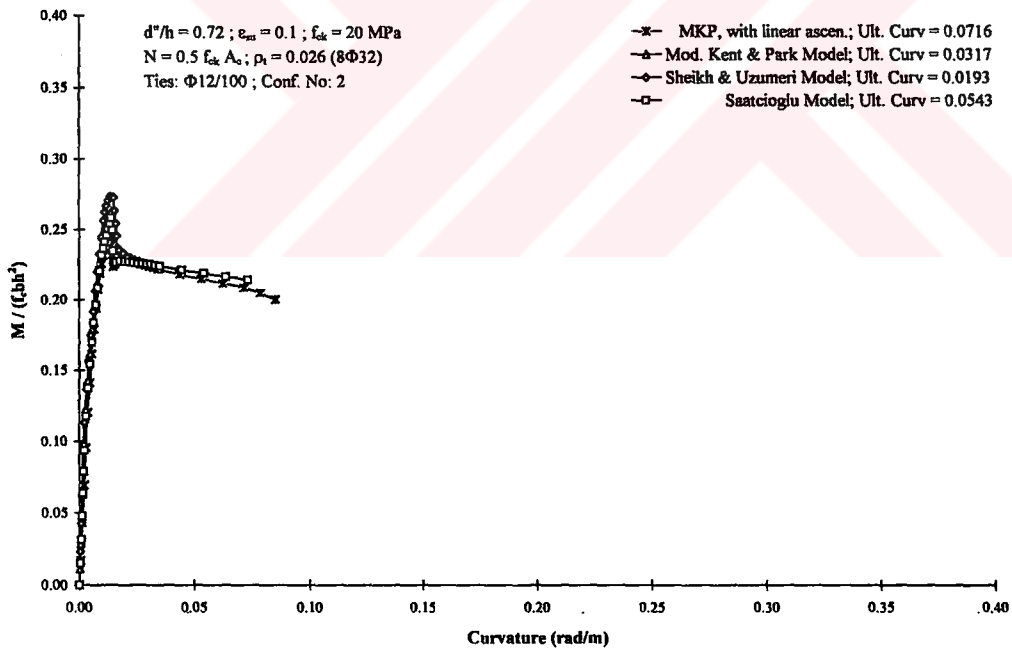


Figure A.123: Influence of ratio of longitudinal bars ( $\rho_t=A_{st}/A_c$ ) in R/C columns;

Group XIII



**Figure A.124:** Influence of confined concrete models on moment curvature diagrams of R/C columns; Group XIII A



**Figure A.125:** Influence of confined concrete models on moment curvature diagrams of R/C columns; Group XIII B

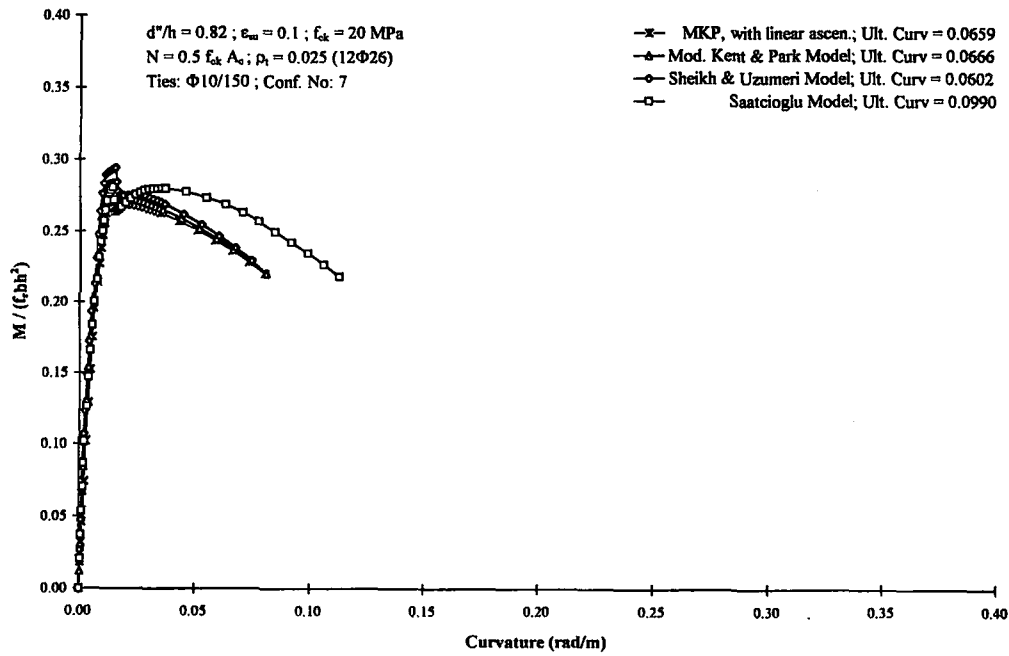


**Figure A.126:** Influence of confined concrete models on moment curvature diagrams of R/C columns; Group XIIC

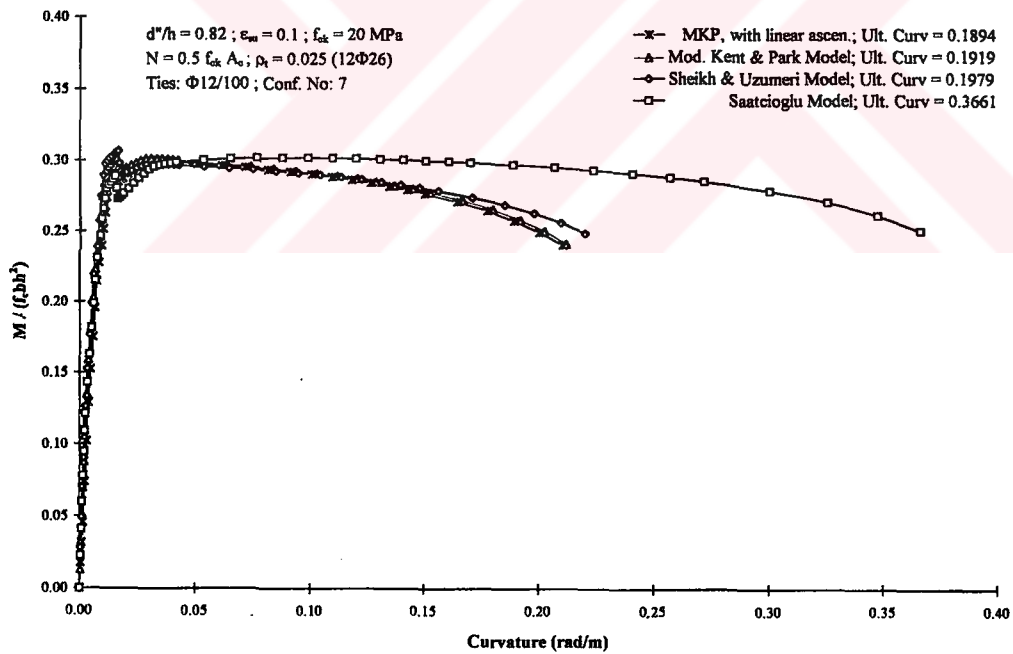


**Figure A.127:** Influence of confined concrete models on moment curvature diagrams of R/C columns; Group XIID



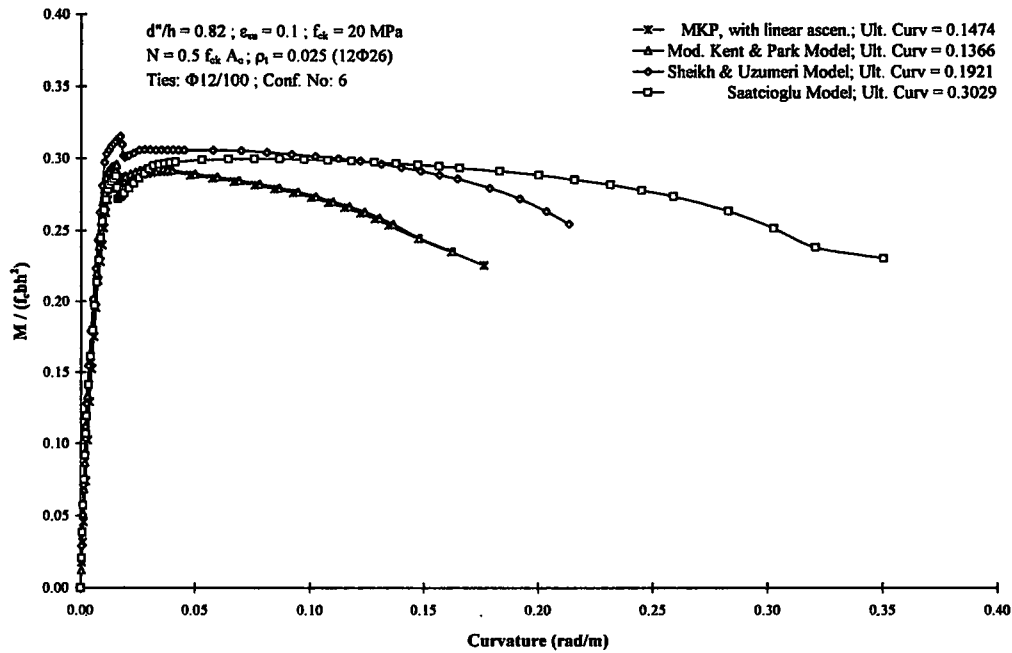


**Figure A.128:** Influence of confined concrete models on moment curvature diagrams of R/C columns; Group XIII E

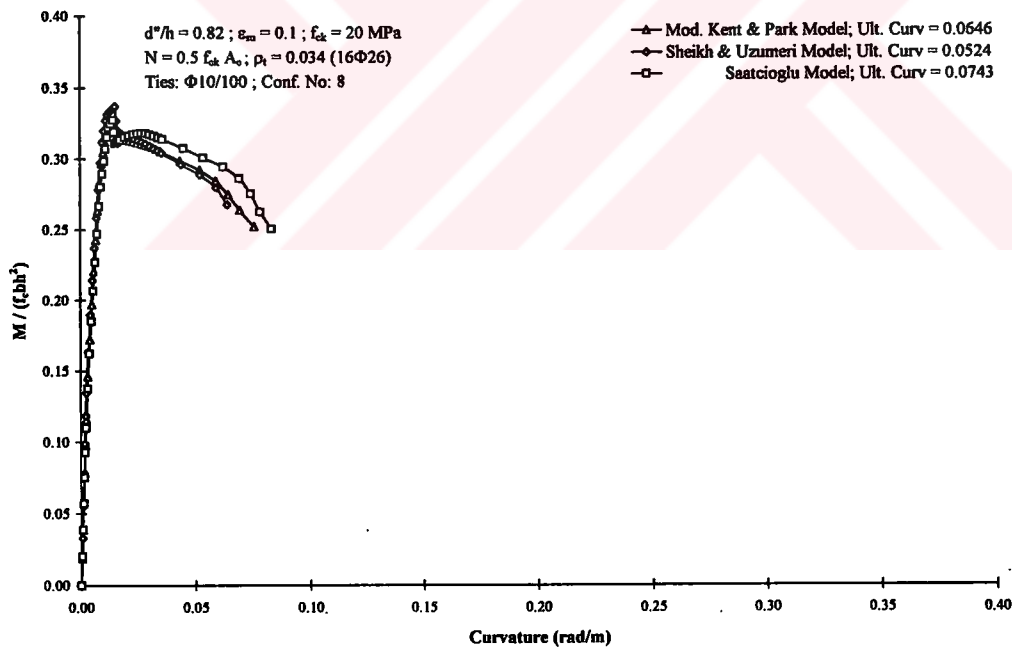


**Figure A.129:** Influence of confined concrete models on moment curvature diagrams of R/C columns; Group XIII F

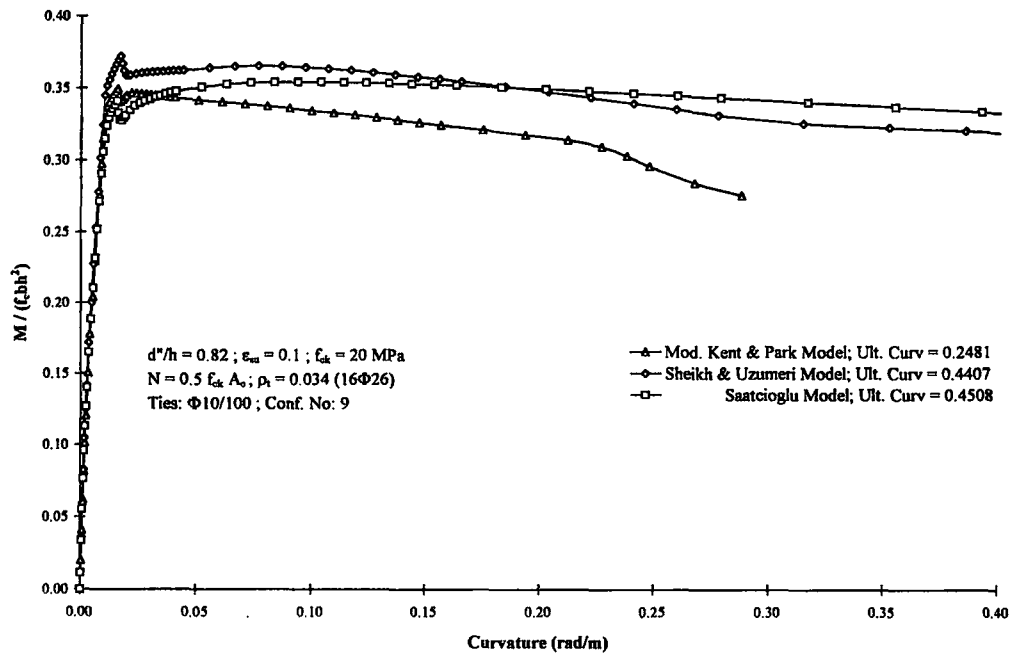


**Figure A.130:** Influence of confined concrete models on moment curvature diagrams of R/C columns; Group XIII G

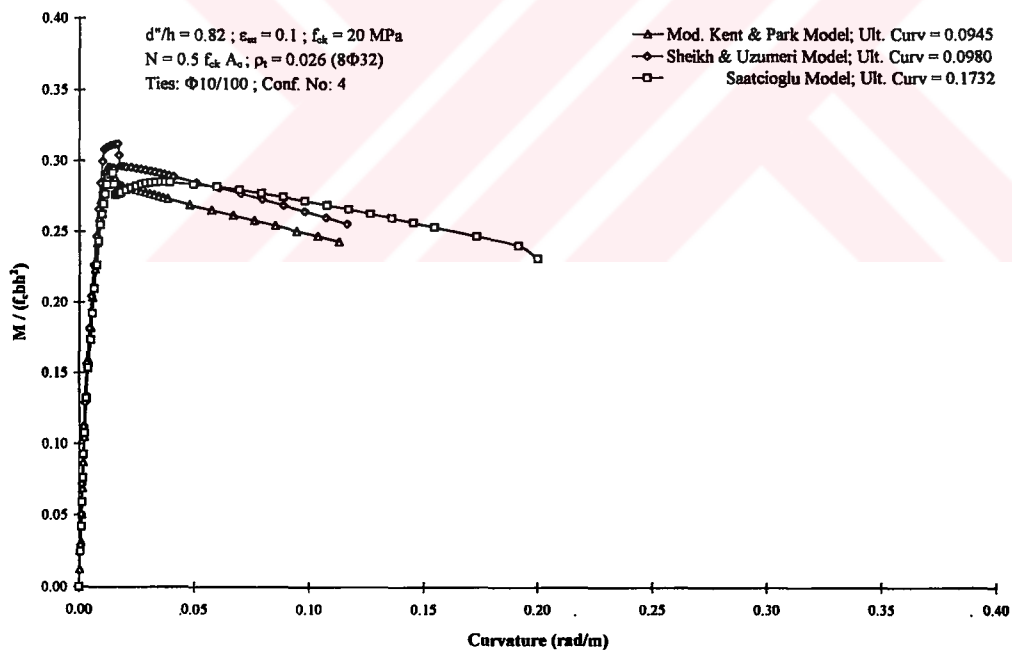


**Figure A.131:** Influence of confined concrete models on moment curvature diagrams of R/C columns; Group XIII H

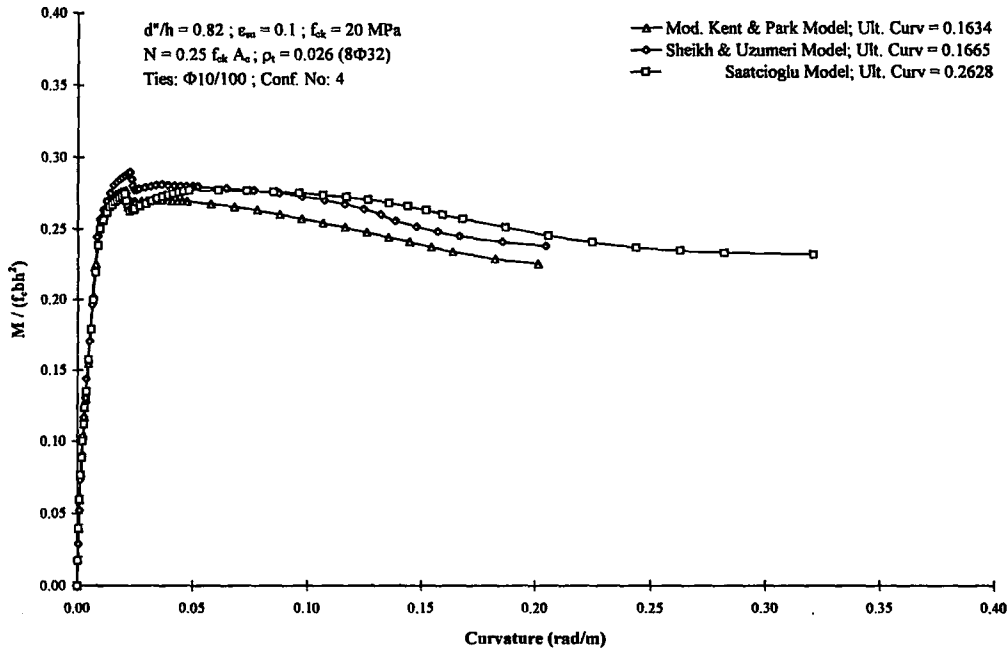


**Figure A.132:** Influence of confined concrete models on moment curvature diagrams

of R/C columns; Group XIIIJ

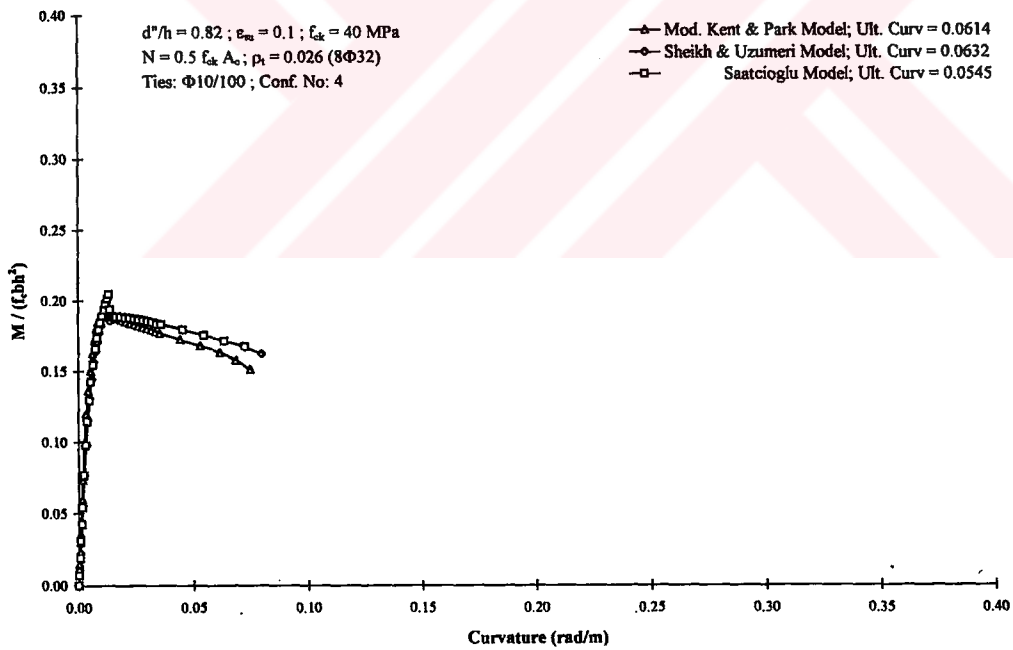


**Figure A.133:** Influence of confined concrete models on moment curvature diagrams

of R/C columns; Group XIIIK

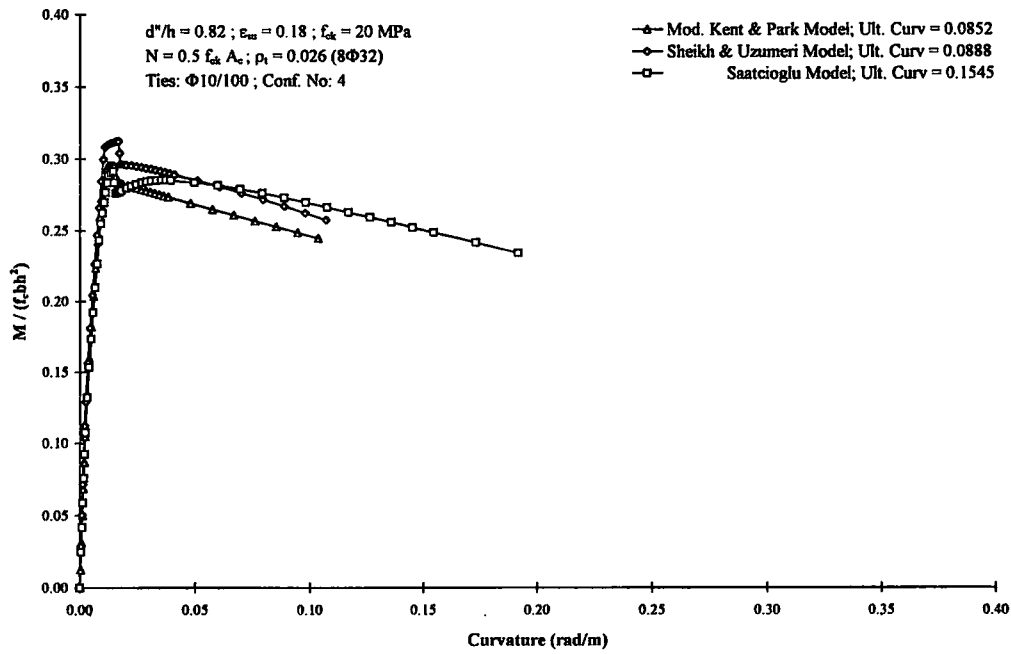


**Figure A.134:** Influence of confined concrete models on moment curvature diagrams of R/C columns; Group XIII

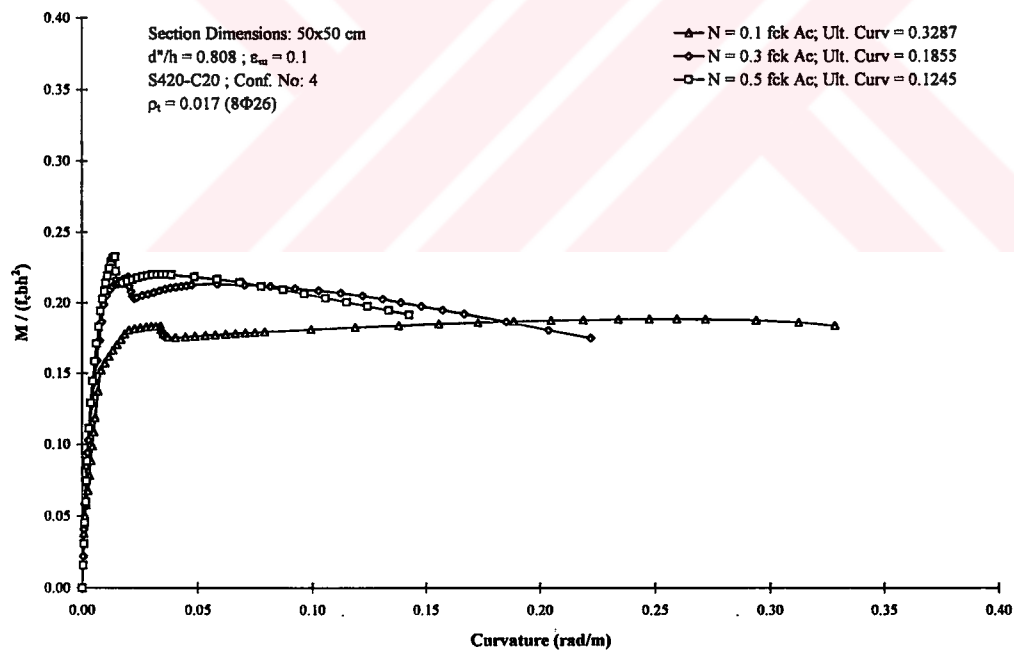


**Figure A.135:** Influence of axial load level ( $N/f_{ck}A_c'$  ratio) in R/C columns; Group XIVA

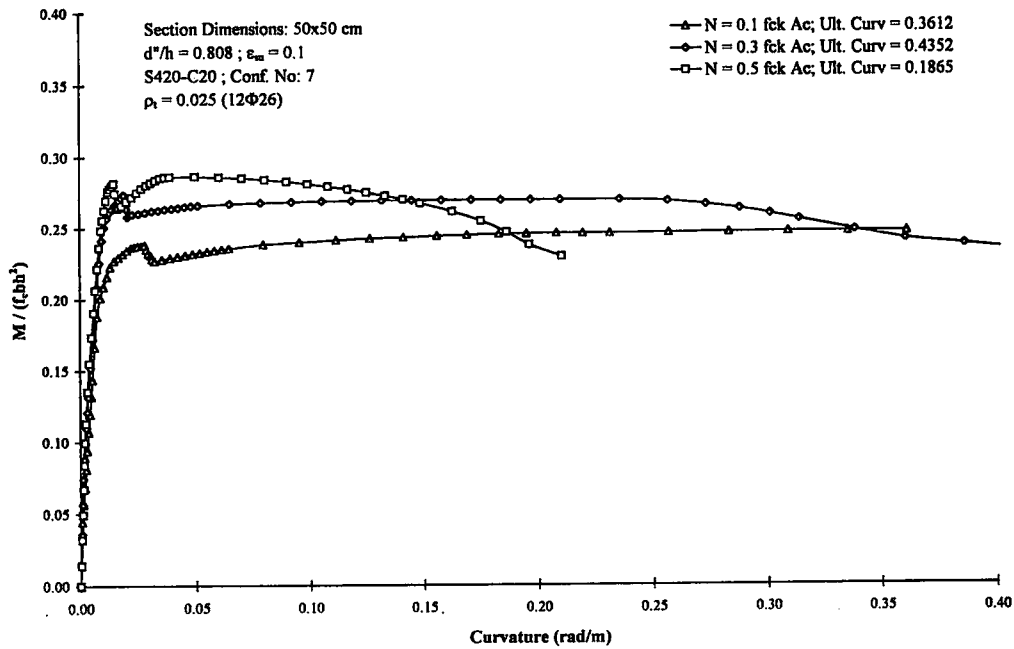


Figure A.136: Influence of axial load level ( $N/f_{ck}A_c$  ratio) in R/C columns; Group

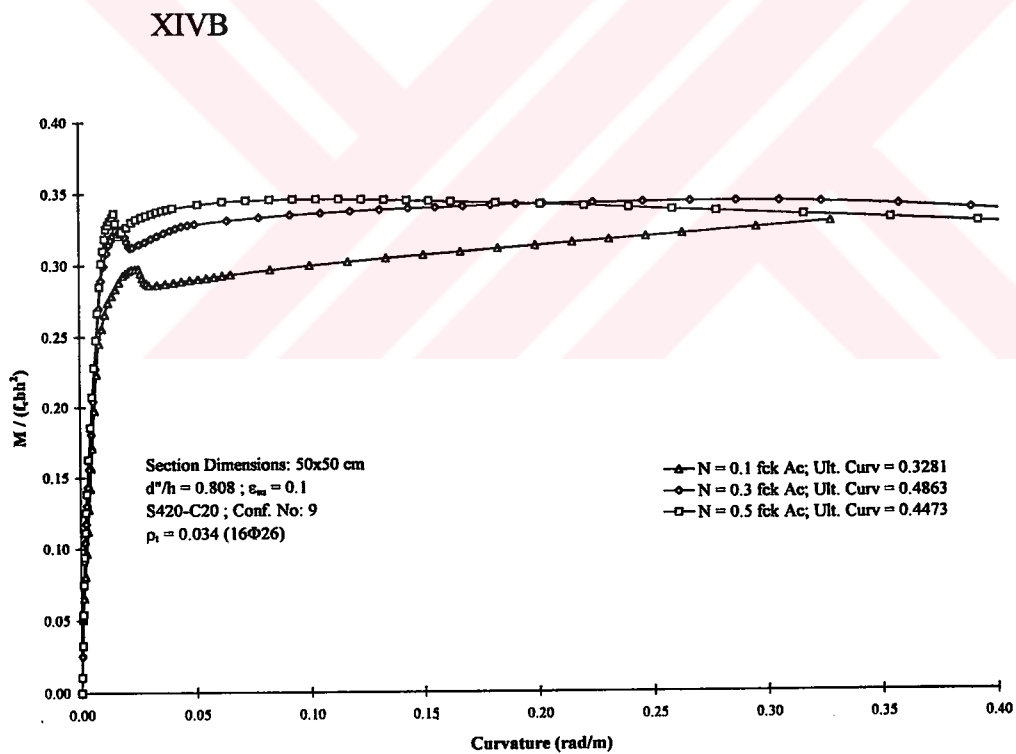


Figure A.137: Influence of axial load level ( $N/f_{ck}A_c$  ratio) in R/C columns; Group

XIVC

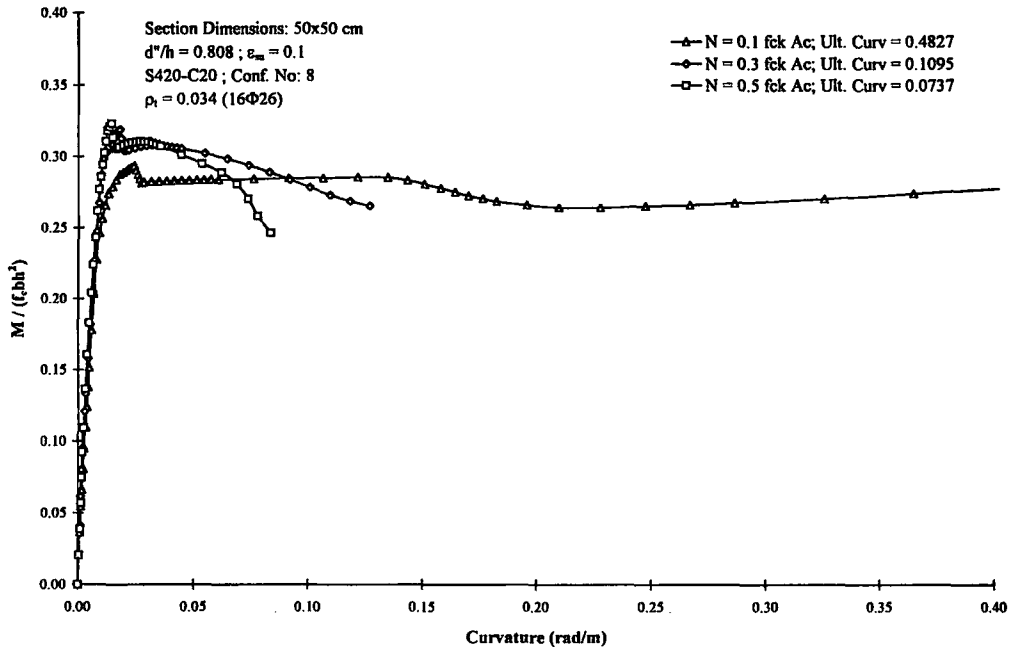


Figure A.138: Influence of axial load level ( $N/f_{ck}A_c'$  ratio) in R/C columns; Group XIV

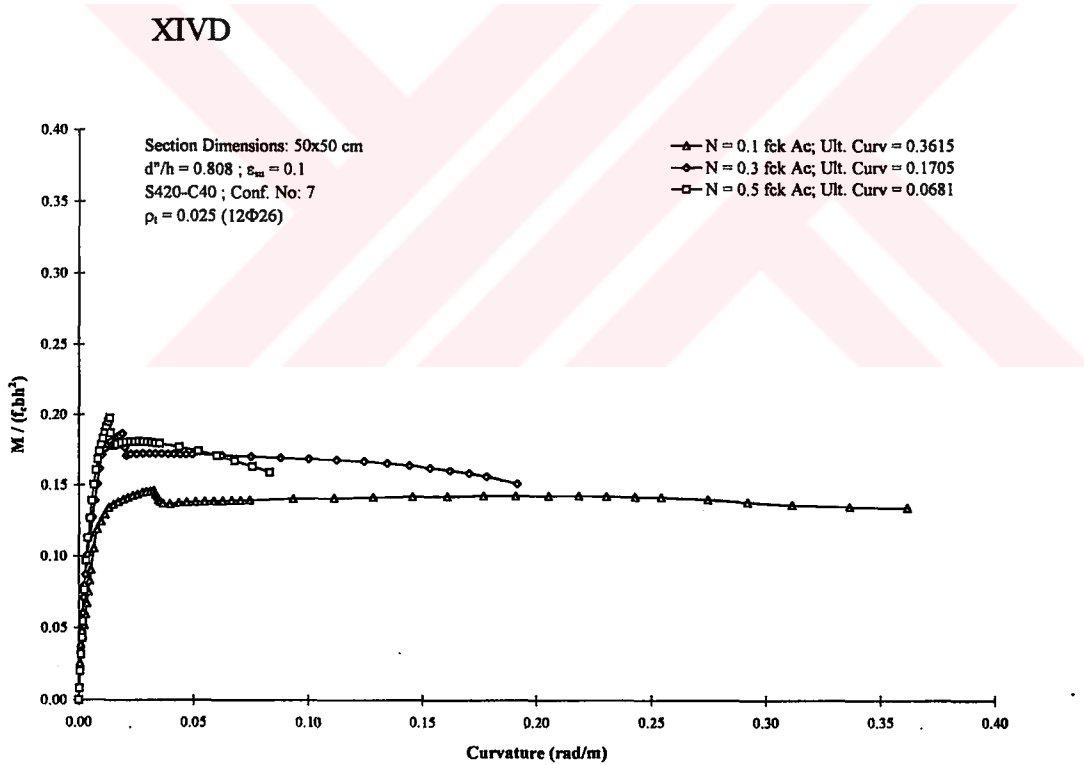


Figure A.139: Influence of axial load level ( $N/f_{ck}A_c'$  ratio) in R/C columns; Group XIVE

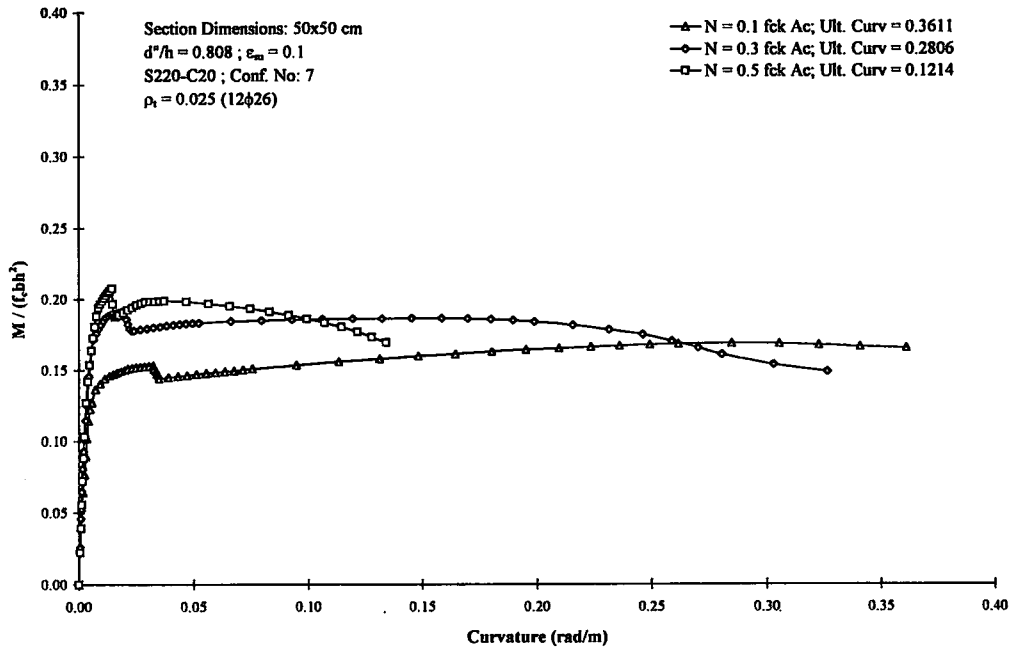


Figure A.140: Influence of axial load level ( $N/f_{ck}A_c'$  ratio) in R/C columns; Group

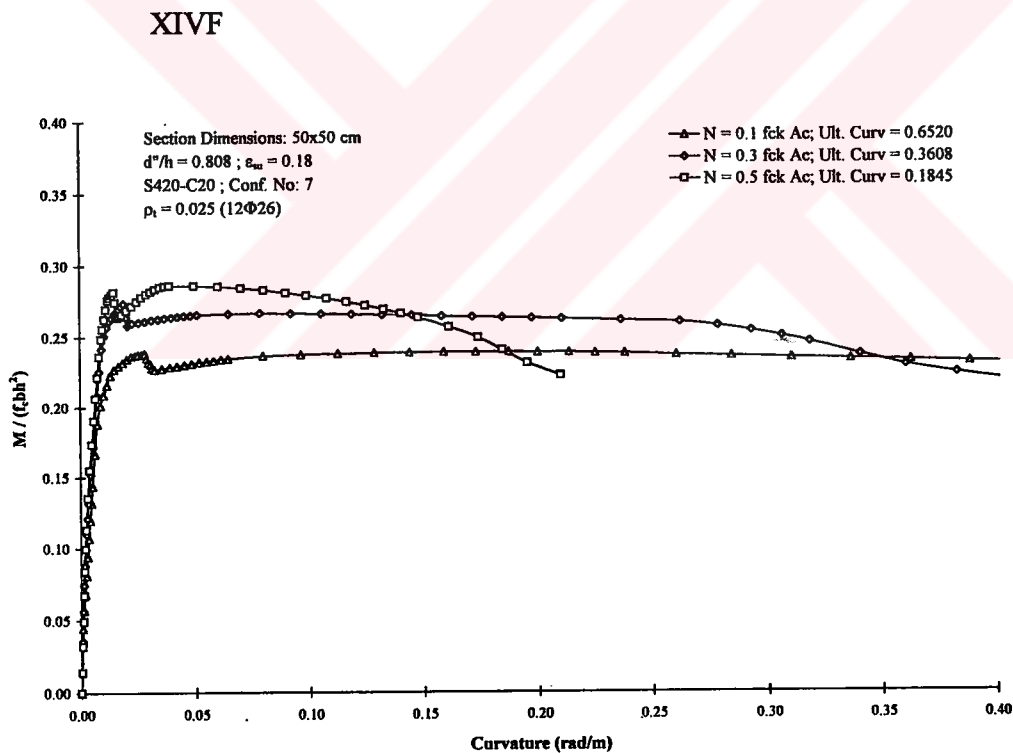


Figure A.141: Influence of axial load level ( $N/f_{ck}A_c'$  ratio) in R/C columns; Group

XIVG

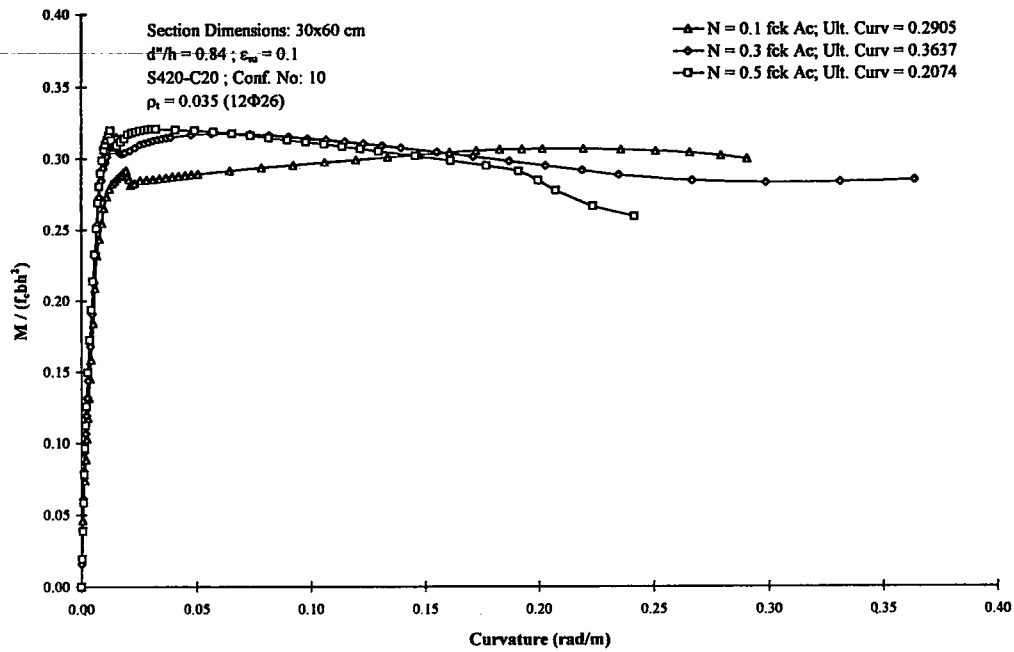


Figure A.142: Influence of axial load level ( $N/f_{ck}A_c'$  ratio) in R/C columns; Group

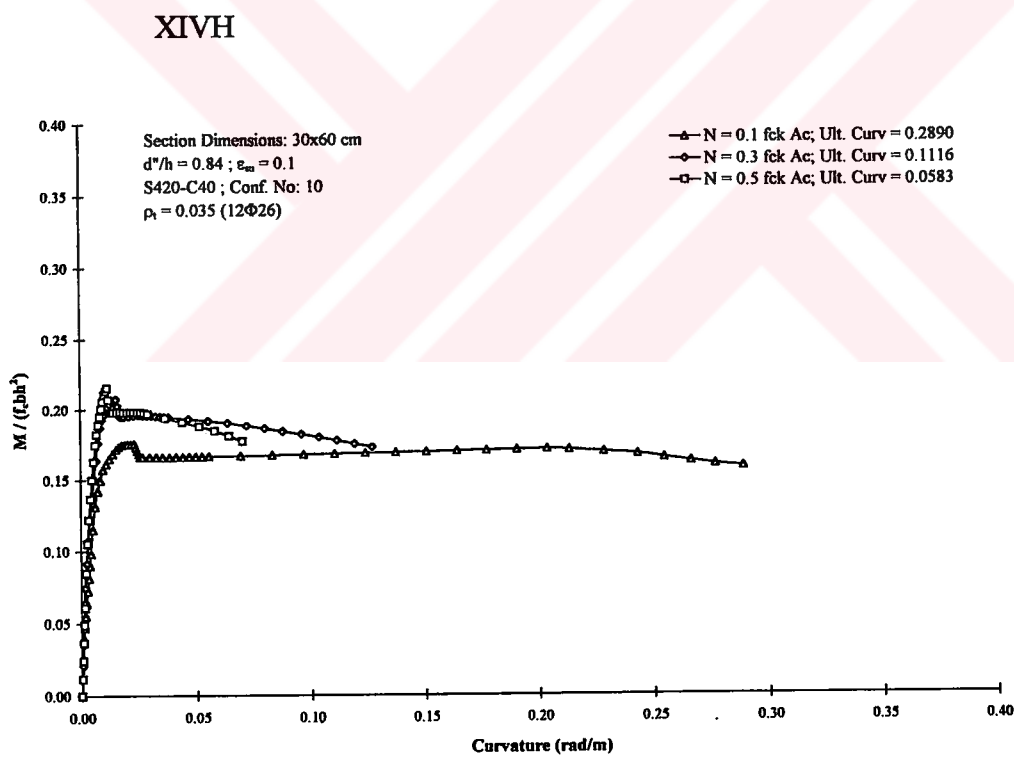


Figure A.143: Influence of axial load level ( $N/f_{ck}A_c'$  ratio) in R/C columns; Group

XIVJ



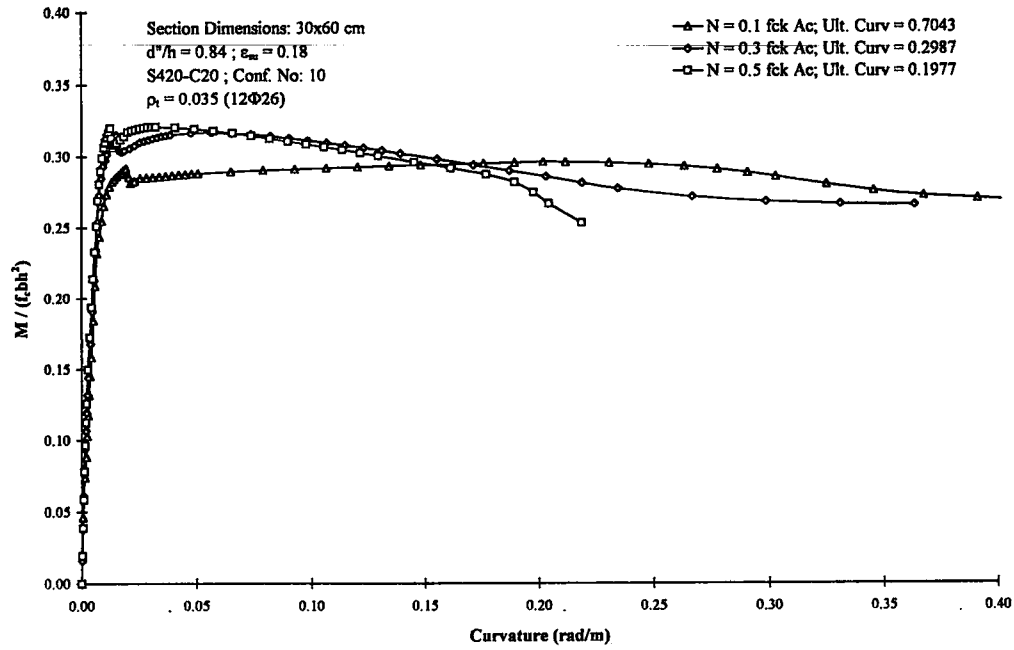


Figure A.144: Influence of axial load level ( $N/f_{ck}A_c$  ratio) in R/C columns; Group

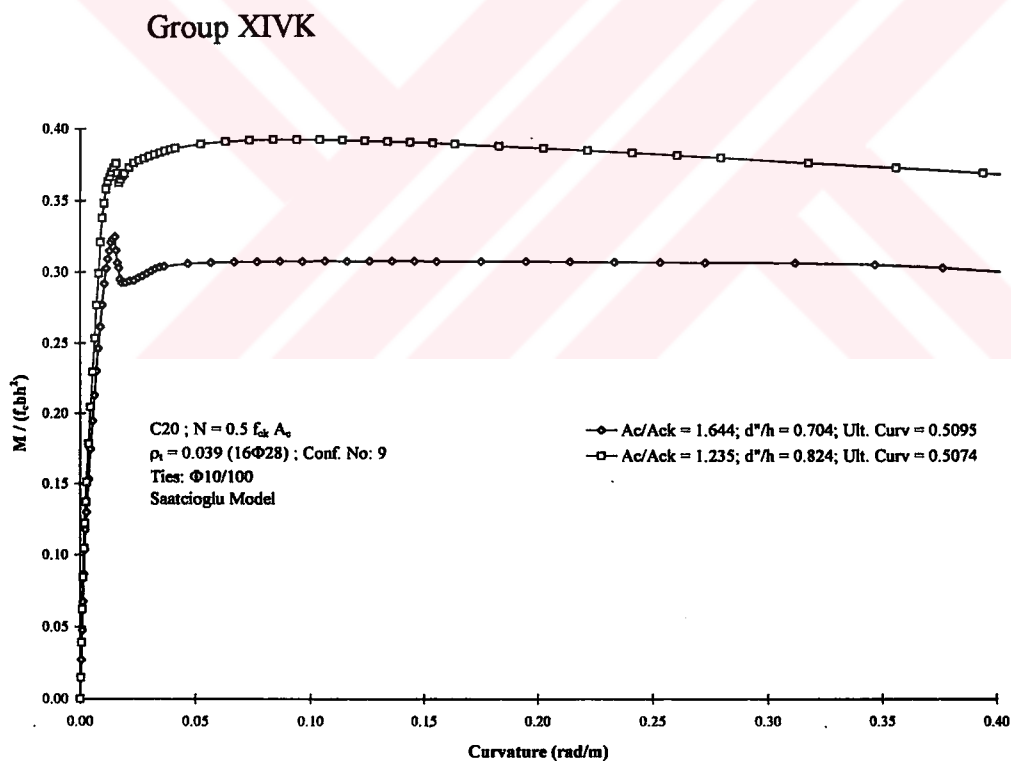
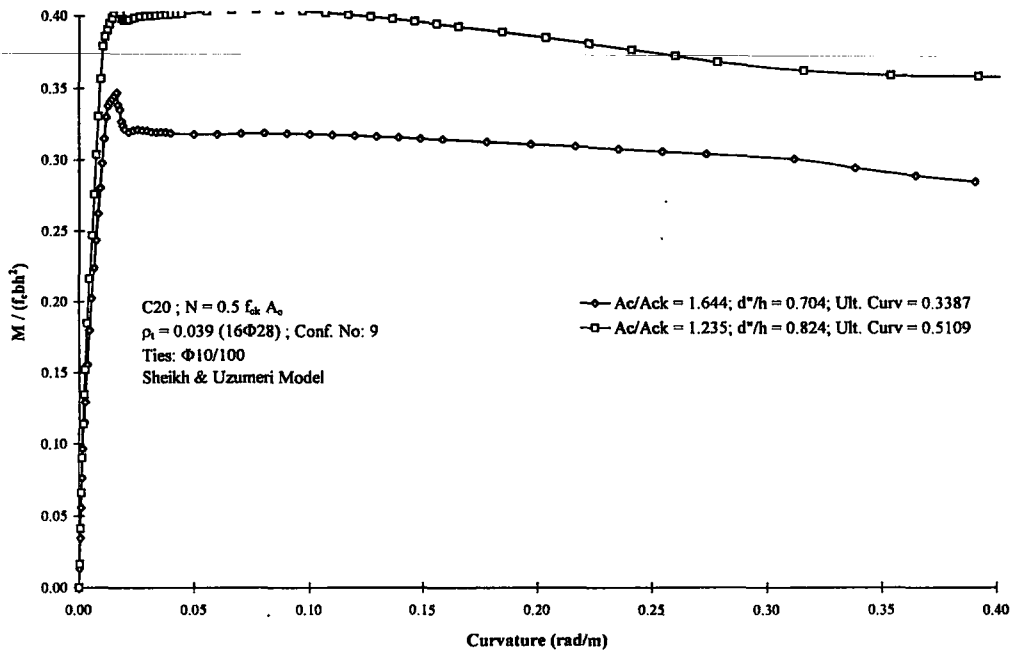
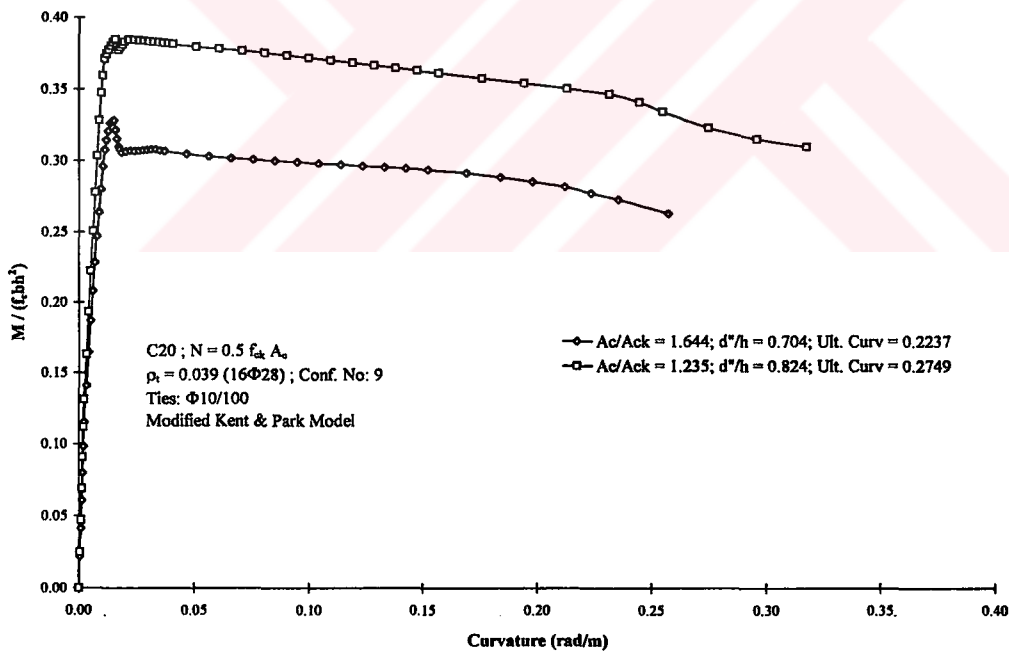


Figure A.145: Influence of ratio of the gross area to the confined area ( $A_c/A_{ck}$ ) in R/C columns; Group XVA



**Figure A.146:** Influence of ratio of the gross area to the confined area ( $A_c/A_{ck}$ ) in R/C columns; Group XVB



**Figure A.147:** Influence of ratio of the gross area to the confined area ( $A_c/A_{ck}$ ) in R/C columns; Group XVC

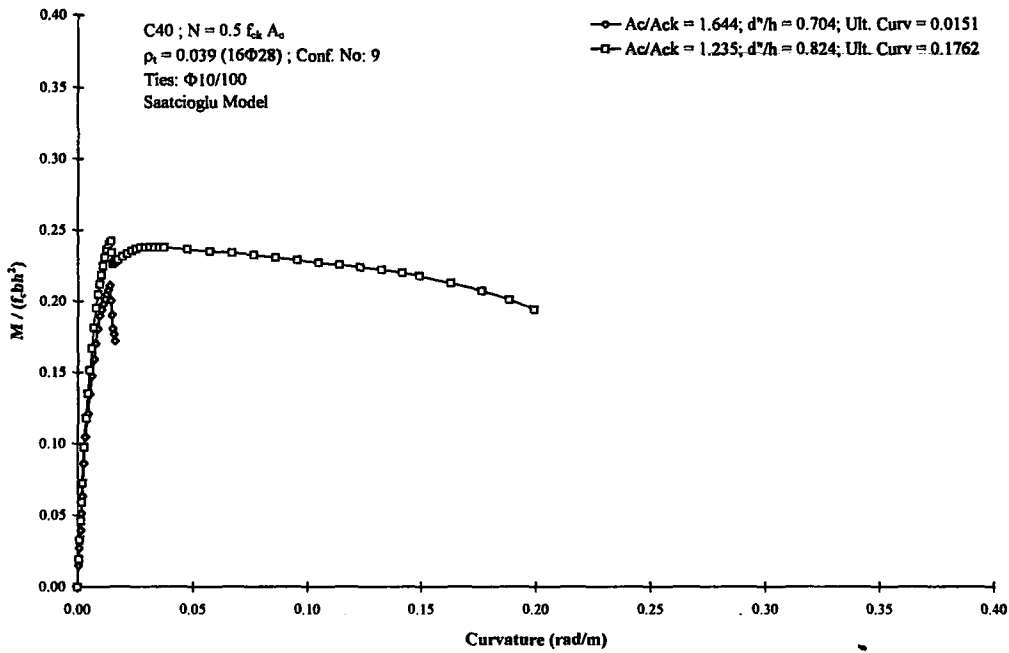


**Figure A.148:** Influence of ratio of the gross area to the confined area ( $A_g/A_{ck}$ ) in R/C columns; Group XVD

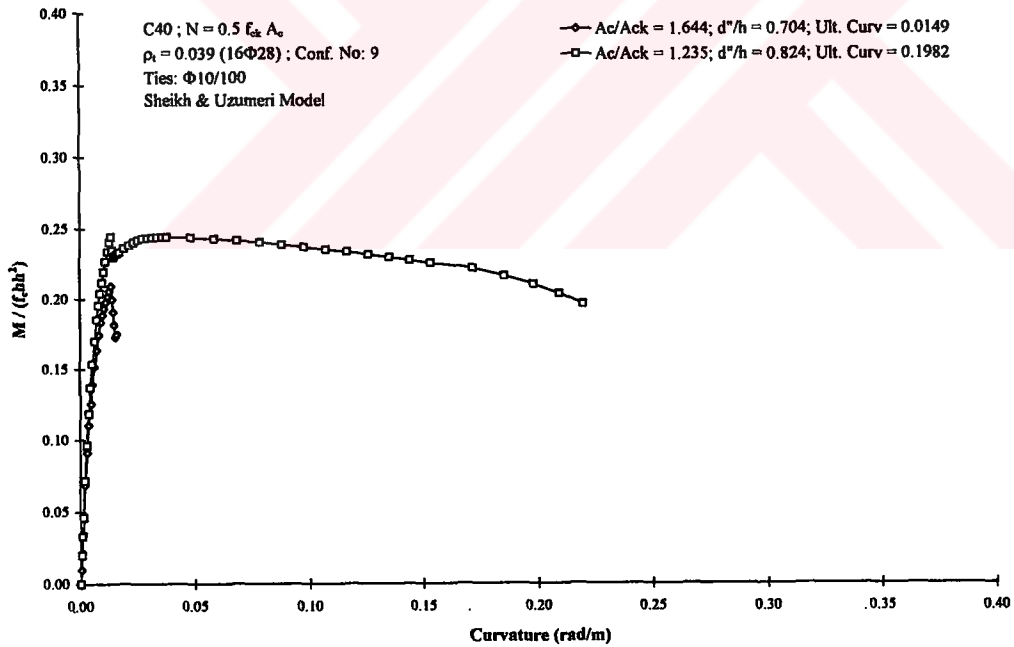


**Figure A.149:** Influence of ratio of the gross area to the confined area ( $A_g/A_{ck}$ ) in R/C columns; Group XVE

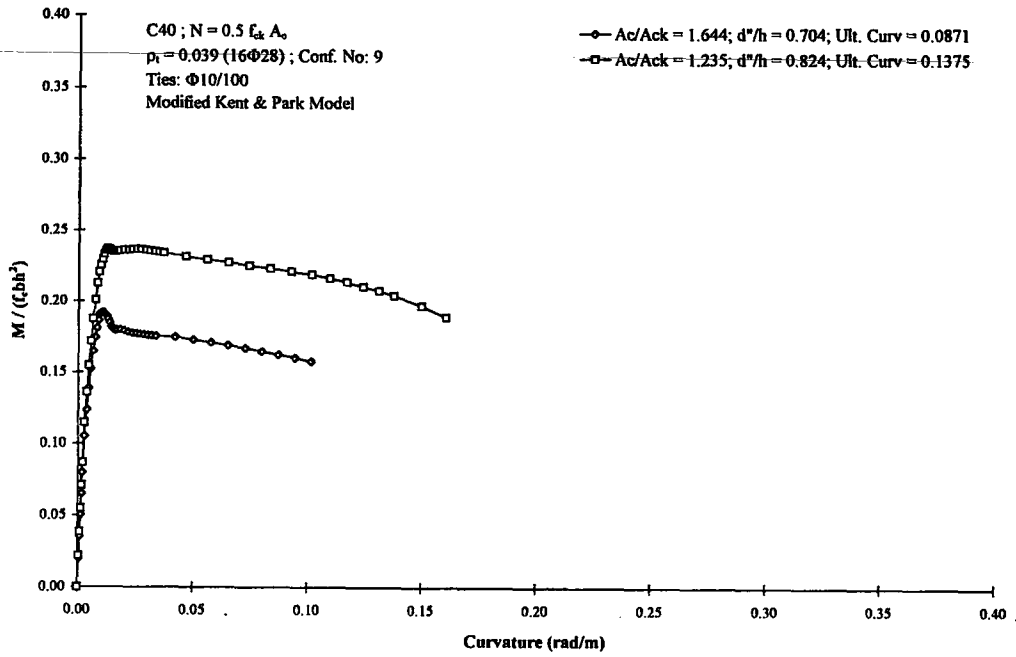


**Figure A.150:** Influence of ratio of the gross area to the confined area ( $A_g/A_{ck}$ ) in R/C columns; Group XVF

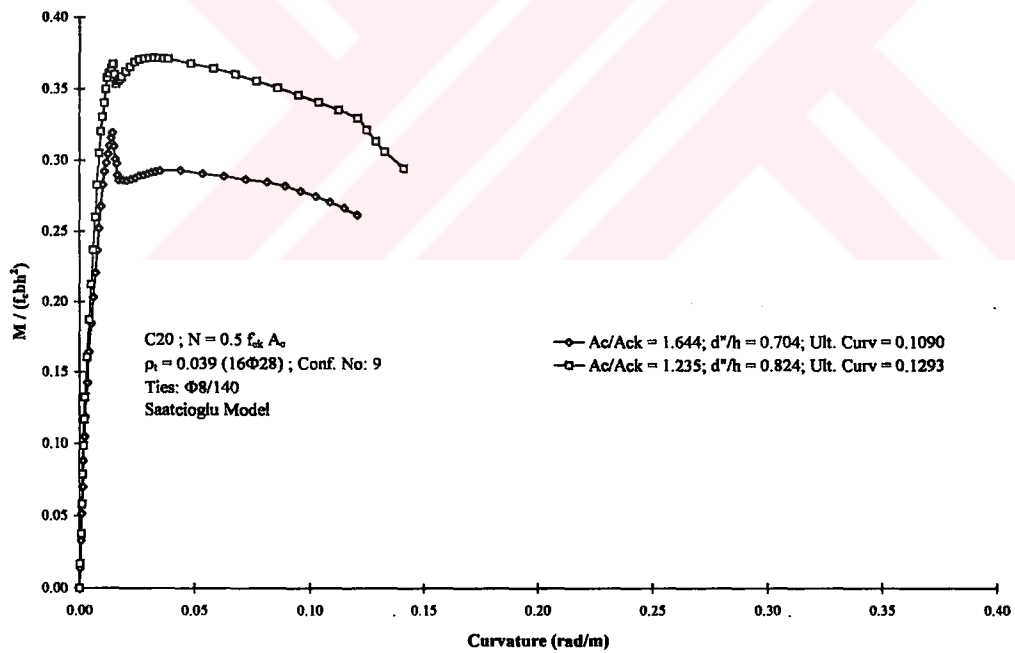


**Figure A.151:** Influence of ratio of the gross area to the confined area ( $A_g/A_{ck}$ ) in R/C columns; Group XVG

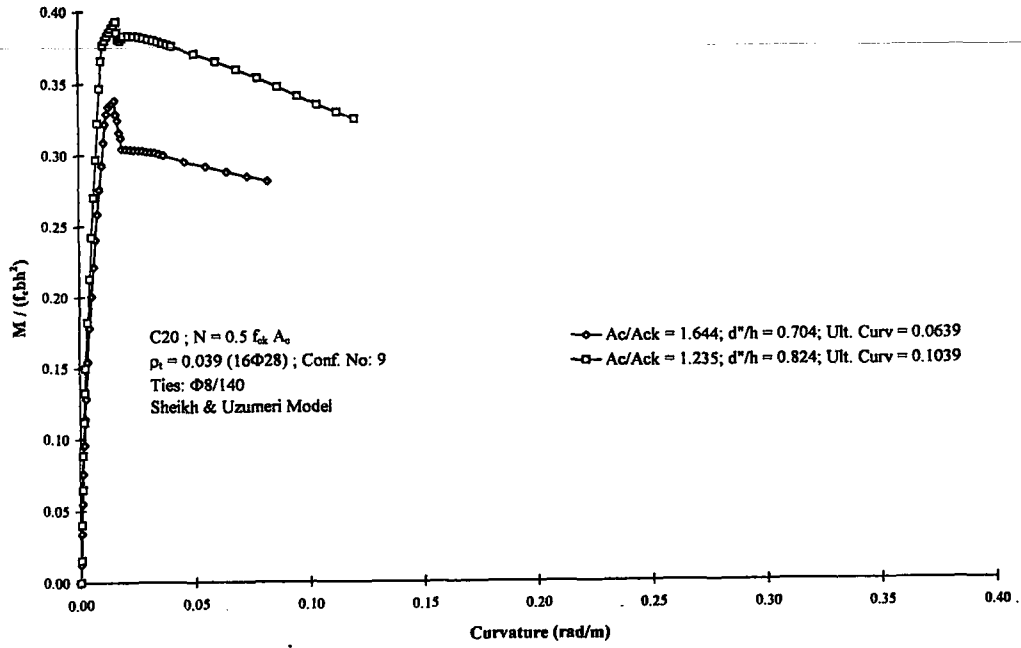


**Figure A.152:** Influence of ratio of the gross area to the confined area ( $A_c/A_{ck}$ ) in

R/C columns; Group XVH

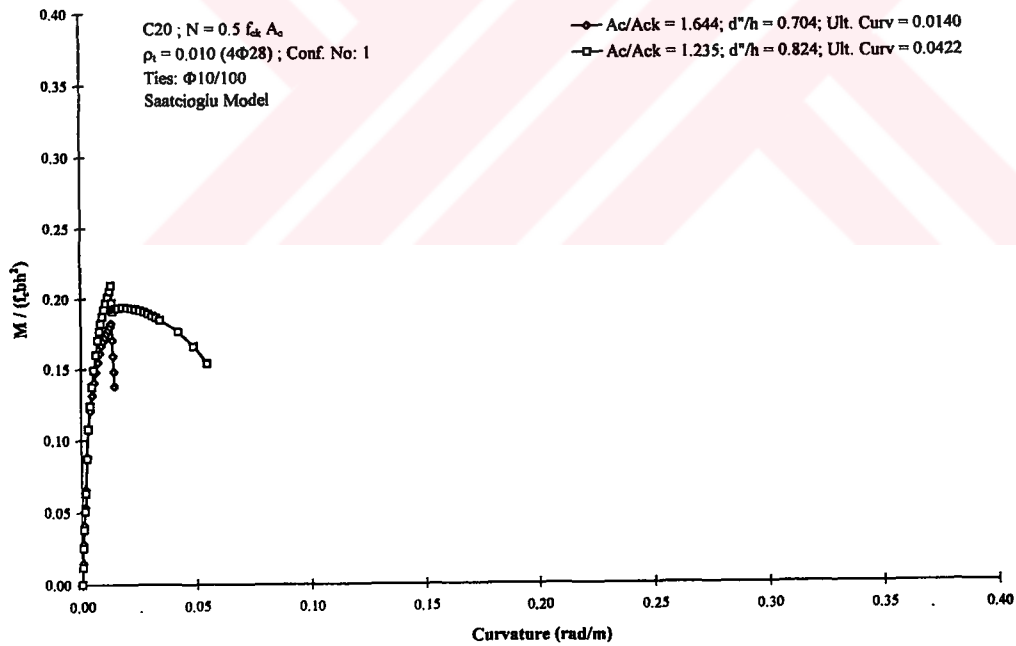


**Figure A.153:** Influence of ratio of the gross area to the confined area ( $A_c/A_{ck}$ ) in

R/C columns; Group XVJ

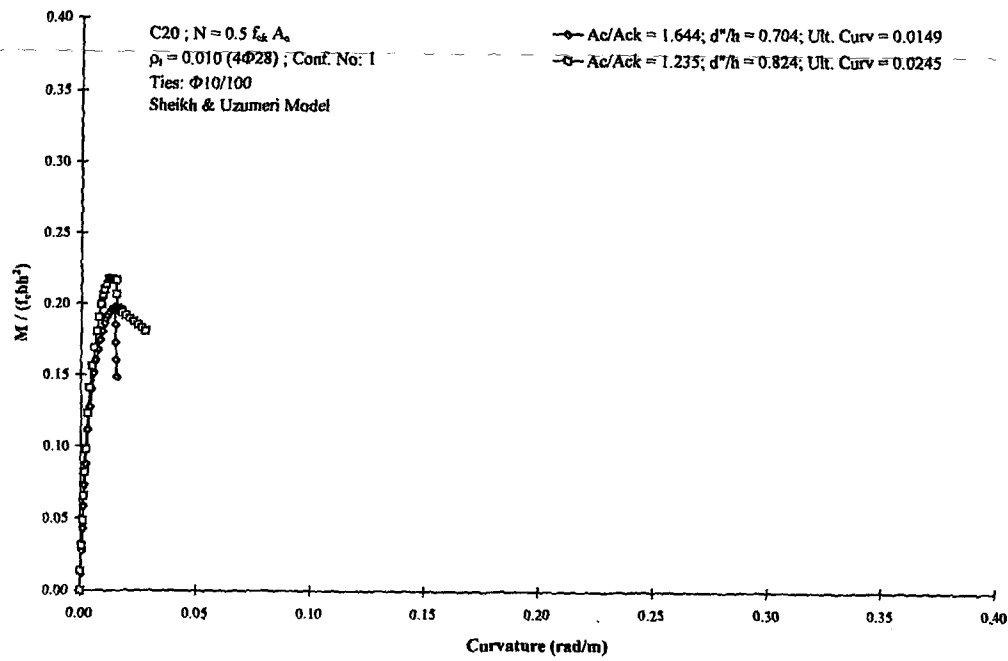


Figure A.154: Influence of ratio of the gross area to the confined area ( $A_g/A_{ck}$ ) in R/C columns; Group XVK

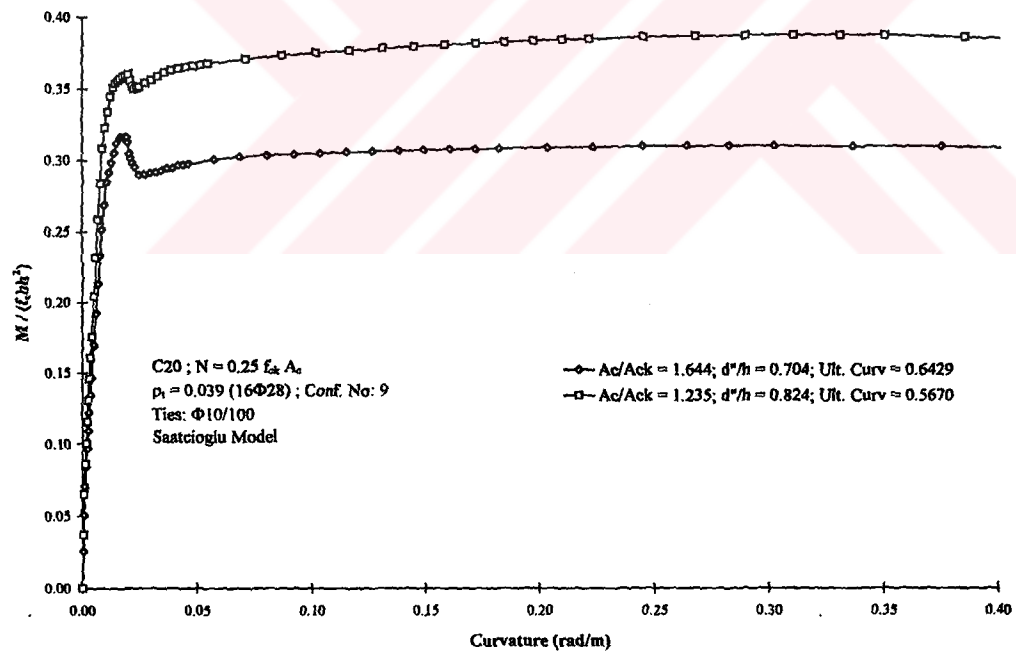
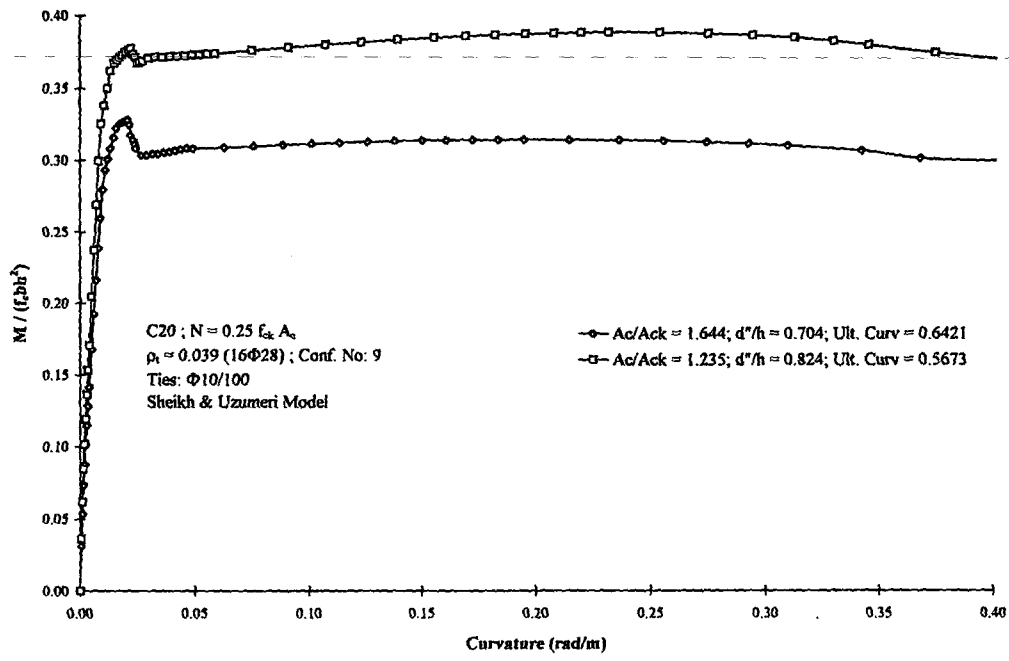


Figure A.155: Influence of ratio of the gross area to the confined area ( $A_g/A_{ck}$ ) in R/C columns; Group XVI



**Figure A.156:** Influence of ratio of the gross area to the confined area ( $A_c/A_{ck}$ ) in R/C columns; Group XVM

## APPENDIX B

In Appendix B, interaction diagrams of columns investigated in Chapter 5 are presented. Diagrams were drawn using unconfined concrete model for both cover & core concrete. For steel elasto-plastic model was used.

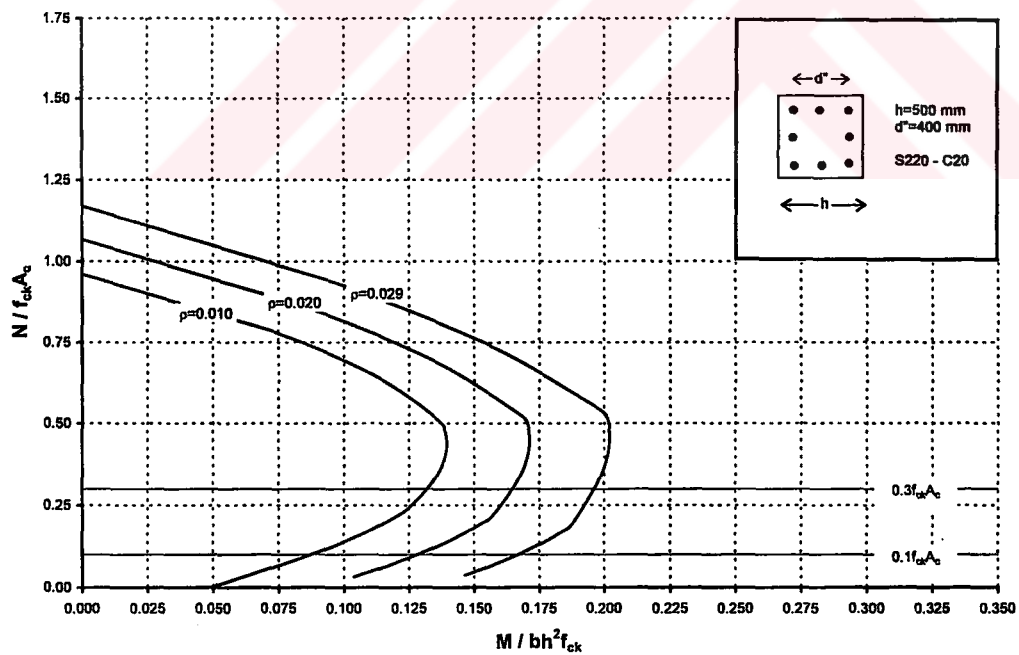


Figure B.1: Interaction diagrams; S220-C20 combination, 8 longitudinal bars



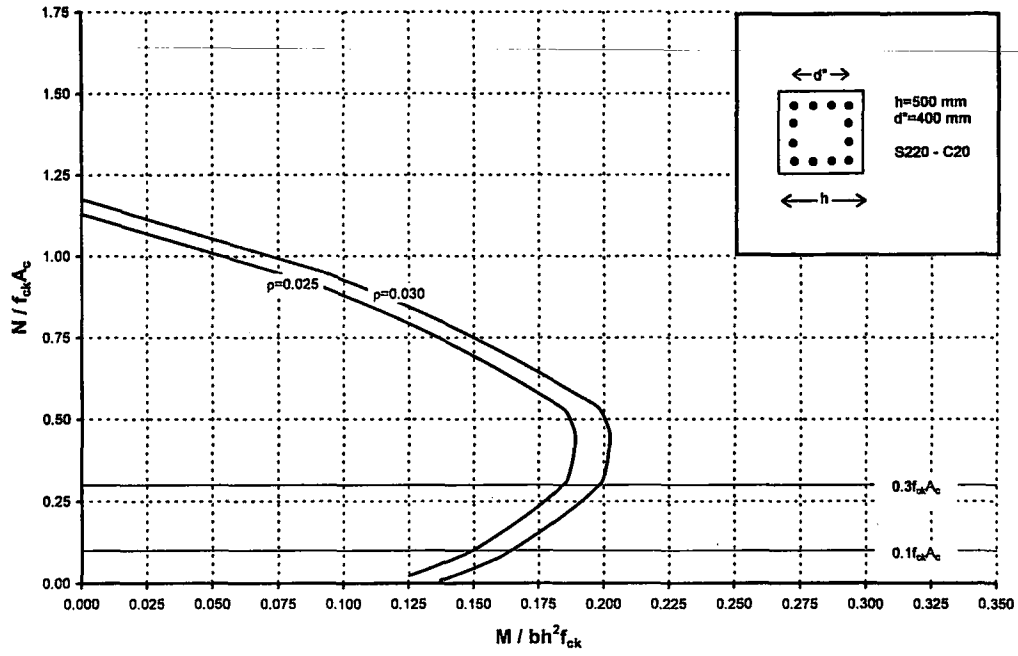


Figure B.2: Interaction diagrams; S220-C20 combination, 12 longitudinal bars

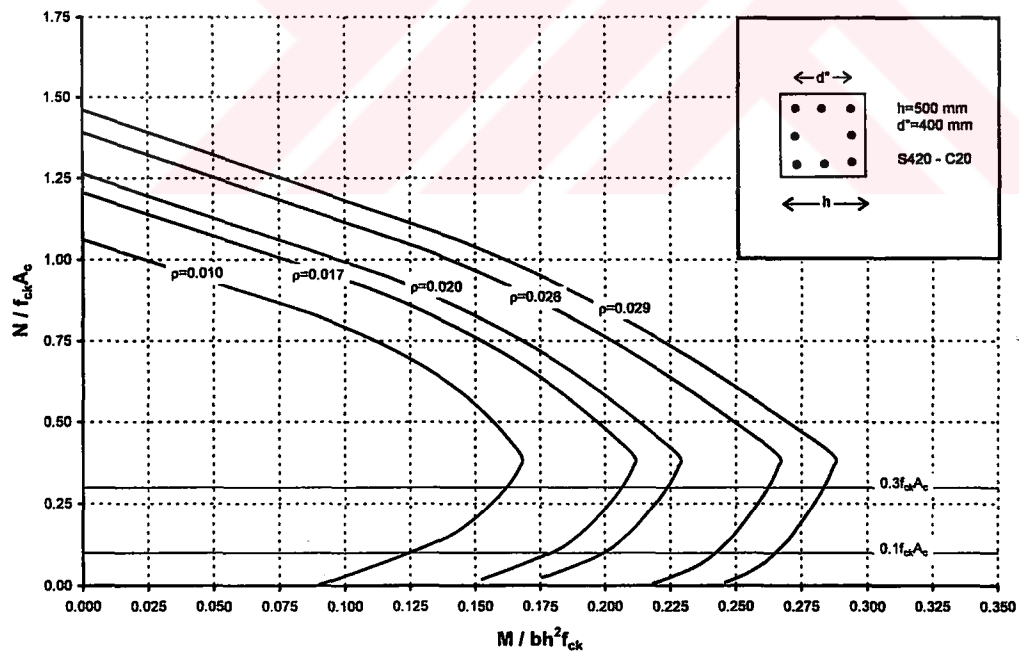
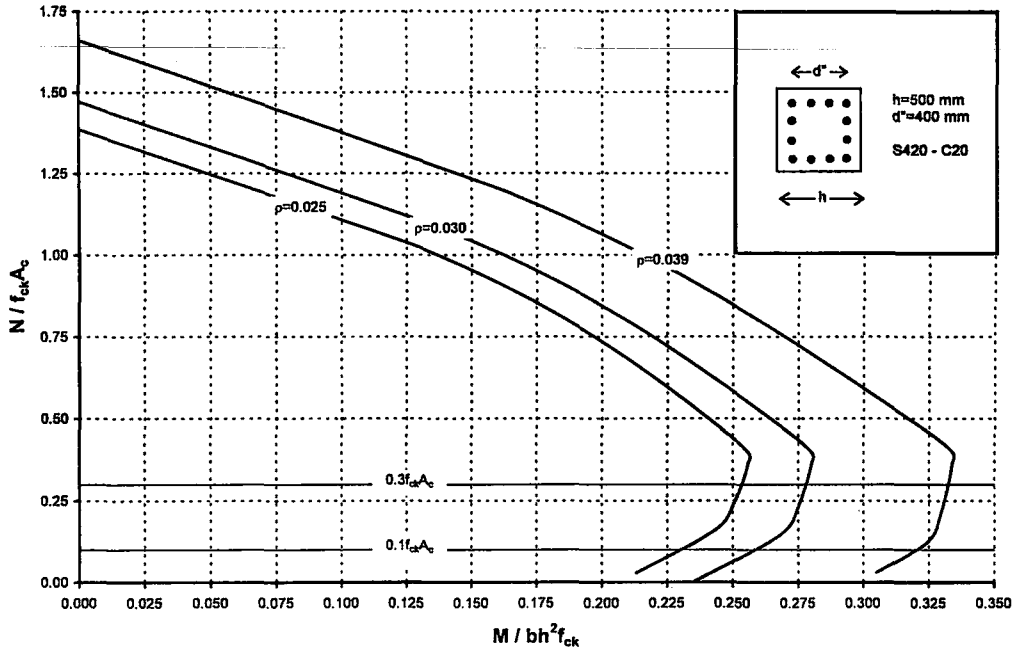
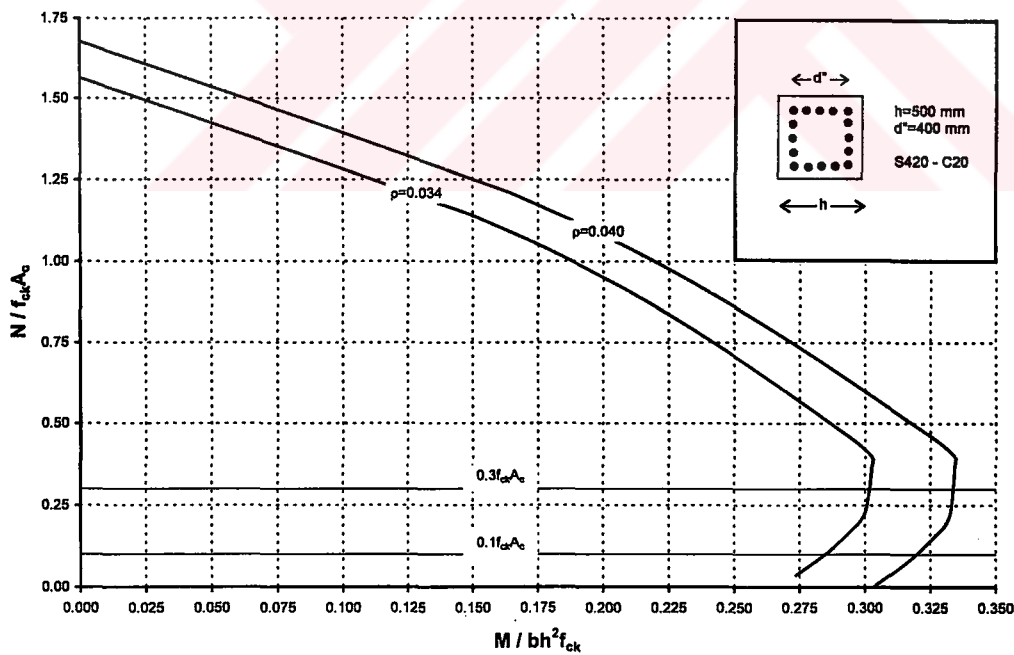


Figure B.3: Interaction diagrams; S420-C20 combination, 8 longitudinal bars



**Figure B.4:** Interaction diagrams; S420-C20 combination, 12 longitudinal bars



**Figure B.5:** Interaction diagrams; S420-C20 combination, 16 longitudinal bars

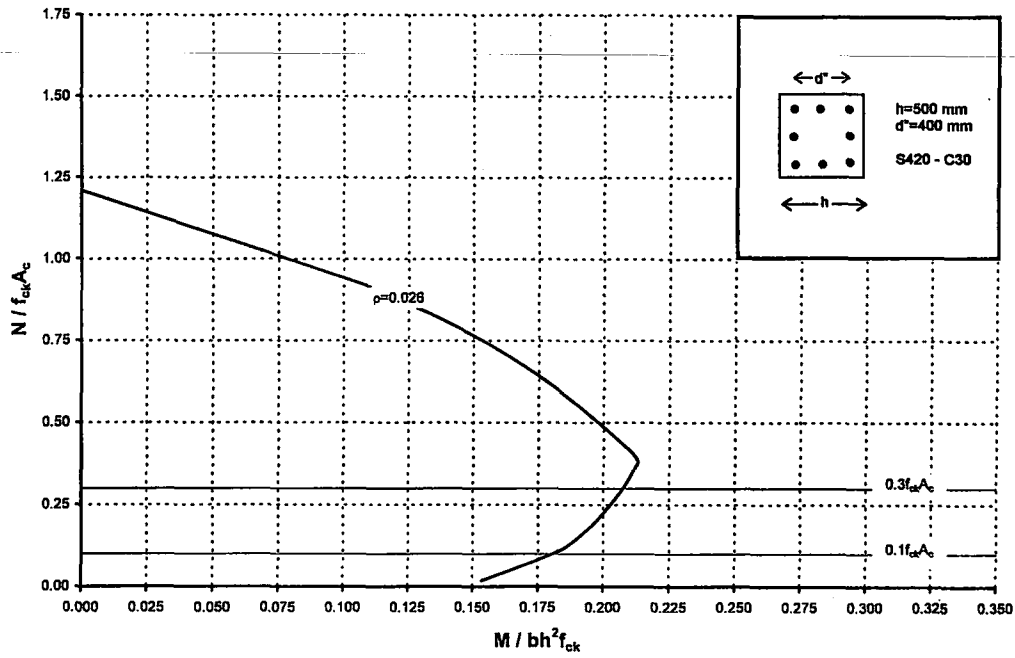


Figure B.6: Interaction diagrams; S420-C30 combination, 8 longitudinal bars

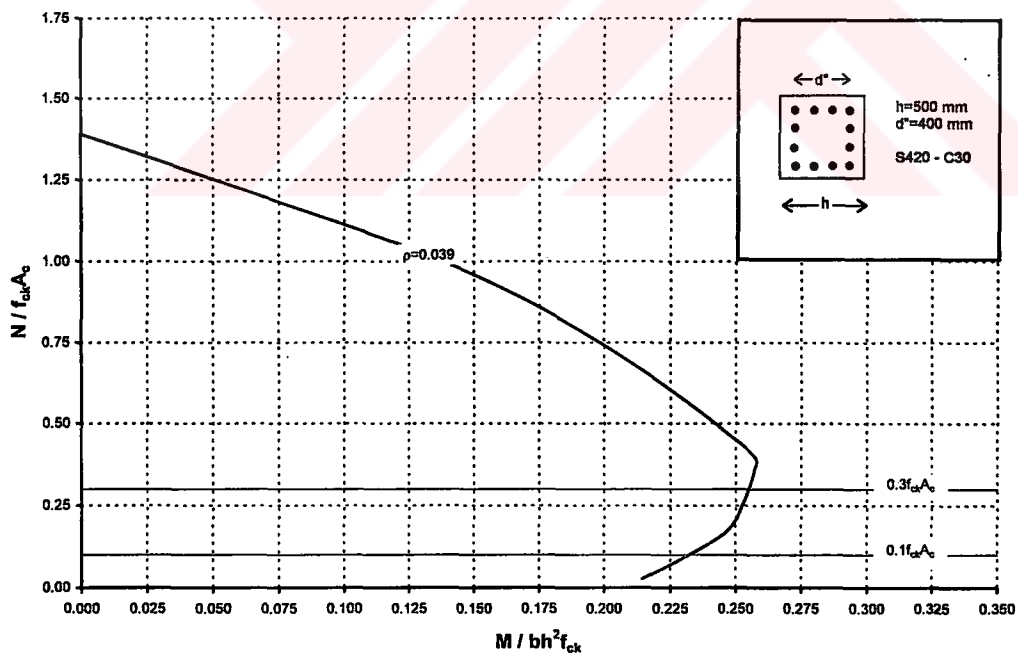
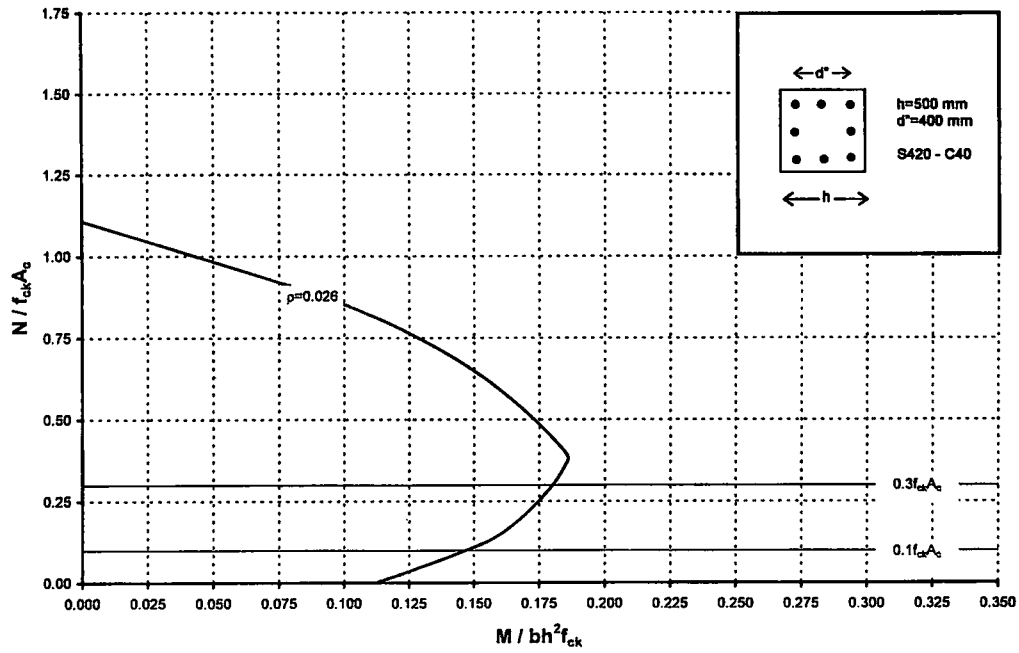
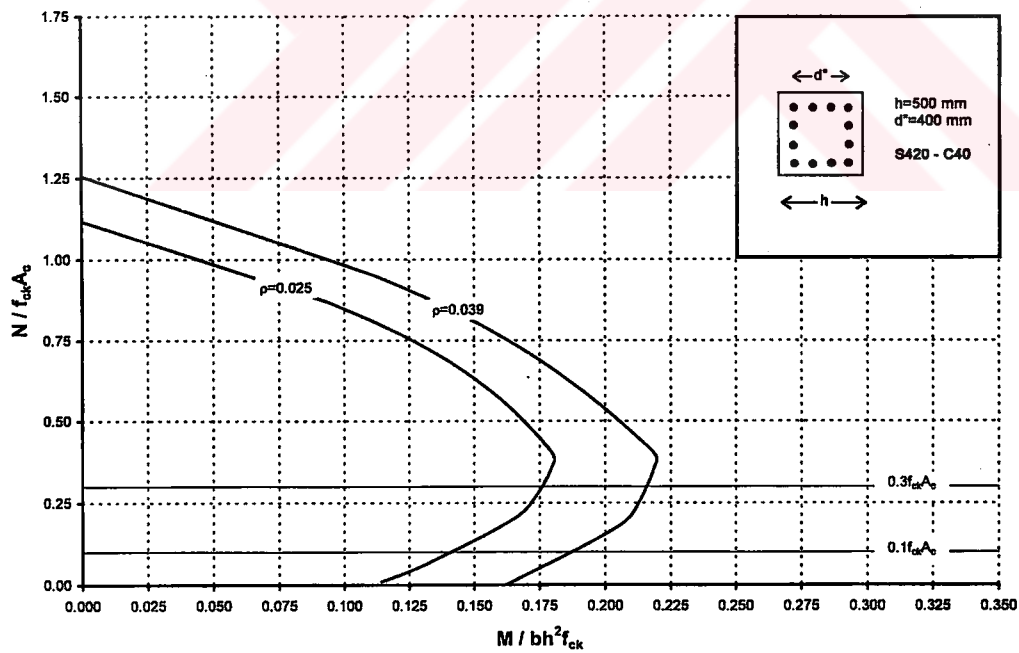


Figure B.7: Interaction diagrams; S420-C30 combination, 12 longitudinal bars

INSTITUT TEKNIK SURABAYA  
FAKULTAS TEKNIK SIPIL DAN PERENCANAAN  
LABORATORIUM MEKANIKA STRUKTURAL



**Figure B.8:** Interaction diagrams; S420-C40 combination, 8 longitudinal bars



**Figure B.9:** Interaction diagrams; S420-C40 combination, 12 longitudinal bars

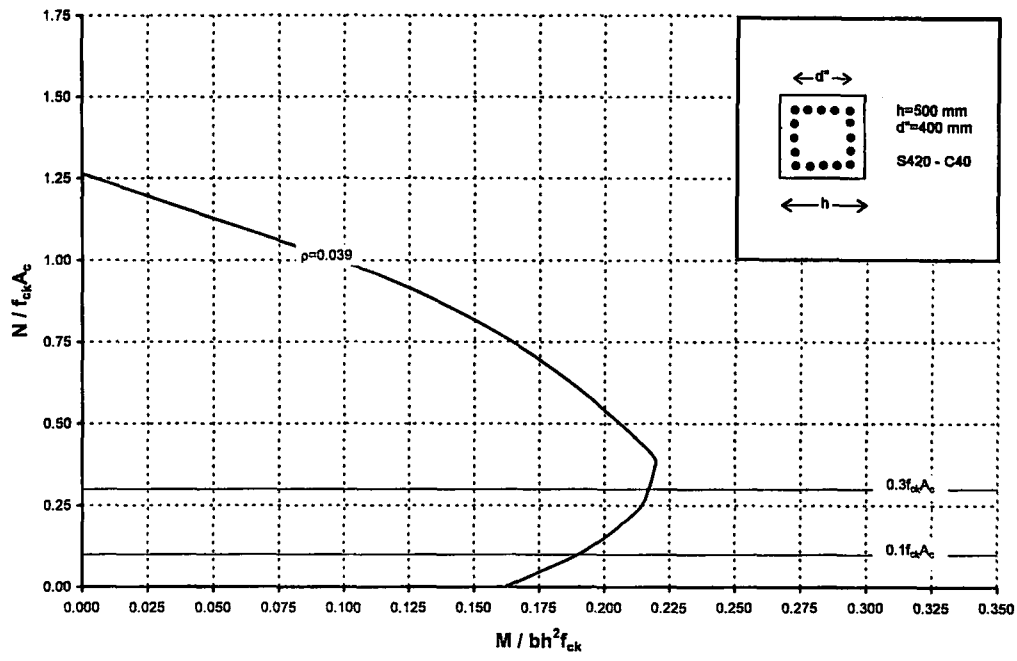


**Figure B.10:** Interaction diagrams; S420-C40 combination, 16 longitudinal bars